TURKISH JOURNAL OF SCIENCE AND TECHNOLOGY (TJST)

Year: 2018 Vol: 13 Number: 1

Address:
Fırat Universitesi
Fen Bilimleri Enstitüsü
23119, Elazig - TURKEY

Tel: 0 424 212 27 07
Fax: 0 424 236 99 55
e-mail: fenbilimdergi@firat.edu.tr

New ISSN
Online: 1308-9099
Printed: 1308-9080

Old ISSN
Online: 1306 – 8555
Printed: 1306 – 8547

Refereed journal. Published twice a year

http://web.firat.edu.tr/fenbilimleri/Dergiler/TJST/index.html

TURKISH JOURNAL OF SCIENCE & TECHNOLOGY (TJST)

Published by Firat University

Fırat Üniversitesi Turkish Journal of Science & Technology (TJST)
12-1, 2017

İÇİNDEKİLER / CONTENTS

Turkish Journal of Science & Technology
Volume 13(1), 1-7, 2018

Free Vibration of Cracked Cantilever Beams: Analytical and Experimental Modelling

Volkan Kahya*, Sebahat Karaca
Karadeniz Technical University, Faculty of Engineering, Department of Civil Engineering, 61080 Trabzon, Turkey
*volkan@ktu.edu.tr

(Received: 10.02.2017; Accepted: 11.04.2017)

Abstract

This study presents free vibration of cantilever beams with multiple cracks. The problem is solved analytically by the transfer matrix method, and is validated experimentally by the operational modal analysis. Six damage scenarios are considered to study crack effect on the natural frequencies and corresponding mode shapes. Graphs and tables for numerical results are given and discussed. Results show that crack occurrence in a beam significantly changes its dynamic behavior.

Keywords: Crack, Beam, Free vibration, Transfer matrix method, Experimental model

Çatlaklı Konsol Kirişlerin Serbest Titreşimi: Analitik ve Deneysel Modelleme

Özet

Bu çalışmada birden fazla çatlak içere konsol kirişlerin serbest titreşimleri incelenmiştir. Problem analitik olarak transfer matrisi metoduyla çözülmüş ve operasyonel modal analiz ile deneysel doğrulama yapılmıştır. Çatlağın doğal frekanslar ve mod şekillerini üzerindeki etkilerini incelemk üzere altı farklı hasar durumu göz önüne alınmıştır. Sayısal sonuçlar grafik ve tablolarla sunulmuştur. Sonuçlar, çatlak varlığının kirişin dinamik davranışını önemli ölçüde değiştirdiğini göstermiştir.

Anahtar Kelimeler: Çatlak, Serbest titreşim, Transfer matrisi metodu, Deneysel model

1. Introduction

Engineering structures are exposed to different types of environmental loads such as earthquakes, wind and traffic loads etc. Over time, stresses and strains due to these loadings lead to reduce in lifetime of the structure, and may cause damages (cracks), which is a serious threat to performance of structure. Early detection of any structural damage is important to prevent structural failures that causes human casualties and financial costs. Thus, an accurate and comprehensive study on structures including cracks are necessary.

Beams are structural elements in which cracks are commonly observed. Therefore, they have been frequently studied by researchers with through different analytical, numerical and experimental techniques. Dimarogonas [1] presented a comprehensive review of various methods in studying structural members with cracks.

Dimarogonas and Paipetis [2] proposed the local flexibility concept to model an open edge crack in a beam, which can be derived from the stress intensity factors in the theory of fracture mechanics. The cracked section in a beam can be replaced by massless rotational springs representing the local flexibility of the crack. Studies on vibrations of cracked beams using the local flexibility concept have generally focused on two main aspects: The first is to estimate the effects of cracks on the eigen-parameters of beams as a direct problem, and the second is to detect the location and size of the crack from the measured information as an inverse problem. Direct analysis of beam vibrations in the presence of cracks is, however, required for solution of the inverse problem.

Methods in studying free vibration of beams with cracks are, in general, divided into two main

groups: continuous and discrete methods. In continuous methods, the beam is divided into several sub-beams connected by massless springs. Differential equations are, then, solved for each sub-beam individually with considering the boundary and continuity conditions. As a continuous method, the transfer matrix method is an efficient tool for free vibration of cracked beams, and have been widely preferred [3-8]. Viola et al. [9] derived the explicit dynamic stiffness matrix of a cracked axially loaded beam under coupled bending–torsion with considering the effects of the rotatory inertia and the shear deformation. Among discrete methods, the finite element method [10-12] and the discrete element method [13] can be mentioned.

Experimental measurements including ambient and forced vibration tests have also been used to extract the dynamic characteristics of cracked beams during operational conditions as well as to verify their analytical and/or numerical models [14-16]. Experimental measurements can also be used to identify cracks in a beam in inverse problems.

As can be seen in the literature summarized above, there are many studies on cracked beam vibrations using different analytical/numerical and experimental methods. However, the studies on extracting dynamic characteristics of cracked beams by operational modal analysis (OMA), and validating the experimental results with analytical solution are limited. This study presents free vibration analysis of cantilever beams with multiple cracks. The problem is solved analytically by the transfer matrix method (TMM), and is validated experimentally by the operational modal analysis (OMA). The cantilever beam is assumed to obey Bernoulli-Euler theory. Six damage scenarios are considered to study crack effect on the natural frequencies and corresponding mode shapes. Comparative graphs and tables for numerical results are given and discussed.

2. Theoretical Formulation

2.1. Analytical model

Consider a cantilever beam with N cracks along its length, and has a rectangular cross-section of width b and height h shown in Fig. 1. The beam is assumed to be connected by massless rotational springs at cracked section as shown in Fig. 2. Equation of motion for each segment of the beam is given by

$$EI\frac{\partial^4 Y_i(x,t)}{\partial x^4}+\rho A\frac{\partial^2 Y_i(x,t)}{\partial t^2}=0 \quad (i=1,2,...,N+1) \tag{1}$$

where $Y_i(x,t)$ is the deflection function, EI is the flexural rigidity, ρ is the mass density, $A=bh$ is the cross-sectional area of the beam. Introducing

$$\bar{x}=x/L \tag{2}$$

into (1) yields

$$\frac{EI}{L^4}\frac{\partial^4 y_i(\bar{x},t)}{\partial \bar{x}^4}+\rho A\frac{\partial^2 y_i(\bar{x},t)}{\partial t^2}=0 \quad (i=1,2,...,N+1) \tag{3}$$

where $Y(x,t)\equiv y(\bar{x},t)$.

Assuming the solution of (3) as

$$y_i(\bar{x},t)=X_i(\bar{x})e^{i\omega t} \quad (i=1,2,...N+1) \tag{4}$$

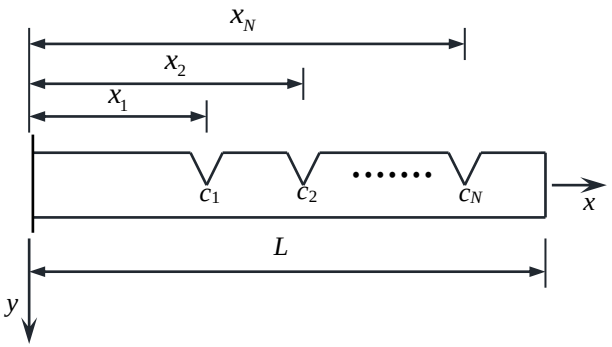

Figure 1. A cantilever beam with multiple cracks

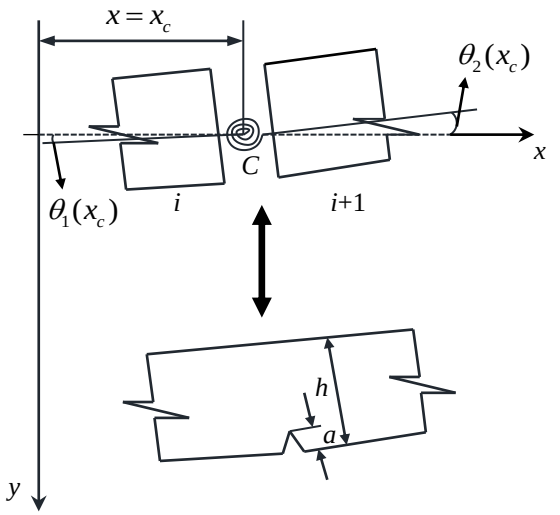

Figure 2. Cracked section represented by massless rotational spring.

where $X_i(\bar{x})$ denotes the modal shape function, and ω is the natural frequency of the beam, and substituting it into (3) gives the following:

$$\frac{d^4 X_i}{d\bar{x}^4} - \beta^4 X_i = 0 \quad (i = 1,2,...,N+1) \tag{5}$$

where

$$\beta^4 = \frac{\rho A L^4}{EI}\omega^2 \tag{6}$$

Solution of (5) is

$$X_i(\bar{x}) = A_i \sin\beta\bar{x} + B_i \cos\beta\bar{x} + C_i \sinh\beta\bar{x} + D_i \cosh\beta\bar{x} \quad (i = 1,2,...N+1) \tag{7}$$

where A_i, B_i, C_i and D_i are constants to be determined from the boundary and continuity conditions given by

$$y(0,t) = y'(0,t) = -EIy''(1,t) = -EIy'''(1,t) = 0 \tag{8}$$

$$\begin{aligned} &y_i(\bar{x}_i,t) = y_{i+1}(\bar{x}_i,t) \\ &y_i'(\bar{x}_i) = y_{i+1}'(\bar{x}_i) - (h/L) f(a_i) y_{i+1}''(\bar{x}_i) \\ &y_i''(\bar{x}_i,t) = y_{i+1}''(\bar{x}_i,t) \\ &y_i'''(\bar{x}_i) = y_{i+1}'''(\bar{x}_i) \end{aligned} \tag{9}$$

where $f(d_i)$ is a dimensionless function, which is given by single-sided open cracks as

$$f(d_i) = 2[d_i/(1-d_i)]^2 (5.93 - 19.69 d_i + 37.14 d_i^2 - 35.64 d_i^3 + 13.12 d_i^4) \tag{10}$$

where $d_i = a_i / h$ is dimensionless crack depth.

Substituting (4) into (9), we have the following:

$$\mathbf{P}_i \mathbf{a}_i = \mathbf{Q}_i \mathbf{a}_{i+1} \quad (i = 1,2,...,N) \tag{11}$$

where $\mathbf{a}_i = \{A_i \quad B_i \quad C_i \quad D_i\}^T$ and

$$\mathbf{P}_i = \begin{bmatrix} \sin\beta\bar{x}_i & \cos\beta\bar{x}_i & \sinh\beta\bar{x}_i & \cosh\beta\bar{x}_i \\ \cos\beta\bar{x}_i & -\sin\beta\bar{x}_i & \cosh\beta\bar{x}_i & \sinh\beta\bar{x}_i \\ -\sin\beta\bar{x}_i & -\cos\beta\bar{x}_i & \sinh\beta\bar{x}_i & \cosh\beta\bar{x}_i \\ -\cos\beta\bar{x}_i & \sin\beta\bar{x}_i & \cosh\beta\bar{x}_i & \sinh\beta\bar{x}_i \end{bmatrix} \tag{12}$$

$$\mathbf{Q}_i = \mathbf{P}_i + \mathbf{S}_i \tag{13}$$

where

$$\mathbf{S}_i = \chi \begin{bmatrix} 0 & 0 & 0 & 0 \\ -\sin\beta\bar{x}_i & -\cos\beta\bar{x}_i & \sinh\beta\bar{x}_i & \cosh\beta\bar{x}_i \\ 0 & 0 & 0 & 0 \\ 0 & 0 & 0 & 0 \end{bmatrix} \tag{14}$$

where $\chi = -\beta(h/L) f(a_i)$. From (11), we have

$$\mathbf{a}_{i+1} = \mathbf{Q}_i^{-1} \mathbf{P}_i \mathbf{a}_i \quad (i = 1,2,...,N) \tag{15}$$

Considering (15), the following relation between the constants of $(N+1)$ th and those of first segment can be written:

$$\mathbf{a}_{N+1} = \mathbf{Q}_N^{-1}\mathbf{P}_N \mathbf{Q}_{N-1}^{-1}\mathbf{P}_{N-1} \cdots \mathbf{Q}_1^{-1}\mathbf{P}_1 \mathbf{a}_1 = \mathbf{T}\mathbf{a}_1 \tag{16}$$

where $\mathbf{T}$ is the transfer matrix.

Using the first two conditions of (8) into (7) gives $D_1 = -B_1$ and $C_1 = -A_1$. Substituting the latter two of (8) into (7) gives

$$\mathbf{W}\mathbf{a}_{N+1} = \mathbf{0} \tag{17}$$

where

$$\mathbf{W} = \begin{bmatrix} -\sin\beta & -\cos\beta & \sinh\beta & \cosh\beta \\ -\cos\beta & \sin\beta & \cosh\beta & \sinh\beta \end{bmatrix} \tag{18}$$

Substituting (16) into (17) gives

$$\mathbf{Z}\mathbf{a}_1 = \mathbf{0} \tag{19}$$

where $\mathbf{Z} = \mathbf{W}\mathbf{T}$. Re-calling $D_1 = -B_1$ and $C_1 = -A_1$ and re-arranging equation (19), we have

$$\begin{bmatrix} Z_{11} - Z_{13} & Z_{12} - Z_{14} \\ Z_{21} - Z_{23} & Z_{22} - Z_{24} \end{bmatrix} \begin{bmatrix} A_1 \\ B_1 \end{bmatrix} = \begin{bmatrix} 0 \\ 0 \end{bmatrix} \tag{20}$$

Equation (20) has real roots different from zero when the determinant of its coefficient matrix is zero. Thus,

$$\det \begin{bmatrix} Z_{11} - Z_{13} & Z_{12} - Z_{14} \\ Z_{21} - Z_{23} & Z_{22} - Z_{24} \end{bmatrix} = 0 \tag{21}$$

which gives a characteristic equation as $f(m, \bar{x}_i, d_i) = 0$ depending on natural frequencies, crack size and location. Using the roots β_n $(n = 1,2,\ldots)$ of the characteristic equation into (6), the natural frequencies of beam can be obtained from

$$\omega_n = \frac{\beta_n^{\,2}}{L^2}\sqrt{\frac{EI}{\rho A}} \tag{22}$$

For modal shape functions, constants $\mathbf{a}_i$ for each segment can, then, be obtained from (20) for $i = 1$ and (15) for $i = 2,3,\ldots$.

2.2. Experimental model

Three steel cantilever beams are constructed for laboratory tests. A typical representation of the model is shown in Fig. 3. The beam has uniform rectangular cross-section along its length. In experimental measurements, B&K3560 data acquisition system with 17 channels, B&K8340-type uni-axial accelerometers and uni-axial signal cables are used as test equipment. Six

sensitive accelerometers are located on the laboratory model to extract natural frequencies and corresponding mode shapes of the beam shown in Fig. 4.

Measurements are performed during 10 minutes for all cases (damaged and undamaged) considered. Frequency range, FFT analyzers and Multi-buffer are selected to be 0-800Hz, 800 lines and 100 averages, 50 size and 500m update, respectively. The signals from the accelerometers are recorded on the computer with applying FFT process in PULSE [17] software. This transformed data is, then, filtered by the weight functions in OMA [18] software. Modal parameters are obtained by Enhanced Frequency Domain Decomposition (EFDD) method in frequency domain which gives the spectral density functions of the signals in each channel. Natural frequencies and modal damping ratios are, then, determined using the spectral density functions. Fig. 5 shows the spectral density functions obtained from OMA. In there, the peak points which are selected manually show natural frequencies of the beam.

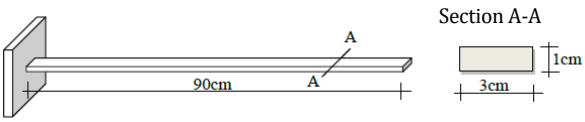

Figure 3. Dimensions of the steel cantilever beam.

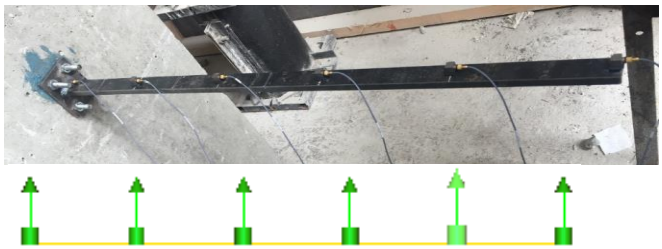

Figure 4. Laboratory model and accelerometer locations.

Table 1. Damage scenarios considered.

Scenario	Crack location (mm)			Crack depth (mm)		
	x_1	x_2	x_2	a_1	a_2	a_3
Damage-1	90	-	-	3	-	-
Damage-2	90	270	-	3	3	-
Damage-3	90	270	450	3	3	3
Damage-4	90	270	450	6	3	3
Damage-5	90	270	450	6	6	3
Damage-6	90	270	450	6	6	6

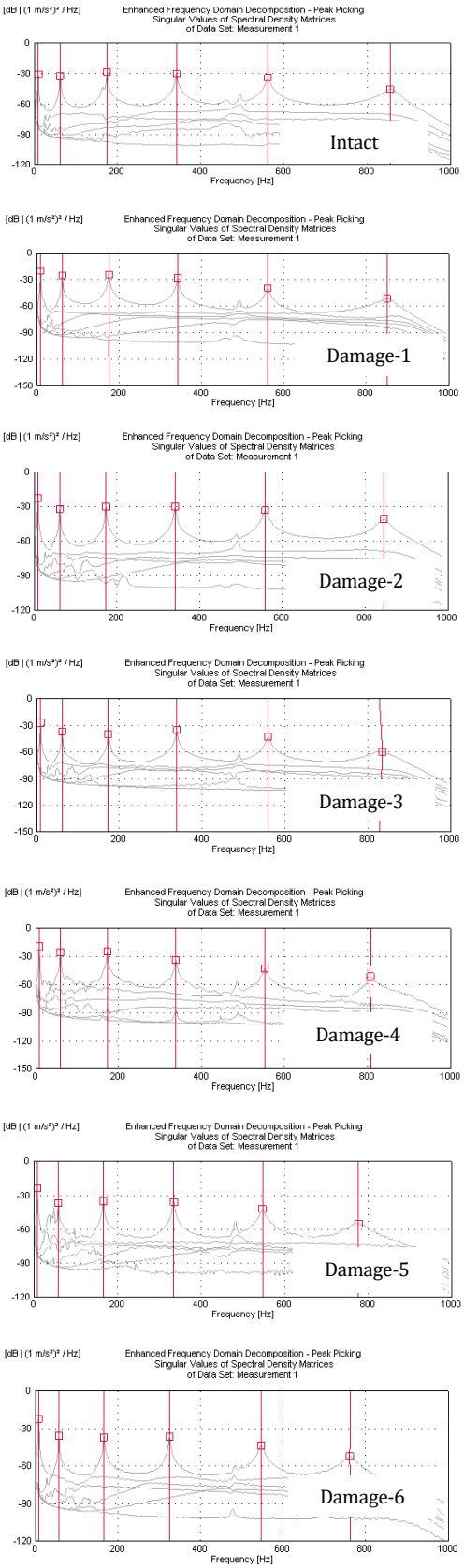

Figure 5. Singular values of spectral density matrices.

Table 2. First six natural frequencies (Hz) calculated from TMM.

Mode	Natural frequencies (Hz)						
	Intact	Damage-1	Damage-2	Damage-3	Damage-4	Damage-5	Damage-6
1	10.25	10.10	10.04	10.03	9.18	8.87	8.77
2	64.24	63.88	63.73	63.16	61.27	60.47	57.07
3	179.83	179.64	178.07	178.02	177.11	168.58	168.58
4	352.42	352.42	351.17	347.91	347.91	342.20	323.51
5	582.60	581.61	580.83	580.75	575.82	571.73	571.73
6	870.24	866.22	857.95	849.86	830.07	796.00	767.36

Table 3. First six natural frequencies (Hz) measured by OMA

Mode	Natural frequencies (Hz)						
	Intact	Damage-1	Damage-2	Damage-3	Damage-4	Damage-5	Damage-6
1	9.92	9.77	9.69	9.75	8.93	8.68	8.59
2	62.53	62.26	61.98	61.56	59.96	59.34	57.54
3	175.30	175.21	173.40	173.70	172.80	167.20	166.90
4	342.10	341.80	340.90	338.60	338.30	334.80	325.30
5	562.00	560.60	559.10	560.00	552.10	548.20	547.50
6	856.70	850.30	844.40	828.60	808.60	776.70	763.50

Table 4. Change in natural frequencies (%) with increasing damage severity.

Case	Change in natural frequencies (%)					
	f_1	f_2	f_3	f_4	f_5	f_6
Undamaged *vs.* Damage-1	1.48	0.55	0.10	0.00	0.17	0.46
Damage-1 *vs.* Damage-2	0.59	0.24	0.87	0.35	0.13	0.95
Damage-2 *vs.* Damage-3	0.11	0.89	0.03	0.93	0.01	0.94
Damage-3 *vs.* Damage-4	8.44	2.98	0.51	0.00	0.85	2.33
Damage-4 *vs.* Damage-5	3.35	1.30	4.82	1.64	0.71	4.11
Damage-5 *vs.* Damage-6	1.14	5.63	0.00	5.46	0.00	3.59

3. Results

Comparisons between the calculated and measured values are given. Material properties are E = 206GPa and ρ = 7800kg/m^3. Free vibration analyses are performed for six damage scenarios in Table 1. Analytical results are obtained through a computer code written in MATLAB environment.

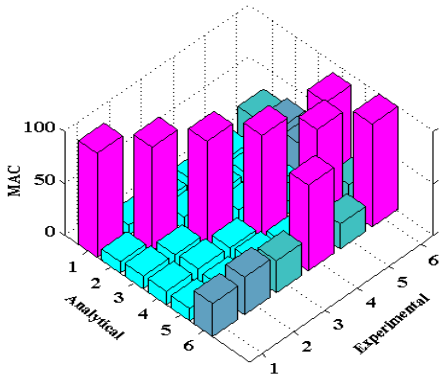

Figure 6. MAC representation between analytical and experimental mode shapes for undamaged case.

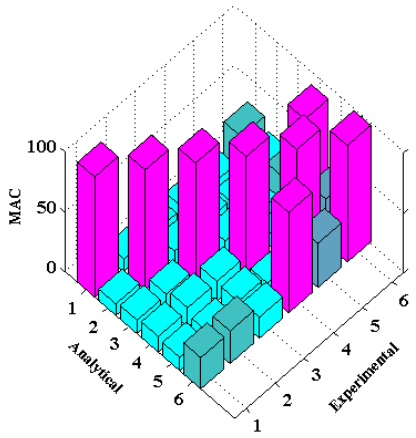

Figure 7. MAC representation between analytical and experimental mode shapes for Damage-6 case.

Tables 2-4 show the first six natural frequencies of the cantilever beam for all cases considered. As can be seen, the natural frequencies decrease with increasing the damage severity. This is more notable when the crack depth increases, i.e., between Damage-3 and Damage-4 cases. Results obtained from TMM and OMA slightly differ. This may be from several reasons such that: (a) fixed support

condition at left-end cannot be provided exactly in laboratory environment, and (b) the beam cross-section, thus the flexural rigidity, cannot be uniform along the beam length. The modal updating, which is already out of the scope of this study, is therefore required.

Modal Assurance Criterion (MAC) is used to establish the correlation between the measured and the calculated results, which is defined by

$$\mathrm{MAC}\left(X_a, X_e\right) = \frac{\left|X_a^T X_e\right|^2}{\left(X_a^T X_a\right)\left(X_e^T X_e\right)} \qquad (23)$$

where X_a and X_e denote analytical and experimental mode shapes. MAC values are greater than 90% means the mode shapes are good correlated [19]. Figs. 6 and 7 show MAC values between analytical and experimental mode shapes for undamaged and Damage-6 cases, respectively. As seen, the correlation between the calculated and measured mode shapes are very good, which verifies the laboratory measurements performed

4. Conclusions

Free vibration of cracked cantilever beams is considered by analytical and experimental methods. Results are in good agreement. The followings can be drawn from the study:

a) Natural frequencies are strongly affected by crack presence in the beam.
b) Crack depth is more effective on the natural frequencies compared to the number of cracks.
c) Operational modal analysis is very suitable for experimental analyses of cracked beams. For more accurate results, modal updating should be recommended.
d) Transfer matrix method gives the frequency equation to solve the inverse problem for damage detection. However, the solution is required more symbolic computation and thus computing time when the number of cracks increases.

5. References

1.Dimarogonas, A.D. (1996). Vibration of cracked structures: a state of the art review. *Engineering Fracture Mechanics*, **55**(5): 831-857.

2. Dimarogonas, A.D. and Paipetis, S.A. (1983). Analytical Methods in Rotor Dynamics, Applied Science Publisher, London.

3. Shifrin, E.I. and Ruotolo, R.. (1999). Natural frequencies of a beam with an arbitrary number of cracks. *Journal of Sound and Vibration*, **222**(3): 409-423.

4. Lin, H.P., Chang, S.C. and Wu, J.D. (2002). Beam vibrations with an arbitrary number of cracks. *Journal of Sound and Vibration*, **258**(5): 987-999.

5. Zheng, D.Y. and Fan, S.C. (2003). Vibration and stability of cracked hollow-sectional beams. *Journal of Sound and Vibration*, **267**: 933-954.

6. Lin, H.P. (2004). Direct and inverse methods on free vibration analysis of simply supported beams with a crack. *Engineering Structures*, **26**: 427–436.

7. Loya, J.A., Rubio, L. and Fernández-Sáez, J. (2006). Natural frequencies for bending vibrations of Timoshenko cracked beams. *Journal of Sound and Vibration*, **290**: 640-653.

8. Attar, M. (2012). A transfer matrix method for free vibration analysis and crack identification of stepped beams with multiple edge cracks and different boundary conditions. *International Journal of Mechanical Sciences*, **57**: 19-33.

9. Viola, E., Ricci, P. and Aliabadi, M.H. (2007). Free vibration analysis of axially loaded cracked Timoshenko beam structures using the dynamic stiffness method. *Journal of Sound and Vibration*, **304**: 124-153.

10. Ruotolo, R. and Surace, C. (2004). Natural frequencies of a bar with multiple cracks. *Journal of Sound and Vibration*, **272**: 301-316.

11. Lee, J. (2009). Identification of multiple cracks in a beam using natural frequencies. *Journal of Sound and Vibration*, **320:** 482-490.

12. Nandakumar, P. and Shankar, K. (2014). Multiple crack damage detection of structures using the two-crack transfer matrix. *Structural Health Monitoring*, **13**(5): 548–561.

13. Neves, A.C., Simões, F.M.F. and Pinto da Costa, A. (2016). Vibrations of cracked beams: Discrete mass and stiffness models. *Computers and Structures*, **168**: 68–77.

14. Sinha, J.K., Friswell, M.I. and Edwards, S. (2002). Simplified models for the location of cracks in beam structure using measured vibration data, *Journal of Sound and Vibration*, **251**: 13-38.

15. Patil, D.P. and Maiti, S.K. (2005). Experimental verification of a method of detection of multiple cracks in beams based on frequency measurements. *Journal of Sound and Vibration*, **281**: 439-451.

16. Nandakumar, P. and Shankar, K. (2015). Structural crack damage detection using transfer matrix and state vector. *Measurement*, **68**: 310–327.

17. PULSE (2006). Analyzers and Solutions, Release 11.2. Bruel and Kjaer, Sound and Vibration Measurement A/S, Denmark.

18.OMA (2006). Operational Modal Analysis, Release 4.0. Structural Vibration Solution A/S, Denmark.

19. Ewins, D.J. (1995). Modal Testing: Theory and Practice, John Wiley & Sons, Inc, New York.

Turkish Journal of Science & Technology
Volume 13(1), 9-17, 2018

Feasibility Analysis of NDT Methods Using to Estimate the Concrete Strength as Part of Urban Regeneration

Kürşat Esat Alyamaç[1], Merve Açıkgenç Ulaş[2]*, Yavuzhan Taş[3], Ehsan Ghafari[4]
[1]Fırat University, Faculty of Engineering, School of Civil Engineering, Elazig, TURKEY
[2]Fırat University, Faculty of Architecture, School of Architecture, Elazig, TURKEY
[3]Ministry of Transport, 8th Regional Directorate of Highways, Elazig, TURKEY
[4]Purdue University, Faculty of Engineering, School of Civil Engineering, West Lafayette, USA
*merveacikgenc@firat.edu.tr

(Received: 15.02.2017; Accepted: 10.04.2017)

Abstract

Most of the countries are placed in a seismic zone which has high activity and has extremely experienced large-scale losses due to several destructive earthquakes such as Turkey. Therefore, governments are seriously trying to produce the projects that will significantly reduce the earthquake effects. The most important part of these projects is urban regeneration. Within the context of urban regeneration activities, renewal of the buildings which have low earthquake-resistant is targeted. While the earthquake resistance level of a building is decided, one of the important steps is the determination of the strength of the building materials. There are many standard NDT methods that will be able to be used to determine the compressive strength. However, it is necessary to choose the appropriate methods in order to quickly and reliably estimate the strength properties of the materials. The purpose of this study is to determine the optimum NDT method for the urban regeneration. So, feasibility analysis was carried out for the standard NDT methods, and the performance of these methods was evaluated based on the cost and the accuracy. The result is the requirement new NDT method which is the practical and efficient for the large-scale projects such as urban regeneration.

Keywords: NDT, Compressive Strength, Urban Regeneration, In-Place Test, Earthquake.

Kentsel Dönüşüm Sürecinde Beton Dayanımının Tahmini İçin Kullanılan Hasarsız Deney Metotlarının Fizibilite Analizi

Özet

Dünya ülkelerinin çoğu, yüksek aktivite gösteren ve Türkiye gibi birçok yıkıcı deprem nedeniyle büyük çapta kayıplar yaşayan bir sismik bölgeye yerleşmiştir. Bu nedenle hükümetler, deprem etkilerini önemli ölçüde azaltacak projeler üretmek için ciddiyetle çalışmaktadırlar. Bu projelerin en önemli olanı kentsel dönüşümdür. Kentsel dönüşüm faaliyetleri bağlamında, depreme dayanıklı olmayan binaların yenilenmesi hedeflenmektedir. Bir binanın depreme dayanıklılık seviyesi belirlenirken, önemli adımlardan birisi yapı malzemelerinin dayanımının belirlenmesidir. Basınç dayanımını belirlemek için kullanılabilecek birçok standart hasarsız deney yöntemi mevcuttur. Bununla birlikte, malzemelerin mukavemet özelliklerini hızlı ve güvenilir bir şekilde hesaplamak için uygun yöntemleri seçmek gereklidir. Bu çalışmanın amacı kentsel dönüşüm için uygun hasarsız deney yöntemini belirlemektir. Böylece, standart hasarsız deney yöntemleri için fizibilite analizi gerçekleştirilmiş ve bu yöntemlerin performansı maliyet ve doğruluğa dayalı olarak değerlendirilmiştir. Sonuç, kentsel yenilenme gibi büyük ölçekli projeler için pratik ve verimli olan yeni hasarsız deney yönteminin gerekliliğidir.

Anahtar Kelimeler: Hasarsız Deney Yöntemleri, Basınç Dayanımı, Kentsel Dönüşüm, Yerinde Test, Deprem.

1. Introduction

The most popular performance measure which is used by design engineers to estimate the actual strength of concrete is the compressive strength, which is usually measured by breaking cylindrical or cubic specimens in a compression-testing machine. The compressive strength results can be used for the quality control, the formwork stripping times, the curing times, the fault diagnosis on the existing reinforced concrete/masonry structures, the research works,

and the in-place testing of concrete/mortar strength. Specifically, it is critical to estimate the in-place compressive strength of concrete, mortar and rock to establish the safety of the concrete and the masonry buildings. Because, most of the countries in the world are frequently exposed to the destructive earthquakes. After these earthquakes and tragedies, millions of buildings were severely damaged or collapsed [1-7]. To figure out this problem, the governments have been trying to renew the buildings by using urban regeneration/transformation policy or post-earthquake rehabilitation and reconstruction before the earthquakes [8, 9], for instance, Turkey is one of these countries. Urban regeneration was regulated with the Law: "The Regeneration of the Areas under Disaster Risk (Law No: 6306)" in Turkey in May 2012. Decreasing the risk before the disasters, which are especially earthquakes, is aimed at this law [10]. Minimizing the risk before the earthquakes means that hundreds of thousands of existing buildings, which have low earthquake resistance or insufficient resistance, should be renewed. First of all, earthquake resistance of these buildings, namely safety, must be determined. The in-situ strength of concrete, mortar and rock is an important part to establish the safety of the buildings [11].

Urban regeneration projects where the buildings have been rebuilt include not only a building but also at least dozens of buildings. Although the earthquake resistance of these buildings, which are usually reinforced concrete or masonry buildings, are estimated to be weak or inadequate, this problem still legally needs to be proven. For this reason, it is necessary to estimate the in-place compressive strength of the concrete in the buildings. Standard non-destructive (NDT) methods and drilling core method are usually used together to estimate the strength properties of the concrete. However, since the number of buildings is very high, the cost of determining the strength of the concrete is greatly increasing. In addition, a considerable amount of time is lost. It is critical to determine the concrete strength quick and reliable so that urban regeneration projects continue economically and rapidly.

Many standard NDT methods, such as UPV, rebound hammer, and penetration tests, are presently used to estimate the strength of the concrete. In this paper, the most preferred standard NDT methods are evaluated in terms of cost, reliability and practicality, and a feasibility analysis is carried out considering carefully requirements and expectations. The purpose of this study by the feasibility analysis is to provide the possibility of comparing the NDT methods for the researchers and engineers. So, they will be able to determine the most effective method for their projects at the earliest convenience. Consequently, a practical graphic-based method is proposed to choose the NDT methods to be used in urban regeneration projects.

2. NDT Methods

There are many NDT techniques used to determine the concrete strength. The most known of these can be listed as follows:

- Rebound Number (Schmidt Hammer Test) [12, 13]
- Ultrasonic Pulse Velocity [12, 14]
- Penetration Resistance (Probe and Pin Tests) [12, 15]
- Pullout Test [12, 16]
- Break-off Number [12, 17]
- Maturity Method [12, 18]
- Cast-in-place Cylinders [12, 19]
- PNT-G Test [20]
- Drilling Resistance [21]
- Nail Penetration [22]
- Twist-off Test [23]

For the feasibility analysis, the NDT methods just used in the standard, current, and for existing buildings have been taken into consideration, and their characteristics have been clearly presented.

2.1. Rebound number test

The rebound number test is technically a test for surface hardness, and it approximately provides for establishing relationship between the rebound hammer number and the compressive strength of concrete. The Rebound Hammer has been around since the late 1940s and today is a commonly utilized method for estimating the in-place compressive strength of

the concrete. Basic operation of the rebound hammer test is illustrated in Fig. 1. Schmidt Hammer is usually used for this test [24].

The tests can be carried out in horizontal, vertically upward, downward or any intermediate angled positions. The rebound hummer is simple to use, and a large number of readings may be obtained in a relatively minimum amount of time. This method is non-destructive and characteristically more economical than other NDT methods. However, with these advantages come disadvantages related to technical limitations on accuracy, and the need for exact calibration and correlation with cores for assessment of an existing structure [25]. The surface texture, moisture content, and carbonation significantly affect the rebound (R) number of the tests.

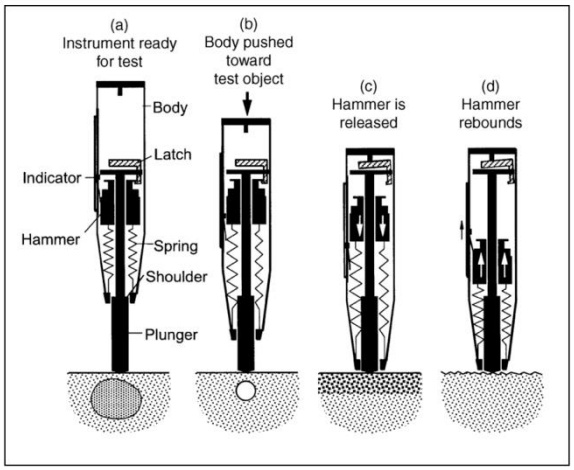

Figure 1. Operation of the rebound hammer as schematic [12].

The advantages and limitations of the rebound hammer test should be recognized and figured on if the rebound hammer will be used for a large-scale project about existing buildings.

2.2. Ultrasonic Pulse Velocity (UPV) Test

Pulses of the waves are produced by an acoustical transducer that is kept in contact with one surface of the concrete under evaluation. After traversing through the concrete, the pulses are gotten and altered into electrical energy by a second transducer placed a distance (L) from the transmitting transducer. The transit time (T) is directly measured electronically. The pulse velocity (V) is calculated by dividing L by T. The operational principle of modern testing equipment is illustrated in Fig. 2 [14].

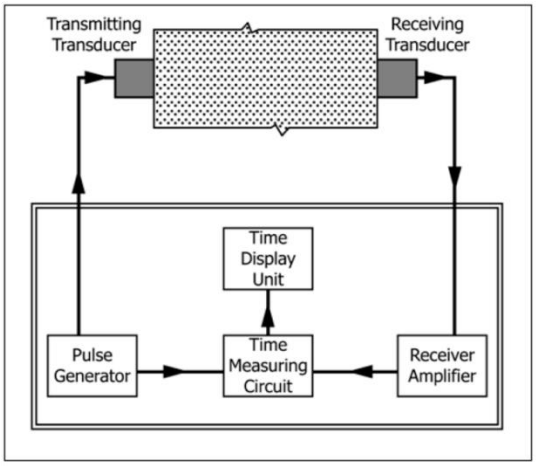

Figure 2. Schematic diagram of the pulse velocity test [14].

UPV can be utilized for the following properties [26]:

- Estimation of the relationship between the strength and the pulse velocity.
- Estimation of uniformity of the concrete.
- Assessment of alters obtaining with time in the common properties of the concrete.

There are three possible configurations where the transducers can be settled as illustrated in Fig. 3. These are direct transmission (Fig. 4a), semi-direct transmission (Fig. 4b), and indirect (surface) transmission (Fig. 4c). Indirect transmission should be used when only one face of the concrete is available. These configurations provide significant advantages for estimation of the in-place strength of the concrete [25].

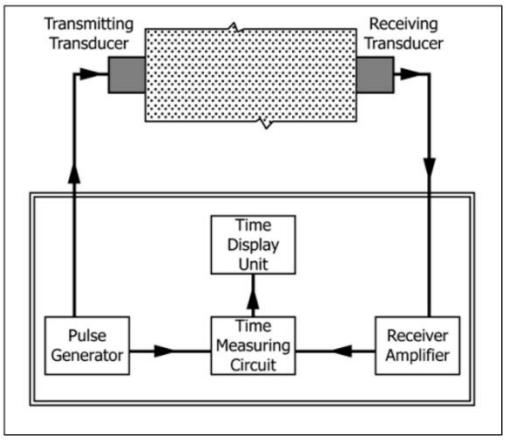

Figure 3. Configration of the UPV test application [25].

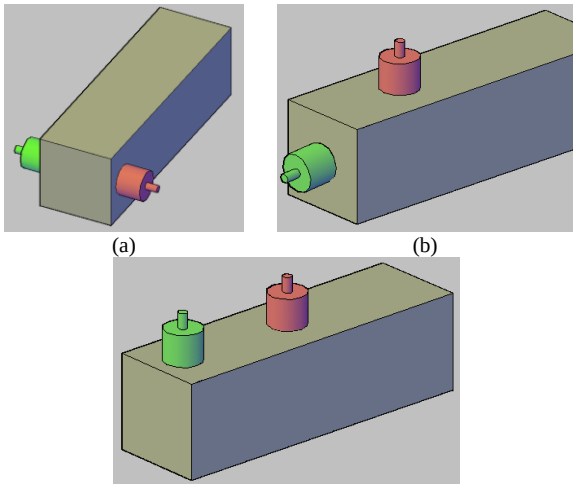

Figure 4. a) Direct transmission, b) semi-direct transmission, and c) indirect (surface) transmission

UPV method adequately provides the examination of relationship between the compressive strength and the pulse velocity of the sample, but the test results of UPV are affected by moisture content, properties of aggregates, cracks, voids. The usability of UPV test is much more limited to predict the compressive strength of concrete, mainly owing to steel reinforcement bars in concrete because the pulse velocity through steel is about 40% greater than through concrete. These limitations should be considered before preferred the UPV method [27, 28].

2.3. Pin Penetration Test

Nasser and Al-Manaseer described an NDT in which a new production hammer that forces a steel pin into the concrete is used to estimate the when it is safe to remove the concrete forms [29]. The apparatus occurs a spring-loaded hammer which may follow a pin of 3.56mm diameter and 30.5mm length with the tip machined [15].

The spring is forced by pressing the hammer against the surface of the concrete, and is released by a trigger causing the pin and the attached shaft and hammer to strike the surface of the concrete with energy of about 108 Nm. After cleaning, the hole depth generated is measured with a dial gauge device (Fig. 5) [28]. There is an acceptable correlation between the pin penetration and the compressive strength of the concrete. Pin penetration (depth of the blind hole in the concrete element) test which requires less energy than the Windsor probe test. The pin test, although easy in concept, has technical disadvantages. The pin penetrates only a small depth into the concrete, and thus, the results can be seriously infected by the properties of the concrete at the surface.

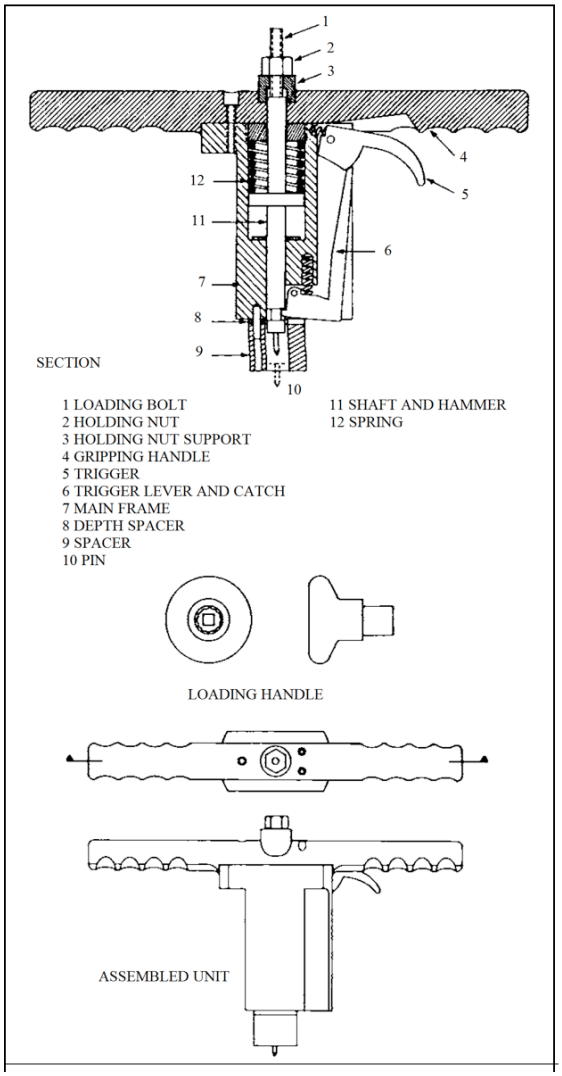

Figure 5. Configuration of the pin penetration test application [29].

2.4. Windsor Probe Test

The probe-penetration technique requires the use of a specially designed gun to run the steel probe into the concrete [15]. (This test system is commonly known as the Windsor Probe Test, as seen in Fig. 6).

Figure 6. Windsor Probe Test equipments.

The Windsor probe test, like the rebound hammer test, is a hardness tester, and its inventors maintain that the penetration of the probe shows the exact compressive strength in a localized area is not certainly true [30]. Nevertheless, the probe penetration does refer to the some property of the concrete, so it has been possible to improve empirical correlations between the compressive strength and the probe penetration [25]. Schematically, failure of the concrete during Windsor probe penetration test is illustrated in Fig 7.

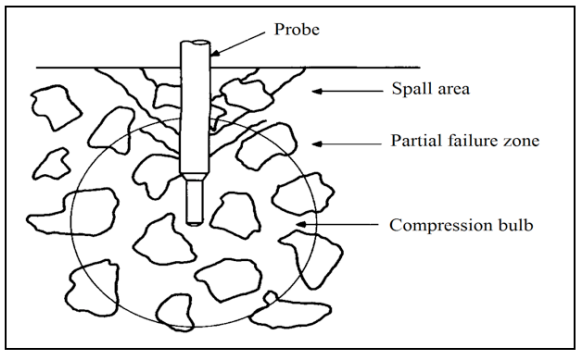

Figure 7. Failure of the concrete during Windsor test schematically [28].

The advantages of the Windsor probe test are [25, 28, 31]:

- The test is adequately fast, and the result is obtained immediately provided an appropriate curve with good correlation is ready for use.
- The correlation with the concrete compressive strength is changed by a relatively small number of variables.
- Application is only required to one surface.

The limitations of the Windsor probe test are [25, 28, 31]:

- The test damages an about 8 mm blind hole in the sample in which the probe penetrated and, in elder concrete, this zone around the point of the penetration is usually broken.
- The least distance from a test location to any edges of the concrete sample or between two tests location is of the order of 150 mm to 200 mm.
- The distance from reinforcement can also be affected the depth of the penetration, especially if the distance is less than about 100 mm.
- The least thickness of the sample, that can be tested, is about three times the estimated depth of steel probe penetration.
- The costs of the operations are really high.

Although the PR method has some advantages, it is particularly sensitive to characteristics of aggregate and minimum member thickness, which can be tested. The advantages and limitations of the Windsor probe test should be recognized and taken into account if this test will be utilized for the existing buildings.

3. Urban Regeneration and the In-Place Test

Turkey connects the tectonic plates that are including the Eurasian, Arabian, and African and the Anatolian plates [32] and Turkey has a high seismic activity because of its location. Many destructive earthquakes occurred in the past two decades in Turkey and the social and economic damages were really huge [33]. So, Turkey is really important model to evaluate for the urban regeneration.

The Turkish earthquake knowledge and data regarding urban projects are seriously little and limited. In urban areas, risks related not only community services and infrastructure but also housing [34]. Erzincan earthquake which occurred in 1992 supplied valuable data to understand the dangerous of the building stock which has not been enough earthquake resistance. However, unfortunately, this experience was not enough to protect from the

disasters which were occurred in Kocaeli (1999), Bingol (2003), Van (2011) et al [7].

Critical amount of Turkey's building stock does not comply with either the design codes or standards, and specifications that were efficient at the time of their built, or the ever more stringent modern design code applied today. It is not practicable to perform reliable estimates of seismic losses due to aforementioned complexities. However, researches based on the scenario earthquakes possible to Istanbul harshly predict 30.000 – 40.000 heavily damaged structures and eleven billion in direct losses due to damage to buildings [33]. The building stock which has low earthquake resistance is a very serious problem threatening many countries like Turkey. To solve this problem, governments are trying to produce efficient urban generation projects.

Urban regeneration is a first step in the rebuilding of a part of the cities, and that it has been designed as a governments-assisted urban regeneration strategy. The origin of the conversation of urban regeneration within the Turkish planning literature was an extension of government programs that were formed by efforts to secure a place in the 1980s world order [35]. Disaster risk resulted from the destructive earthquakes has become the main theme of the urban regeneration in Turkey, especially, in the last decade, and has soon become the primary reason for the application of urban regeneration projects with the Law on the 6306, "Regeneration of Areas under the Risk of Disasters', which was accepted on 16.05.12. This has added to the "legality" of urban regeneration projects that will be implemented all over the country with a quick and public model of rebuilding [36].

One of the most important parts of the existing urban regeneration projects is to determine earthquake risk levels of the buildings. When the risk levels of the buildings are determined, one of the basic steps is estimation of the compressive strength of the concrete. Determination of the strength of the concrete by just using the core drilling method is expensive, difficult and time-consuming. Therefore, as far as possible, the destructive methods should be used as minimum and NDT methods usually should be used. Even so, it is not easy to select the most suitable one/more from many NDT methods. Accordingly, in this study, a feasibility analysis was carried out for NDT methods in line with the urban regeneration requirements.

For the urban regeneration projects, estimation of the in-place strength of the concrete is the topic of discussion, because all NDT is unsuitable for determination of the in-place concrete strength. Thus, also any NDT may not be suitable for urban generation projects.

Since the 1900s, there has been an ongoing investigation of the in-place strength of the concrete [37]. Although there are many in-place test methods, very few of them are standard [38, 39]. The standard methods have many advantages such as comparability with the previous works, experience, and easy reachability to the test equipment.

4. Feasibility Analysis of the NDT Methods

Feasibility analyses are originally formed by social scientist. In this study, the feasibility studies made is one of the first examples of its kind, and these methods will hopefully be more commonly performed in the future researches. A feasibility analysis estimates and observes an economic opportunity based on certain theory and estimations that have been put forward in the process of starting a new project [40]. Feasibility analyses aim to decide whether a business opportunity is possible, practical, and workable [41]. A number of the factors are considered and assessed in a feasibility analysis to calculate the most effective results.

Within the framework of urban regeneration projects, to determine the in-place strength of the concrete, priority expectations from the NDT methods are listed below:

- Economy (cost of the operation)
- Time (minimum labor and test time)
- Accuracy (more than 90%, if possible)

The critical issue for the project is that the cost of the operation should be more economical than the cost of the test equipment. The approximate cost of the operations and test equipment are presented in Table 1.

Table 1. Cost information for the NDTs

NDT Methods	Operation Cost ($)	Equipment Cost ($)
Rebound Hammer	Only labor	$300.00

Table 1. Cost information for the NDTs

NDT Methods	Operation Cost ($)	Equipment Cost ($)
UPV	Only labor	$4000.00
Pin Penetration	$10/each	$5000.00
Windsor Probe	$18/each	$5500.00

In order to be able to apply the tests in Table 1, there must be no plaster or coating on the surfaces of the concrete elements. If it is present, it has to be removed from the concrete surface. So, it is assumed that the labor that is for removing the coating will be in equal amounts, $100, for all the tests.

At least three tests should be performed to determine the compressive strength of the concrete. These three tests are accepted as a set. In order to compare NDT methods, a certain number of tests must be taken into account in feasibility analysis. Windsor probe test is taken as reference to determine this numerical value. This value is the test number that makes the cost of the operation equal to the cost of the equipment. The number of the tests = 5500 / 18 ≅ 305.

Two parameters were used for feasibility analysis. The first is based on cost; the second is based on the benefit. The parameters of the analysis are explained in Table 2.

Table 2. Parameters of the feasibility analysis

NDT Methods	CO/CE[a]	T[b]	A[c]	T/A[d]
Rebound Hammer	0.3	3	3	1
UPV	> 0.1	2	2	1
Pin Penetration	0.63	3	2	1
Windsor Probe	1	3	1	3

[a.] CO/CE=(Cost of operation + labor) / cost of the equipment

[b.] T: Application Time (0~15 min: 3, 16~60 min: 2, more than 60 min: 3)

[c.] A: Accuracy (Excellent: 1, Good: 2, Approximate: 3)

[d.] T/A: Time/Accuracy

The rate of CO/CE is developed to consider the cost effect on the choosing of the NDT. The rate of T/A is developed to consider the technical benefit on the selecting of the NDT.

Graphic based feasibility analysis is illustrated in Fig. 8. If it is desired to determine as fast, practical and approximate whether an NDT method is suitable for an urban regeneration project, first, the numerical values of the parameters of this method, CO/CE and T/A, are calculated. And then, these parameters are marked on the graphics, finally; the feasibility region is determined by Fig 8. The RED, YELLOW and GREEN Zones mean the unfeasible, acceptable and feasible NDT methods, respectively.

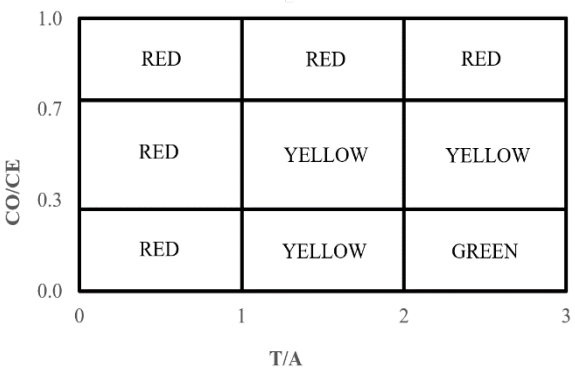

Figure 8. Graphic of the feasibility analysis.

5. Discussion and Results

Graphic based feasibility analysis is performed for the standard NDT methods, and results of the feasibility analysis are given in Table 3.

Table 3. Feasibility result of the NDT method

NDT Methods	Feasibility Zone
Rebound Hammer	YELLOW
UPV	YELLOW
Pin Penetration	YELLOW
Windsor Probe	RED

Rebound hammer, UPV, pin penetration, and Windsor probe tests are in the yellow and red zones, respectively. Existing methods are not feasible but acceptable methods to utilize for the urban regeneration projects. These methods which are in the yellow zone are neither economical nor sufficiently useful. The Windsor probe test is unfeasible because of the cost of the operation. This method is reliable and practical. However, cost of the operation of Windsor Probe test is so high. It is evident how large the economic loss will be, if it is assumed that the test will be used for tens of thousands of buildings in urban regeneration projects.

The proposed method in the current paper is a preliminary and practical method. This feasibility analysis can be used in non-standard NDT methods. However, accuracy must be carefully determined. The most important thing is that these analyses are done by experienced

engineers. If every numerical result passes from the engineer's filter, it gains significant value.

6. Conclusion

Urban regeneration has become a strategy to avoid the earthquake damages in many countries like Turkey. Because the target is building stock, the strength of the concrete, which is the most-used material to produce the buildings needed to be determined. A feasibility analysis was carried out for the methods of determining the in-place concrete strength in this study. Following are some of the important conclusions.

- The number of drilled core specimens should be reduced as much as possible while the concrete strength is determined as the number of buildings in urban regeneration projects is too high. Even if it is possible, reliable results should be tried to be obtained without using destructive methods. It can be economically and quickly carried out.
- The efficiency of an NDT method by the help of the graphic based feasibility method can be evaluated with cost, time and accuracy limiters.
- None of the existing methods are in the green zone when the feasibility analysis performed. This conclusion implies that a new feasible NDT method is required.
- Windsor probe test has high accuracy but not economic. So, it can be used for the specific works.
- None of the existing NDT methods can be applied to surface that has coating. Before the NDT is applied, the coating/plaster must be removed. Therefore, a new NDT is required to test the concrete elements without removing the coating, especially for the urban regeneration projects.

7. References

1.Bikce, M. and Celik, T.B. (2016). Failure analysis of newly constructed RC buildings designed according to 2007 Turkish Seismic Code during the October 23, 2011 Van earthquake. Eng. Fail. Anal., **64**: 67-84.

2.Dogangun, A. (2004). Performance of reinforced concrete buildings during the May 1, 2003 Bingol Earthquake in Turkey. Eng. Struct., **26**(6): 841-856.

3. Norio, O., Ye T., Kajitani, Y., Shi, P.J. and Tatano, H. (2011). The 2011 Eastern Japan Great Earthquake Disaster: Overview and Comments. Int. J. Disaster. R. Sci., **2**(1): 34-42.

4. Saatcioglu, M., Ghobarah, A. and Nistor, I. (2006). Performance of structures in Indonesia during the December 2004 great Sumatra earthquake and Indian Ocean tsunami. Earthq. Spectra., **22**: S295-S319.

5. Sezen, H., Whittaker, A., Elwood, K. and Mosalam, K. (2003). Performance of reinforced concrete buildings during the August 17, 1999 Kocaeli, Turkey earthquake, and seismic design and construction practise in Turkey. Eng. Struct., **25**(1): 103-114.

6. Zhao, B., Taucer, F. and Rossetto, T. (2009). Field investigation on the performance of building structures during the 12 May 2008 Wenchuan earthquake in China. Eng. Struct., **31**(8): 1707-1723.

7. Yon, B., Sayin, E., Calayir, Y., Ulucan, Z.C., Karatas, M., Sahin, H., Alyamac, K.E. and Bildik, A.T. (2015). Lessons learned from recent destructive Van, Turkey earthquakes. Earthquakes and Structures, **9**(2): 431-453.

8. Karaman, O. (2013). Urban Renewal in Istanbul: Reconfigured Spaces, Robotic Lives. Int. J. Urban Regional, **37**(2): 715-733.

9. Anthony, O.S. (1990). Post-Disaster Housing Reconstruction and Social Inequality: A Challenge to Policy and Practice. Disasters, **14**(1): 7-19.

10. Gunay, Z., Koramaz, T.K. and Ozuekren, A.S. (2015). "From Squatter Upgrading to Large-scale Renewal Programmes: Housing Renewal in Turkey," in Renewing Europe's Housing, (Ed) Turkington, R. and Watson, C., Thu University of Chicago Press, 215-243.

11. Alyamac, K. (2014). Earthquake Resistance and Future Planning of the Existing Building Stock in Elazig/TURKEY. The International Congress on Elazig from the Past to the Present. Prime Ministry of Turkish Republic, Ataturk Culture Language and History Higher Institution, Ataturk Research Center. 583-600.

12. ACI_2281r_03 (2003). In-Place Methods to Estimate Concrete Strength. American Concrete Institute: Farmington Hills. p. 44.

13. ASTMC805/C805M−13a. (2014). Standard Test Method for Rebound Number of Hardened Concrete. ASTM International: West Conshohocken. p. 4.

14. ASTMC597-09. (2010). Standard Test Method for Pulse Velocity Through Concrete. ASTM International: West Conshohocken. p. 4.

15. ASTMC803/C803M-03. (2010). Standard Test Method for Penetration Resistance of Hardened Concrete. ASTM International: West Conshohocken. p. 4.

16. ASTMC900-15. (2015). Standard Test Method for Pullout Strength of Hardened Concrete. ASTM International: West Conshohocken. p. 10.
17. ASTMC1150-96. (1996). Standard Test Method for The Break-Off Number of Concrete. ASTM International: West Conshohocken. p. 4.
18. ASTMC1074−11. (2011). Standard Practice for Estimating Concrete Strength by the Maturity Method. ASTM International: West Conshohocken. p. 10.
19. ASTMC873/C873M−15. (2016). Standard Test Method for Compressive Strength of Concrete Cylinders Cast in Place in Cylindrical Molds. ASTM International: West Conshohocken. p. 4.
20. Gucci, N. and Barsotti, R. (1995). A non-destructive technique for the determination of mortar load capacityin situ, Mater. Struct., **28**(5): 276-283.
21. Rodrigues, J.D., Pinto, A.F. and da Costa, D.R. (2002). Tracing of decay profiles and evaluation of stone treatments by means of microdrilling techniques. J. Cult. Herit., **3**(2): 117-125.
22. Selcuk, L., Gokce, H.S., Kayabali, K. and Simsek, O. (2012). A Nondestructive Testing Technique: Nail Penetration Test. ACI Struct. J., **109**(2): 245-252.
23. Naderi, M. (2007). New twist-off method for the evaluation of in-situ strength of concrete. J. Test. Eval., **35**(6): 602-608.
24. Kolek, J. (1958). An appreciation of the Schmidt rebound hammer. Magazine of Concrete Research, **10**(28): 27-36.
25. Malhotra, V.M. and Carino, N.J. (2004). Handbook on Nondestructive Testing of Concrete. CRC Press.
26. Panzera, T.H., Christoforo, A.L., Cota, F.P., Borges, P.H.R. and R.B.C. (2011). "Advances in Composite Materials–Analysis of Natural and Man-Made Materials, chapter 17," in Ultrasonic Pulse Velocity Evaluation of Cementitious Materials. InTech.
27. Yaman, I.O., Inci, G., Yesiller, N. and Aktan, H.M. (2001). Ultrasonic pulse velocity in concrete using direct and indirect transmission. ACI Materials Journal, **98**(6): 450.
28. Hellier, C.J. (2003). Handbook of Nondestructive Evaluation. The McGraw-Hill Companies, Inc.
29. Nasser, K. and Al-Manaseer, A. (1987). New non-destructive test. Concrete International, **9**(1): 41-44.
30. Malhotra, V. (1974). Evaluation of the Windsor probe test for estimating compressive strength of concrete. Matériaux et Construction, **7**(1): 3-15.
31. Bin Ibrahim, A., Bin Ismail, P., Forde, M., Gilmour, R., Kato, K., Khan, A., Ooka, N., Siong, S., Terada, K. and Wiggenhauser, H. (2002). "Guidebook on non-destructive testing of concrete structures. International Atomic Energy.
32. Bommer, J., Spence, R., Erdik, M., Tabuchi, S., Aydinoglu, N., Booth, E., Del Re, D. and Peterken, O. (2002). Development of an earthquake loss model for Turkish catastrophe insurance. Journal of Seismology, **6**(3): 431-446.
33. Gunes, O. (2015). Turkey's grand challenge: Disaster-proof building inventory within 20 years. Case Studies in Construction Materials, **2**: 18-34.
34. Erdik, M. (1994). "Developing a comprehensive earthquake disaster masterplan for Istanbul," in Issues in Urban Earthquake Risk. Springer. 125-166.
35. Güzey, Ö. (2009). Urban regeneration and increased competitive power: Ankara in an era of globalization. Cities, **26**(1): 27-37.
36. Güzey, Ö. (2016). The last round in restructuring the city: Urban regeneration becomes a state policy of disaster prevention in Turkey. Cities, **50**: 40-53.
37. Jones, R. (1949). The non-destructive testing of concrete*. Magazine of Concrete Research, **1**(2): 67-78.
38. McCann, D. and Forde, M. (2001). Review of NDT methods in the assessment of concrete and masonry structures. NDT&E Int, **34**(2): 71-84.
39. Uomoto, T. (2000). “Non-destructive testing in civil engineering 2000”. Elsevier.
40. Blocher, E.J. (2009). Teaching cost management: A strategic emphasis. Issues in Accounting Education, **24**(1): 1-12.
41. Hassan, A. and Jones, S. (2012). Non-destructive testing of ultra high performance fibre reinforced concrete (UHPFRC): A feasibility study for using ultrasonic and resonant frequency testing techniques. Construction and Building Materials, **35**: 361-367.

Turkish Journal of Science & Technology
Volume 13(1), 19-23, 2018

Determination of Friction Angles Between Soil and Steel – FRP Piles

H. Suha Aksoy[1], Mesut Gör[1*], Esen İnal[2]
[1]Firat University Engineering Faculty Civil Engineering Department, Elazığ, Turkey
[2]Karayolları 8. Bölge Müdürülüğü, Elazığ, Turkey
[*]mgor@firat.edu.tr

(Received: 18.01.2017; Accepted: 01.03.2017)

Abstract

Forces of friction between structure and soil are taken into account in the design of geotechnical engineering constructions such as piles, retaining walls, sheet piles and diaphragm walls. Although many studies were carried out about the soil-structure interaction in recent years. However, in pile design, frictional forces are still calculated by using the empirical formulas proposed in the first half of the 20th century. Throughout history, wood was often used as friction piles. Steel piles are used extensively in practice. Nowadays, in harsh environmental conditions fiber-reinforced polymer (FRP) piles come into use in numerous cases. As is known, the effect of pile point tip resistance on the bearing capacity is ignored particularly in loose sands and the bearing capacity is fully taken equal to the skin friction. Hence, it is understood that correct determination of skin friction angle is very important in engineering calculations. In this study, various ratios of low plasticity clays (CL) were added to the sandy soil and compacted to standard Proctor density. Thus, soils with various internal friction angles were obtained. By performing interface shear tests (IST), skin friction angles of these soils with steel (st37) and FRP were determined. Based on the data obtained from the test results, a chart was proposed, which engineers can use in pile design. By means of this chart, the skin friction angles of the soils, of which only the internal friction angles are known, with steel and FRP materials can be determined easily.

Keywords: Skin Friction; Design Chart; Pile Materials; Direct Shear Test.

Çelik ve FRP Kazıklar ile Zemin Arasındaki Sürtünme Açısının Belirlenmesi

Özet

Zemin ile yapı elemanları arasındaki sürtünme kuvvetleri temel mühendisliği açısından hayati öneme sahiptir. Son yıllarda zemin-yapı etkileşimi konusunda çok sayıda çalışma yapılıyor olsa da sürtünme kuvvetlerinin belirlenmesi için hala 20. yüzyılın ilk yarısında önerilen yaklaşık bağıntılar kullanılmaktadır. Tarih boyunca sürtünme kazığı olarak genellikle ahşap kullanılmıştır. Son yüzyılda ise çelik kullanılmaya başlanmıştır. Günümüzde ise bu malzemelere alternatif olarak özellikle olumsuz çevre koşullarında uzun yıllar hizmet edebilmesi nedeniyle FRP (fiber-reinforced polymer) kazıklar yoğun şekilde kullanılmaktadır. Bilindiği gibi özellikle gevşek kumlu zeminlerde kazık uç direncinin taşıma gücüne etkisi ihmal edilmekte ve taşıma gücü tamamen yüzey sürtünmesine eşit alınmaktadır. Buradan, mühendislik hesaplamalarında yoğun bir şekilde kullanılan yüzey sürtünme açısının doğru olarak belirlenmesinin ne kadar önemli olduğu anlaşılmaktadır.
Bu çalışmada, kum zemine farklı oranlarda düşük plastisiteli kil (CL) eklenmiş ve Proctor sıkılığında sıkıştırılmıştır. Bu sayede farklı içsel sürtünme açılarına sahip zeminler elde edilmiştir. Bu zeminlerin, çelik (st37) ve FRP malzemeleri ile yaptıkları yüzey sürtünme açıları belirlenmiştir. Deney sonuçlarından elde edilen verilerden yola çıkarak mühendislerin kazık tasarımında kullanabileceği bir abak önerilmiştir. Bu abak sayesinde sadece içsel sürtünme açısı bilinen zeminlerin çelik ve FRP malzemeleriyle yaptıkları yüzey sürtünme açıları kolaylıkla belirlenebilmektedir.

Anahtar Kelimeler: Yüzey Sürtünmesi; Tasarım Kartı; Kazık Malzemeleri; Direkt Kesme Deneyi.

1. Introduction

Skin friction angle between soil and pile materials emerges as an important component in the designs made by geotechnical engineers. Frictional forces between structure and soil are taken into consideration in the design of civil engineering constructions such as retaining walls, sheet piles, diaphragm walls and piles. As is known, the effect of pile point tip resistance on the bearing capacity is ignored particularly in loose sand soils and the bearing capacity is fully taken equal to the skin friction. Hence, it is understood that correct determination of skin friction angle is very important in geotechnical design.

Many geotechnical engineers consider the skin friction angle (δ) as equal to 2/3 of the internal friction angle (ϕ) of soil in their designs [1]. However, it is known that δ can change in the event of frictions between the same soil and different materials. Even today, skin friction angles (δ) between soil and pile materials are not exactly known and design engineers use approximate values. δ values used in designs are of essential in the determination of pile number, diameter and length. A low δ value leads making non-economic designs and increases project costs substantially. On the other hand, a high δ value causes to safety problems.

Wood was used as a driven pile material up to the first half of the 20th century. However, the use of wood declined almost non-existing in today due to increasing costs. Nowadays, steel is commonly used as the driven pile material. Plastic composite materials have also been started to be used in recent years as alternative to steel. Today, FRP (fiber-reinforced polymer) material is ever-increasingly used due to the reasons such as being economic, having high tensile and compressive strengths and its resistance to harsh environmental conditions.

Potyondy (1961) conducted interface shear tests (IST) on the soils prepared in four sand/clay ratios and determined the skin friction angles of wood, steel and concrete materials. When examine the IST results, it is seen that the critical value for the cohesion is the situation where sand/clay ratio is 1. The cohesion rises quickly in all values over this ratio [2]. Uesugi and Kishida (1986) determined the friction between mild steel and dry sand by using IST. They found that the type and mean grain diameter of sand (D_{50}) had significant effects on friction angle [3]. There are many studies where the frictions between geosynthetics and sands were analyzed thorough IST [4, 5, 6, 7]. When articles in the literature are examined, it is generally seen that the frictions of clean sands (without fine-grained soils) and pile material surfaces were determined [6, 8, 9, 10]. However, clean sands are hardly seen in nature. Therefore, mixing various ratios of sand and clay soils will allow more realistic results to be obtained in the in laboratory of the soils encountered in the field [11].

Clayey sand soils containing various ratios (0%, 20%, 30%, 40% and 45%) of clay were used in laboratory tests. The produced soils have different internal friction angles, skin friction angles between the soils and pile materials (steel and FRP) were obtained. As a result of the laboratory studies, a chart was proposed, which shows the relationship between the internal and skin friction angles. By means of this chart, the skin friction angles between soil and pile materials can be obtained based only on the internal friction angles of soils.

2. Material and Method

The index properties of the sand and low plasticity clay (CL) soil used in the tests were determined and given in Table 1. Black basalt originated river sand (specific gravity 2.77) used in the tests. The sieve analyses, Atterberg limits tests and specific gravity tests were conducted according to standards [12, 13, 14]. Sieve analysis of sand and clay soils can be seen in Figure 1.

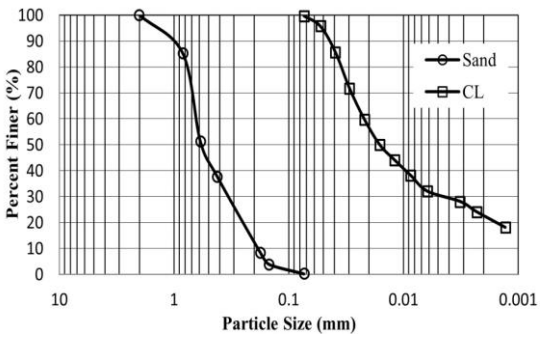

Figure 1. Grain size distribution of soils.

CL at the ratios of 0%, 20%, 30%, 40% and 45% in weight were mixed in the sand and optimum water contents (w_{opt}) were determined by performing standard Proctor tests on these mixtures [15]. w_{opt} values and soil classifications according to Unified Soil Classification System (USCS) are shown for each mixture in Table 2. The mechanical properties of the steel and FRP materials used in the tests are shown in Table 3.

Table 1. Index properties of soils.

	Sand	**CL**
D_{30} (mm)	0. 33	0.0045
D_{50} (mm)	0.57	0.016
Liquid Limit, W_L (%)	-	30
Plastic Limit, W_P (%)	-	15
Specific Gravity, γ_s	2.77	2.68

Table 2. Mixing ratios and optimum moisture content.

Mixture	**Clay (%)**	**Sand (%)**	**Soil Group (USCS)**	w_{opt} **(%)**
m_0	0	100	SP	6.0
m_{20}	20	80	SC	9.0
m_{30}	30	70	SC	10.0
m_{40}	40	60	SC	11.5
m_{45}	45	55	SC	13.0

Table 3. Properties of pile materials.

	Steel (st37)	**FRP (50% glass)**
Compression strength (Mpa)	240	200
Tensile strength (Mpa)	360	240
Tensile Elasticity Modulus (Gpa)	210	23
Density (gr/cm^3)	7.85	1.8

The direct shear test (DST) was performed to obtain the internal friction angles (ϕ) of the soil mixtures [16]. Interface shear tests (IST) were conducted in order to determine the skin friction angles (δ) between the produced soil samples and steel, FRP [17]. Test setups can be seen in Figure. 2. and Figure 3. DST and IST tests were performed at a rate of 0.5 mm/min horizontal displacement. Samples prepared at the standard Proctor density and optimum water content were used in DST and IST tests and the results obtained from the tests can be seen in Table 4.

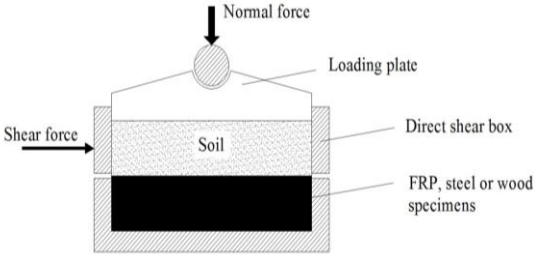

Figure 2. Sketch of interface shear test setup.

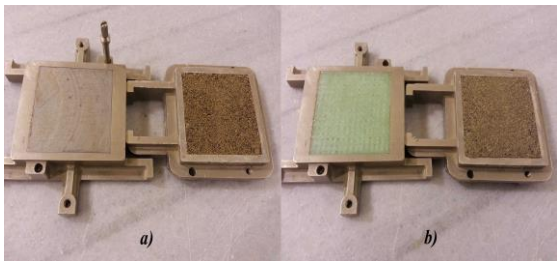

Figure 3. Interface shear test setup; a) IST (steel soil) b) IST (FRP-soil).

Table 4. Direct shear test (DST) and interface shear test (IST) results.

Mixture	**Internal friction angle of soil, ϕ (°)**	**Skin friction angle, δ (°)**	
		Steel	**FRP**
m_0	43.0	26.5	34.5
m_{20}	39.5	31.5	37.0
m_{30}	41.5	29.2	36.0
m_{40}	35.0	27.0	32.0
m_{45}	28.0	18.0	22.7

Even today, in most projects, skin friction angle is calculated by using $\delta=2\phi/3$ equation. But every material have different skin friction angle with soils [11]. Especially for FRP this equation gives significantly lower δ values than test results. For example, for $\phi=35°$ it is calculated that δ =23.3°. This δ value obtained from IST tests for FRP as 32.0°. Therefore, as skin friction angle assumed lower values causes increase in number, diameter and depth of piles. Consequently non-economical designs can be made by using this equation.

3. Skin Friction Chart

The results determined from the tests and then analyzed. A skin friction chart was proposed to be used in pile design (Figure 4.).

Thanks to this chart, geotechnical engineers will be able to obtain the skin friction angles between the soil and pile materials based on the internal friction angle of soil in the field.

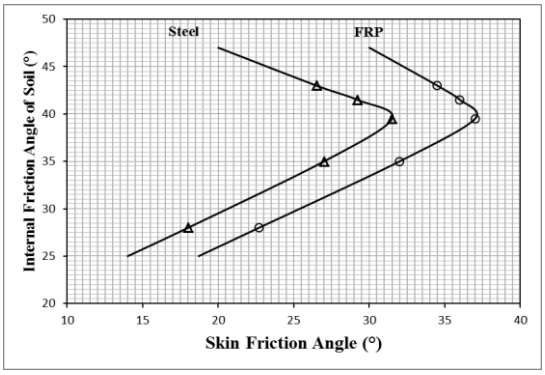

Figure 4. Skin friction chart for steel and FRP.

4. Literature Review with Cases

The results determined through the chart and the studies conducted in the past are shown in Table 5. When the table is examined, it is seen that the δ values obtained through the proposed chart and the values determined in the study performed by Potyondy (1961) show nearly 100% similarity for steel [2]. When results of the chart and the study of Pando et al. (2002) are compared, it is seen that the δ values obtained for FRP material show approximately 90% of similarity [18]. When the results of the chart are compared with the study of Sakr et al. (2005), the δ values show 91% similarity for steel and 94% for FRP material [8]. And when the results of the chart and the studies of Tiwari et al. (2010) and Tiwari and Al-Adhadh (2014) are compared, it is seen that δ values show approximately 90% similarity for steel [10, 19].

Consequently, when δ values obtained from the chart and the studies conducted in the past are compared, these values show similarity more than 90%. The small differences around 10% are considered to arise from types of pile materials (steel hardness and FRP types) used in the tests and the use of dry sand in most studies.

Table 5. Comparison between chart and other studies

Soil (ϕ) (°)	Potyondy (1961), δ (°)		Pando *et al.* (2002), δ (°)		Sakr *et al.* (2005), δ (°)		Tiwari *et al.* (2010), δ (°)	Tiwari and Al-Adhadh (2014), δ (°)		Skin Friction Chart δ (°)		Similarities between Literature and Skin Friction Chart (%)	
	Steel	FRP	Steel	FRP	Steel	FRP	Steel	Steel	FRP	Steel	FRP	Steel	FRP
31.0	-		-	-	24.4	-	-	21.7	26.7	89	-		
31.4	-	-	-	-	-	26.1	22.4	27.4	86	-			
33.1	-	-	-	-	27.6	-	24.6	29.7	89	-			
33.3	-	-	-	-	28.5	-	24.9	29.8	87	-			
33.4	-	-	-	-	-	27.4	25.1	30.0	92	-			
34.7	-	29.2	-	-	-	-	26.6	31.4	-	93			
37.0	-	-	26.6	32.3	-	-	29.1	34.2	91	94			
40.0	31.5	-	-	-	-	-	31.2	37.0	99	-			
43.4	-	29.5	-	-	-	-	25.8	33.9	-	87			
44.5	24.2	-	-	-	-	-	24.3	32.8	100	-			

5. Conclusions

The use of different pile materials, significantly changes the angle of skin friction (δ). Diameter, length and number of piles are considerably affected from these changes.

- IST were performed on the interfaces between soils and pile materials (steel and FRP). The skin friction angles between these materials and various soils were determined.
- In laboratory studies, soils with internal friction angles ranging between 28° and 43° were used.
- When the results determined from the tests and then analyzed, a chart is proposed which allows acquiring the angle of skin friction to take place between soil, the internal friction angle of which is known, and various pile materials.
- Many articles are found in the literature and then these studies were compared with the chart proposed and it was observed conformity over 90% in the δ values determined. Nowadays, design engineers use equations that accept δ

values equal for all pile materials ($\delta=2\phi/3$). This approach prevents make more realistic designs. True skin friction angles (δ) can be determined by means of the proposed chart. Thus, more economic designs can be made by selecting reasonable pile diameter, length and number.

When the internal friction angles (ϕ) of sand-clay mixture soils are examined, it can be seen that ϕ value decreases as the clay percentage increases. However, a slight increase occurred in ϕ in any cases where the clay content is around 30%. These slight increases in the internal friction angles of sand-clay mixtures with the increase of the clay content were observed by Dafalla (2013) and Bayoğlu (1995) as well [20, 21].

6. References

1. Terzaghi, K. & Peck, R.B. (1948). Soil Mechanics in Engineering Practice. *John Wiley and Sons*, N. York.

2. Potyondy, J., G. (1961). Skin friction between various soils and construction materials. *Geotechnique*, 11(4): 339-353.

3. Uesugi, M., Kishida, H. (1986). Influential factors of friction between steel and dry sands. *Soils and Foundations*, 26(2): 33-46.

4. O'Rourke, T., Druschel, S., and Netravali, A. (1990). Shear strength characteristics of sand-polymer interfaces. *J. Geotech. Geoenviron. Eng.*, 116(3): 451-469.

5. Izgin, M. and Wasti, Y. (1998). Geomembrane–sand interface frictional properties as determined by inclined board and shear box tests. *Geotextiles and Geomembranes*, 16(3): 207-219.

6. Frost, J. and Han, J. (1999). Behavior of interfaces between fiber-reinforced polymers and sands. *J. Geotech. Geoenviron. Eng.*, 125(8): 633-640.

7. Palmeira, E. M. (2009). Soil-geosynthetic interaction: modelling and analysis. *Geotextiles and Geomembranes*, 27(5): 368-390.

8. Sakr, M., El Naggar, M., and Nehdi, M. (2005). Interface characteristics and laboratory constructability tests of novel fiber-reinforced polymer/concrete piles. *J. Compos. Constr.*, 9(3): 274-283.

9. Gireesha, N. T., and Muthukkumaran, K. (2011). Study on soil structure interface strength property. *International Journal of Earth Sciences and Engineering*, 4(6) SPL: 89-93.

10. Tiwari, B. and Al-Adhadh, A. R. (2014). Influence of relative density on static soil–structure frictional resistance of dry and saturated sand. *Geotechnical and Geological Engineering*, 32(2): 411-427.

11. Aksoy, H. S.,Gör, M. and İnal E. (2016). A new design chart for estimating friction angle between soil and pile materials. *Geomechanics and Engineering*, 10(3): 315-324.

12. ASTM D422-63(2007)e2 (2007). ASTM International, Standard test method for particle-size analysis of soils, West Conshohocken, PA.

13. ASTM D4318-10e1 (2010). ASTM International, Standard test methods for liquid limit, plastic limit, and plasticity index of soils, West Conshohocken, PA.

14. ASTM D854-14 (2014). ASTM International, Standard test methods for specific gravity of soil solids by water pycnometer, West Conshohocken, PA.

15. ASTM D698-12e1 (2012). ASTM International, Standard test methods for laboratory compaction characteristics of soil using standard effort (12 400 ft-lbf/ft3 (600 kN-m/m3)), West Conshohocken, PA.

16. ASTM D3080 / D3080M-11 (2011). ASTM International, Standard test method for direct shear test of soils under consolidated drained conditions, West Conshohocken, PA.

17. ASTM D5321 / D5321M-14 (2014). ASTM International, Standard test method for determining the shear strength of soil-geosynthetic and geosynthetic-geosynthetic interfaces by direct shear, West Conshohocken, PA.

18. Pando, M., Filz, G., Dove, J. and Hoppe, E. (2002). Interface shear tests on frp composite piles. *Deep Found.*, 1486-1500.

19. Tiwari, B., Ajmera, B., and Kaya, G. (2010). Shear strength reduction at soil structure interface. *GeoFlorida* 2010: 1747-1756.

20. Dafalla, M. A. (2013). Effects of clay and moisture content on direct shear tests for clay-sand mixtures. Advances in Materials Science and Engineering, 2013, Article ID 562726: 1-8.

21. Bayoğlu, E. (1995). Shear strength and compressibility behavior of sand - clay mixtures. *M.Sc. Thesis*, Middle East Technical University, Ankara, Turkey.

Turkish Journal of Science & Technology
Volume 13(1), 25-29, 2018

Implementation of Two Cell Non-Autonomous CNN Model on FPGA

Bariş Karakaya*, Vedat Çelik, Arif Gülten
Fırat University, Electrical – Electronics Engineering, Faculty of Engineering, 23119 Elazig, Turkey
*bkarakaya@firat.edu.tr

(Received: 05.01.2017; Accepted: 27.02.2017)

Abstract

This paper presents implementation of a chaotic Cellular Neural Network (CNN) on Field Programmable Gate Array (FPGA). The network has two non-autonomous cells and exhibits chaotic behavior. In the implementation stage, Verilog Hardware Description Language (HDL) is used and discrete time model of the network is coded on Xilinx ISE Design Suite 13.2. It seems that the chaotic attractor can be used as entropy source or short key (seed) of chaos based random number generator design.

Keywords: Cellular Neural Network, Chaos, FPGA, Random Number Generator.

İki Hücreli Özerk Olmayan HYSA Modelinin FPGA'da Gerçeklenmesi

Özet

Bu çalışma, kaotik bir Hücresel Yapay Sinir Ağı'nın (HYSA) Alanda Programlanabilir Kapı Dizileri'nde (FPGA) gerçeklenmesini sunmaktadır. Ağ, özerk olmayan iki hücreye sahiptir ve kaotik davranış sergilemektedir. Gerçekleme aşamasında, Verilog Donanım Tanımlama Dili kullanılmakta ve ağın ayrık zamanlı modeli Xilinx ISE Design Suite 13.2'de kodlanmaktadır. Görülmektedir ki kaotik çeker, kaos tabanlı rasgele sayı üreteci tasarımında entropi kaynağı veya tohum olarak kullanılabilir.

Anahtar Kelimeler: Hücresel Yapay Sinir Ağı, Kaos, FPGA, Rasgele Sayı Üreteci.

1. Introduction

Chaos can be defined as unpredictable behaviors that are sensitive to initial conditions in a nonlinear deterministic system [1]. As chaotic behavior can be undesirable in some applications, there are a lot of application areas which use the chaotic behavior in their structures. In [2], the use of the Field Programmable Gate Array (FPGA) as a controller of a DC-DC boost converter, controlling the output current of a photovoltaic cells and minimizing the effect of the boost converter chaotic behavior on the output voltage are discussed. Micro controllers, Digital Signal Processors (DSP) and FPGAs can be used to design implementations of chaotic systems [3-6]. FPGA realizations of chaotic systems are studied in [7, 8] by using Euler algorithm with both integer arithmetic and floating-point number format. Especially, the Lorenz's chaotic system is implemented onto a FPGA with the help of the fourth order Runge-Kutta (RK4) algorithm in [9]. The chaotic behavior can be used in Random Number Generator (RNG) applications in order to generate exactly true random number series which are required for secure communication systems. In literature, the realizations of chaotic systems are proposed by using the Xilinx System Generator technology in order to have the HDL code. In [10], the Lorenz's chaotic system is implemented onto FPGA to obtain chaotic sequence for information security issue and in this design the Xilinx System Generator technology is also used. As Cellular Neural Network (CNN) proposed by Chua [11, 12] has complex dynamics, chaotic behavior can occur in the CNN structures [13]. In this paper, a chaotic attractor is observed with two non-autonomous cell CNN using opposite-sign template. This network is reported in [14] and solved with Runge-Kutta iterative solution method.

In recent years, many chaotic CNN applications are implemented on the FPGA. Main advantage of the usage of the FPGA is that it can be programmed with more flexibility during implementation of design. Furthermore,

development of any design on FPGA is easier and faster than other microprocessors [15]. Implementation of CNN structure on FPGA platform presents all advantages in the meaning of higher operating frequency, minimum resource utilization, reconfigurable systems and more secure applications.

Herewith this introduction, CNN structure and its mathematical model which exhibits chaotic behavior, are presented in Section 2. In Section 3, the implementation of discrete time chaotic CNN model on FPGA platform is also presented. At the end, final section concludes the paper.

2. The Chaotic CNN Structure

The two-cell non-autonomous CNN model given in [14] is described by state equations as follow:

$$\begin{aligned} \dot{x}_1 &= -x_1 + pf(x_1) - sf(x_2) + g(t) \\ \dot{x}_2 &= -x_2 + sf(x_1) + pf(x_2) \end{aligned} \tag{1}$$

$$f(x_i(t)) = \frac{1}{2}\left(|x_i(t)+1| - |x_i(t)-1|\right), \qquad i = 1,2 \tag{2}$$

$$g(t) = A\sin\left(\frac{2\pi t}{T}\right) \tag{3}$$

where $p > 1$, $s > 0$; x_1, x_2 are state variables of each cell and $f(\cdot)$ is an odd piecewise-linear function as defined in Eq. (2). For the CNN parameters $p = 2$, $s = 1.2$, initial condition $x(0) = (0.14, -0.1)$ and a sinusoidal input signal parameters $A = 4.04$ and $T = 4$, the non-autonomous CNN with two-cell given in [14] and chaotic portrait of the system are shown in Fig.1 and Fig.2, respectively.

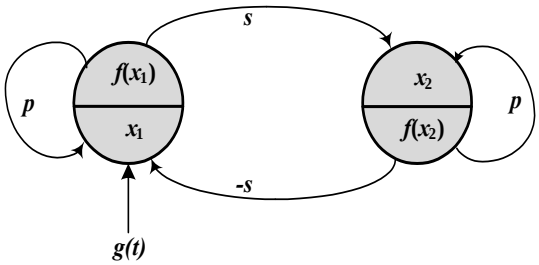

Figure 1. The non-autonomous CNN with two-cell.

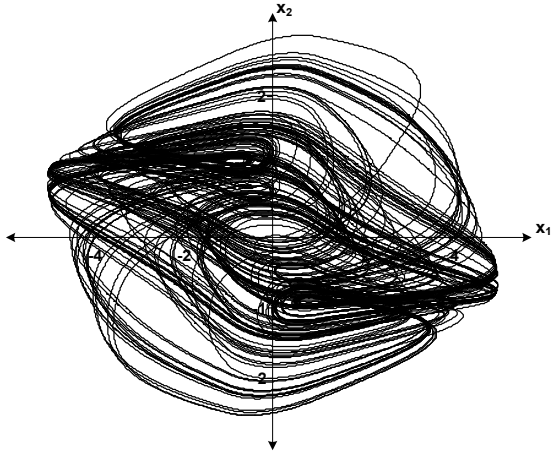

Figure 2. Phase plane portrait of system with initial condition of $x(0) = (0.14, -0.1)$.

In Fig 2, the chaotic behavior is observed. It is clearly appeared that the attractor has a roughly point symmetric property. If the Poincaré map of (x_1, x_2)-plane is obtained, it can be seen that the attractor possesses the horseshoe structure [14].

3. Implementation of Discrete Time Chaotic CNN Model

In order to implement the model on microprocessor, state equations must be discretized. Discrete time model of the CNN based chaotic system is determined as below.

$$\begin{aligned} x_1[n+1] &= \frac{1}{a}\left[\left(\frac{x_1[n]}{T}\right) + pf(x_1[n]) - sf(x_2[n]) + \mathrm{g[n]}\right] \\ x_2[n+1] &= \frac{1}{a}\left[\left(\frac{x_2[n]}{T}\right) + sf(x_1[n]) + pf(x_2[n])\right] \end{aligned} \tag{4}$$

$$f(x_i[n]) = \frac{1}{2}\left(|x_i[n]+1| - |x_i[n]-1|\right), \qquad i = 1,2 \tag{5}$$

$$g[n] = 4.04\sin(\pi n/2) \tag{6}$$

Discrete time response of the model can be acquired by using CNN parameters as $p = 2$, $s = 1.2$, initial conditions $x(0) = (0.14, -0.1)$, $T = 0.005$, $a = 1 + (1/T) = 201$.

In arithmetic operations, fractional numbers are used as well as integers. There are two types of binary number representation format which are floating-point and fixed-point format. Any of

them can be chosen to represent a fractional number as a fractional binary number. A fractional number representation format should be considered that it represents the fractional number as a decimal and then converts it to a fractional binary number by multiplying the decimal number by 0.5 repeatedly. A binary coded number can be defined by equation,

$$...b_2b_1b_0.b_{-1}b_{-2}... = \sum_i b_i x 2^i \quad (7)$$

where there is a binary radix point in the above equation before b_{-1} [16].

In this study, the fixed-point number format is chosen because of advantages on easy coding. In this format, a signed/unsigned number is stored and this number is scaled by a fixed factor which is determined by user with respect to format parameters. This method implies shifting operation the radix point to the left side [16].

Qm.n is the representation of fixed-point number format that has *m* bit for integer part and *n* bit for fractional part as shown in Fig. 3. As we use signed numbers in discrete time model of our network, *Qm.n* format has to be arranged as it contains signed two's complement fixed-point fractional binary number [16].

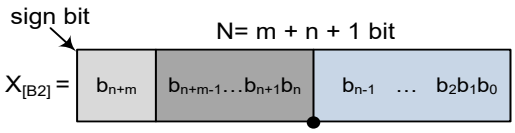

Figure 3. Structure of the *Qm.n* fixed-point signed number format.

Since initial values of state variables and parameters are chosen signed numbers as 16-bits in width, the format is arranged to *Q3.12* and 1 bit is reserved for the sign.

$$x_{[B10]} = \frac{1}{2^n}\left[-2^{N-1}b_{N-1} + \sum_{i=0}^{N-2} 2^i b_i\right] \quad (8)$$

Regarding to equation above (8) where $x_{[B10]}$ represents fractional number in decimal, N = 16, x_{min} = -2^m = -8, x_{max} = 2^m -2^{-n} = 7.99975 and resolution = 2^{-n} = 2.4414.10-3 are determined for *Q3.12* signed two's complement format.

In the implementation stage, three peripheral circuits are used in the CNN core design. These are Clock Generator, CNN Circuit and CNN Cache.

The Clock Generator generates the low frequency clock signal by using the 50 MHz clock signal on FPGA chip. Generated low frequency clock signal is used for iterative solution of model. In FPGA applications, instead of for loop operation, a counter module is arranged in order to calculate the next value of state variables repeatedly. Each increment of counter value is admitted as the beginning of the new loop.

The CNN circuit has two state variables, four parameters for state variables, sampling period register and external sinusoidal input register which are all in 16 bit width. The CNN circuit solves the equations (4), (5) and (6) iteratively by using the clock pulse of the Clock Generator circuit. The model requires previous values of the state variables in order to determine the current values. Therefore, the CNN Cache circuit is used.

The CNN Cache needs 20 KB of total memory in order to emulate the discrete time chaotic CNN model. Since FPGA chip has enough memory in BlockRAM, no external memory is needed. 2 BlockRAM modules are defined for this implementation each one of module has 10 KB capacity. Defined BlockRAM modules have a dual-port interface. Therefore, the values at different addresses can be accessible at the same time.

The CNN core is designed, implemented on Spartan 3e XC3S1600e FPGA development board and programmed by Xilinx ISE Design Suite 13.2. When core is programmed, initial values of state variables and parameters are transferred to the core by using built-in communication interfaces and functions in MATLAB. The whole system is illustrated in Fig.4. Table 1 illustrates resource utilization of the CNN core design.

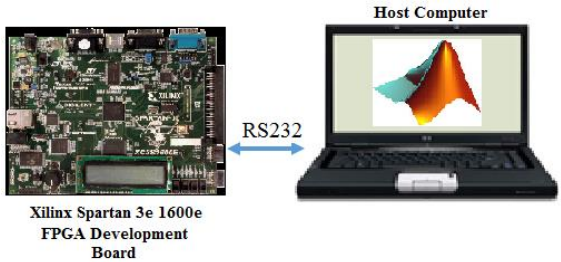

Figure 4. The scheme of the CNN Core Design.

Table 1. Resource utilizations of the design.

Resources	Arithmetic Unit	
	Clock Generator Circuit	CNN Core Design
Used slices	24	4013
Used FFs	33	5214
Used LUTs	47	6589

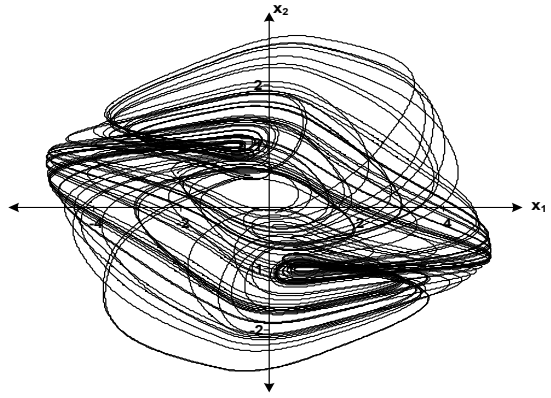

Figure 5. Discrete time response of the model with given parameters.

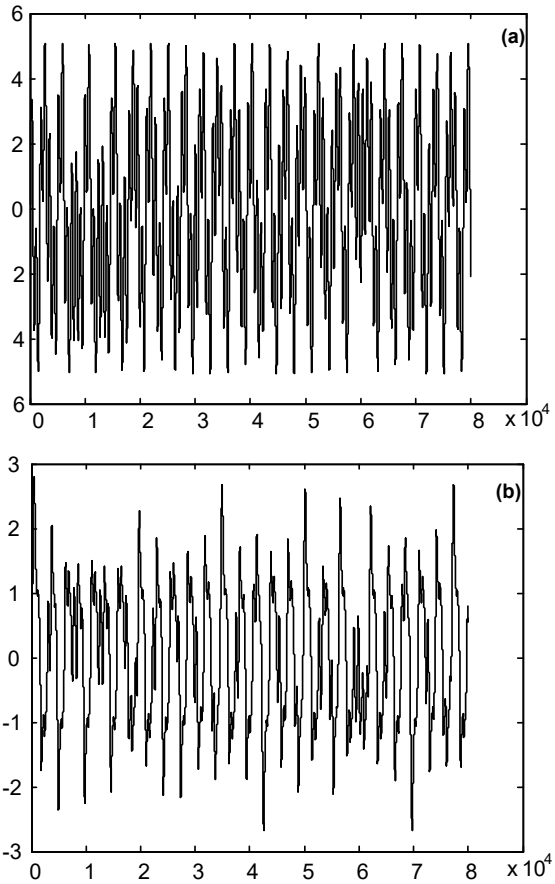

Figure 6. Discrete time response of a) x_1[n], b) x_2[n].

After the whole design is implemented, the programming bit stream of the design is generated and FPGA chip is programmed by Xilinx ISE Design Suite. The maximum operating frequency is obtained as 24.67 MHz from Xilinx ISE Design Suite. Fig. 5 shows the discrete time response of the model, which is very similar to the continuous time response given in Fig. 2. Also, Fig.6 illustrates the discrete time response of each cell. Fig. 5 and Fig. 6 are plotted in MATLAB and the data are obtained from implementation results on Xilinx ISE Design Suite for FPGA of the chaotic discrete time CNN model.

4.Conclusion

In this study, we have presented the implementation of two cell non-autonomous CNN model on FPGA. This study shows that the implemented CNN model have chaotic behaviors and model can be easily adapted to RNG applications using FPGA not only the entropy source of RNG but also the seed of pseudo random number generator application.

5. References

1. Strogatz S.H., Herbert D.F., (1996). Nonlinear dynamics and chaos. Medical Physics-New York-Institute of Physics, **23**(6), 993-995.
2. Natsheh A.N., Al-Habibah E.M.S., (2015). Chaos control DC-DC boost converter by FPGA. *2015 IEEE 42nd Photovoltaic Specialist Conference (PVSC)*, New Orleans, LA, 1-6.
3. Hidalgo R.M., Fernndez J.G., Rivera R.R., Larrondo H.A., (2001). Versatile dsp-based chaotic communication system. Electronic Letters, **37**, 1204–1205.
4. Ali-Pacha A., Said N.H., M'Hamed A., Belgoraf A., (2007). Lorenz's attractor applied to the stream cipher (alipacha generator). Chaos, Solitons and Fractals, **33**(5), 1762-1766.
5. Mazzini G., Setti G., Rovatti R., (1997). Chaotic complex spreading sequences for aynhchronous ds-cdma-part 1: System modeling and results. IEEE Trans. Circuits Sys. 1, **44**(10), 937–947.
6. Setti G., Balestra M., Rovatti R., (2000). Experimental verification of enhanced electromagnetic compatibility in chaotic fm clock signals. in Proceedings of ISCAS'00. IEEE Circuits and Systems Society, III-229–232.
7. Gonz´alez C.M., Larrondo H.A., Gayoso C.A., Arnone L.J., (2003). Generaci´on de secuencias binarias pseudo aleatorias por medio de un mapa ca´otico 3d. in Proceedings del IX Workshop de IBERCHIP.
8. De Micco L., Zabaleta O.G., Gonzlez C.M., Arizmendi C.M., Larrondo H.A., (2010). Estocasticidad de un atractor catico determinista implementado en fpga. Proceedings Iberchip.

9. De Micco L., Larrondo H.A., (2011). FPGA implementation of a chaotic oscillator using RK4 method. *2011 VII Southern Conference on Programmable Logic (SPL)*, Cordoba, 185-190.doi: 10.1109/SPL.2011.5782646.
10. Merah L., Ali-Pacha A., Said N.H., Mamat M., (2013). Design and FPGA implementation of Lorenz chaotic system for information security issues. Applied Mathematical Sciences, **7**(5), 237-246.
11. Chua L.O., Yang L., (1988). Cellular neural networks: Theory. IEEE Trans. Circuits Syst., **35**, 1257-1272.
12. Chua L.O., Yang L., (1988). Cellular neural networks: applications. IEEE Transactions on Circuits and Systems, **35**(10), 1273-1290.
13. Zou F., Nossek J.A., (1993). Bifurcation and chaos in cellular neural networks. IEEE Transactions on Circuits and Systems I: Fundamental Theory and Applications, **40**(3), 166-173.
14. Zou F., Nossek J.A., (1991). A chaotic attractor with cellular neural networks. in *IEEE Transactions on Circuits and Systems*, **38**(7), 811-812.
15. Gerosa A., Bernardini R., Pietri S., (2001). A fully integrated 8-bit, 20MHz, truly random numbers generator, based on a chaotic system. In: Proceedings of the Southwest Symposium on Mixed-Signal Design, SSMSD, 87–92.
16. Karakaya B., Yeniceri R., Yalcin M.E., (2015). Wave computer core using fixed-point arithmetic. 2015 IEEE International Symposium on Circuits and Systems (ISCAS), Lisbon, 1514-1517.

Turkish Journal of Science & Technology
Volume 13(1), 31-36, 2018

Determination of Fracture Paramaters of Effective Crack Model by Wedge-Splitting Test

A. Tevfik Bildik*, Ragıp İnce
Firat University Engineering Faculty Civil Engineering Department Elazığ
*tbildik@firat.edu.tr

(Received: 07.02.2017; Accepted: 17.04.2017)

Abstract

Although the cracked beams have been widely utilized in fracture mechanics of concrete, there have been some advantages of the cubical/cylindrical specimens such as compactness and lightness. In the present work, the wedge-split-tension tests on cubical specimens with different cement contents and water/cement ratios were initially performed for the effective crack model. Finally, some relationships based on regression between the fracture parameters and the strength properties of concrete were derived. The results of the split-tension cube tests look viable and very promising.

Keywords: Concrete; Effective Crack Model; Wedge-splitting Test.

Kama-Yarma Testi ile Efektif Çatlak Modelinin Kırılma Parametrelerinin Belirlenmesi

Özet

Betonun kırılma mekaniğinde genellikle çentikli kiriş numuneler kullanılmakla birlikte küp ve silindir numunelerin de bazı avantajları vardır. Bu çalışmada, çimento miktarları ve su/çimento oranları farklı olan kama-yarma numuneleri efektif çatlak modeline göre teste tabi tutulmuştur. Sonuç olarak betonun kırılma parametreleri ile basınç ve yarma-çekme mukavemetleri arasında bazı regresyon bağıntıları türetilmiştir.

Anahtar Kelimeler: Beton; Efektif Çatlak Modeli; Kama-Yarma Testi.

1. Introduction

Fracture mechanics applications of cement-based materials were initiated by Kaplan [1]. However, in 1970s, experimental investigations on concrete fracture revealed that Linear Elastic Fracture Mechanics (LEFM) has been no longer valid for cementitious materials such as rock and concrete [2]. Because of the existence of a relatively large process zone in front of and around the tip of the main notchs and this inelastic zone is ignored by LEFM, it is inapplicable for concrete. Therefore, several deterministic fracture-mechanics approaches have been developed to describe fracture-dominated failure of concrete structures [3-8].

These models can be categorized as cohesive crack models [3, 4] and effective crack models [5-8]. LEFM uses a single fracture parameter such as the critical strain energy release rate, but these models need at least two experimentally determined fracture parameters to estimate failure of concrete/reinforced concrete structures.

The cracked beam tests have been widely utilized, because they were used in the first LEFM standard test for metals in order to estimate fracture parameters of quasi-brittle materials. Nevertheless, there are some important advantages of cubical/cylindrical specimens as follows [9-13]:

1) They are compact and lighter than notched beams. Therefore they are useful for investigating the size effect.

2) They can be easily cast at the construction site by using the same molds as for strength tests.

3) The self-weight of the specimens can be neglected in the computing of fracture parameters, contrary to cracked beams.

The tests on the cylinder and cube samples in fracture mechanics of concrete can be classified as split-tension tests and wedge-splitting tests.

The wedge-splitting tests have been performed on the cylinder/cube specimens with an edge crack. The wedge-splitting tests are also useful for the effective crack models although they were initially developed for the cohesive crack fracture models [9].

In the present work, the wedge-splitting tests (WST) on cube specimens with different cement contents and water/cement ratios were initially performed for the effective crack fracture model (ECM). Finally, some relationships based on regression between the strength properties and the fracture parameters of concrete were determined.

2. Effective Crack Model (ECM)

The effective notch length a_e in the effective crack model for the fracture of cementitious materials recommended by Nallathambi and Karihaloo [6] is computed from the secant stiffness of the real concrete body at the maximum load. The main idea behind this approach may be emphasized with Figure 1, in which the load and deflection curve of the cracked three-point beam up to maximum load is indicated. When the secant stiffness of the real body is equal to tangent stiffness of the body, of which the notch length is a_e, the fracture toughness achieves its critical value K_{Ic}^e. Consequently, according to the effective crack model, the fracture of cement-based materials is defined by two-parameter: the critical fracture toughness K_{Ic}^e and the effective notch length a_e.

Though the effective notch length is computed from the load and displacement curves by trial and error approach in practice, it can also be calculated by the following regression formula:

$$\frac{a_e}{d} = \gamma_1 \left(\frac{\sigma_u}{E_c}\right)^{\gamma_2} \left(\frac{a_0}{d}\right)^{\gamma_3} \left(1 + \frac{d_{\max}}{d}\right)^{\gamma_4} \qquad (1)$$

in which a_0 is the initial notch length, d is the specimen depth, d_{max} is the maximum aggregate size, the nominal strength $\sigma_u = 6M_u/(bd^2)$, M_u is the maximum moment and γ_1 = 0.088, γ_2 = -0.208, γ_3 = 0.451 and γ_4 = 1.653. When elasticity modulus of cement-based materials E_c is estimated from the separate experiments, these constants are γ_1 = 0.198, γ_2 = -0.131, γ_3 = 0.394 and γ_4 = 0.600 [14]. Nevertheless, elasticity modulus of cementitious materials in Eq. (1) may be determined according to the following expression [15]:

$$E_C = 4730\sqrt{f_c'} \qquad (2)$$

where f_c' is the cylindrical strength for concrete. E_c and f_c' in Eq. (2) are in [MPa]. The critical fracture toughness K_{Ic}^e according to the effective crack model may be determined from Eq. (3):

$$K_{Ic}^e = \sigma_u \sqrt{a_e} Y(\alpha_e = a_e/d) \qquad (3)$$

in which α is the relative notch length (a/d) and $Y(\alpha)$ is the function of geometry for computing the fracture toughness of the notched three-point beam and may be obtained from any fracture mechanics handbook [16].

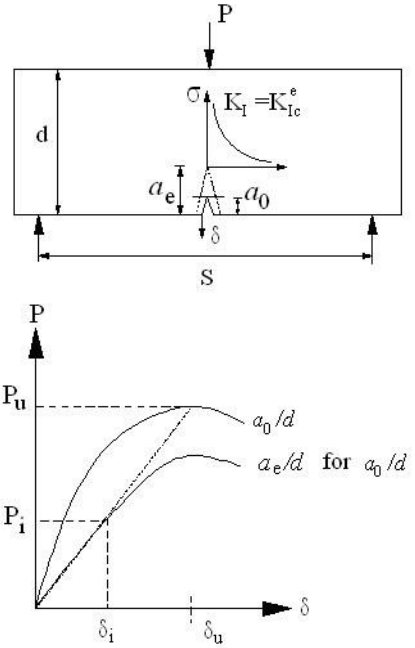

Figure 1. Determination of fracture parameters of concrete according to ECM

3. Wedge-Splitting Test

Although notched-beam specimens have been widely used in concrete fracture mechanics, compact tension (CT) and wedge-splitting (WS) specimens have some advantages over beams,

such as compactness and lightness (Fig. 2). CT specimens were initially used by Wittmann et al. [10] to determine the fracture energy and evaluate the strain-softening behavior of cement-based materials. Brühwiler and Wittmann [9] proposed a popular wedge-splitting test, which has been used in recent years in concrete fracture testing with test specimens.

A WS specimen can be considered a compact form of the three-point bending beam, as shown in Fig. 2b. WS specimens with grooves were developed for use as CT specimens, as shown in Fig. 2c. WS and CT testing can be conducted on both cylindrical and cubical specimens. The use of cylindrical test specimens, which may be obtained from existing concrete/reinforced concrete structures by coring, offers the great advantage of estimating the fracture properties of existing structures based on fracture mechanics. In WS testing, the load is applied to the specimen by means of a wedge and a loading device with roller bearings, as illustrated in Fig. 2d. The horizontal load P_H acts on the rollers because of the vertical load (P_V) on the wedge, as shown in Fig. 2e. Friction forces also occur between the rollers and the wedge. However, the friction forces can be ignored when the wedge angle θ=15°. The horizontal load can be calculated as follows:

$$P_H = \frac{P_V}{2\tan\theta} \qquad (4)$$

For CT and WS test samples, the fracture toughness can be computed as follows:

$$K_I = \frac{P_H}{bd}\sqrt{d}\,Y(\alpha) \qquad (5)$$

where the dimensionless function $Y(\alpha)$ is given by the following equation [16]:

$$Y(\alpha) = \frac{(2+\alpha)\left(0.886+4.64\alpha-13.32\alpha^2+14.72\alpha^3-5.6\alpha^4\right)}{(1-\alpha)^{3/2}} \qquad (6)$$

The accuracy of Eq. (6) is ±0.5 % for α>0.2.

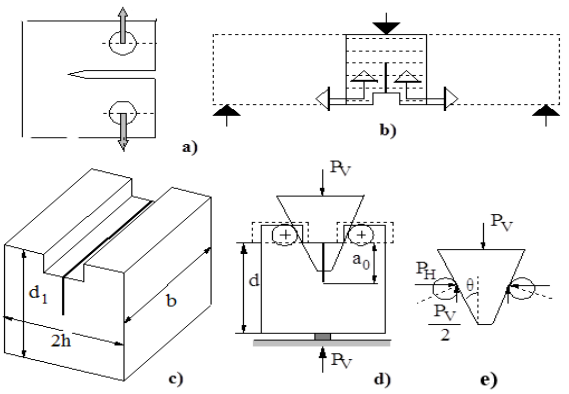

Figure 2. Wedge-splitting test
a) Standard CT specimen **b)** WS specimen as "compact" three-point bending specimen [9] **c)** Specimen configuration **d)** Loading **e)** Wedge forces

4. Experimental Studies

Cubical wedge-splitting (WS) specimens with 150 mm were used in this study (Figure 2). The maximum aggregate diameter of 16mm was used. The cement contents varied from 250 kg/m^3 to 490 kg/m^3 whereas the water-cement ratios (w/c) varied from 0.44 to 0.81. The batches were designed for two slump values=6±1 and 12±2 cm. Eight series specimens (48 cube specimens), namely A, B, C, D, E, F, G and H, were tested concerning the above variables in different combinations. The test specimens in each batches were cast from the same mix of concrete. The cracks were precast in all test samples. The test specimens in all series were of the same size, but they had different notch lengths for each specimen geometry. Table 1 summarizes the cement content, the initial crack length, a_0, the concrete compressive strength, f'_c, and the ultimate vertical load, P_V, of the test specimens.

Three identical cube specimens with 150 mm were also cast from each mix of concrete in order to estimate the compressive strength of concrete. All test specimens and identical test cubes were removed from the mold after 1 day and then were cured at 20 °C in water until testing at 28-day. The compression tests and the split-tension tests were made by using a digital compression machine with a capacity of 100 kN. Typically, approximately 3 min (± 30 sec) elapsed before the peak load capacity for each test specimen was reached. Identical cubes were tested at an age similar to the other specimens.

5. Analysis of Test Results

In this study, WS specimens were analyzed according to ECM. For this, equations 1-6 were utilized. The nominal strength in Eq. (1) may be computed for WS specimens according to the principles of the classical strength of materials as follows:

$$\sigma_u = \frac{P_H}{bd} + \frac{6P_H\, d/2}{bd^2} = \frac{4P_H}{bd} \qquad (7)$$

The computed fracture parameters of concrete based on ECM: the effective fracture toughness and the relative effective notch length values were also given in the last two columns in table 2. It is well known that there is a very strong correlation between f'_c and water-cement ratio. f'_c decreases with increasing w/c. The following formula by Abrams may utilized to stabilize the effects of the factors related to curing conditions, concrete age and cement properties, which directly influence the internal structure of cement-based materials:

$$f_c = \frac{K_1}{K_2^{w/c}} \qquad (8)$$

where K_1 and K_2 are the empirical constant and the constants which depends on the cement properties, respectively [17]. These constants may be computed as $K_1=A$ and $K_2=e^{-C}$ from the regression based on exponential function performed on $Y=AX+C$ with Y=f'_c, X=w/c. Fig. 3 shows the two relation-ships K_{Ic}^e - f'_c and K_{Ic}^e - w/c. The two empirical formulas were derived in this figure. The results indicate that K_{Ic}^e increases with increasing f'_c while K_{Ic}^e decreases with increasing w/c.

Tests have revealed that fracture parameters of cement-based materials are generally influenced by the four material parameters; namely compressive strength, aggregate type, maximum aggregate diameter and water/cement ratio (*w/c*) [11-13, 18-20]. It is noted that fracture parameters of concrete can also be affected by other material parameters such as cement type, aggregate/sand ratio, curing conditions and porosity etc. Therefore, these empirical formulas are approximate and they should only be utilized for preliminary design and for the bodies of low fracture sensitivity although their correlation coefficients are very high r>0.900.

Table 1. Experimental results and analysis results

Series-Slump	Cement kg/m^3	w/c	f'_c MPa	a_0 mm	P_v kN	K_{Ic}^e MPa$\sqrt{m}$	a_e/d
A-12	250	0.81	19.24	50	2.59	0.883	0.523
				50	2.71	0.914	0.520
				80	1.23	0.843	0.695
				80	1.21	0.836	0.696
				95	0.71	0.948	0.799
				95	0.70	0.945	0.800
B-6	250	0.76	22.45	50	2.78	0.949	0.524
				50	2.93	0.988	0.520
				80	1.42	0.944	0.689
				80	1.36	0.922	0.692
				95	0.89	1.056	0.783
				95	0.87	1.051	0.786
C-12	330	0.58	35.56	50	3.37	1.160	0.527
				50	3.65	1.234	0.521
				80	1.68	1.149	0.694
				80	1.68	1.149	0.694
				95	1.01	1.299	0.794
				95	0.90	1.275	0.806
D-6	325	0.56	36.97	50	3.45	1.186	0.526
				50	3.35	1.159	0.528
				80	1.72	1.174	0.694
				80	1.71	1.171	0.694
				95	0.97	1.311	0.800
				95	0.78	1.281	0.823
E-12	410	0.54	44.07	50	3.71	1.280	0.527
				50	3.71	1.280	0.527
				80	1.78	1.247	0.699
				80	1.63	1.193	0.707
				95	0.96	1.412	0.811
				95	0.97	1.413	0.809
F-6	400	0.53	46.63	50	3.60	1.258	0.531
				50	3.64	1.269	0.531
				80	1.82	1.279	0.699
				80	1.83	1.282	0.699
				95	1.00	1.454	0.809
				95	0.99	1.452	0.810
G-12	490	0.45	51.35	50	3.99	1.378	0.528
				50	4.18	1.428	0.524
				80	1.86	1.324	0.702
				80	1.78	1.295	0.706
				95	1.03	1.523	0.811
				95	0.95	1.513	0.820
H-6	480	0.44	54.07	50	3.87	1.353	0.531
				50	4.11	1.418	0.527
				80	1.79	1.316	0.708
				80	1.93	1.366	0.701
				95	1.06	1.563	0.811
				95	0.95	1.550	0.823

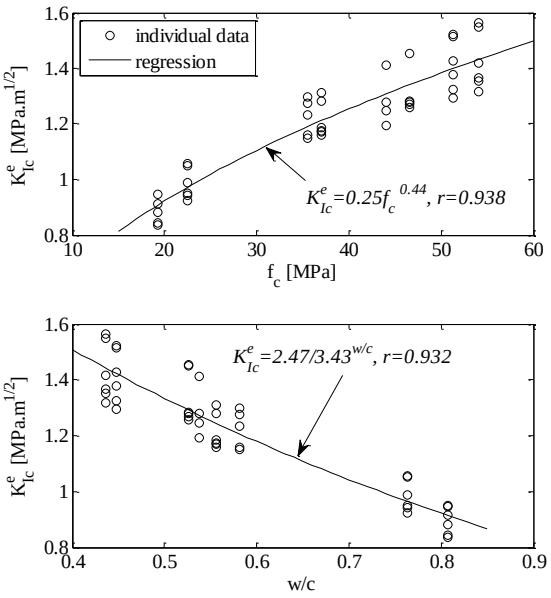

Figure 3. Variation of K^e_{Ic} with f'_c and w/c

6. Conclucions

In recent years, splitting specimens such as compact-tension, wedge-splitting and cylindrical/cubical splitting tension test specimens have been commonly preferred over beams for use in concrete fracture testing. Wedge-splitting test results were used for the first time in this study to determine the fracture parameters of cement-based materials via the effective crack model. The following conclusions should be drawn from the results of this study:

1) Notched compact tension specimens and beams have been used with the effective crack model. The results of this study indicate that the effective crack model can be successfully applied to wedge-splitting specimens.2)Many structural laboratories do not have sophisticated testing equipment such as closed-loop testing systems and displacement-controlled testing machines. The effective crack model offers the great advantage of requiring measurement of only the maximum load applied to specimens to determine the values of the fracture parameters of concrete.

3) The fracture parameters of cementitious materials required for the effective crack model were investigated in this study. Nevertheless, the results obtained may easily be transformed to other fracture models, such as the size effect fracture model, the two-parameter model and the double-K model by the related LEFM formulas.

7. References

1. Kaplan, M.F. (1961). Crack propagation and the fracture of concrete. *ACI J.,* **58(11):** 591-610.

2. Kesler, C.E., Naus, D.J. and Lott, L.L. (1972). Fracture mechanics-its applicability to concrete. *The Soc. of Mater. Sci.,* **4:** 113-124.

3.Hillerborg, A., Modeer, M. and Petersson, P.E. (1976). Analysis of crack formation and crack growth in concrete by means of fracture mechanics and finite elements. *Cem. Conc. Res.*, **6:** 773-782.

4. Bazant, Z.P. and Oh, B.H. (1983). Crack band theory for fracture concrete. *Mater. and Struct. (RILEM),* **16(93):** 155-157.

5. Jenq, Y.S. and Shah, S.P. (1985). Two-parameter fracture model for concrete. *ASCE J. Engng. Mech.,* **111(10):** 1227-1241.

6. Nallathambi, P. and Karihaloo, B.L. (1986). Determination of the specimen size independent fracture toughness of plain concrete. *Mag. Conc. Res.,* **38(135):** 67-76.

7. Bazant, Z.P. and Kazemi, M.T. (1990). Determination of fracture energy, process zone length, and brittleness number from size effect with application to rock and concrete. *Int. J. of Fract.,* **44(2):** 111-131.

8. Xu, S. and Reinhardt, H.W. (1999). Determination of double-K criterion for crack propagation in quasi-brittle fracture, Part II: Analytical evaluating and practical measuring methods for three-point bending notched beams. *Int. J. of Fract.,* **98:** 151-177.

9. Brühwiler, E. and Wittmann, F.H. (1990). The wedge splitting test, a method of performing stable fracture tests. *Engng. Fract. Mech.,* **35:** 117-126.

10. Wittmann, F.H, Rokugo, K., Brühwiler, E., Mihashi, H. and Simonin, P. (1988). Fracture energy and strain softening of concrete as determined by means of compact tension specimens. *Mater. and Struct.,* **21:** 21-32.

11. Ince, R. (2010). Determination of concrete fracture parameters based on two-parameter and size effect models using split-tension cubes. *Engng. Fract. Mech.,* **77:** 2233-2250.

12. Ince, R. (2012). Determination of concrete fracture parameters based on peak-load method with diagonal split-tension cubes. *Engng. Fract. Mech.,* **82:** 100-114.

13. Ince, R. (2012). Determination of the fracture parameters of the Double-K model using weight functions of split-tension specimens. *Engng. Fract. Mech.,* **96:** 416-432.

14. Karihaloo, B.L. and Nallathambi, P. (1989). An improved effective crack model for the determination

of fracture toughness of concrete. *Cem. Conc. Res.*, **19:** 603-610.

15. ACI-318. (2002). Building code requirements for structural concrete and commentary. Farmington Hills, Michigan.

16. Tada, H., Paris, P.C. and Irwin, G.R. (2000). The Stress Analysis of Cracks Handbook. ASME Press.

17. Neville, A.M. (1995). Properties of Concrete. Fourth Edition, Longman, London.

18. Bazant, Z.P. and Becq-Giraudon, E. (2002). Statistical prediction of fracture parameters of concrete and implications for choice of testing standard. *Cem. Conc. Res.*, **32:** 529-556.

19. Ince, R. (2004). Prediction of fracture parameters of concrete by artificial neural networks. *Engng. Fract. Mech.*, **71:** 2143-2159.

20. Ince, R. (2010). Artificial neural network-based analysis of effective crack model in concrete fracture. *Fatigue. Fract. Engng. Mater. Struct.*, **33(9):** 595-606.

Turkish Journal of Science & Technology
Volume 13(1), 37-44, 2018

Investigation of Soft Stories in Buildings with Hollow Block Slab

Ozan Ince[1*], Humeyra Sahin[1], Kursat Esat Alyamac[1], Zulfu Cinar Ulucan[1]
1. Fırat Ünv. Mühendislik Fak. İnşaat Müh. Bölümü, Elazığ
[*]o.ince@firat.edu.tr, ozann.ince@gmail.com

(Received: 21.01.2017; Accepted: 05.04.2017)

Abstract

Hollow block slab is a floor slab system that consists of a thin slab and joists. In hollow block slab system, nonstructural materials are used between joists. Hollow block slab usually consists of wide and shallow beams. Because of low beam height in this system, its lateral stiffness is less than beam floor systems. Because hollow block slab has low lateral stiffness, using of this slab type increases soft-story risk in buildings that have soft-story risk. Therefore, in building with hollow block slab should be detailedly investigated regarding soft-story. For this reason, in this study buildings with stores of 5, 8 and 11, which constructed with hollow block slab were numerically investigated for different ground story height. According to analysis, lateral drift ratios was obtained for each story. As ground story height increased, the lateral drift ratios of ground story with hollow block slab were increased nearly between 33% and 50%. As the number of stories increased, the lateral drift ratios have approached upper limit which is recommended by TEC-2007. The high values of lateral drift ratios in ground stories increase soft-story risk. This situation has a negative effect on building performance under lateral loads. For improving this negative effect shear walls was added to the systems and analysis was repeated. Because shear walls have decreased lateral drift ratios of ground stories nearly between 40% and 60%, negative effect of increment in ground story was decreased. It is agreed on that in high seismic zone, buildings with hollow block slab should be designed as a frame-wall system for better building performance.

Keywords: Hollow block slab, Soft-story, Lateral drift ratio, Reinforced concrete building

Asmolen Döşeme Sistemli Binalarda Yumuşak Kat Düzensizliğinin İncelenmesi

Özet

Asmolen döşeme sistemi ince bir plak tabakası ve dişlerden oluşan döşeme sistemidir. Asmolen döşeme sisteminde, dişlerin arası taşıyıcı özelliği bulunmayan dolgu malzemesi ile doldurulur. Asmolen döşeme sistemi genellikle geniş ve sığ kirişlerden oluşmaktadır. Sığ kiriş yüksekliğinden dolayı, bu sistemlerin yatay ötelenme rijitlikleri kirişli plak döşemeli sistemlere oranla düşüktür. Asmolen döşeme sistemi, düşük yatay ötelenme rijitliğine sahip olmasından dolayı, yumuşak kat düzensizliği riski bulunan binalarda, bu döşeme tipinin kullanılması yumuşak kat düzensizliği riskini arttıracaktır. Bundan dolayı, asmolen döşeme sistemine sahip binalar yumuşak kat düzensizliği açısından detaylı bir biçimde incelenmelidir. Bu amaçla, bu çalışmada asmolen döşeme sistemli 5, 8 ve 11 katlı binalar, farklı zemin kat yükseklikleri için sayısal yöntem kullanılarak incelenmiştir. Analizler neticesinde, her kat için göreli kat ötelenme değerleri elde edilmiştir. Zemin kat yüksekliği arttıkça, asmolen döşeme sistemli yapıların zemin katında oluşan göreli kat ötelenmelerinin yaklaşık %33 ile %50 arasında arttığı tespit edilmiştir. Kat sayısı arttıkça, zemin kattaki ötelenmelerin artarak TDY-2007 tarafından önerilen üst sınıra yaklaştığı görülmüştür. Zemin kattaki yüksek göreli kat ötelenmeleri, yumuşak kat düzensizliği riskini arttırmaktadır. Bu durum yatay yükler altında binanın deprem performansını olumsuz etkilemektedir. Bu sakıncalı durumu düzeltmek için betonarme perdeler sistemlere eklenmiş ve analizler tekrarlanmıştır. Betonarme perdelerin, binaların zemin katında oluşan göreli kat ötelenme değerlerini yaklaşık %40 ile %60 arasında azaltarak, zemin kat yüksekliğinin artmasından kaynaklanan olumsuz durumun etkisini azalttığı görülmüştür. Asmolen döşeme sistemine sahip binaların, deprem tehlikesinin yüksek olduğu bölgelerde güvenli bir şekilde tasarımının yapılması için, perde-çerçeve sistem olarak tasarlanmasının uygun olduğu görülmüştür.

Anahtar kelimler: Asmolen döşeme sistemi, Yumuşak kat düzensizliği, Göreli kat ötelenmesi, Betonarme bina

1. Introduction

Hollow block slab is a floor slab system that consists of a thin slab and joists. There are nonstructural materials between joists. Hollow block slab provides important advantages such as effective using of story height and interior design in buildings for architects. Furthermore, hollow block slab that has a flat slab ceiling reduce formwork and construction time. Because of these advantages, the using of this type slabs have become more common.

Hollow block slab usually consists of wide and shallow beams for providing a flat slab ceiling. The height of hollow block slab is determined compatible with nonstructural materials (styrofoam, briquette, tile) that use between joists. In Turkey, the thickness of the hollow block slab is usually 300 mm or 320 mm [1]. Because of low beam height in this system, its lateral stiffness is less than beam floor systems. Because hollow block slab has low lateral stiffness, lateral drift ratio in this system may be more under lateral loads, and this system may show weak performance under earthquake load.

In Turkey, the ground story of buildings that is existed two sides of main streets is used as commercial areas. For this reason, the height of this story is more than other stories and infill walls that are existed in upper stories between frames partly or completely remove in ground story. Recent years, in this building, using of hollow block slab system have become more common for using story height effectively and for providing a flat slab ceiling. This situation reduces the lateral stiffness of buildings especially in ground story and increase the risk of soft-story. This situation has a risk for buildings in Turkey where has earthquake zones. In Turkey, the soft-story effect is one of the main reason of damage sustained by reinforced concrete buildings during earthquakes [2, 3]. After Van Earthquake (2011), it was reported that soft story was the most common irregularity in collapsed buildings [4].

In this study, soft-story in building with hollow block slab was numerically investigated for different ground story height. For numerically studys 5, 8, 11 stories buildings that are used commonly in Turkey were investigated. Structure analysis software SAP2000 and IdeCAD was used for analysis [5, 6]. According to analysis, lateral drift ratios was obtained for each story. It is shown that as ground story height increased, the lateral drift ratios of buildings have reached limits that have negative effects on building performance under earthquake load. For restricting lateral drift ratios and improving building performance under earthquake load, shear walls added to the system and analysis was repeated. It is shown that because shear walls restrict lateral drift ratios of ground story, the earthquake performance of the building is improved.

2. The Earthquake Performance of Building with Hollow Block Slab

Over three decades, because of advantages of hollow block slab have been commonly used in Middle East countries including Turkey [7]. Because there is not enough experimental and numerical study that investigate the performance of hollow block slab under lateral loads, the performance of this system under earthquake loads doesn't know as much as beam floor systems. Because there is not enough experimental study that investigates the performance of hollow block slab under earthquake loads, most country's earthquake codes prevent using this system in seismic regions or allow with some requirement about dimensions or spacing of reinforcement using this system in seismic regions [8, 9].

Figure 1. A building with hollow block slab

Hollow block slab (Figure 1) usually consists of wide and shallow beams. Because of low beam height in this system, its lateral stiffness is low. Because hollow block slab has low drift stiffness,

this system may have more lateral drift ratio under lateral loads. In the building, more lateral drift ratios may cause more second order effect. This situation has a negative effect on building performance under earthquake loads. For example, in 2011 Van Earthquake, it is shown that damage of infill walls in building with hollow block slab are more than beam floor system. The reason is that hollow block slab that has shallow beam can't restrict the rotation at the end of the column at enough level under lateral loads, and big lateral drift ratios happen in building [10].

Figure 2. A damaged building with hollow block slab after Van Earthquake (2011)

Hollow block slab, because of weak performance has been restricted by Turkey Earthquake Code (TEC). TEC-1975 allows using this system in a seismic zone with a requirement which buildings higher than certain height must have shear walls [11]. TEC-1998 and TEC-2007 allow using of hollow block slab in high seismic zones only if structural elements (column, beam and beam-column joints) are designed ductile, if the structural elements are not ductile, shear walls have to be used in the system [12, 13]. But, in existing buildings with hollow block slab, TEC requirements are neglected, and buildings with largely weak performance under earthquake loads have been built. The most important proof of this situation is that these type buildings were heavily damaged in Bingöl Earthquake (2003) [2]. Figure 2 shows damaged building with hollow block slab after Van Earthquake (2011).

3. Soft-Story Effect

In Turkey, the ground story of buildings that exist two sides of main streets is used as commercial areas. For this reason, the height of this story is more than other stories. Furthermore, infill walls that exist in the upper story between frames partly or completely remove in ground story. In this situation, in the ground story that has big earthquake loads, lateral stiffness of building is decreased, and because of lateral drift ratio, the building experiences degradation of strength. Furthermore, recent years, in these buildings, using of hollow block slab have become more common for using story height effectively and for providing a flat slab ceiling. Authors think that in these type buildings, the using of hollow block slab reduces the performance of building under earthquake loads.

Designing of the ground story with more height than upper story and removing of infill walls of the ground story have negative effects on reinforced concrete (RC) building performance under earthquake load. Because infill walls restrict lateral drift ratios of the building, infill walls increase the load carrying capacity of the building. For example, under Lorca earthquake, a research investigates performance of RC buildings with one-way slabs with wide beams, for buildings, three wall densities are considered: no walls, low wall density, and high wall density. Results show that infill walls increase the lateral stiffness of buildings and decrease lateral drift ratios of buildings under earthquake loads [14]. Especially, because infill walls that exist in the upper story between frames partly or completely remove in ground story, ground story have more lateral drift ratio than the upper story. Past studies show that if infill walls of the ground story are removed, the lateral load carrying capacities of building reduce 30% and the maximum lateral drift ratios of building increase 10% [3, 15]. Although TEC-2007 in the design of reinforced concrete building considers the weight of infill walls, it neglects the effect of infill walls on frame system [13]. The real performances of the buildings can't be calculated due to this negligence. For this reason, they think that design of these type buildings should be detailedly investigated. Authors are planning a long-term

study that considers the effect of infill walls on the building.

4. Numerical Study

In this study, soft-story in buildings with hollow block slab was numerically investigated for different ground story height. For numerical analysis 5, 8 and 11 stories square floor plan of buildings was investigated. Figure 3 show the typical square floor plan of buildings. According to common using heights of the first floor was determined for 3.0m, 3.5m, 4.0m, 4.5m. Except for height of ground story, all heights of stories are 3.0m.

In hollow block slab, the dimension of joists was chosen as 150/320 mm and the dimension of the slab as 70 mm. The nonstructural material was chosen as styrofoam. For providing a flat slab ceiling, heights of all beams of frames was chosen as 320 mm, and for providing enough stiffness, wide of all beams was chosen as 600 mm. Material properties were chosen 25 MPa for concrete compressive strength and 420 MPa yield strength for steel.

Buildings were designed minimum requirement accordance with TEC-2007 and TS-500 (*Turkish Building Code*) [13, 16]. Buildings were designed for first earthquake zone and Z3 soil class. Dimensions of the column in a building stayed unchanged so that only effect of changing of ground story height is investigated. Table 1 shows the dimension of columns and beams.

For linear analysis of designed buildings, structure analysis software SAP2000 and IdeCAD was used for analysis [5, 6]. According to analysis, lateral drift ratios was obtained for each story. Two different softwares, in these sensitive systems, were considered for investigating accuracy rating of software. According to analysis, lateral drift ratios were obtained for each story. For the different height of the ground story, changing of obtained lateral drift ratios have been presented in tables and graphics. The lateral drift ratios that were obtained from structure analysis software IdeCAD have been shown in graphics (Figure 4-9). The lateral drift ratios that were obtained from structure analysis software SAP2000 have been presented in tables (show in Table 2). The limited number of paper influences this presentation.

According to analyses result in a frame system, as ground story height increased, the lateral drift ratios became more. For designing safety building against to earthquake, TEC-2007 state that 2% is limit of the lateral drift ratios [13]. But it is shown that as the number of stories increased, the lateral drift ratios have approached limits and the lateral drift ratios of 11 stories building have reached 2% (this can be seen in Table 2). This increment increases the risk of soft-story.

Table 1. Dimensions of columns and beams(mm)

	Dimensions of Columns		Dimensions of Beams
	Inside	*Outside*	
5 stories	450/450	450/450	600/320
8 stories	500/500	450/450	600/320
11 stories	550/550	500/500	600/320

For reducing the lateral drift ratios, in the both direction in systems, as much as 1% of the area plan, shear walls added to system and analysis was repeated. In both direction, four shear walls that have 30/210 dimension symmetrically added to the system. It is shown that shear walls have considerably reduced the lateral drift ratios and have reduced negative effects from the increment of ground story height. It is shown that in the frame-wall system, lateral drift ratios have reached maximum 1.4%. Because shear walls have decreased lateral drift ratios of ground stories, negative effect of increment in ground story was decreased.

5. Conclusion

In this study, lateral drift ratios of buildings with hollow block slab under earthquake loads was numerically investigated regarding the effect of the ground story height on lateral drift ratios.

For numerically study, lateral drift ratios of 5, 8, 11 story RC buildings was obtained. According to analyses;

- For frame structures, it is shown that when the height of ground story increased from 3.0m to 4.5m, lateral drift ratios of ground story increased nearly 50%.
- As the number of stories increased, the lateral drift ratios approach upper limit 2% which is recommended by TEC-2007. For 11 stories buildings, drift ratios that are obtained

from using structure software SAP2000 reached this limit.

The effect of infill walls was not considered for this study. In case infill walls which are usually used for design are removed in ground story, it is thought that the increasing in lateral drift ratios will exceed the limit 2% value. Because TEC-2007 don't consider the effect of infill walls on the frame in design, the risk of soft-story is high in these type buildings. For preventing the risk of soft-story, shear walls should be added the systems. It is shown that shear walls reduce the lateral drift ratios of 5 stories buildings on average 65%, 8 stories buildings on average 55%, 11 stories buildings on average 45%. In the frame-wall system, lateral drift ratios reached maximum 1.4%.

Because hollow block slab has low lateral stiffness, it shows weak performance under earthquake loads. This type slabs in the high seismic zone should be carefully designed as a frame-wall system. Furthermore, lateral drift ratios in hollow block slab should be investigated with the effect of infill walls on the building.

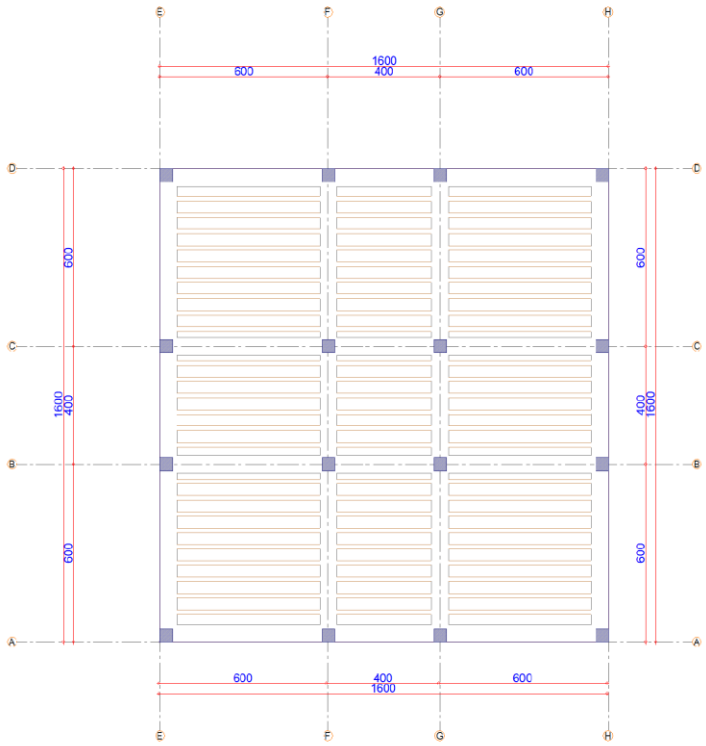

Figure 3. Square floor plan of a building

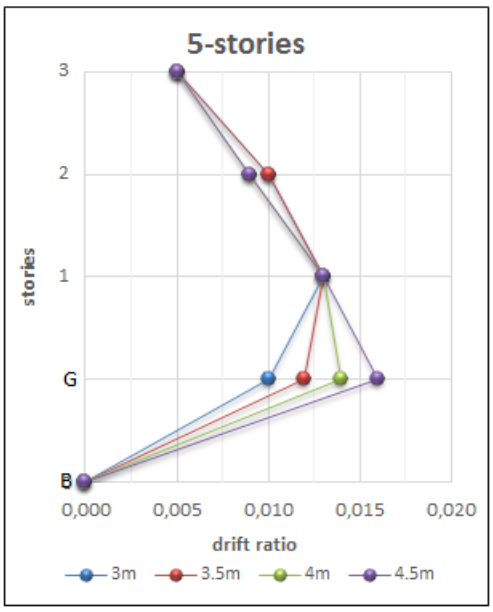

Figure 4. Frame structure with story of 5

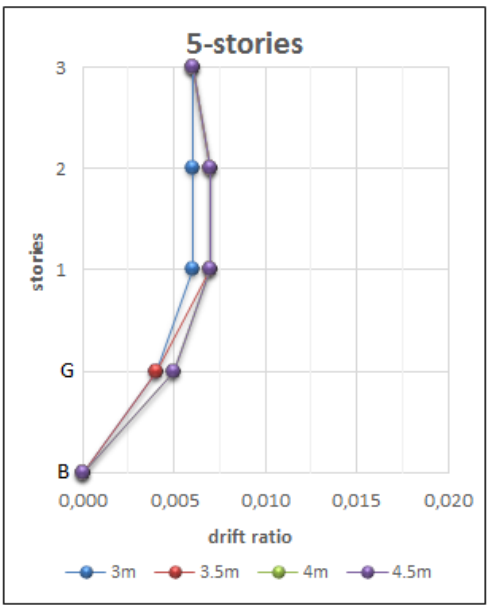

Figure 5. Frame-wall structure with story of 5

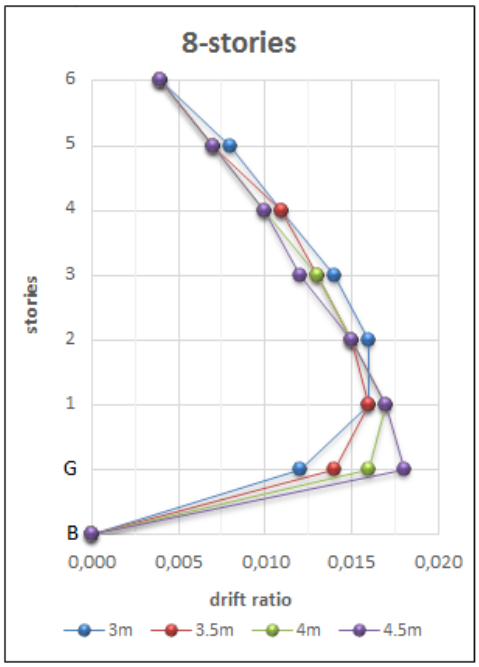

Figure 6. Frame structure with story of 8

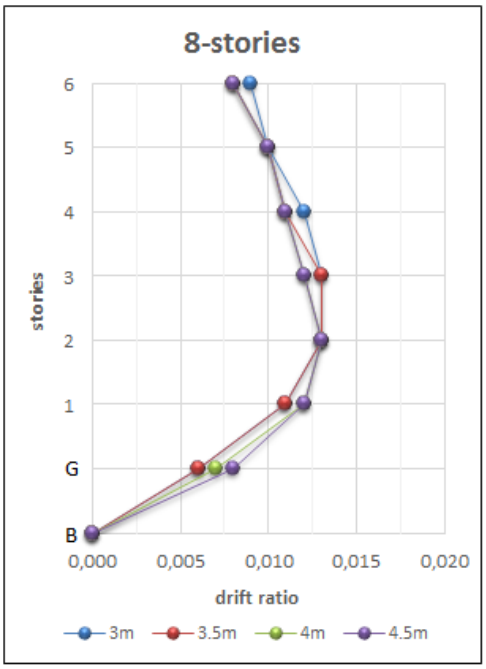

Figure 7. Frame-wall structure with story of 8

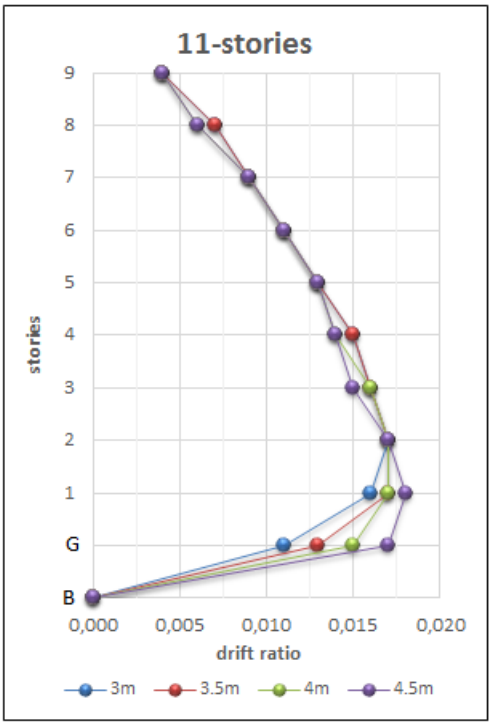

Figure 8. Frame structure with story of 11

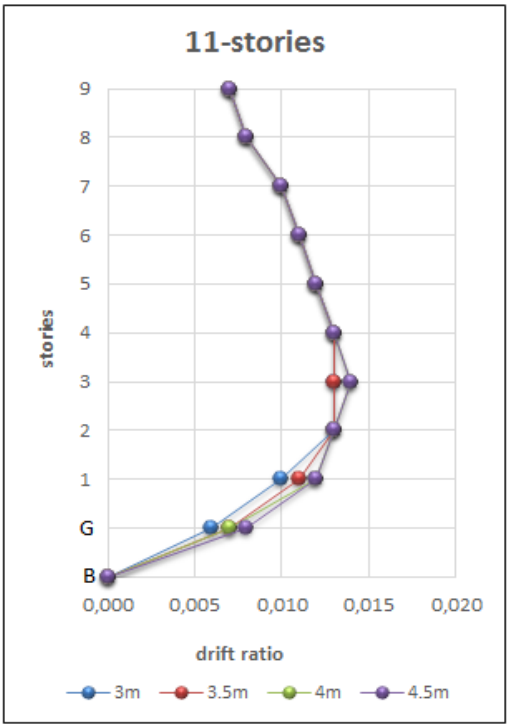

Figure 9. Frame-wall structure with story of 11

Table 2. Lateral drift ratios of buildings from sap2000

5 Stories frame structure					
Ground story H (m)	B	G	1	2	3
3	0.000	0.010	0.014	0.010	0.006
3.5	0.000	0.012	0.014	0.010	0.005
4	0.000	0.014	0.014	0.009	0.005
4.5	0.000	0.016	0.013	0.009	0.005
5 Stories frame-wall structure					
Ground story H (m)	B	G	1	2	3
3	0.000	0.003	0.005	0.005	0.005
3.5	0.000	0.003	0.005	0.006	0.005
4	0.000	0.004	0.006	0.006	0.005
4.5	0.000	0.004	0.006	0.006	0.006

8 Stories frame structure								
Ground story H (m)	B	G	1	2	3	4	5	6
3	0.000	0.012	0.017	0.016	0.014	0.011	0.007	0.004
3.5	0.000	0.014	0.017	0.016	0.013	0.011	0.007	0.004
4	0.000	0.016	0.017	0.015	0.013	0.010	0.007	0.004
4.5	0.000	0.018	0.018	0.015	0.013	0.010	0.007	0.004
8 Stories frame-wall structure								
Ground story H (m)	B	G	1	2	3	4	5	6
3	0.000	0.005	0.009	0.01	0.01	0.009	0.008	0.007
3.5	0.000	0.005	0.009	0.01	0.01	0.009	0.008	0.007
4	0.000	0.006	0.01	0.011	0.01	0.009	0.008	0.007
4.5	0.000	0.006	0.01	0.011	0.01	0.009	0.008	0.007

11 Stories Frame Structure											
Ground story H (m)	B	G	1	2	3	4	5	6	7	8	9
3	0.000	0.012	0.019	0.02	0.018	0.017	0.015	0.012	0.01	0.007	0.004
3.5	0.000	0.014	0.019	0.02	0.018	0.017	0.014	0.012	0.01	0.007	0.004
4	0.000	0.016	0.02	0.02	0.018	0.016	0.014	0.012	0.009	0.007	0.004
4.5	0.000	0.018	0.021	0.019	0.018	0.016	0.014	0.012	0.009	0.006	0.004
11 Stories frame-wall structure											

Ground story H (m)	B	G	1	2	3	4	5	6	7	8	9
3	0.000	0.006	0.01	0.012	0.013	0.013	0.012	0.011	0.009	0.008	0.006
3.5	0.000	0.006	0.011	0.013	0.013	0.013	0.012	0.011	0.009	0.008	0.006
4	0.000	0.007	0.011	0.013	0.013	0.013	0.012	0.01	0.009	0.007	0.006
4.5	0.000	0.007	0.012	0.013	0.013	0.013	0.012	0.011	0.009	0.008	0.006

6. References

1. Sezen H, Elwood KJ, Whittaker AS, Mosalam KM, Wallace JW, Stanton JF, 2000. Structural Engineering Reconnaissance of the August 17, 1999 Kocaeli (Izmit), Turkey Earthquake, PEER 2000/09, Technical Report, Berkeley, CA., Pacific Earthquake Engineering Research Center, University of California.

2. Dogangun, A., (2004). Performance of reinforced concrete buildings during the May 1, 2003 Bingol Earthquake in Turkey, Eng Struct,. **26**(6): 841-856.

3. Ozturk, M., (2013). Field Reconnaissance of the October 23, 2011, Van, Turkey, Earthquake: Lessons from Structural Damages, J. Perform. Constr. Facil., **29**(5): 04014125.

4. ODTU, (2011). 23 Ekim 2011 M_w 7.2 Van Depremi Sismik ve Yapısal Hasarlara İlişkin Saha Gözlemleri, METU/EERC 2011-04, Ankara.

5. SAP2000. Integrated Finite Element Analysis and Design of Structures, Computer and Structures Inc., Berkeley, California, USA.

6. IdeCAD, structure analysis software, http://idecad.com.tr/

7. Benavent-Climent, A., X. Cahis, J.M. Vico, (2010). Interior wide beam-column connections in existing RC frames subjected to lateral earthquake loading. *Bulletin of Earthquake Engineering*, **8**(2): 401-420.

8. Fadwa, I.,vd., (2014). Reinforced concrete wide and conventional beam-column connections subjected to lateral load, *Engineering Structures*, **76**: 34-48.

9. Gentry, T.R., (1992). Reinforced concrete wide beam-column connections under earthquake-type loading, PhD Thesis, University of Michigan.

10. ODTU (2012). 9 Kasım 2011 M_w 5.6 Van-Edremit Depremi Sismik ve Yapısal Hasara İlişkin Gözlemler, METU-EERC / İMO 2012-01, Ankara

11. Turkish Earthquake Code (TEC), (1975). Afet Bölgelerinde Yapılacak Binalar Hakkında Yönetmelik, (Regulation for Structures in Disaster Areas), *Ministry of Public Works and Settlement*, Ankara, Turkey.

12. Turkish Earthquake Code (TEC), (1998). Afet Bölgelerinde Yapılacak Binalar Hakkında Yönetmelik, (Regulation for Structures in Disaster Areas), *Ministry of Public Works and Settlement*, Ankara, Turkey.

13. Turkish Earthquake Code (TEC), (2007). Deprem Bölgelerinde Yapılacak Binalar Hakkında Yönetmelik, (Regulation for Buildings in Seismic Areas), *Ministry of Public Works and Settlement*, Ankara, Turkey.

14. Domínguez, D., López-Almansa, F. and Benavent-Climent, A., (2016). Would RC wide-beam buildings in Spain have survived Lorca earthquake (11-05-2011)?, *Engineering Structures*, **108**, 134-154

15. Arslan, M. H., and Korkmaz, H. H., (2007). What is to be learned from damage and failure of reinforced concrete structures during recent earthquakes in Turkey. *Engineering Failure Analysis*, **14**(1), 1–22.

16. TS-500 (TSE), (2000). Requirements for design and construction of reinforced concrete structures. Turkish Standards Institution, Ankara, Turkey.

Turkish Journal of Science & Technology
Volume 13(1), 45-53, 2018

Investigation of the Properties of Warm Mix Asphalt Involving Organic Additive

Ali Topal[a], Baha Vural Kök[b] , Derya Kaya[*a], Burak Şengöz[a], Peyman Dokandari[a], Mehmet Yılmaz[b]

[a] Department of Civil Engineering, Dokuz Eylul University, Izmir, Turkey
[b] Department of Civil Engineering, Fırat University, Elazig, Turkey
[*]e-mail: d.kaya@deu.edu.tr

(Received: 28.01.2017; Accepted: 03.04.2017)

Abstract

Demand for sustainable pavements increases day by day in asphalt paving industry. Warm Mix Asphalt (WMA) technology has begun to be an interesting topic for researchers owing to sustainability and environmental issues. Within the scope of this study, the effect of an organic WMA additive was evaluated in terms of mixture characteristics and performance. The fundamental and rheological properties of bitumen samples involving organic WMA additive were determined by conventional bitumen tests and dynamic shear rheometer (DSR). Mixtures modified with organic WMA additives were produced according to Marshall mix design method and the optimum bitumen content of the samples were determined. Following the determination of optimum bitumen content, the effect of the organic WMA additive was investigated in terms of indirect tensile stiffness modulus, fatigue and creep behaviour. Hamburg wheel tracking device was also applied to evaluate the permanent deformation characteristics of WMA mixtures in comparison to Hot Mix Asphalt (HMA) mixtures. The results appraised the effect of the organic WMA additive on rheological and performance characteristics of bituminous mixtures.

Keywords: Warm mix asphalt, Organic additive, Mixture characteristics, Dynamic shear rheometer, Fatigue behaviour, Hamburg wheel tracking device.

Organik Katkı İçeren Ilık Karışım Asfaltın Özelliklerinin İncelenmesi

Özet

Asfalt kaplama endüstrisinde sürdürülebilir kaplama gereksinimi her geçen gün artmaktadır. Ilık Karışım Asfalt (WMA) teknolojisi sürdürülebilirlik ve çevre sorunları nedeniyle araştırmacılar için ilgi çekici bir konu olmaya başlamıştır. Bu çalışma kapsamında, organik bir WMA katkı maddesinin karışım özellikleri ve performansı üzerindeki etkisi değerlendirilmiştir. Organik WMA katkısı içeren bitüm numunelerinin temel ve reolojik özellikleri, geleneksel bitüm deneyleri ve dinamik kayma reometresi (DSR) deneyi ile belirlenmiştir. Organik WMA katkı maddesi ile modifiye edilmiş karışımların tasarımı Marshall karışım tasarımı yöntemine göre yapılmış ve karışımın optimum bitüm içeriği tespit edilmiştir. Optimum bitüm içeriği belirlendikten sonra, indirekt çekme rijitlik modülü, yorulma ve sünme davranışı açısından organik WMA katkı maddesinin etkisi araştırılmıştır. Ayrıca WMA karışımlarının kalıcı deformasyon özelliklerini Sıcak Karışım Asfalt (HMA) ile kıyaslayabilmek amacıyla Hamburg tekerlek izi deneyi de uygulanmıştır. Sonuçlar, organik WMA katkısının bitümlü karışımların reolojik ve performans özellikleri üzerinde etkili olduğunu göstermiştir.

Anahtar Kelimeler: Ilık karışım asfalt, Organik katkı maddesi, Karışım özellikleri, Dinamik kayma reometresi, Yorulma davranışı, Hamburg tekerlek izi cihazı.

1. Introduction

Most of the field pavement practices around the world consist of conventional hot mix asphalt (HMA). For the last decade, implementing of warm mix asphalt (WMA) technologies has gained popularity in Europe and in some other countries as well as in the USA. The goal of WMA technologies is to obtain required strength and durability which is equivalent to or even better than HMA pavements [1]. The use of WMA technologies offers many benefits to asphalt industries. Many studies have common sight about the various advantages of the

utilization of WMA technologies. These advantages are all originated from the major feature of WMA additives which is reducing the viscosity of the bitumen [2]. This reduction results in increasing workability and ease of use, ecological benefits due to less emissions and reduction in costs due to less energy use. In terms of workability, the reduced viscosity helps the aggregates to be coated more easily [3, 4]. When discussing about environmental benefits, there are serious worries about the greenhouse gases emissions in HMA pavement applications. Due to lower application temperatures of WMA mixes, the emission of carbon dioxide (CO2) and other so called greenhouse gases are lowered in comparison with HMA mixes [5]. Besides, the evaporation of less heavy components of bitumen occurs less than conventional applications. This causes less odours in asphalt plants, therefore provides more pleasant working conditions. Builders comments also indicate that the fumes are rather less in WMA production in comparison with HMA production [6]. The fuel consumption of WMA technologies is rather less than conventional HMA mixtures. Energy consumption for WMA production has been reported as 60–80% of HMA production [4]. Some studies have also reported the range of 20–35% of savings in burner fuel with use of WMA technologies [5]. In asphalt industry, a common way of achieving lower application temperatures in order to produce WMA is the utilization of WMA additives. All of the current WMA additives facilitate lowering of production temperature by either lowering the viscosity and/or expanding the volume of the bitumen at a given temperature [7, 8]. There are many kinds of WMA additives, these additives are categorized as chemical, zeolite or organic additive etc. Organic WMA additives those are the most common as aforementioned, WMA additives used to improve workability by reducing the viscosity of bitumen [9]. By lowering the viscosity, asphalt can be produced at lower temperatures compared to conventional HMA. Organic WMA additives are reported as resistance improvers against permanent deformation by composing crystallized structures after cooling [10].

In this research, WMA mixture has been prepared with an optimum rate of organic WMA additive that is based on the recommendation of manufacturers. The mechanical performances of the samples were evaluated by Marshall stability test. Following, WMA samples involving organic WMA additive; indirect tensile stiffness modulus (ITSM) and fatigue behaviour of WMA were analyzed and compared with control specimens (HMA). Hamburg wheel tracking device was also used to determine the rutting performance of WMA mixture.

2. Material and Method

In this study, 50/70 penetration grade base bitumen provided from Aliağa/Izmir petroleum refinery was used. In order to characterize the properties of the base bitumen, conventional tests such as: penetration test, softening point test, Rolling Thin Film Oven Test (RTFOT) and etc. were conducted. These tests were performed in conformity with the relevant standards. Results are presented in Table 1.

Table 1. Properties Of Base Bitumen

Test	Specifications	Results	Limits
Penetration (25 °C; 0.1 mm)	ASTM D5/D5M-13 TS EN 1426	55	50-70
Softening point (°C)	ASTM D36/D36M-12 TS EN 1427	49	46-54
Viscosity at (135 °C)-Pa.s	ASTM D4402/D4402M-13	412.5	-
Viscosity at (165 °C)-Pa.s	ASTM D1754/D1754M-09 TS EN 12607-2	-	-
Change of mass (%)	-	0.04	0.5(max.)
Retained penetration after RTFO (%)	ASTM D5/D5M-13 TS EN 1426	25	-
Softening point rise after RTFO (°C)	ASTM D36/D36M-12 TS EN 1427	54	48 (min)
Specific gravity	ASTM D70-09e1 TS EN 15326	1.03	-
Flash point (°C))	ASTM D92-12b TS 123 EN 22592	260	230 (min)

The aggregates used in this study consist of a mix of basalt and limestone aggregates provided from Dere Madencilik Inc. quarry located in Belkahve/Izmir. The mix gradation of basalt and limestone was intentionally chosen to provide desired performance in conformity with Turkish specifications concerning the Type 1 wearing course. Basalt plays the role of

strengthening constituent as coarse aggregate while limestone participates in the fine aggregate framework. Table 2 presents the final gradation chosen for basalt–limestone aggregate mixture. The properties of the aggregate were investigated by several tests such as specific gravity, Los Angeles abrasion resistance, sodium sulphate soundness, fine aggregate angularity and flat and elongated particles. Test results conducted on both aggregate types are presented in Table 3.

Table 2. Gradation For Basalt–Limestone Aggregate Mixture

Test	19 – 12,5 mm Basalt	12,5 – 5 mm Basalt	5 – 0 mm Limestone	Combined Grad. (%)	Spec. Limits
Mix.(%)	15	45	40		
(3/4)″	100	100	100	100	100
(1/2)″	35.7	100	100	90.5	83-100
(3/8)″	2.5	89	100	80.5	70-90
No.4	0.4	16	100	47.3	40-55
No.10	0.3	1.2	81	33	25-38
No.40	0.2	0.7	33	13.5	10-20
No.80	0.15	0.4	22	9	6-15
No.200	0.10	0.2	13	5.3	4-10

Table 3. The Properties Of Both Basalt And Limestone

Test	Specifications	Results		Spec. Limits
		Limestone	Basalt	
Specific Gravity (Coarse Agg.)	ASTM C127-12			
Bulk		2.686	2.666	-
SSD		2.701	2.810	-
Apparent		2.727	2.706	-
Specific Gravity (Fine Agg.)	ASTM C128-12			
Bulk		2.687	2.652	-
SSD		2.703	2.770	-
Apparent		2.732	2.688	-
Specific Gravity (Filler)		2.725	2.731	-
Los Angeles Abrasion (%)	ASTM C131-06 TS EN 1097-2	24.4	14.2	maks. 45 maks. 27
Flat and Elongated Particles (%)	ASTM D4791-10 TS EN 933-3	7.5	5.5	maks 10 maks. 25
Sodium Sulphate Soundness (%)	ASTM C88-13			maks. 10-20
Fine Aggregate Angularity	ASTM C1252-06	47.85	58.1	min. 40

Sasobit® is an organic WMA additive which is product of Sasol Wax Inc. It is a long-chain aliphatic polymethlene hydrocarbon produced from the Fischer-Tropsch (FT) chemical process with a melting temperature of 120°C. The longer chains help keep the wax in solution, which reduces bitumen viscosity at typical asphalt production and compaction temperatures. Based on the literature, dosages for organic additive ranged from 1.0% to 4.0% by weight of the bitumen [11–13]. In this research, the organic additive content was chosen as 3.0% based on the past research [14]. Organic additive added to the virgin bitumen at 120°C and mixed by using the high shear mixer for 10 minutes.

2.1. Test methods

2.1.1. Conventional bitumen tests

The base bitumen and the bitumen sample containing organic additive were subjected to the following conventional bitumen tests; penetration, ring and ball softening point, thin film oven test (TFOT), penetration and softening point after TFOT as well as the storage stability test determined by the difference in softening point test results taken from the top and bottom of the tube (ASTM D5-06 2006; ASTM D36-95 2000; ASTM D 1754-97 2002) [15–17]. In addition, the temperature susceptibility of the bitumen samples has been calculated in terms of penetration index (PI) using the results obtained from penetration and softening point tests [18].

The viscosity defined as resistance of a fluid to flow is significant since it affects the workability of the bitumen [19]. Brookfield viscometer was employed to inspect the mixing and compaction temperatures of the mixtures in according to ASTM D4402-06 [20]. The test was performed at 135°C and 165°C and the temperatures corresponding to bitumen viscosities 170±20 mPa.s and 280±30 mPa.s were chosen as mixing and compaction temperatures respectively.

2.1.2. Mechanical properties

The effect of organic WMA additive on the mechanical properties of WMA has been determined by Marshall mix design method (ASTM D3549) in terms of stability, flow and air void content as well as by indirect tensile stiffness modulus test and indirect tensile fatigue test [21-24]. The tests were conducted on WMA samples at recommended contents and on HMA as control samples. Asphalt concrete specimens were prepared with a compaction effort of 75 blows simulating heavy traffic loading conditions. The ITSM test is a non-destructive test that is used to evaluate the relative quality of materials and study the effect of temperature and loading rate. The ITSM Sm in MPa is defined as below [23];

$$Sm = F(R + 0.27)/LH \quad (1)$$

Where F is the peak value of the applied vertical load (repeated load, N), H is the mean amplitude of the horizontal deformation (mm) obtained from five applications of the load pulse, L is the mean thickness of the test specimen (mm), and R is the Poisson's ratio (assumed as 0.35). The test was performed by way of a universal testing machine (UTM) in deformation-controlled mode. The magnitude of the applied force was adjusted by the system during the first five conditioning pulses such that the specified target peak transient diametral deformation was obtained. An appropriate value was chosen to ensure that sufficiently high signal amplitudes were obtained from the transducers which would produce consistent and accurate results. Accordingly, this value was selected as 5 mm for this test. The rise time, which is measured from the origination of load pulse and denotes the duration of the applied load rising from zero to the maximum value, was set at 124 ms. The load pulse application was adjusted to 3.0 s. ITSM tests were conducted at three different temperatures (20 oC, 25 oC and 30 oC).

The indirect tensile fatigue test is one of the constant stress test that characterizes the fatigue behaviour of the mixture [25]. In this study, the fatigue test was performed in a controlled stress mode based on BS DD ABF standard [24]. The UTM was also used for this purpose. The loading frame was housed in an environmental chamber to control temperature during the test. The desired load level, load rate and load duration were controlled by a computer. The deformation of the specimen was monitored through linear variable-differential transducers (LVDTs). The LVDTs were clamped vertically onto the diametrical side of the specimen. A repeated dynamic compressive load at 350 kPa was applied to specimens at 20oC, 25oC and 30oC test temperatures, across the vertical cross-section along the depth of the specimen using two loading strips 12.5 mm in width. Finally, the resulting total deformation corresponding to the applied force was measured.

2.1.3. Rheological properties

The DSR test was performed on WMA samples by using a Bohlin Gemini II DSR rheometer to evaluate their rheological characterization. The test was performed under controlled stress loading conditions using low (0.01 Hz) and high (10 Hz) frequency sweeps at temperature between 30 oC and 80 oC (for every 10 oC). The stress amplitude for all the tests was confined within the linear visco-elastic response of the bitumen.

2.1.4. Rutting test

The loss of pavement serviceability is a common result from rutting which is defined as the formation of the longitudinal depressions under the wheel paths caused by the progressive movement of materials under traffic loading in the asphalt pavement layers [26]. The Hamburg wheel tracking device is designed to evaluate the rutting characteristics of bituminous mixtures by dint of aggregate structure, bitumen properties, moisture susceptibility and adhesion between bitumen and aggregates. The test is carefully contemplated to simulate bearing capacity of pavement under actual wheel tracks.

The working principle is to roll a steel wheel with a specified diameter over a bituminous mixture specimen with a standard thickness for a specified number of wheel passes. The test measures the depth of rut after the specified number of passes is reached. Various organizations may define their own

specifications with different testing conditions such as specimen dimensions, wheel diameter, rolling length, applied load and temperature. Within this context, there are many devices designed to carry out the task under various conditions.

The test device used within the scope of this study, was an electronically powered device which rolls a steel wheel (capable of using rubber wheel) with a diameter of 203 mm and width of 50 mm over a well compacted specimen with dimensions of 430×280×50 mm. The device is capable of making about 50 passes in minute over the specimen's surface by rolling length of 230 mm. The applied load was chosen as 710 N by default as per EN 12697-22 standard test method [27]. Prior to compaction of the specimens, HMA and WMA mixtures were carefully mixed at their pre-defined mixing temperatures using a mixer capable of mixing adequate amount of materials at desired temperature. The Hamburg wheel tracking device comes with a roller compactor in order to compact mixtures within standard molds to fit in wheel tracking device frames. The roller compactor also makes it convenient to prepare specimens with desired thickness (50 mm) with specified air voids (4%). The amount of loose mix to reach the desired compacted bulk specific gravity corresponding to 4% air voids considering mold dimensions was calculated and poured into compaction molds. After cooling the specimens at room temperature, the specimens were subjected to 30.000 passes of wheel tracks. In this study, two specimens of HMA and WMA were prepared and tested for right and left wheels. The rut depth was measured and recorded for right and left wheels simultaneously by an electronic system at every 5.000 passes while the test was running.

3. Results and Discussion

3.1. Conventional test results

The conventional properties of the bitumen prepared with organic additive are presented in Table 4. As depicted in Table 4, the addition of the organic WMA additive decreased the penetration values and increases the softening point values.

As seen in Table 4, WMA sample exhibits higher penetration index values (which is an indicator of reduced temperature susceptibility) compared to base bitumen. Asphalt mixtures containing bitumen with higher PI are more resistant to low temperature cracking as well as permanent deformation [28]. Storage stability test indicate that, the bitumen samples with WMA additive is much more storage stable compared to HMA.

As depicted in Table 4, the additive reduce the viscosity of bitumen which indicates that, WMA additives increase the workability and make relatively reductions for mixing and compaction temperatures. The viscosity of results related to WMA additive 135°C and 165°C are drawn at semi logarithmic figure and the temperature corresponds to compaction and mixing range is also summarized in Table 5. Based on the Table 5, it can be seen that, the addition of organic WMA additive reduced the mixing and compaction temperature between 10-15°C.

Table 4. Conventional Properties Of Base And Organic Wma Modified Bitumen

Test	Base bitumen	Bitumen including Organic WMA Additive
Penetration (0.1mm)	55	37
Softening point (°C))	49.1	69.3
Viscosity at (135 °C) (mPa.s)	412.5	287.5
Viscosity at (165 °C)-(mPa.s)	137.5	75.0
Loss of mass (%)	0.04	0.07
Retained penetration (after TFOT (%)	75	87
Softening point rise after (afterTFOT (°C)	5.0	4.0
Pen. In	-1.20	1.95
Storage Stability	0	1.6

Table 5. Mixing And Compaction Temperatures

Additive Content (%)	Mixing Temperature Range(ºC)	Compaction Temperature (ºC)
0	156-163	143-149
3	144-149	134-138

3.2. Results of mechanicalpProperties

In this study, the optimum bitumen content related to HMA mixture as well as WMA

mixture containing organic WMA additive were determined by the Marshall mix design method, retrieved directly as the bitumen content corresponding to 4% air voids on content–air voids graphic based on second degree polynomial trend lines. The optimum bitumen content for HMA mixture and WMA mixture containing organic WMA additive were determined as 4.76%, and 4.25% respectively. The ITSM values at 20°C, 25°C and 30°C temperatures for HMA and WMA mixtures containing organic WMA additive are shown in Fig. 1. As depicted in Fig. 1, the ITSM values of WMA are higher than HMA mixtures at all tested temperatures. The ITSM values of HMA mixtures and WMA mixtures containing Organic WMA additive have significantly decreased by increase in temperature.

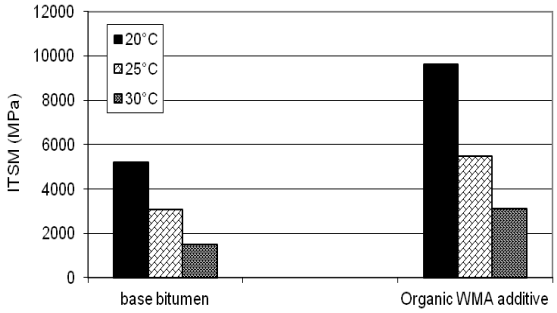

Figure 1. ITSM values of HMA WMA mixtures including organic WMA additive

The variation of load cycle numbers by temperature change is given in semi-logarithmic graphs in Fig. 2. As presented in Fig. 3, the load cycle numbers which caused the specimens to be cracked declined considerably as the temperature increased.

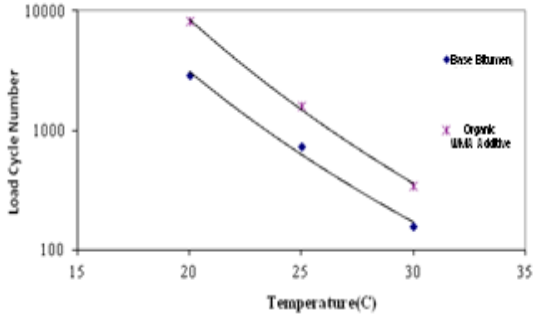

Figure 2. Variation of load cycle numbers by temperature change

The deformation of the specimens was monitored through linear variable–differential transducers (LVDTs) during the indirect tensile fatigue test. The graphs for the load cycle number corresponding permanent deformation are given in Fig. 3 for HMA and WMA mixtures at 20°C temperature. As shown in Fig. 3, HMA and WMA mixtures were cracked at approximate values of 4.3 mm, 4 mm deformation strains respectively. The specimens prepared with organic WMA additive could withstand higher load cycles and have cracked at lower deformation strains.

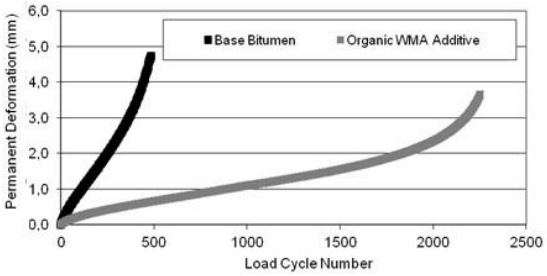

Figure 3. Permanent deformations corresponding load cycle numbers

3.3. Results of rheological properties

The variation of complex modulus (G*) of the base bitumen and the bitumen samples involving variable content of organic WMA additive at low (0.01 Hz) and high frequency level (10 Hz) and at six different temperatures are presented in Figs. 4a and 4b. As depicted in Figs. 4a-4b complex modulus increases by the decrease of temperature. An increment in G* indicates higher elastic part, thus an improved elastic behaviour. Besides, G* increases with increase in frequency. This is due to the rheological behaviour of the bitumen samples since bitumen under shorter loading times (high frequency level) exhibit elastic behaviour. G* values of the samples involving organic WMA additive are greater than G* of base bitumen for all temperatures and frequencies as seen in Figs. 4a and 4b.

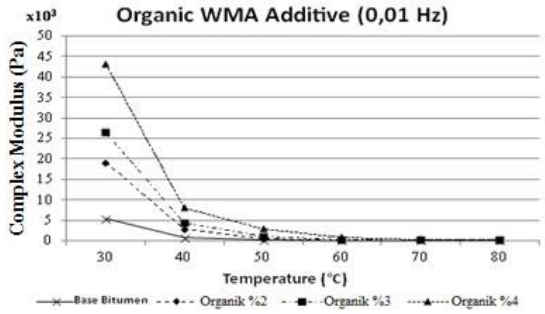

Figure 4a. Complex Modulus of organic WMA additive at 0.01 Hz.

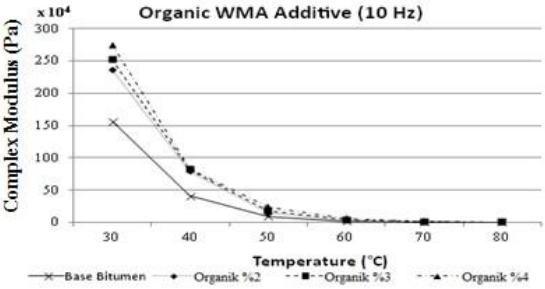

Figure 4b. Complex Modulus of organic WMA additive at 10 Hz.

3.4. Rutting test results

The Hamburg wheel tracking test was performed in accordance with EN 12697-22 standard [27]. The rut depths at 50°C are presented in Figure 5. Results are given as percent values indicating the ratio of actual rut depth over the total thickness of tested specimen (50 mm). The real rut depths (mm) are obtainable by halving the percent values. The rut depths at 50°C of HMA and WMA mixtures involving organic WMA additive were determined at each 5.000 passes initiating at 5.000 and ending at 30.000.

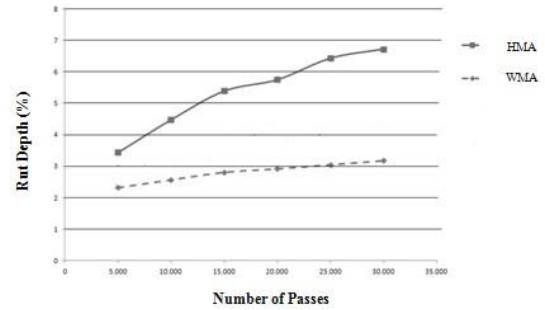

Figure 5. The rut depth % values corresponding number of passes for HMA and WMA mixtures including Organic WMA Additive

As expected the rut depth values typically increased with increase in the number of passes. Based on each number of passes, WMA mixture involving organic additive performed better than HMA mixture in terms of rut depth.

4. Conclusion

Lowering mixing and compaction temperatures and consequently the reduction of energy costs as well as emissions are the dominant advantages of utilization of WMA technologies. The utilization of organic WMA additive helps in the reduction of viscosity values which in turn reduces the mixing and compaction temperatures.

The results obtained from Marshall design demonstrated that the optimum bitumen content decreases by WMA additive. This reduction can be described as an advantage of using organic WMA additive in terms of initial cost.

ITSM values regarding HMA mixture and WMA mixture showed that the utilization of organic WMA additive increases the stiffness of mixtures. The ITSM values of all mixtures tested within the scope of this study significantly decreased by increase in temperature. As well as PI values of bitumen containing organic additive exhibited that the use of WMA additive potentially improves the temperature susceptibility.

When evaluating the load cycle numbers which caused the specimens to be cracked, WMA additive improves the repetitive loading strength of bituminous mixtures. The load cycle numbers of all mixtures significantly decrease by increase in temperature. Taking into consideration the deformation strains, WMA mixture exhibits better performance under constant loading cycles. The utilization of organic WMA additive improves the ability of asphalt pavements against permanent deformation and increases the rigidity of bituminous mixtures. The formation of crack in lower deformation levels as a result of repetitive loading is an indicator for brittle susceptibility level of a specimen.

Detailed investigation performed by DSR test at low and high frequency level and at different temperatures indicated that, the complex modulus value increases with increase

in frequency and decreasing temperature. Increment in G* is attributed to improved elastic behaviour of the sample.

In the light of findings from rutting test, it is possible to consider that the organic WMA additive improves resistance to rutting characteristics of bituminous mixtures. Organic WMA additive has structural modification effects on bituminous mixtures.

5. Acknowledgment

This research was sponsored by the Scientific and Technological Research Council of TURKEY (TUBITAK) under the project number 110M567 for which the authors are greatly indebted. The findings and evaluations of the results of this study are not the official view of TUBITAK.

6. References

1. Newcomb, D. (2006). An introduction to warm-mix asphalt. National Asphalt Pavement Association.
2. Hurley, G. C., Prowell, B. D. (2006). Evaluation of potential process for use in warm mix asphalt. J Assoc Asphalt Paving Technol., vol. 75, pp. 41-90.
3. Kristjansdottr, O., Muench, S. T., Michael, L., Burke, G. (2007). Assessing potential for warmmix asphalt technology adoption. Transport Res Rec., vol. 2040, pp. 91-99.
4. Rubio, M. C., Martinez, G., Baena, L., Moreno, F. (2012). Warm mix asphalt: an overview. J Cleaner Prod., vol. 24, pp. 76-84.
5. D'Angelo, J., Harm, E., Bartoszek, J., Baumgardner, G., Corrigan, M., Cowsert, J., et al. (2008). Warm-mix asphalt European practice. American Trade Initiatives.
6. Croteau, J. M., Tessier, B. (2008). Warm mix asphalt paving technologies: a road builder's perspective. The 2008 Annual Conference of the Transportation Association of Canada.
7. Button, J. W., Estakhri, C., Wimsatt, A. (2007). A synthesis of warm-mix Asphalt. Texas Transportation Institute, The Texas A&M University.
8. Hurley, G. C., Prowell, B. D. (2005). Evaluation of Sasobit for use in warm mix asphalt. National Center for Asphalt Technology.
9. Jamshidi, A., Hamzah, M. O., You, Z. (2013). Performance of Warm Mix Asphalt containing Sasobit®: State-of-the-art. Construction and Building Materials, vol. 38, pp. 530-553.
10. Zaumanis, M. (2010). Warm mix asphalt investigation. M.Sc. Thesis, Technical University of Denmark, Kgs.Lyngby.
11. D'Angelo, J., Harm, E., Bartoszek, J., Baumgardner, G., Corrigan, M., Cowsert, J., Harman, T., Jamshidi, M., Jones, W., Newcomb, D., Prowell, B., Sines, R., Yeaton, B. (2008). Warm-mix asphalt: European practice. American Trade Initiatives.
12. Austerman, A. J., Mogawer, W. S., Bonaquist, R. (2009). Evaluating the effects of warm mix asphalt technology additive dosages on the workability and durability of asphalt mixtures containing recycled asphalt pavement. Transportation Research Board 88th Annual Meeting.
13. Kanitpong, K., Nam, K., Martono, W., Bahia, H. (2008). Evaluation of a warm mix asphalt additive. Construction Materials. vol. 161(1), pp. 1-8.
14. O'Sullivan, K., Wall, P. (2009). The effect of warm mix asphalt additives on recycled asphalt pavement. Worcester Polytechnic Institute.
15. American Society for Testing and Materials (2006). ASTM D5-06: Standard test method for penetration of bituminous materials. West Conshohocken, PA.
16. American Society for Testing and Materials (2000). ASTM D36-95: Test method for softening point of bitumen (ring and ball apparatus). West Conshohocken, PA.
17. American Society for Testing and Materials (2002). ASTM D 1754-97: Standard test method for effects of heat and air on asphaltic materials (thin-film oven test).; West Conshohocken, PA.
18. Read, J., Whiteoak, D. (2003). The Shell bitumen handbook. Thomas Telford Publishing, London.
19. Specht, L. P., Khatchatourian, O., Brito, L. A. T., Ceratti, J. A. P. (2007). Modelling of asphalt-rubber rotational viscosity by statistical analysis and neural networks. Materials Research. vol. 10(1), pp. 69-74.
20. American Society for Testing and Materials (2002). ASTM D4402-06: Standard test method for viscosity determination of asphalt at elevated temperatures using a rotational viscometer. West Conshohocken, PA.
21. American Society for Testing and Materials (2011). ASTM D3549-11: Standard test method for thickness or height of compacted bituminous paving mixture specimens. West Conshohocken, PA.
22. American Society for Testing and Materials (2012). ASTM D6931-12: Standard test method for indirect tensile (IDT) strength of bituminous mixtures. West Conshohocken, PA.
23. British Standards Institution (1993). BS DD 213: Method for determination of the indirect tensile stiffness modulus of bituminous mixtures. Draft for development, London.
24. British Standards Institution (1997). BS DD ABF: Method for determination of the fatigue characteristics of bituminous mixtures using indirect tensile fatigue. Draft for development, London.

25. Nejad, F. M., Aflaki, E., Mohammadi, M. A. (2010). Fatigue behavior of SMA and HMA mixtures. Constr Build Mater., vol. 24, pp. 1158-1165.

26. Nejad F. M., Azarhoosh, A., Hamedi, G.H., Roshani, H. (2014). Rutting performance prediction of warm mix asphalt containing reclaimed asphalt pavements. Road Materials and Pavement Design, vol. 15(1), pp. 207-219.

27. European Committee for Standardization (2003). EN 12697-22. Bituminous mixtures - Test methods for hot mix asphalt - Part 22: Wheel tracking.

28. Sengoz, B., Isikyakar, G. (2008). Analysis of styrene-butadiene-styrene polymer modified bitumen using fluorescent microscopy and conventional test methods. Journal of Hazardous Materials, vol. 150, pp. 424-432.

Turkish Journal of Science & Technology
Volume 13(1), 55-59, 2018

Linear Elastic Analyses of Masonry Walls

Erkut Sayın[1*], Yusuf Calayır[2]
[1]Firat University Engineering Faculty Civil Engineering Department Elazığ
[*]esayin@firat.edu.tr

(Received: 07.02.2017; Accepted: 05.04.2017)

Abstract

Masonry structures are commonly used in many countries. Load bearing masonry walls are the most important structural element in the masonry structures. In this study, a computer program was written in MATLAB for linear elastic analyses of masonry walls. In addition, a mesh program which meshes the wall as two dimensional model was written in MATLAB. These models were constituted with macro modelling approach. Three different load cases were applied to two dimensional masonry model with opening. The obtained results from the linear elastic analysis were compared with ANSYS software results.

Keywords: Masonry walls, Linear elastic behaviour, Finite element method

Yığma Duvarların Lineer Elastik Analizi

Özet

Yığma yapılar birçok ülkede yaygın olarak kullanılır. Bu yapılardaki en önemli yapı elemanı taşıyıcı duvarlardır. Bu çalışmada, yığma duvarların lineer elastik analizi için MATLAB dilinde bir bilgisayar programı yazılmıştır. Ayrıca yine MATLAB dilinde duvarın iki boyutlu olarak sonlu eleman modelini oluşturabilen bir program yazıldı. Yığma duvar modelleri makro modelleme yaklaşımıyla modellendi. Pencere açıklığına sahip duvar modellerine üç farklı yükleme uygulanarak elde edilen lineer elastik analiz sonuçları ANSYS program sonuçları ile karşılaştırıldı.

Anahtar Kelimeler: Yığma duvar, Lineer elastik davranış, Sonlu eleman metodu

1. Introduction

Masonry is the oldest building material that still finds wide use in today's building industries [1]. Masonry structures are the construction systems where walls, comprised of mortar and masonry units such as briquette, brick, stone and adobe, are used as load bearing system. Undoubtedly, the most important structural element for masonry structures is the load bearing walls. These structures are commonly used in many countries all over the world. The most important characteristic of masonry construction is its simplicity. Laying pieces of stone, bricks or blocks on top of each other, either with or without cohesion via mortar, is a simple, though adequate, technique that has been successfully used ever since remote ages [2]. Half of the existing building stock is consist of masonry structures in Turkey [3]. The vast majority of these structures are located in the rural areas and neighborhoods around the city. Masonry structures prefer over other structural systems because the relevant materials can be easily obtained and their construction and workmanship are easier. For this reason, the ratio of masonry structures increase to 82% in rural regions [4]. Masonry structures can be divided into three groups as confined, unreinforced and reinforced masonry structures. These structures are commonly constructed as to be unreinforced masonry in Turkey. These structures are constructed with traditional techniques using locally available materials. Nearly no engineering services are used in these buildings.

2. Modelling of Masonry

Masonry is a material which exhibits distinct directional properties due to the mortar joints which act as planes of weakness. In general, the approach towards the numerical representation of masonry can focus on the

micro-modeling of the individual components, unit (brick, block, etc.) and mortar, or the macro-modeling of masonry as a composite [5]. Depending on the level of accuracy and the simplicity desired, it is possible to use one of the modeling strategies. Three different strategies which called detailed micro modeling, simplified micro modeling and macro modeling are used for modeling the masonry structure. One modeling strategy cannot be preferred over the other because different application fields exist for micro and macro models. In the detailed micro modelling, the material specifications of the masonry units and the mortar, i.e., the modulus of elasticity, density and Poisson ratio are evaluated separately. The masonry units are widened by as much as half of the mortar layer in the simplified micro-modelling. Thus, the mortar layer is neglected, and the masonry units are separated from each other with interface lines. Macro-modelling is an equivalent material model that assumes the construction elements to be a composite without any exception among stone, brick and mortar. These modeling strategies are given in Figure 1.

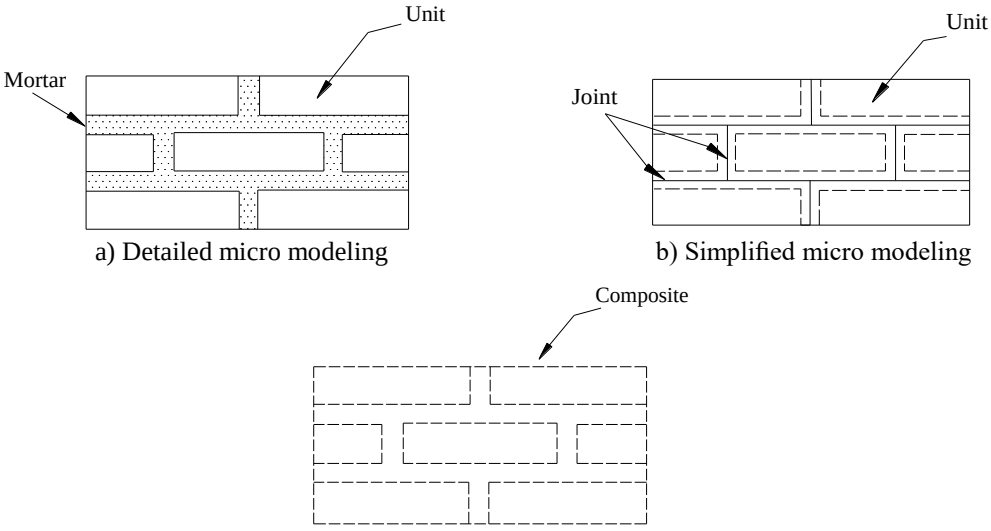

a) Detailed micro modeling

b) Simplified micro modeling

c) Macro modeling

Figure 1. Modeling strategies of masonry structures [1]

3. Linear Elastic Analyses

In this study, linear elastic analyses of a masonry wall was performed. For this purpose, a program that can perform linear analyses of masonry walls was written in MATLAB. The program was named as masonry-lin. Also, a mesh program was written in MATLAB that can draw the wall with and without opening and prepare the necessary information as input file for the masonry-lin [6]. The mesh program model the masonry wall as two dimensional by means of the macro modelling approach. Node coordinates, element and node numbers, element connectivity, restrained nodes and material properties are prepared with the mesh program as the input file for the masonry-lin. Finite element mesh of the wall with and without opening created by the mesh program was presented in Figure 2. In this figure, black and blue numbers on the wall show node points and element numbers, respectively. The masonry-lin. uses this input file and starts the analysis. It calculates displacement, stress and strain values of the node points.

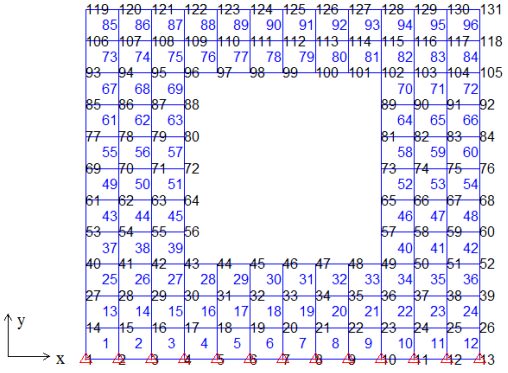

a) with opening

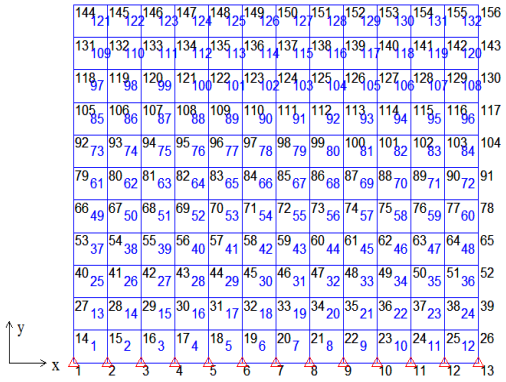

b) without opening

Figure 2. Finite element mesh of the masonry wall

In finite element implementation, finite element model of the masonry wall is constructed using quadrilateral elements, with four nodal points and two degrees of freedom on each nodal point. Element stiffness matrixes were found using 2x2 Gauss integration rule. The flow diagram of the masonry-lin. is presented in Fig. 3.

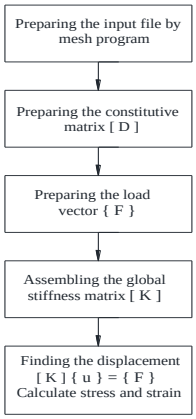

Figure 3. Flow diagram of the masonry-lin

Three different load cases were applied to two dimensional masonry model with opening. The base nodes of the wall were fixed in x and y directions at all load cases. For first and second load case, single load was applied at horizontal and vertical direction, respectively. For third load case, these two single loads were applied together to the masonry wall model.

Value of the single load was considered as 50 kN. The modulus of elasticity, mass per volume and Poisson's ratio for the masonry unit was considered as $5x10^3$ Mpa, 1.2 t/m^3, and 0.20, respectively. The dimension of the masonry wall used in the analysis was shown in Figure 4.

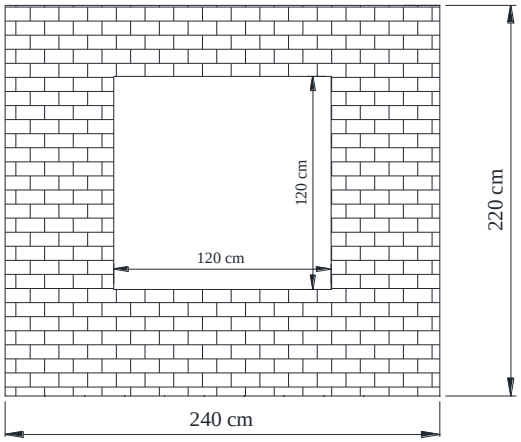

Figure 4. Dimension of the masonry wall

For first load case, the single load was applied in the x direction at nodal point 119. For second load case, the single load was acted in the negative y direction at nodal point 125. For third load case, these two single loads were applied at the same nodes and at the same directions (Fig. 5).

Deformed and undeformed shape of the masonry wall for three different load cases obtained the masonry-lin. is shown in Figure 5. In this figure, solid blue and dashed green lines show the undeformed and deformed shape of the masonry wall.

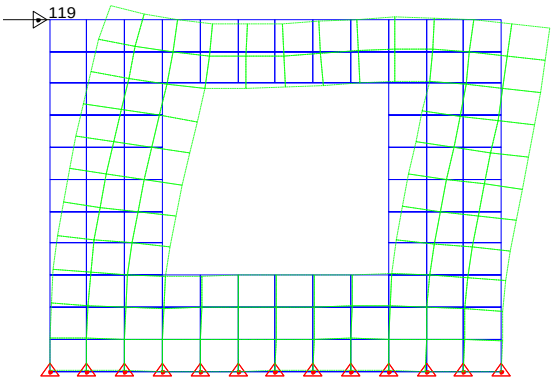

a) First load case

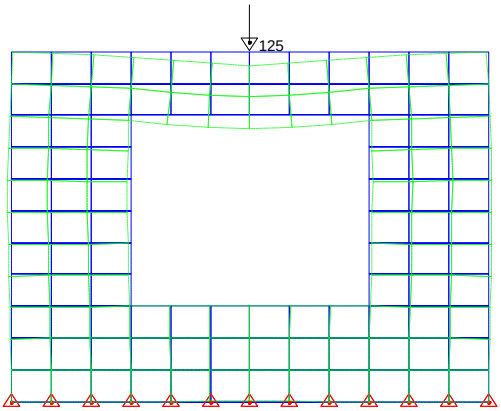

b) Second load case

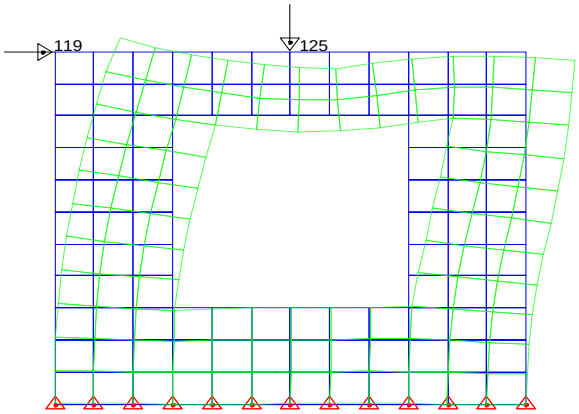

c) Third load case

Figure 5. Undeformed and deformed shape of the masonry wall with different load cases

Two node points was selected on the masonry wall for comparing displacement and stress values acquiring from masonry-lin and ANSYS software. These points is given in Figure 6. Displacement values of the node point 131 obtained from the masonry-lin. and ANSYS software under first, second and third load cases is presented in Table 1.

Also, the masonry-lin. can calculate the maximum and minimum principal stress of the node points. Maximum and minimum principal stress values of the node point 117 under first, second and third load cases is presented in Table 2. Same displacement and stress values were obtained according to the analysis results.

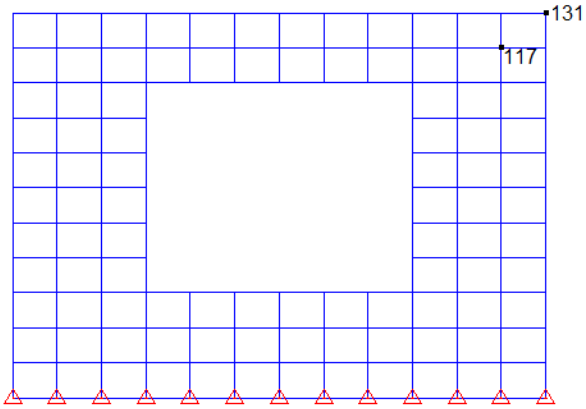

Figure 6. Selected node points

Table 1. Displacement values of the node point 131

Load cases	Masonry-lin.		ANSYS	
	x (mm) direction	y (mm) direction	x (mm) direction	y (mm) direction
First load case	1.285	-0.277	1.285	-0.277
Second load case	-0.0542	-0.0104	-0.0542	-0.282
Third load case	1.233	-0.282	1.233	-0.282

Table 2. Maximum and minimum principal stress of the node point 117

Load cases	Masonry-lin.		ANSYS	
	max. principal stress (kPa)	min. principal stress (kPa)	max. principal stress (kPa)	min. principal stress (kPa)
First load case	144.24	-141.06	144.24	-141.06
Second load case	84.45	-94.17	84.45	-94.17
Third load case	227.60	-232.95	227.60	-232.95

4. Conclusion

In this study, a computer program was written in MATLAB to perform linear elastic analyses of masonry walls. Furthermore, a mesh program which meshes the wall as two dimensional was written in MATLAB. These masonry walls were constituted with macro modelling approach. Three different load cases were applied to these walls. Accuracy of the results obtained from the masonry-lin. were compared with ANSYS software results.

6. References

1. Lourenco, P.B. (1996). Computational strategies for masonry structures, Delft University of Technology, Netherlands.

2. Lourenco, P.B. (1998). "Experimental and numerical issues in the modelling of the mechanical behaviour of masonry", *Structural Analysis of Historical Constructions II*, Barcelona.

3. Building Census, (2000). State Institute of Statistics Prime Ministry Republic of Turkey, Ankara, Turkey.

4. Erdik, M. and Aydınoğlu, N. (2003). "Earthquake vulnerability of buildings in Turkey", *Third International Symposium on Integrated Disaster Risk Management,* Kyota, 3-5 July 2003, Japan.

5. Rots, J.G. (1991). "Numerical simulation of cracking in structural masonry." *Heron,* 36(2) , 49-63.

6. Sayın, E. (2009). Nonlinear static and dynamic analysis of masonry structures, Fırat University, *Graduate School of Natural and Applied Sciences*, (in Turkish).

7. ANSYS. (2015). Finite Element Software. Houston, TX, USA: Swanson Analysis System. Inc.

8. MATLAB. (2014). The MathWorks, Inc.

Turkish Journal of Science & Technology
Volume 13(1), 61-64, 2018

The Effect of Centric Steel Braced Frames with High Ductility Level on the Performance of Steel Structures

Mustafa Ülker[1*], Ercan Işık[2], Mehmet Ülker[3]
[1]Bitlis Eren University, Technical Sciences VHS, Bitlis
[2]Bitlis Eren University Engineering, Faculty, Civil Engineering Department, Bitlis
[3]Fırat University, Engineering Faculty, Civil Engineering Department, Elazığ
[*] mulker444@gmail.com

(Received: 11.01.2017; Accepted: 07.03.2017)

Abstract

The basic functions expected from any structure are generally sufficient rigidity, ductility and stiffness. In this study, the effect of steel ducts with high ductility level on the performance of steel structures was investigated. For this purpose, calculations were made using five different types of central steel curtains for steel flues of any hospital building. Period, frequency, modal addition rates, displacement and rotation values are calculated and compared for each different central steel screen. The aim of the study is to be informed about the central steel slabs with high ductility level and to have information about which of the most suitable central steel slabs will be chosen.

Keywords: Ductility, High Ductility, Steel Structures, Performance, Steel Cross Braced Frame

Süneklik Düzeyi Yüksek Merkezi Çelik Perdelerin Çelik Yapıların Performansına Etkisi

Özet

Herhangi bir yapıdan beklenen temel işlevler genel olarak yeterli rijitlik, süneklik ve dayanımdır. Bu çalışmada süneklik düzeyi yüksek merkezi çelik perdelerin çelik yapıların performansına etkisi incelenmiştir. Bu amaçla herhangi bir hastane binasına ait çelik baca için beş farklı merkezi çelik perde çeşidi kullanılarak hesaplamalar yapılmıştır. Her bir farklı merkezi çelik perde için periyot, frekans, modal katkı oranları, yer değiştirme ve dönme değerleri hesaplanarak karşılaştırmalar yapılmıştır. Çalışmadaki amaç süneklik düzeyi yüksek merkezi çelik perdeler hakkında bilgi verilerek en uygun merkezi çelik perdenin hangisinin seçileceği hususunda bilgi sahibi olmaktır.

AnahtarKelimeler: Süneklik, Süneklik Düzeyi Yüksek, Çelik Yapılar, Performans, Çelik Perde

1. Introduction

Rigidity, ductility and strength must be sufficient to ensure that the earthquake loads are transmitted continuously and safely to the foundation of the earthquake loads as well as in each of the elements constituting the earthquake loads at the same time [1]. Adequate rigidity, strength and ductility are at the top of the principles considered in the design of earthquake-affected structures. In the regulation of the structural bearing system, the material strength, the ductility and stiffness concepts in the elements are important parameters [2]. These parameters need to be built into the structure.

Generally, ductile conveying systems are the foreground in the depressive structure design. However, it is emphasized that the selection of the regular carrier system in the horizontal and vertical sections and the encouragement to be shown in the junctions of the elements.

Ductility is defined as the extent of displacement of a section, of an element or of a carrier system, without significant change in external load, beyond the elastic limit, and the system ductility rate is proportional to the linear shape changes of the total shape changes in the displacement order. The result of the system

ductility ratio taking large values ensures that the structure can change its nonlinear shape sufficiently before migration.

Central crossed structures are very popular for medium height structures. Design and production are simple and the required horizontal stiffness and strength can be obtained with low cost. The horizontal stiffness of the central steel cross curtains is provided by vertically positioned cage beams. This lattice behaviour is obtained by crossing the column and the beams [3, 4, 5].

In this study, calculations were made in the case of using five different centric steel braced frames for a steel chimney belonging to a structure designed as a hospital building. The results were compared and recommendations were made.

2. Materials and Methods

Structural engineering is the science and art of designing and making, with elegance and economy, buildings, bridges, frameworks and other similar structures so that they can safely resist the forces to which they may be subjected [6]. The main purpose of structural design is to produce suitable structure. We must consider not only the initial cost, but also the cost of maintenance, damage and failure. Thus, the optimum design of a structure requires a general view on the total process [7].

The design of steel seismic resistant structures took a dramatic turn after the last Californian and Japanese events. The heavy damage observed as a result of these earthquakes was never before recorded in the history of building design. These events gave rise to a general effort all over the world to improve the seismic resistance of steel structures. A comprehensive program started to evaluate both the design specifications and detail rules. In this perspective, clear attention has been paid to the evaluation of local ductility erosion at the level of sections [2].

Ductility is a measure of the ability of a section, an element, or a carrier system to deform beyond the elastic limit, without significant change in external load. The numerical definition of the system ductility ratio is the ratio of the total shape change to the linear shape change during the displacement.

The two most important features of steel are energy absorption capacity under ductility and repeated inelastic loading. In terms of behavior against depression, horizontal load carrier systems of steel buildings are separated into two classes in terms of ductility level [2].

In Turkish Seismic Code, TEC-2007, based on their behaviour against seismic events, the lateral load bearing systems of the steel constructions are classified in two sections based on their ductility.

a. *Systems with High Ductility*

b. *Systems with Low Ductility*

based on this, the classifications are further divided to

• Frames with High Ductility,
• Shears with Steel Cross Beam Bars with High Ductility,
• Shears with Outer Steel Cross Beam Bars with High Ductility,
• Frames with Standard Ductility" and
• Shears with Steel Cross Beam Bars with Standard Ductility,
to form a list with five different titles with descriptions in seismic activity regulations.

In this study, centric steel braced frames with high ductility level are shown in Figure 1. The lateral load carrying capacity of these systems is large, along with their bending strength. Obviously, these shear wall systems can be interpreted as earthquake walls in a reinforced concrete structure.

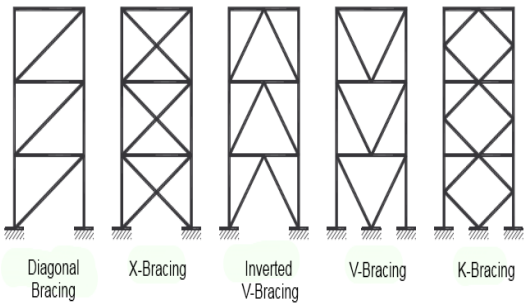

Figure 1. Centric Steel Braced Frames with High Ductility

As a numerical application, a steel chimney of hospital structure was analyzed. In the project, the steel chimney was transferred to the

rectangular truss system. The steel chimney has an area of 3,125 m^2 and a span of 2.5 m. The building height is 12 m. 150 * 150 * 5 mm was used for the structural system columns and 60 * 60 * 4 mm box profiles were used for the beams and bracing members (Figure 2).

Fe37 steel was used as material. In Fe37 steel σ_{saf} = 14.1 kN /cm^2, σ_{yield} = 24 kN /cm^2, σ_{weld} = 11 kN/cm^2 were taken.

In calculations, truss span L = 2,50 m, truss space L' = 1,25 m and number of truss were two.

The wind load is taken as q = 0.8 kN /m^2 from TS498 Specification [8].

The steel chimney was modelled and analyzed in the SAP2000 package program [8]. It is modelled as a 12-storey structure while modelling a 12 m high chimney system. Five different centric steel braced frames were used in this study. Centric steel braced frame types considered in the study are taken from the SAP2000 program and shown in Figure 3.

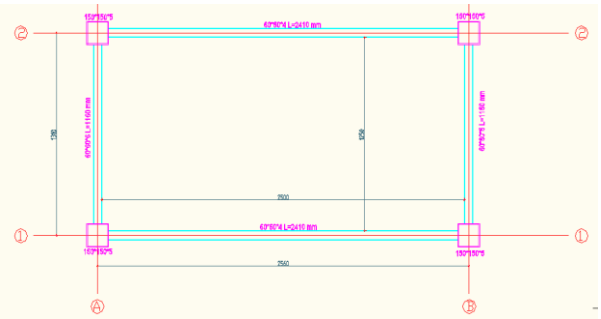

Figure 2. Steel Chimney Plan

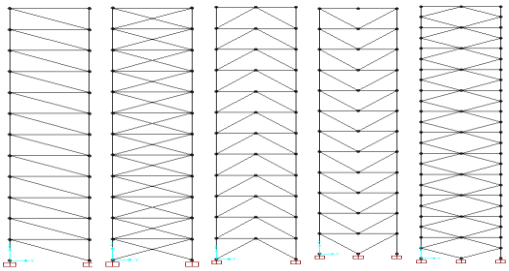

Figure 3. SAP2000 model of Centric Steel Braced Frames

In the dynamic analysis of the chimney system, the seismic parameters and function values shown in Figure 4 are entered. Period, frequency and eigen values are calculated for each braced type with these values.

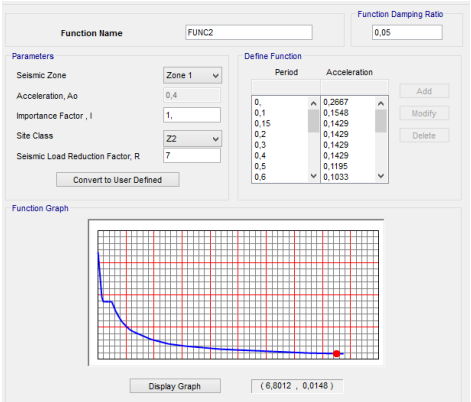

Figure 4. Seismic parameters in SAP2000 program

The displacements and rotations calculated in the SAP2000 program for the five different steel braced frames given in Figure 3 above are presented in Table 1.

Table 1. Displacements and rotations of centric steel braced frames

	Displacements [mm]			Rotations [rad]		
Frame Type	U_X	U_Y	U_Z	R_X	R_Y	R_Z
Diagonal Bracing	10,40	-0,10	-0,70	0,00000	0,00095	-0,00013
X-Bracing	8,90	0,27	-0,70	0,00000	0,00090	-0,00010
Inverted V-Bracing	8,20	0,00	-0,50	0,00000	0,00082	0,00000
V-Bracing	10,70	0,00	-0,70	0,00000	0,00100	0,00000
K-Bracing	8,90	0,00	0,60	0,00000	0,00090	0,00000

3. Results

In this study, the effects of five frames with high ductility level centric steel braced frames were investigated. Horizontal displacement values occurring in the building under lateral loads (earthquake and wind loads) are given in Table 1. The limitation given by the specifications is provided with confidence. That is, the frame with high ductility level centric steel braced frames is provided with a rigidity of about four times.

As shown in Table 1, the maximum lateral displacement is calculated as $u_x = 10.7$ mm at the top of the steel chimney. In the specifications, displacement is generally given as $u_x \leq \Delta_{max} = H/300$ limit. From here, if the constraint is checked, $u_x = 10.7$ mm $\leq \Delta_{max} = 12000/300 = 40$ mm will be seen. H/300 limit. From here, if the constraint is checked, $u_x = 10.7$ mm $\leq \Delta_{max} = 12000/300 = 40$ mm will be seen.

Nearly the same performance was achieved with five types of centric steel braced frames applied to lateral displacements.

With the classic Moment-resisting frames, larger lateral displacements are obtained and displacement limits cannot be achieved.

Finally, it is concluded that the systems providing the best limitations for earthquake performance and specifications are high ductility level centric steel braced frames.

References

1. Turkish Earthquake Code (2007), Turkish earthquake code-specification for structures to be built in disaster areas, Turkey.

2. Ülker, M., Işık, E., Bakır, D., Karaşin, İ.B., (2016). The effects of concrete strength to rigidity in RC buildings, *International Conference on Natural Science and Engineering (ICNASE-2016)*, Kilis, Turkey

3. ANSI/AISC 341-10 (2010), Seismic Provisions for Structural Steel Buildings, American Institute of Steel Construction, Chicago, Illinois, USA.

4. Denavit, M. D., Hajjar, J. F., Perea, T. and Leon, R. T. (2016). Seismic performance factors for moment frames with steel-concrete composite columns and steel beams, *Earthquake Engineering and Structural Dynamics*, **45(10)**, 1685-1703.

5. Montuori, R., Nastri, E. and Piluso, V. (2015), Seismic response of EB-frames with inverted Y-scheme: TPMC versus eurocode provisions, *Earthquakes and Structures*, **8(5)**, 1191-1214.

6. Petroski, H. J. (1985). Simple models for the stability of a crack in a cantilever beam subject to impact. *Engineering Fracture Mechanics*, **21(2)**, 377-381.

7 . Terán-Gilmore, A., Bertero, V. V., Youssef, N. F. (1996). Seismic rehabilitation of infilled non-ductile frame buildings using post-tensioned steel braces. *Earthquake spectra*, **12(4)**, 863-882.

8. TS-498 (1997), Design Loads for Buildings, Turkish Standards Institution, Ankara, Turkey.

9. SAP2000 (2015) Integrated Finite Elements Analysis and Design of Structures, Computers and Structures, Inc, Berkeley, CA.

Turkish Journal of Science & Technology
Volume 13(1), 65-68, 2018

Multy Variable Grey Method For Multy Point Deformation Analysis

Levent Taşçi[1*], Erkan Köse[2]
[1]Fırat University, Engineering Faculty, Geomatics Department, Elazığ, TURKEY
[2]Nuh Naci Yazgan University, Engineering Faculty, Industrial Engineering Department, Kayseri, TURKEY
[*]ltasci23@gmail.com

(Received: 15.02.2017, Accepted: 01.04.2017)

Abstract

Grey theory is one of the methods used to study uncertainty. The uncertain systems characterized by small sample and poor information are the study object of grey system theory. Multivariable grey prediction models are part of grey forecasting system. They are presented if there are mutual relations among the factors in the system. They believe that all the influencing factors are not independent of each other and should be regarded as a whole. In multivariable grey forecasting models, the future value of a variable is tried to be forecasted considering the other influential factors in the system. In this study, deformation consisting on the crest of a Dam is aimed to determine by using multivariable grey prediction models.

Keywords: Deformation, Grey method, Deformation predict

Çok Noktalı Deformasyon Analizi İçin Çok değişkenli Gri Sistem

Özet

Gri teori, belirsizliği incelemek için kullanılan yöntemlerden biridir. Sınırlı bilgi ve küçük örnekler ile karakterize edilmiş belirsiz sistemler, gri sistem teorisinin inceleme konusudur. Çok değişkenli gri tahmin modelleri gri tahmin sisteminin parçasıdır. Sistemdeki faktörler arasında karşılıklı ilişkiler varsa onlar temsil edilirler. Etkileyen faktörler birbirinden bağımsız değildir ve bir bütün olarak kabul edilmektedir. Çok değişkenli gri tahmin modeli, bir değişkenin gelecek değerini sistemdeki diğer etkilenen faktörleri göz önüne alarak tahmin etmeye çalışmaktadır. Bu çalışmada, çok değişkenli gri tahmin modeli kullanarak bir barajın kreti üzerinde oluşan deformasyonların tahmin edilmesi amaçlanmıştır.

Anahtar Kelimeler: Deformasyon, Gri yöntem, Deformasyon tahmini

1. Introduction

The evaluation of measurements and geodetic deformation measurements covers a significant portion of the engineering measurements. The monitoring of the movements of big engineering structures begins during the construction of the building and continues throughout life. The evaluation of the data and the interpretation phase of the results is the last and most important part of the deformation study. There are damages that can't be compensated by a wrong decision. As a result, it is necessary to be very careful and the results must be absolutely reliable. A large number of measures are needed to be able to give decisions about the behavior of constructions and to interpret the results. But, being able to make more accurate decisions with less data is very important in every circumstance.

The main strength of grey prediction is that it only requires short-term, current and limited data. Grey systems theory was first proposed by Deng [1]. Grey theory is one of the methods used to study uncertainty. The uncertain system characterized by small sample and poor information are the study object of grey system theories. The grey system puts each stochastic variable as a grey quantity that changes within a given range. It does differ from statistical analysis method to deal with the grey quantity. It deals directly with the original data and searches the intrinsic regularity of the data [2].

2. Materials and Methods

2.1. Multy Variable Grey Forecast Model

Multivariable grey prediction models are part of grey forecasting system. They are presented if there are mutual relations among the factors in the system. They believe that all the influencing factors are not independent of each other and should be regarded as a whole. In multivariable grey forecasting models, the future value of a variable is tried to be forecasted considering the other influential factors in the system. Because of high accuracy and easy application procedures, multivariable grey models have been applied to many areas in the literature [3-9].

MGM (1, N) model is set up by using Accumulating Generation Operator (AGO). The primitive data are subjected to the AGO to smooth the randomness of the data and to weaken the tendency of variation [10]. Assume that $X^{(0)} = \{x^{(0)}(1), x^{(0)}(2),\ldots., x^{(0)}(m)\}$ is an original, non-negative data series taken in consecutive order and at equal time intervals, then $X^{(1)}=\{x^{(1)}(1), x^{(1)}(2),\ldots., x^{(1)}(m)\}$ is called 1-AGO where $x^{(1)}(k)=\sum_{j=1}^{k} x^{(0)}(j)$, $k = 1, 2,\ldots..m$. Suppose that the number of variable is represented by n and the number of observation period by m, MGM(1,N) procedure is described in the following parts [10]. The first-order ordinary differential equation for the MGM (1, N) can be written as follows:

$$\begin{aligned}
\frac{dx_1^{(1)}}{dt} &= a_{11}x_1^{(1)} + a_{12}x_2^{(1)} + \ldots + a_{1m}x_m^{(1)} + b_1 \\
\frac{dx_2^{(1)}}{dt} &= a_{21}x_1^{(1)} + a_{22}x_2^{(1)} + \ldots + a_{2m}x_m^{(1)} + b_2 \\
&\ldots\ldots\ldots\ldots\ldots\ldots\ldots\ldots\ldots\ldots\ldots\ldots \\
\frac{dx_n^{(1)}}{dt} &= a_{n1}x_1^{(1)} + a_{n2}x_2^{(1)} + \ldots + a_{nm}x_m^{(1)} + b_n
\end{aligned} \quad (1)$$

marked as:

$$\frac{dX_1^{(1)}}{dt} = AX^{(1)} + B \quad (2)$$

The estimate value is obtained by using the least square method:

$$H=(L^TL)^{-1}L^TY \quad (3)$$

where

$$L=\begin{bmatrix}
\bar{x}_1^{(1)}(2) & \bar{x}_2^{(1)}(2) & \ldots & \bar{x}_n^{(1)}(2) & 1 \\
\bar{x}_1^{(1)}(3) & \bar{x}_2^{(1)}(3) & \ldots & \bar{x}_n^{(1)}(3) & 1 \\
\ldots\ldots & \ldots\ldots & \ldots\ldots & \ldots\ldots & \ldots\ldots \\
\bar{x}_1^{(1)}(m) & \bar{x}_2^{(1)}(m) & \ldots & \bar{x}_n^{(1)}(m) & 1
\end{bmatrix}$$

$$Y=\begin{bmatrix}
x_1^{(0)}(2) & x_2^{(0)}(2) & \ldots & x_n^{(0)}(2) \\
x_1^{(0)}(3) & x_2^{(0)}(3) & \ldots & x_n^{(0)}(3) \\
\ldots\ldots & \ldots\ldots & \ldots\ldots & \ldots\ldots \\
x_1^{(0)}(m) & x_2^{(0)}(m) & \ldots & x_n^{(0)}(m)
\end{bmatrix}$$

and $\bar{x}_i^{(1)}(k)=\frac{1}{2}(x_i^{(1)}(k)+x_i^{(1)}(k-1))$. The estimated value $\hat{A}$ and $\hat{B}$ can be obtained from H:

$$\hat{A}=\begin{bmatrix}
\hat{a}_{11} & \hat{a}_{21} & \cdots & \hat{a}_{n1} \\
\hat{a}_{12} & \hat{a}_{22} & \cdots & \hat{a}_{n2} \\
\ldots\ldots & \ldots\ldots & \ldots\ldots & \\
\hat{a}_{1m} & \hat{a}_{2m} & \cdots & \hat{a}_{nm}
\end{bmatrix}, \quad \hat{B}=\begin{bmatrix}
\hat{b}_1 \\ \hat{b}_2 \\ \ldots \\ \hat{b}_n
\end{bmatrix} \quad (4)$$

Then accumulated predicted values can be calculated by using Equation (4).

$$\hat{X}^{(1)}(k)=e^{\hat{A}(k-1)}(\hat{X}^{(1)}(1)+\hat{A}^{(-1)}\hat{B})-\hat{A}^{(-1)}\hat{B} \quad (5)$$

where

$$e^{\hat{A}(k-1)}=I+\sum_{i=1}^{\infty}\frac{\hat{A}^i}{i!}(k-1)^i \quad (6)$$

After the inverse first-order accumulated generation operation (1-IAGO), we obtain the sequence as $\hat{X}^{(0)}(k)=\hat{X}^{(1)}(k)-\hat{X}^{(1)}(k-1)$. The average fitting precision of the model is

$$\sigma^2=\frac{\sum_{i=1}^{n}V_i^TV_i}{nm} \quad (7)$$

where

$$v_ik=x_i^{(0)}(k)-\hat{x}_i^{(0)}(k), V_i=(v_i(1),v_i(2),\ldots v_i(m))^T \quad (8)$$

3. Application

Multy Variable Grey Prediction Model which is very efficient methodology in the situation of the limited number of the data has

been used to predict deformation in a dam. In this study 11 periods' real measurement values has been used to predict deformations depending on the water level for object points 11, 12 and 13 which are located in the middle of the rockfill dam crest. The first 6 periods' measurements have been used to establish multivariable grey prediction model, and the last six periods' measurement are used to test the accuracy of the proposed method. The original and predicted values are shown in Table 1. The outcomes also presented in Figure 1-3.

The 7th column in the Table 1 shows predicted values for object point 11 depending on the water level. 8th and 9th columns show the predicted values when we apply grey prediction procedure for two object points at the same time. The last three columns show the results if we apply prediction procedure for all object points in this study.

Table 1. Original and predicted values

Years	Period	Heights of Point AS11 (m.)	Heights of Point AS12 (m.)	Heights of Point AS13 (m.)	Dam Lake Water Level (m.)	Multy Variable					
						MGM(1,2)	MGM(1,3)		MGM(1,4)		
						AS11	AS11	AS12	AS11	AS12	AS13
						Predicted value	Predicted value	Predicted value	Predicted value	Predicted value	Predicted value
13.01.1975	1.Period	851.659	851.727	851.796	803.960	851.660	851.659	851.727	851.659	851.727	851.796
21.03.1975	2.Period	851.653	851.721	851.791	805.290	851.620	851.555	851.623	851.6049	851.673	851.7416
24.06.1976	3.Period	851.540	851.605	851.662	842.090	851.564	851.391	851.456	851.475	851.539	851.597
01.06.1977	4.Period	851.506	851.568	851.623	836.210	851.532	851.299	851.361	851.413	851.475	851.531
24.03.1978	5.Period	851.493	851.554	851.610	828.040	851.411	851.231	851.292	851.379	851.441	851.496
20.11.1979	6.Period	851.502	851.563	851.618	828.500	851.501	851.173	851.234	851.356	851.417	851.472
30.07.1980	**Predicted.1**	**851.448**	**851.508**	**851.563**	**841.400**	**851.471**	**851.115**	**851.176**	**851.335**	**851.396**	**851.451**
04.03.1982	**Predicted.2**	**851.398**	**851.456**	**851.514**	**834.290**	**851.441**	**851.057**	**851.118**	**851.315**	**851.377**	**851.432**
17.05.1982	**Predicted.3**	**851.402**	**851.496**	**851.514**	**844.350**	**851.411**	**850.995**	**851.056**	**851.295**	**851.357**	**851.412**
15.11.1984	**Predicted.4**	**851.369**	**851.420**	**851.479**	**831.830**	**851.381**	**850.941**	**851.002**	**851.276**	**851.338**	**851.392**
14.05.1985	**Predicted.5**	**851.361**	**851.419**	**851.475**	**835.210**	**851.350**	**850.881**	**850.942**	**851.256**	**851.319**	**851.373**

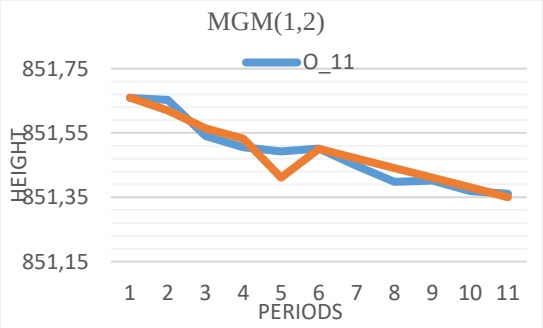

Figure 1. Multivariable Grey Model (1, 2)

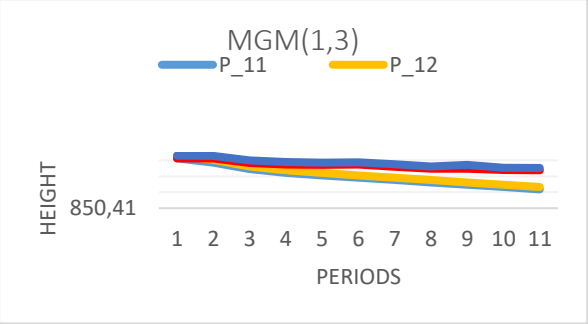

Figure 2. Multivariable Grey Model (1, 3)

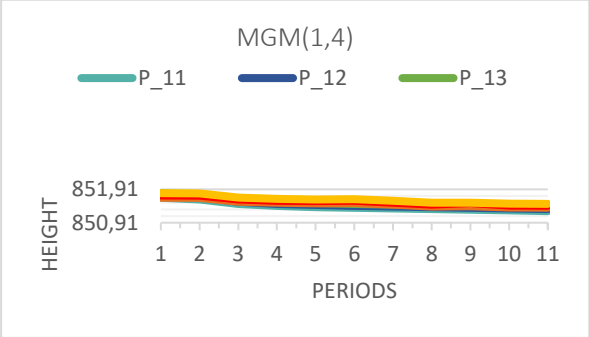

Figure 3. Multivariable Grey Model (1, 4)

4. Results

The Grey System Theory provides a solution to the problem even in the case of very limited number of data. The Multi Variable Grey Prediction Model can be used to predict deformation not only for one point but also for many points at the same time. In this study deformation level of the three different object points in a dam crest has been tried to be forecasted depending on the water level by multi variable grey model. Results show that there are great consistency between grey prediction values and real values. Based on the outcomes it is possible to conclude that grey prediction model is a very reliable prediction model in limited data circumstances.

5. References

1. Deng, J.L. (1982). Control problems of grey systems. *S.ystems and Control Letters*, **1**(5): 211–215.
2. Huang, Y.P. and C.C. Huang, C.C. (1996). The integration and application of fuzzy and grey modeling methods. *Fuzzy Sets and Systems*, **78**(1): 107-119.
3. T. Tien. (2005). The indirect measurement of tensile strength of material by the grey prediction model GMC(1,n). *Measurement Science and Technology*, **16**(6): 1322–1328.
4. Wu, W.Y. and Chen, S.P. (2005). A prediction method using the grey model GMC(1,n) combined with the grey relational analysis a case study on internet access population forecast. *Applied Mathematics and Computation*, **169**(1): 198–217.
5. Hsu, L. (2009). Forecasting the output of integrated circuit industry using genetic algorithm based multivariable grey optimization models. *Expert Systems with Applications*, **36**(4): 7898–7903.
6. Hsu, L. and Wang, C. (2009). Forecasting integrated circuit output using multivariate grey model and grey relational analysis. *Expert Systems with Applications*, **36**(2): 1403–1409.
7. Luo,Y.X., Wu,X., Li,M. and Cai, A.H. (2009). Grey dynamic model GM(1,N) for the relationship of cost and variability. *Kybernetes*, **38**(3): 435–440.
8. Tien, T.L. (2012) A research on the grey prediction model GM(1,n). *Applied Mathematics and Computation*, **218**(9): 4903–4916.
9. Niu, W., Zhai, Z., Wang, G., Cheng, J. and Guo, Y. (2011). Adaptive multivariable grey prediction model. *Journal of Information Computer Science*, **8**(10): 1801-1808.
10. Hui, H., Li, F., and Shi, Y. (2013). An Optımal Multı-Varıable Grey Model for Logıstıcs Demand Forecast. *International Journal of Innovative Computing, Information and Control*, **9**(7): 2907-2918.

Turkish Journal of Science & Technology
Volume 13(1), 69-75, 2018

Adopted Material Properties of Historical Masonry Structures for Finite Element Models: Mosques and Bridges

Onur Onat[1*], Burak Yön[1]
[1]Munzur University Engineering Faculty Civil Engineering Department Tunceli, Turkey
[*]onuronat@munzur.edu.tr

(Received: 07.01.2017; Accepted: 07.03.2017)

Abstract

This paper aims to present adopted material properties of masonry elements to historical mosque and bridge structures. The importance of this study is to adopt correct material properties with reliable reference according to material types and structure types.

Keywords: material properties; historical structures; historical mosques; historical bridges.

Sonlu Elemanlar Modelleri için Tarihi Yığma Yapılarda Kullanılan Malzeme Özellikleri: Camiler ve Köprüler

Özet

Bu çalışmada, yığma yapı ile yapılmış camii ve köprülerde kullanılan malzeme özelliklerinin sunulması amaçlanmıştır. Bu çalışmanın önemi, yığma yapılarda kullanılan malzeme özelliklerini güvenilir kaynaklara dayandırarak malzeme çeşidine ve yapı tipine göre sınıflandırarak sunmaktır.

Anahtar Kelimeler: malzeme özellikleri, tarihi yapılar, tarihi camiler, tarihi köprüler

1. Introduction

Historical structures are the most important part of civilization where constructed. Therefore, these cultural heritages of the urban population should be protected through centuries against external extreme loads. Conservation of cultural heritages are commonly considered as suitable restoration. However, with developing numeric analysis tools, it is possible to estimate global behavior of a historical structures available and after restoration situation under severe loads like earthquake. Structural characteristics of a historical monument mostly depend on the availability of local construction materials during construction era [1]. Moreover, it is difficult to determine the engineering properties of materials adopted to the historical structures due to the lack of experimental data and forbidden destructive test by authorities [2]. For this reason, indirect methods are developed to evaluate historical structures to reveal information related to available conditions. These indirect assessment methods are based on visual inspection, geometrical and crack pattern survey, surface decay mapping, radar, geoelectric and ultrasonic testing. Listed indirect methods are not convenient for the assessment of historical masonry structure alone. In addition, these methods cannot be substituted by destructive testing [3]. These are necessary to understand the damages and their causes and carry out a first interpretation of the phenomena [4].

During the analytical modelling, defining incorrect or uncertain material properties causes unavoidable wrong results. For a typical masonry heritage, the most difficult step is defining input parameter to quantify the material properties of masonry and mortar assembly. When developing a (FE) models, especially for historic masonry structure, it is possible to define imprecise input parameters that can result in unrealistic models and erroneous solutions [5]. Indefinite references or insufficient material data force researcher to use wide range of data with lower boundary and upper boundary [6]. The aim of using upper and lower boundary material data is to adapt randomly selected engineering property due to insufficient material data for

modelled structure. The reliability of the selected material properties depends mostly on model calibration of the FE model. Basic philosophy of model calibration is to compare dynamic identification test result of investigated structure with FE model of the same structure on the base of natural vibration period and frequencies. The success of model calibration depends not only on selecting the correct comparative quantitative but also in updating the correct quantitative. Thus, if the extreme use of the FE model is to assess damage in historical structures, the engineering properties must be adapted well to represent linearity and nonlinearities. Model calibration includes engineering judgment and self-intuition about selecting calibration parameters. Moreover, the unforeseen dependencies or correlations of parameters possibly arise among the calibrated inputs. If these dependencies or correlations are strong, this will raise the problem of the calibration of one parameter compensating for imprecision in another [5]. Besides, purchasing accelerometer always not possible due to extreme cost of test set up and non-destructive application. For listed reason above, it is very important to define certain and robust material properties for investigated historical structures.

This study presents 14 different study composed of mosques and bridges.

2. Structure Types

2.1. Mosques

Mosques are one of the most prominent religious structures in the history. Nearly all dominated sultans let to construct mosque to shown power. Many of the available mosques are still in use. For this reason, response of their behavior against external loads needs to be assessed. Koçak and Köksal (2010) investigated seismic behavior of Little Hagia Sophia with FE modelling. Adopted material properties were suited with destructive and non-destructive methods [7] and addressed to Aköz and Yüzer (1995) [8]. Teomete and Aktaş (2010) implemented destructive tests on historical masonry and brick elements of an historical Urla Kamanlı mosque in İzmir Turkey [9]. Demir and İlki (2014) studied on material properties and characterization of single layer and multi-layer Küfeki stone in other words limestone which is commonly used to construct mosques [10]. Demir and İlki (2014) characterized the multi layered Küfeki stone in other words limestone according to sample dimensions 40x30 cm, 40x26 cm and 40x20 cm respectively [10]. Altunışık et al. (2015) assessed the performance of Kaya Çelebi Mosque in Turkey. For this purpose, dynamic modal analysis and seismic spectral analysis were performed on model [11]. Material properties were adopted by Altunışık et al. (2015) addressed to Can et al. (2012) [12], Dal-Cin and Russo (2014) [2014] and Saloustros (2015) [14]. Cakir et al. (2015) modelled and analyzed Erzurum Lala Pasha Mosque. For this purpose, firstly material characterization was implemented and then FE model was prepared. Compressive strength and tensile strength of materials were obtained from experimental characterization. However, elasticity modulus and density adapted from literature [15]. Nohutcu et al. (2015) studied Hafsa Sultan Mosque in Turkey. In their study, ultrasonic pulse velocity was used to obtain mechanical properties of granite and stone. Homogenization approach was used to determine mechanical properties of FE model [16]. Nohutcu et al. (2015) obtained mechanical properties by using ultrasonic pulse velocity test and then these values evaluated as bigger to adapt complete model of masonry elements [16]. Güllü and Karabekmez (2016) investigated seismic behavior of 125 years old Gaziantep Kurtuluş mosque. Material properties were adopted from literature [17]. Elasticity modulus, poisson ratio and compressive strength values were obtained from predicting with genetic algorithm by Baykasoğlu et al. (2008) [18]. Tensile strength value is adopted like 1/fc. İlerisoy and Soyluk (2012) studied on Şehzade Mehmet mosque to assess seismic performance [19]. Adopted material properties was addressed to similar studies by Kaya et al. (1998) [20]. Addressed reference contains a numeric study related to Süleymaniye mosque. Altunışık et al. (2016) studied on seismic safety of Kaya Çelebi mosque [21]. Material properties were adopted from Can et al. (2012) [12], Dan Cin and Russo (2014) [13] and Saloustros et al. (2015) [14]. Mangia et al. (2016) assessed seismic performance of Eltihatun Mosque located in Tunceli province.

Adopted material properties obtained from literature on the base of medium hard masonry elements [22]. These properties can be seen in Table 1. There are eight mosques and experimental studies related to mosque. Material properties of these investigated mosques can be seen in Table 1.

Table 1. Adopted material properties to mosques

Author(s)	Age and Material Properties				
	Age	***Density (kg/m^3)***	***Young's Modulus (MPa)***	***Compressive Strength (MPa)***	***Tensile Strength (MPa)***
Koçak and Köksal (2010)	536	NA	10000	10	1
Teomete and Aktaş (2010)	14th century	1700	2700	4.25	0.425
Demir and İlki (2014)	15th century	2050	2615	7.91	1.6
Altunışık et al. (2015)	1660	2000	1600	0.3	NA
Cakir et al. (2015)	1562	1900	350	17.49	2.69
Nohutcu et al. (2015)	16th century	2200	1500 (1210)	7.42	0.74
Güllü and Karabekmez (2016)	1892	2500	25000	40	4
İlerisoy and Soyluk (2012)	1548	2190 (Arch), 2000 (Dome)	8500 (Arch), 3000 (Dome)	NA	NA
Altunışık et al (2016)	1663	2400	1200	NA	NA
Mangia et al. (2016)	1252	2200	1500	3	0.15

The numbers in bracket demonstrates calibrated parameters

2.2. Bridges

There are many historical bridges either restored or non-restored in our country. A few of these bridges were studied by researchers. Hacıefendioğlu et al. (2015) assessed seismic behavior of masonry arch Kurt bridge in Turkey against blast induced ground motion [23]. Material properties of bridge adopted from Sevim et al. (2011) [24]. Güllü and Jaf (2016) modelled a historical arch bridge with two different boundary condition approach. One of them is soil structure interaction and other of them is with fixed base boundary condition [25]. Material properties were adopted from similar study by Ural and Doğangün (2007) [2]. However, Ural and Doğangün estimated material properties on the base of their experiences for the same arch bridge. Altunışık et al. (2015) modelled a historical arch bridge called as Göderni bridge. Adopted material properties were obtained from laboratory test results. Sayın (2016) performed nonlinear dynamic analysis on a historical masonry arch bridge called as Nadir bridge [27]. The source of adopted material parameters is addressed to literature. Sevim et al. (2011) presented earthquake response of historical masonry arch bridge [24]. Adopted material properties were referenced to similar studies by Frunzio et al. (2001) [28], Toker and Unay (2001) [29] and Brencich and Sabia (2008) [30].

Table 2. Adopted material properties to bridge

Author(s)	Age and Material Properties				
	Age	***Density (kg/m^3)***	***Young's Modulus (MPa)***	***Compressive Strength (MPa)***	***Tensile Strength (MPa)***
Hacıefendioğlu et al. (2015)	13th century	2140.7	3000	NA	NA
Güllü and Jaf (2016)	18th century	2354, 2353, 1961	3000, 2500, 1000	NA (Arch), NA (Spandrel), NA (Parapet)	NA
Altunışık et al. (2015)	19th	2000	5000 (Arch),	NA	NA

Author(s)	Age and Material Properties				
	Age	***Density (kg/m³)***	***Young's Modulus (MPa)***	***Compressive Strength (MPa)***	***Tensile Strength (MPa)***
	century		3000 (Abutment)		
Sayın (2016)	1569	2300, 2200	2500 (Arch), 2000 (Spandrel)	NA	0.5, 0.4
Sevim et al. (2011)	19th century	1600, 1400	3000 (Arch), 2500 (Side Wall)	NA	NA

3. Statistical Analysis

This section contains statistical evaluation and correlation of Young's modulus and compressive strength of historical masonry material. The most common and used masonry materials are limestone and brick. Statistical evaluations are performed on these materials to easily obtain missing parameters with a known parameter.

3.1. Limestone

Limestone is of the most used material among historical masonry structures. Even if material properties are more abundant while compared with other materials, abrasion factor and environmental interference change the material properties of this material based on local conditions.

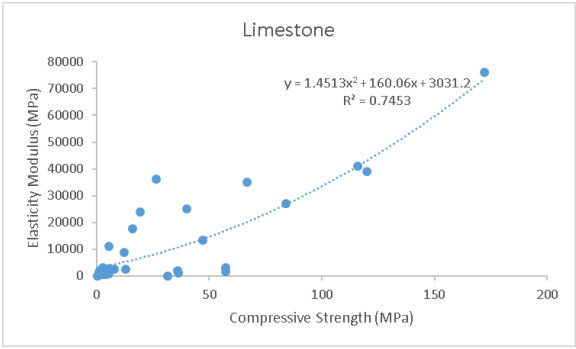

Figure 1. Young's modulus versus compressive strength of Limestone

As seen from the Figure 1, correlation between the Young's modulus and compressive strength is polynomial. This correlation can be defined with an equation indicated in the figure above. The confidence percent is 74.53%. This equation is proposed to determine unknown parameter with known one.

3.2. Brick

Brick is one another abundant material after stone masonry. One of the most important property of brick is more consistent than stone masonry. Because, while plotting the data and fitting the best curve to this material type, none of the data was ignored.

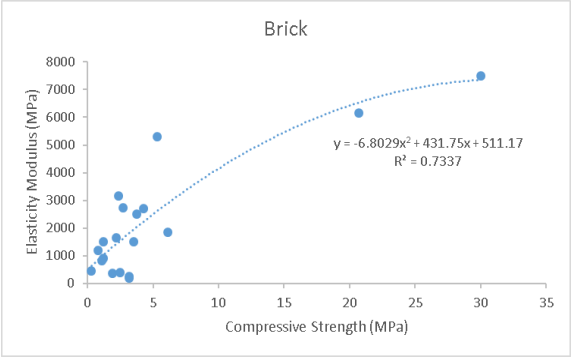

Figure 2. Young's modulus versus compressive strength of Brick

The best fitted curve between the Young's modulus and compressive strength is polynomial as seen in Figure 2. Confidence percent is 73.37%.

4. Discussion

After the FE modelling procedure, one of the most important key point is to define correct parameter of historical heritage. Many researchers are missing a few important parameters like poison ratio, compressive strength or tensile strength. However, each parameter has own importance. Ural and Doğangün (2007) [2] investigated changing mechanical properties of infill and arch material parameters on the seismic performance of historical masonry arch bridge. However, Ural and Doğangün adopted material properties on the base of their experiences and considered intervention of material by external natural events. Güllü and Jaf (2016) [25] modelled a historical masonry arch bridge with soil structure interaction (SSI) and without SSI and then addressed Ural and Doğangün related to material properties of Mataracı bridge located at Trabzon. But, Ural and Doğangün performed sensitivity analysis on the base of masonry arch and infill material properties. Moreover, Ural and Doğangün considered natural intervention on mechanical properties of material [2]. Güllü and Karabekmez (2016) obtained material properties of investigated mosque by prediction with genetic algorithm on the base of in-situ testing [17]. Mangia et al. (2016) obtained material properties from literature referenced to medium strong masonry elements. Indeed, this assumption does not reflect actual behavior of the historical mosque [22]. Sayın (2016) implemented a numeric study on a historical Nadir bridge to assess seismic performance of the bridge [27]. Sayın indicated material properties of historical bridge to reliable references in the mentioned study. One another example is randomly selected material properties on the base of self-experience like Ramos et al. (2010) performed model calibration on historical masonry tower before starting structural analysis [31]. However, randomly 1000 MPa elasticity modulus was selected for FE model of the historical tower. This random selection was implemented on the base of self-experience and high confidence of dynamic identification. However, due to high instrumentation cost, dynamic identification is always not possible for researcher.

5. Conclusions

The purpose of this paper is to present material properties of historical structures. Mosques and bridges were considered for this study. Moreover, this study limited with national historical structures. Recently, there are numerous study revealed by investigators that seek for performance evaluation of historical structures. However, reliability of these investigations depends completely on the adopted material properties of the investigated structure. External intervention is nearly impossible on historical monuments in order not to disturb available property of value. For this purpose, reliable references are required especially for numeric model of the investigated monument. Correct material properties that adapted to numeric model is indispensable to implement risk assessment of any type of historical structure. This study collected all material properties of investigated historical structures either with destructive or non-destructive testing evaluation. Moreover, this study includes experimental tests to determine engineering properties of the historical element or structure. This paper has contributions to the literature on the base of listed aspects;

1. Before performing a numerical assessment of a historical structure, precise material properties should be adopted to the structure with the same material and the structural type.
2. In an investigated structure, material properties of all element type cannot be the same properties. Vault, arch and wall element of the same model may contain different material properties even if these element type composed of the same material.
3. Adopted material properties can be calculated by different approaches like homogenization. This calculated property reflects overall behavior of brick and mortar unit. While calculating these parameters, selected material properties of the unit and mortar should

be selected on the base of individual characterized elements.

4. Adopted material properties should simulate structural intervention and restoration well.

6. References

1. Dogangun, A., Sezen, H. (2012) "Seismic vulnerability and preservation of historical masonry monumental structures". Earthquake and Structures, **3**(1), 83-95.

2. Ural A, Dogangun A, (2007) "Arch bridges in East Blacksea Region of Turkey and effects of infill materials on a sample bridge". In: Lourenco PB, Oliveira DV, Portela A (eds) ARCH'07–5th international conference on arch bridges, proceedings of the 5th international conference on arch bridges, 12–14 September, Madeira, pp 543–550.

3. Wenzel, F., Kahle, M., (1993) Indirect methods of investigation for evaluating historic masonry. IABSE reports, Zurich

4. Binda, L., Tiraboschi, C. (1999) Flat-Jack Test: A slightly destructive technique for the diagnosis of brick and stone masonry structures. International Journal for Restoration of Buildings and Monuments, **5**(5), 449-472.

5. Atamturktur, S., Laman, J. A. (2012) "Finite element model correlation and calibration of historic masonry monuments: review." The Structural Design of Tall and Special Buildings, **21**(2), 96-113.

6. Atamturktur, S., Bornn, L., Hemez, F. (2011) "Vibration characteristics of vaulted masonry monuments undergoing differential support settlement". Engineering Structures, **33**(9), 2472-2484.

7. Koçak, A., Köksal, T. (2010) "An example for determining the cause of damage in historical buildings: Little hagia sophia (Church of St. Sergius and Bacchus)–Istanbul, Turkey. Engineering Failure Analysis, **17**(4), 926-937.

8. Akoz, F., Yüzer, N. (1995) "Investigation of Material Properties of Kucuk Ayasofya Mosque-Sts Sergius and Bacchus of Istanbul". WIT Transactions on The Built Environment, 16.

9. Teomete, E., Aktaş, E. (2010) "Structural analyses and assessment of historical Kamanlı Mosque in Izmir", Turkey. Journal of performance of constructed facilities, **24**(4), 353-364.

10. Demir, C., Ilki, A. (2014) "Characterization of the materials used in the multi-leaf masonry walls of monumental structures in Istanbul, Turkey." Construction and Building Materials, **64**, 398-413.

11. Altunisik, A. C., Kanbur, B., Genc, A. F. (2015) "The effect of arch geometry on the structural behavior of masonry bridges". Smart Structures and Systems, **16**(6), 1069-1089.

12. Can, H., Kubin, J., Unay, A. I. (2012) "Seismic behavior of historical masonry buildings with irregular geometry". Journal of the Faculty of Engineering and Architecture of Gazi University, **27**(3), 679-686.

13. Dal Cin, A., Russo, S. (2014) "Influence of the annex on seismic behavior of historic churches". Engineering Failure Analysis, **45**, 300-313.

14. Saloustros, S., Pelà, L., Roca, P., and Portal, J. (2015) "Numerical analysis of structural damage in the church of the Poblet Monastery". Engineering Failure Analysis, **48**, 41-61.

15. Cakir, F., Seker, B. S., Durmus, A., Dogangun, A., Uysal, H. (2015) "Seismic assessment of a historical masonry mosque by experimental tests and finite element analyses". KSCE Journal of Civil Engineering, **19**(1), 158-164.

16. Nohutcu, H., Demir, A., Ercan, E., Hokelekli, E., Altintas, G. (2015) "Investigation of a historic masonry structure by numerical and operational modal analyses". The Structural Design of Tall and Special Buildings, **24**(13), 821-834.

17.Güllü, H., Jaf, H. S. (2016) "Full 3D nonlinear time history analysis of dynamic soil–structure interaction for a historical masonry arch bridge". Environmental Earth Sciences, **75**(21), 1421.

18. Baykasoğlu, A., Güllü, H., Çanakçı, H., & Özbakır, L. (2008) "Prediction of compressive and tensile strength of limestone via genetic programming". Expert Systems with Applications, **35**(1), 111-123.

19. İlerisoy, Z. Y., Soyluk, A. (2012) "Impact of shallow earthquakes on the Sehzade Mehmet Mosque". Gradevinar, **64**(9), 735-740.

20. Kaya, S. M., Aydinoglu, M. N., Erdik, M., Yuzugullu, O. (1998) "Determination of Dynamic Characteristics of Suleymaniye Mosque by Analytical and Experimental Methods". Compatible Materials for the Protection of European Cultural Heritage. Istanbul, 56-68.

21. Altunisik, A. C., Bayraktar, A., Genc, A. F. (2016) "A study on seismic behaviour of masonry mosques after restoration". Earthquakes and Structures, **10**(6), 1331-1346.

22. Mangia, L., Ghisassi, B., Sayın, E., Onat, O., Lourenço, P. B., (2016) "Pushover Analysis of Historical Elti Hatun Mosque", 12th International Congress on Advances in Civil Engineering, Boğaziçi University, Istanbul

23. Hacıefendioğlu, K., Banerjee, S., Soyluk, K., Alpaslan, E. (2015) "Stochastic dynamic analysis of a historical masonry bridge under surface blast-induced multi-point ground motion". Stochastic Environmental Research and Risk Assessment, **29**(5), 1275-1286.

24. Sevim, B., Bayraktar, A., Altunişik, A. C., Atamtürktür, S., Birinci, F. (2011) "Finite element model calibration effects on the earthquake response of masonry arch bridges". Finite Elements in Analysis and Design, **47**(7), 621-634.
25. Güllü, H., Jaf, H. S. (2016) "Full 3D nonlinear time history analysis of dynamic soil–structure interaction for a historical masonry arch bridge". Environmental Earth Sciences, **75**(21), 1421.
26. Altunisik, A. C., Kanbur, B., Genc, A. F. (2015) "The effect of arch geometry on the structural behavior of masonry bridges". Smart Structures and Systems, **16**(6), 1069-1089.
27. Sayin, E. (2016) "Nonlinear seismic response of a masonry arch bridge". Earthquakes and Structures, **10**(2), 483-494.
28. Frunzio, G., Monaco, M., Gesualdo, A. (2001) "3D FEM analysis of a roman arch bridge". Historical constructions, 591-598.
29. Toker, S., Ünay, A. I. (2004) "Mathematical modeling and finite element analysis of masonry arch bridges". Gazi University Journal of Science, **17**(2), 129-139.
30. Brencich, A., Sabia, D. (2008) "Experimental identification of a multi-span masonry bridge: The Tanaro Bridge". Construction and Building Materials, **22**(10), 2087-2099.
31. Ramos, L. F., Marques, L., Lourenço, P. B., De Roeck, G., Campos-Costa, A., Roque, J. (2010) "Monitoring historical masonry structures with operational modal analysis: two case studies". Mechanical Systems and Signal Processing, **24**(5), 1291-1305.

Turkish Journal of Science & Technology
Volume 13(1), 77-85, 2018

Effects of the Combined Use of Styrene-Butadiene-Styrene and Gilsonite in Bitumen Modification on the Stiffness and Thermal Sensitivity of Bitumens

Özge Erdoğan Yamaç[1]*, Mehmet Yılmaz[1], Baha Vural Kök[1]
[1]Firat University Faculty of Engineering, Department of Civil Engineering, Elazig, Turkey
ozgeerdogan@firat.edu.tr

(Received: 08.01.2017; Accepted: 28.02.2017)

Abstract

In the present study, the effects of styrene-butadiene-styrene (SBS) and American gilsonite (AG) on the stiffness and thermal sensitivity of bituminous binders were investigated in bitumen modification. Şanlıurfa province was chosen as the application field. It was determined that 18% AG and 5% SBS additives should be used separately to obtain the adequate binder for Şanlıurfa province. It was also determined that 13% AG with 2% SBS, 10% AG with 3% SBS and 6% AG with 4% SBS were required to obtain binders with the same performance level. Penetration, softening point and rotational viscometer tests were conducted on neat and modified bitumen to determine the consistency of binders. Furthermore, thermal sensitivities of binders were determined from penetration index and penetration viscosity number values. It was determined that all additives increased the consistency of the binders, the most effective additive type and ratio was 18% AG on penetration values, and all additives had similar effects on the softening point and viscosity values. In addition, it was determined that the temperature susceptibility was reduced with additive use and the most effective contribution came from 5% SBS.

Keywords: Bitumen, Styrene-butadiene-styrene, American Gilsonite, Consistency, Temperature susceptibility.

Bitüm Modifikasyonunda Stiren-Butadien-Stiren ve Gilsonit'in Birlikte Kullanımının Bağlayıcıların Sertliği ve Isı Hassasiyetine Etkileri

Özet

Bu çalışmada, bitüm modifikasyonunda stiren-butadien-stiren (SBS) ve Amerikan Gilsoniti'nin (AG) bitümlü bağlayıcıların sertliği ve ısı hassasiyeti üzerindeki etkileri araştırıldı. Uygulama alanı olarak Şanlıurfa ili seçildi. Şanlıurfa ili için uygun bağlayıcı elde etmek amacıyla % 18 AG ve % 5 SBS katkı maddelerinin ayrı ayrı kullanılması gerektiği tespit edildi. Ayrıca aynı performans seviyesine sahip bağlayıcılar elde etmek için % 2 SBS ile % 13 AG, % 3 SBS ile % 10 AG ve % 4 SBS ile % 6 AG kullanılması gerektiği tespit edildi. Bağlayıcıların kıvamını belirlemek için saf ve modifiye bitümler üzerinde penetrasyon, yumuşama noktası ve dönel viskozimetre deneyleri yapıldı. Ayrıca bağlayıcıların ısı hassasiyetleri, penetrasyon indeksi ve penetrasyon viskozite sayısı değerleri yardımıyla belirlendi. Tüm katkı maddelerinin bağlayıcıların kıvamını arttırdığı, penetrasyon değerleri üzerinde en etkin katkı türü ve oranının % 18 AG olduğu ve tüm katkı maddelerinin yumuşama noktası ve viskozite değerleri üzerinde benzer etkilere sahip olduğu tespit edildi. Buna ek olarak, ısı hassasiyetinin katkı kullanımı ile azaldığı ve en etkin katkının % 5 SBS olduğu saptandı.

Anahtar Kelimeler: Bitüm, Stiren-butadien-stiren, Amerikan gilsonit, Kıvam, Isı hassasiyeti.

1. Introduction

Bitumen obtained by distillation from crude oil is produced from the residues of this process. Bituminous binders are a complex mixture of organic particles containing aliphatic, aromatic and naphthenic hydrocarbons and could be divided into two basic groups, namely maltenes and asphaltenes [1]. The asphaltenes are dispersed in the maltene phase with a continuous phase and the structure that forms the bitumen structure includes saturates (S), aromatics (A), resins (R) and asphaltenes (AS). The complexity, aromaticity and molecular weight of the fractions are ranked as follows: S < A < R < As [2, 3].

The bitumen exhibits binding properties that binds aggregates due to their cohesive properties

in road applications. The bituminous binder also prevents the aggregate particles from falling apart under traffic loads, improves the driving comfort with the smooth surfaces they create, increases mixture stability with its cohesion, and provides impermeability by filling the voids in the mixture. Bituminous binders have a great effect on mixture performance, even though they are used at a low rate of 5 to 7% by weight in hot mix asphalts [4].

Various additives (modifiers) have been used to improve the properties of binders for a long time, thereby increasing the service life of the pavement by preserving its performance for a longer period of time. The additives used for this purpose vary depending usage. To increase the resistance of bitumens and bituminous hot mixes to heat and traffic loads, generally additive materials of polymer origin are added. Mostly Styrene-Butadiene-Styrene (SBS) Block Copolymers are used in these additives. Several previous studies determined that SBS improves the fracture resistance at low temperatures, and the generation of rutting and fatigue resistance at high temperatures [5-9].

Gilsonite is a solid hydrocarbon mineral available in nature with a potential to improve physical and chemical properties of bitumen [10]. Gilsonite can rapidly dissolve in bitumen since it is a kind of natural asphalt binder [11]. Gilsonite offers different advantages over other modifiers such as easy mixing and compatibility with asphalt mixtures [12]. Economically significant Gilsonite mineral is found in the United States and Iran.

When Gilsonite is added to the bitumen, the penetration of the bitumen decreases, its viscosity increases and as a result, a harder modified bitumen is obtained. Mixtures prepared with Gilsonite modified bitumens have higher stability, lower permanent deformation and temperature susceptibility, as well as higher resistance to stripping caused by water when compared to mixtures prepared with unmodified bitumen [13-16].

Several previous studies reported that storage stability of SBS modified bitumen is low, even though the rheological properties of SBS modified bitumen are superior to that of the neat binder [17, 18]. Furthermore, SBS is also a more expensive additive compared to Gilsonite. Using SBS and Gilsonite together in bitumen mixture instead of using only SBS-modified bitumen, so that the resulting performance would be the same, provides economic benefits [19]. The combined use of the two additives has been common during recent years and aimed to remove the negative aspects of the additives and to increase the rheological properties of the bituminous binders, and thus, increasing the performance of the BHMs in different aspects [20-23].

In the present study, the effect of the combined use of SBS and AG in bitumen modification on consistency and temperature susceptibility of the bituminous binders were examined. For this purpose, penetration, softening point and rotational viscometer experiments were conducted with neat and five different modified bitumen samples. Furthermore, using penetration and softening point values, penetration index value, which is the indicator of temperature susceptibility, is determined. Thus, the effect of two different additives on the consistency and thermal sensitivity of the bituminous binders was determined.

2. Material and Method

The binder design was conducted with the Superpave method in the study. Şanlıurfa, the warmest province in Turkey, was selected as the application field. The information on the highest temperature values for 7 consecutive days and the coldest day during the last 21 years was obtained from Regional Meteorology Directorate and it was assumed that the design traffic estimate was 3-30 million standard axle load equivalent and there was low-speed traffic (<50 km / Hour). It was determined that the binder class that should be used in the design criteria determined for Şanlıurfa was PG 76-10.

In the present study, Styrene-Butadiene-Styrene (SBS) Block Copolymer produced by Shell Bitumen Company and American Gilsonite (AG) obtained from American Gilsonite Company were used as additives to B 160/220 grade bitumen that was procured from TÜPRAŞ refinery in Turkey. The mix was obtained by mixing the neat bitumen and additive material for 60 minutes with 1000 rpm. mixer at a

temperature of 180°C (Figure 1). In previous studies, it was determined that when 5% SBS (MB5S), 18% American Gilsonite (MB18G), 2% SBS + 13% AG (MB2S+13G), 3% SBS + 10% AG (MB3S+10G), and 4% SBS + %6 AG (MB4S+6G) were used, the performance level (PG 76-16) was suitable for Şanlıurfa province and the test results for these mixtures were similar. For this reason, 5 different additive ratios determined in the previous study were used.

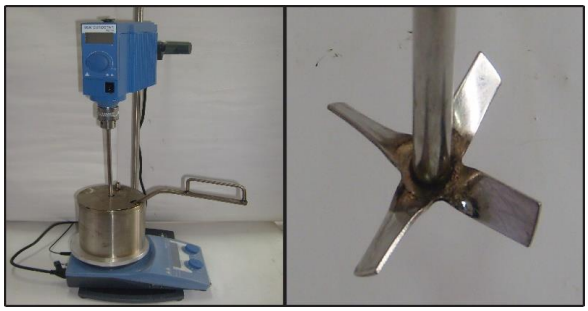

Fig 1. Modified bitumen mixer and mixing apparatus

2.1. Peneteration Test

The penetration test was conducted to determine the stiffness or consistency of the bituminous binder. Penetration is the amount of vertical penetration by a standard needle at a given temperature under a given load, and over a period of time (Figure 2). The unit of penetration is 0.01 cm. In the penetration test, a load of 100 g was applied to the bituminous binder sample at 25°C for 5 seconds.

In the penetration test, the bituminous binder sample is taken according to EN 58 standard and transferred to the sample container after heating. The samples are allowed to cool for 60-90 minutes at a temperature of 5-30°C. The sample containers are then placed in a constant temperature water bath in the transfer chamber for 1-1.5 hours.

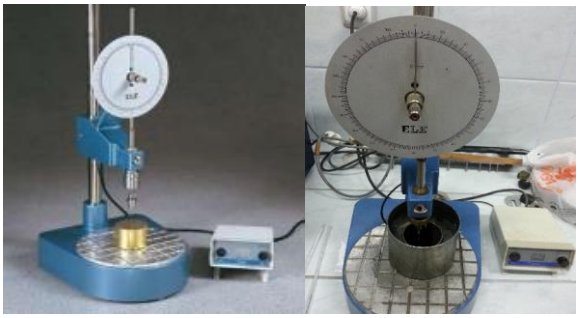

Fig 2. Penetration test apparatus

The transfer container that contains the sample container is placed on the penetration device plate. The needle loaded with the desired weight is adjusted to have contact with the sample surface. At least 3 tests should be conducted using points that are not closer to each other and the side of the container for more than 1 cm. The arithmetic mean of accepted measurements is rounded to the nearest whole number, which is taken as the penetration value.

2.2. Softening Point Test

The softening point test aims to measure the resistance of bituminous binders to high temperatures. Softening point is the temperature at the moment when the softened material touches the base as a result of heating the bituminous material in the standard ring at a certain speed, which was placed in a water bath, with a ball on it. The test setup is shown in Figure 3.

Before the experiment, the bitumen sample is heated and poured into the standard ring up to the top of the ring and cooled for 1 hour. The bitumen overflowing the ring is cut off using a heated spatula.

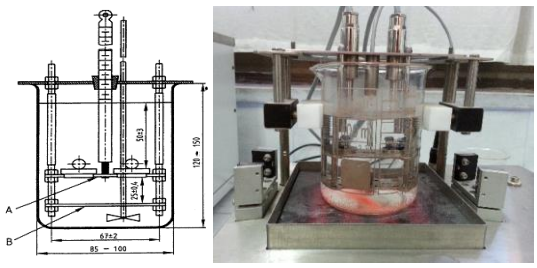

Fig 3. Softening point test apparatus

Pure water at a temperature of 5°C is placed in the beaker and the ring that contains

the sample is submerged into the water. Then the ball is placed in the beaker filled with water. The temperature of the water bath is kept constant at 5°C for 15 minutes. The ball is then placed in the middle of the sample in the ring using a pair of suitable tongs. The water is heated at a rate of 5°C per minute. The temperature read from the thermometer is recorded as the softening point when the softening material touches the base of the bath as a result of the increase in temperature.

2.3. Rotational Viscosimeter (RV) Test (ASTM D 4402)

The Rotational Viscometer (RV) test is conducted to determine the viscosity properties of the bituminous binders at high temperatures. The high temperature viscosity values of binders are identified to determine whether the binders are sufficiently fluid during pumping and mixing procedures. In the experiment, viscosity values are obtained by measuring the resistance of a shaft rotating at 20 rpm within the binder (Figure 4). In the RV test conducted with the original binders, it is best when the viscosity at 135°C does not exceed 3 Pa.s (3000 cP) [24, 25].

Approximately 30 gr. sample is taken and it is heated in a drying oven with a temperature of less than 150°C. Approximately 11 gr. of this material is placed in the sample compartment, and the sample compartment is placed in a temperature-controlled container with a constant temperature. After the sample is kept at a constant temperature for 15 minutes, the test is conducted. After almost equal viscosity values are obtained, three readings are conducted, and the viscosity of the binder is accepted as the average of these three measurements.

Viscosity values are used to determine the mixing and compaction temperatures of hot mix asphalts (HMAs). For this purpose, the RV test is carried out at 135°C and 165°C temperatures. A temperature-viscosity graph is plotted and the viscosity values are marked on the graph and these values are connected by a straight line. The viscosity values of the bituminous binder of 0.170 ± 0.20 Pa.s and a compaction value of 0.280 ± 0.30 Pa.s are desired when mixing HMAs [24]. The temperature values corresponding to these viscosity values are accepted as the mixing and compaction temperatures.

Fig 4. Brookfield Viscosimeter

2.4.Temperature susceptibility of bituminous binders

2.4.1. Peneteration Index Method

Penetration Index (PI) is used to determine the temperature susceptibility of bituminous binders. The Penetration Index is determined with the standard penetration and softening point test results (Formulas 1, 2). P25 in the formula depicts the penetration value of the bitumen at 25°C and TYN indicates the softening point. The PI values decrease as the temperature susceptibility of bitumen binders increases. If the Penetration Index is less than -2, the bitumen is very sensitive to heat, whereas when it is greater than +2, it indicates that the bitumen is less sensitive to heat [26].

$$A = \frac{\log 800 - \log P_{25}}{T_{YN} - 25} \quad (1)$$

$$PI = \frac{20 - 500A}{1 + 50A} \quad (2)$$

2.4.2.Peneteration Viscosity Number Method

Penetration-Viscosity Number (PVN), also called Pen-Vis Number, is an empirical correlation between asphalt cement factors and low temperature pavement cracking experiences. Asphalt cement factors considered in the original correlation are penetrations at 25°C, viscosity at 135°C and equation is proposed for selecting asphalt cements to prevent low

temperature cracking of asphalt concrete pavements. The PVN method is used to quantify temperature susceptibility of an asphalt cement and estimate its ability to prevent low-temperature cracking. Lower values of PVN indicate higher temperature susceptibility, and asphalt mixtures containing binders with lower temperature susceptibility should be more resistant to cracking. The PVN number of a paving asphalt can be calculated precisely from the equations as follows [27];

$$\mathrm{PVN} = -1.5\frac{4.258 - 0.7967\log P_{25} - \log V}{0.795 - 0.1858\log P_{25}} \quad (3)$$

In the formula, P25 indicates the bitumen penetration at 25°C and V indicates the viscosity value at 135°C.

2.5. Experimental study

In the present study, neat and modified binders were subjected to penetration, softening point and rotational viscometer tests to determine their consistency. Furthermore, the penetration index values, which indicate the temperature susceptibility of the bituminous binders, are determined using softening point and penetration values.

3. Results

3.1. Peneteration results

The results obtained from the penetration tests applied to binders are presented in Figure 5.

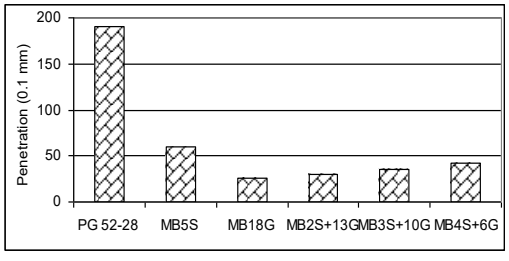

Fig 5. Penetration test results

Figure 5 demonstrates that penetration values decreased with the use of additives. It was determined that the use of 18% AG and 5% SBS were the least effective methods for decreasing the penetration value when compared to the neat bitumen. The penetration values increased as the SBS content increased when dual additives were used. The penetration values of the modified bitumen that contained 5% SBS, 18% AG, 2% SBS + 13% AG, 3% SBS + 10% AG and 4% SBS + 6% AG were 3.14, 7.50, 6.32, 5.34 and 4.56 times lower than neat binder, respectively.

3.2. Softening Point Test results

The results obtained in the softening point tests applied to the binders are presented in Figure 6. Figure 6 demonstrates that the softening point values increased with the use of additives. This indicated that all utilized additives would increase the high temperature resistance of the bituminous binders. When the impact of the additives on the softening point values is considered, it was found that all the additives had similar effects on the softening point and increased the softening point values by about 45% when compared to the neat binder.

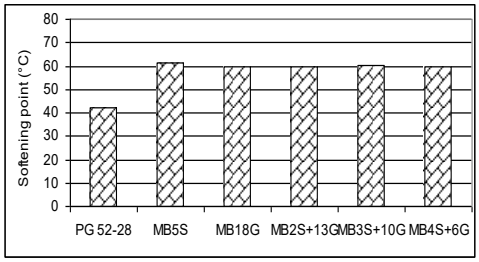

Fig 6. Softening point test results

3.3. Specific gravity of bituminous binders

Specific gravity values of neat and modified bitumen are determined based on the EN 15326 standard. The results obtained in specific gravity tests are presented in Figure 7.

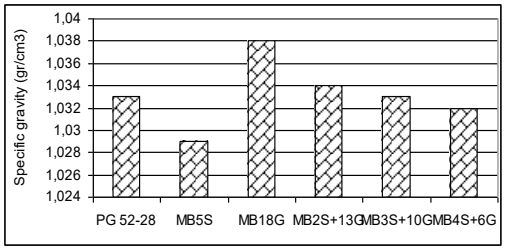

Fig 7. Specific gravity values of neat and modified binders

As can be seen in the figure above, the specific gravity values of bituminous binders

were between the specification limits 1.0-1.1. When the changes in specific gravity with the use of additives were examined, it was observed that the specific gravity of binders increased with the use of American Gilsonite, whereas the specific gravity values decreased with the use of SBS. With the combined use of AG and SBS, specific gravity values increased regularly when compared to the use of 5% SBS, but decreased regularly when compared to 18% AG use.

3.4. Penetration Index values

The Penetration Index values for neat and modified bituminous binders determined using formulas (1) and (2) are given in Figure 8.

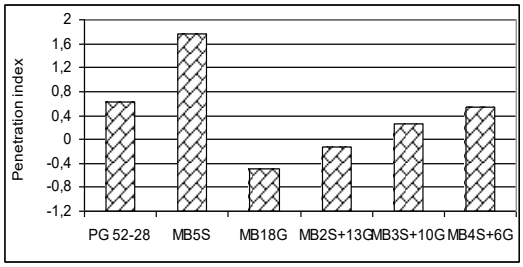

Fig 8. Variation in binder penetration index values with additive use

The Penetration Index results that demonstrate the temperature susceptibility of bituminous binders showed that the PI value increased as the SBS ratio in modified binders increased (Figure 8). Since the temperature susceptibility of bituminous binders decrease as the PI value increased, it could be argued that the use of SBS decreased the temperature susceptibility of bituminous binders. It was determined that as AG content in modified bitumen increases, the PI values decreases and thus, the temperature susceptibility increases. When SBS and AG are used together in the modified bitumen, it was determined that AG had a negative effect on the temperature susceptibility, and that this problem was eliminated by using SBS in conjunction with AG.

3.5. Penetration Viscosity Number values

The Penetration Viscosity Index values for the neat and modified bituminous binders determined using the formula (3) are given in Figure 9.

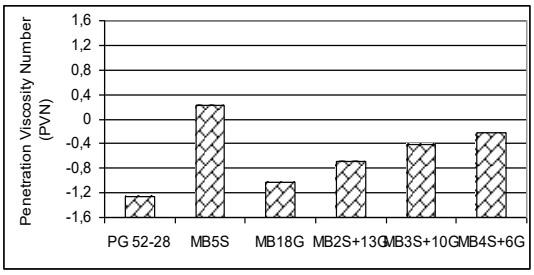

Fig 9. Variations in binder penetration viscosity number values with additive use

When the penetration viscosity number results that reflect the susceptibility of bituminous binders to low temperatures were evaluated, it was determined that the use of AG had a negative effect on temperature susceptibility in PVN values, similar to the PI values, when compared to that of the SBS. It was also determined that SBS can be used to avoid the negative impact of AG on temperature susceptibility. It was determined that the temperature susceptibility decreased with the use of SBS instead of AG in dual modified bitumen (Figure 9).

3.6. Rotational Viscometer Test results

Neat and modified binders were subjected to rotational viscometer tests at 135°C and 165°C temperatures. In the experiment, 20 rpm speed was used. Modification index values were obtained from the ratio of the viscosity value of the modified binder to the viscosity value of the neat binder (ηmodified / ηneat). The viscosity results obtained from the tests are presented in Figure 10. The viscosity and modification index values obtained at high temperatures (135°C and 165°C) demonstrated that SBS increases the stiffness of the binders and reduces the workability at high temperatures.

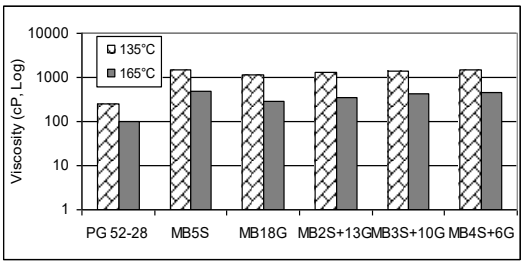

Fig 10. Variations in binder viscosity values with temperature and additive use

Figure 10 demonstrates that the viscosity values of all binders met the Superpave specification limit maximum value of 3000 cP at a temperature of 135oC. With additive use, the viscosity values increased at all temperatures. It was determined that the viscosity values of 5% SBS modified binders were the highest and the bituminous viscosity values with 18% AG were the lowest, despite their similar performance levels. It was determined that as the SBS content in the modified bitumen increased, the viscosity values increased at both temperatures.

The modification index (ηmodified / ηneat) values determined by the ratio of the viscosity value of the modified bitumen to the viscosity value of the neat binder are given in Figure 11. When the modification index values were examined, it was determined that the additive that maximizes the viscosity value at all temperatures was SBS and the least contributing additive was AG. It was determined that the viscosity values of SBS and AG were higher than those of the sole use of AG and the viscosity values increased regularly as the SBS ratio in the mixture increased.

When the bituminous binders are mixed with the aggregates at the plant and the hot mix asphalts are compacted in the field, they must possess adequate workability. It is desirable that the bituminous binder has a viscosity value of 0.170 ± 0.20 Pa.s for compaction and 0.280 ± 0.30 Pa.s for the mixing [24]. In the plotted temperature-viscosity graphs, the viscosity values were marked and these values were joined with a straight line. The temperature values that correspond to these viscosity values are accepted as the mixing and compaction temperatures. As an example, the viscosity-temperature graph that shows the mixing and compaction temperature ranges for the modifier binder that contains 18% AG is presented in Figure 12.

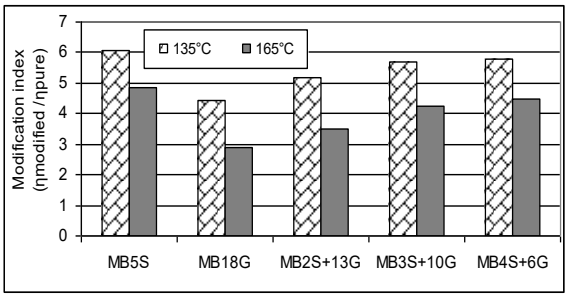

Fig 11. Variations in binder modification indexes with temperature and additive use

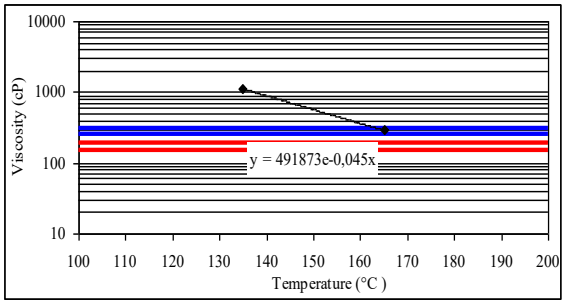

Fig 12. Viscosity-temperature chart for the modified binder including 18% AG

The variation in the mixing and compaction temperatures with the type of additive is presented in Figure 13.

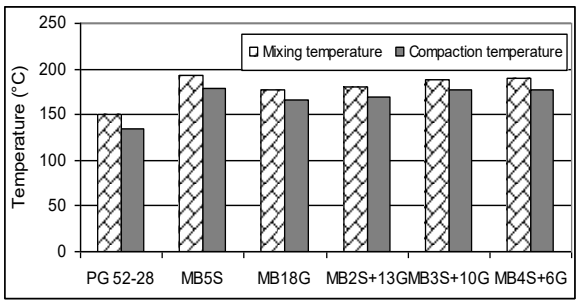

Fig 12. Mixing and compaction temperatures of binders

As shown in Figure 13, higher mixing and compaction temperatures were required with the use of additives. This demonstrates that although higher binder performance is achieved with additive use, higher temperatures will be required during mixing it with the aggregate and compaction of the HMA, thus requiring more energy during the preparation at the plant. When the effects of the additive types and combined use of additives were evaluated, it was determined that the highest mixing and

compaction temperatures were found with 5% SBS modified bitumen and the lowest values were found with 18% AG modified bitumen. As the SBS content in the modified bitumen increased, higher mixing and compaction temperatures were needed.

4. Conclusion

In the study, consistency and specific gravities of neat and 5 different modified bitumen were determined and their temperature susceptibility was evaluated with two different methods. Initially, 18% AG and 5% SBS were used as additives separately, then 2% SBS and 13% AG, 3% SBS and 10% AG, and 6% AG and 4% SBS were used in conjunction to obtain bituminous binders with the same performance level.

- Penetration tests demonstrated that all additives increased the stiffness significantly. It was determined that the most effective additive was 18% AG and the least effective additive was 5% SBS.
- Softening point tests demonstrated that all additives increased the high temperature resistance of the bituminous binders significantly, and all modified bitumen had similar softening point values.
- It was determined that the specific gravity values of AG modified bitumen were higher since both the usage ratio and density of AG was higher than those of SBS as demonstrated in specific gravity tests.
- Penetration index values demonstrated that 5% SBS modified bitumen had the lowest thermal sensitivity and 18% AG modified had the highest. This negative aspect of AG modified binders was reduced with the addition of SBS.
- Penetration viscosity number values were consistent with PI values. With the use of AG additive, the low temperature susceptibility of bituminous binders have increased, and the use of SBS has reduced the low temperature susceptibility.
- It was determined that additive use increased binder stiffness values as observed in viscosity values. Consequently, the mixing and compaction temperatures increased with the modification values. The most effective additive on viscosity values was 5% SBS modification.

Acknowledgment

This study was conducted within the scope of the Scientific and Technological Research Council of Turkey (TUBITAK) project no. MAG-214M669. The authors would like to thank TUBITAK for their support.

5. References

1.Kennedy, T.W., Cominsky, R.J. (1990). Hypotheses and models employed in the SHRP asphalt research program. SHRP-A/WP-90-008, Strategic Highway Research Program, Washington.

2. Claudy, P., Letoffe, J.M., King, G.N., Brule, B., Planche, J.P. (1990). Caracterisation des bitumes routiers par analyse calorimetrique differentielle. Bull Liaison Lab Ponts Chaussees, issue **165**, pp. 85-92.

3. Garcia-Morales, M., Partal, P., Navarro, F.J., Martinez-Boza, F.J., Gallegos, C. (2006). Process rheokinetics and microstructure of recycled EVA/LDPE-modified bitumen. Rheol Acta., vol. **45**, pp. 513-524.

4. Tunç, A. (2004). Esnek Kaplama Malzemeleri El Kitabı. Asil Yayın Dağıtım, 352 s.

5. Lu, X., Isacsson, U. (2000). Laboratory study on the low temperature physical hardening of conventional and polymer modified bitumens. Constr. Build. Mater., vol. **14**, pp. 79-88.

6. Navarro, F.J., Partal, P., Martinez-Boza, F., Valencia, C., Gallegos, C. (2002). Rheological characteristics of ground tire rubber-modified bitumens. Chem. Eng. J., vol. **89**, pp. 53-61.

7. Airey, G.D. (2002). Rheological properties of styrene butadiene styrene polymer modified road bitumens. Fuel, vol. **82(14)**, pp. 1709-1719.

8. Aglan, H., Othman, A., Figueroa, L., Rollings, R. (1993). Effect of styrene-butadiene-styrene block copolymer on fatigue crack propagation behavior of asphalt concrete mixtures. Transp. Res. Rec., vol. **1417**, pp. 178-186.

9. Khattak, M.J., Baladi, G.Y. (1998). Engineering properties of polymer-modified asphalt mixtures. Transp. Res. Rec., vol. **1638**, pp. 12-22.

10. Hamidi, H. (1998). Stiffness Modulus and Permanent Deformation Characteristics of Asphalt Mix Containing Gilsonite, PhD Thesis, Bandung Technology Institute, India.

11. Liu, J., Li, P. (2008). Experimental study on gilsonite-modified asphalt. Proceeding of the 2008 Airfield and Highway Pavement Specialty Conference, Washington, pp. 222-228.

12.URL-1, http://www.asiagilsonite.com/?page=gilsonite Asia Gilsonite. 27 Ocak 2017.

13. Yalçın, E. (2014). Filler Olarak Kireç Kullanımının Modifiye Bitümlerle Hazırlanan Karışımların Performansına Etkisinin İncelenmesi, Yüksek Lisans Tezi, Fırat Üniversitesi, Fen Bilimleri Enstitüsü, Elazığ.

14. Çeloğlu, M.E. (2014). Farklı Doğal Asfaltların Bitüm ve Bitümlü Sıcak Karışımların Özelliklerine Etkileri, Yüksek Lisans Tezi, Fırat Üniversitesi, Fen Bilimleri Enstitüsü, Elazığ.

15. Widyatmoko, I., Elliott, R. (2008). Characteristics of elastomeric and plastomeric binders in contact with natural asphalts. Construction and Building Materials, vol. **22**, pp. 239-249.

16. Babagoli, R., Hasaninia, M., Namazi, N.M. (2015). Laboratory evaluation of the effect of gilsonite on the performance of stone matrix asphalt mixture. Road Materials and Pavement Design, vol. **16(4)**, pp. 889-906.

17. Wen, G., Zhang, Y., Zhang, Y., Sun, K., Fan, Y. (2002). Rheological characterization of storage-stable SBS-modified asphalts. Polymer Testing, vol. **21**, pp. 295-302.

18. Sun, D., Lu, W. (2003). Investigation and improvement of storage stability of sbs modified asphalt. Petroleum Science and Technology, vol. **21(5-6)**, pp. 901-910.

19. Davis, N., Tooman, C.E. (1989). New laboratory tests evaluate the effectiveness of gilsonite resin as a borehole stabilizer. SPE Drilling Engineering, vol. **4(1)**, pp. 47-56.

20. Kök, B.V., Yılmaz, M., Akpolat, M. (2014). Evaluation of the conventional and rheological properties of SBS + Sasobit modified binder. Construction and Building Materials, vol. **63**, pp. 174-179.

21. Carcer, I.A., Masegosa, R.M., Vinas, M.T., Salom, C., Prolongo, M.G., Contreras, V., Barcelo, F., Paez, A. (2014). Storage stability of SBS/Sulfur modified bitumens at high temperature: Influence of bitumen composition and structure. Construction and Building Materials, vol. **52**, pp. 245-52.

22. Pamplona, T.F., Amoni, B.C., Alencar, A.E.V., Lima, A.P.D., Ricardo, N.M., Soares, J.B., Soares, S.A. (2012). Asphalt binders modified by SBS and SBS/Nanoclays: Effect on rheological properties. Journal of the Brazilian Chemical Society, vol. **23(4)**, pp. 639-647.

23. Zaniewski, J.P., Pumphrey, M.E. (2004). Evaluation of performance graded asphalt binder equipment and testing protocol. Asphalt Technology Program, pp. 107.

24. Peng, Y., Ruibo, R., Lizhi, Xiaoning, W., Z. (2012). Characteristic behavior of asphalt with SBS and PE. Sustainable Construction Materials, pp. 421-429.

25. McGennis, R.B., Shuler, S., Bahia, H.U. (1994). Background of Superpave asphalt binder test methods. No. FHWA-SA-94-069, pp. 104.

26. Ullidtz, P. (1987). Pavement Analysis. Elsevier, Amsterdam, pp 318.

27. McLeod, N.W. (1976). Asphalt cements: pen-vis number and its application to moduli of stiffness. Journal of Testing and Evaluation, vol. **4(4)**, pp. 275-282, July.

Turkish Journal of Science & Technology
Volume 13(1), 87-92, 2018

Assessment of Earthquake Behavior of Reinforced Concrete Buildings with Slab Discontinuity

Sibel Sağlıyan[1*], Burak Yön[2]
Fırat University, vocational school of higher education, Construction Department, Elazığ
Munzur University Engineering, Faculty, Civil Engineering Department, Tunceli
*ssagliyan@firat.edu.tr

(Received: 04.02.2017; Accepted: 08.04.2017)

Abstract

The most important principle of the earthquake-resistant design of reinforced concrete structures is that the structural elements must carry both vertical loads and horizontal loads as a whole. For this reason, it is required that the structural elements carry their own weight with sufficient safety and the loads arose from external forces must be transferred safely to the load carrying vertical elements. However, discontinuity of the slabs disturbs the integrity of the structures and causes problems in transferring earthquake loads to the structural elements. In this study, the effect of slab discontinuity in plan on seismic behaviors of multi - storey reinforced concrete structures was investigated by using incremental linear dynamic analysis method. To investigate this irregularity situation, one regular and three irregular multi-storey reinforced concrete building models were selected. Dynamic envelopes of the structures were obtained from the analysis results and compared with each other. Thus, it was observed that the irregular structures subjected to more shear force than the regular structure.

Keywords: Reinforced concrete building, Slab discontinity, Incremental linear dynamic analysis

Döşeme Süreksizliğine Sahip Betonarme Binaların Deprem Davranışlarının Değerlendirilmesi

Özet

Betonarme yapıların depreme dayanıklı tasarımının en önemli ilkesi yapıyı oluşturan taşıyıcı elemanların hem düşey yükleri hem de yatay yükleri bütün bir eleman olarak taşımasıdır. Bu nedenle yapısal elemanlardan kendi ağırlıklarını yeterli güvenlikle taşıması, dış kuvvetlerden gelen yükleri taşıyıcı elemanlara güvenli bir şekilde aktarması istenmektedir. Ancak yapıların bütünlüğünü bozan döşeme süreksizlikleri, deprem yüklerinin taşıyıcı elemanlara aktarılmasında sorunlara neden olmaktadır. Bu çalışmada planda döşeme süreksizliğinin sahip çok katlı betonarme yapıların deprem davranışına etkisi artımsal dinamik analiz yöntemiyle incelenmiştir. Bu düzensizlik durumunun incelenmesi için biri düzenli diğerleri düzensiz olmak üzere toplam altı adet çok katlı betonarme yapı modeli seçilmiştir. Analiz sonuçlarından yapıların dinamik itme zarfları elde edilmiştir. Yapılan değerlendirme sonucunda döşeme süreksizliğine sahip yapıların düzenli yapıya göre daha fazla kesme kuvvetine maruz kaldığı görülmüştür.

Anahtar Kelimeler: Betonarme yapı, Döşeme süreksizliği, Artımsal lineer dinamik analiz

1. Introduction

The earthquake effect is a natural catastrophe that has caused massive devastation on people and the environment. But the main reason of the losses in the earthquakes is that the structures not provided the desired earthquake behavior. While designing the building systems, it is aimed that the buildings resist the earthquake forces at least must be provide life safety level. To provide this performance level, the structure has symmetrical and regular load carrying system. Regular structures; both in practice and in dimensioning, provide simple the calculation and forces are calculated accurately. For this reason, regular construction is the most practical choice for a good design.

Lateral forces are transmitted to the vertical load carrying elements by slabs. It is assumed that the slab behaviors as a rigid diaphragm during the design of structure. But the large openings in the slab invalids rigid diaphragm assumption [1-4]. So, Turkish Seismic Code (TSC-2007) [5] requires some requirements

about this irregularity. These requirements are shown in Fig.1. According to code, In any floor

a) The case where the total area of the openings including those of stairs and elevator shafts exceeds 1/3 of the gross floor area,

b) The case where local floor openings which make the safe transfer of seismic loads difficult to vertical structural elements,

c) The cases of abrupt reductions in the in-plane stiffness and strength of floors.

$$A_b = A_{b1} + A_{b2}$$

$$\frac{A_b}{A} > \frac{1}{3}$$

where

A_b shows sum of the openings and A shows gross floor area, respectively.

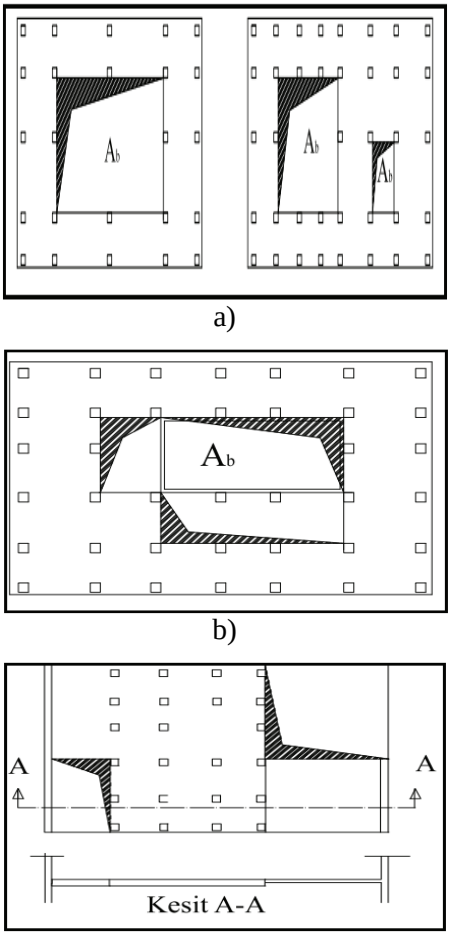

Figure 1. Slab discontinuity situations defined in TSC

To investigate this irregularity situation, one regular and three irregular multi-storey reinforced concrete building models were selected. Incremental linear dynamic analyses were performed and dynamic envelopes of the structures were obtained from the analysis results. In dynamic analysis, elastic diaphragm assumption was made.

2. Material and Methods

Numerical study

A. Selected Building Models

For dynamic analyses three 3D irregular and a regular building models were selected. These models have five stories and height of stories are 3.50 m. The dimensions for columns were selected as 50x50 cm, and dimensions for beams were selected as 30x60 cm. Slab thickness was selected as 13 cm. It was assumed that, the building importance coefficient is 1.0 and, concrete class is C25 and reinforcement steel class is S420. Selected models and rates of slab openings are illustrated in Figs.2-5. In this models, first and end bays are 500 cm and the middle bays are 450 cm in x direction. For y direction first and end bays are 600 cm, the other bays are 500 cm. The dynamic analyses are performed by SAP2000 structural analysis program [6]

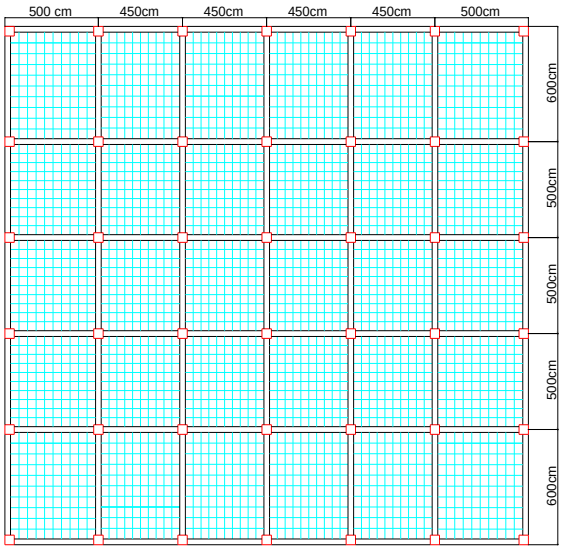

Figure 2. Regular model

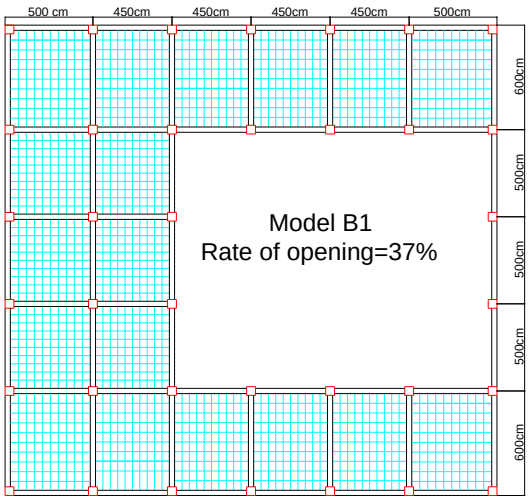

Figure 3. B1 irregular model

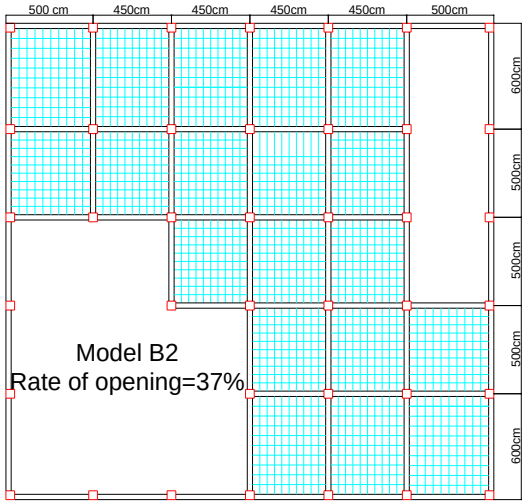

Figure 4. B2 irregular model

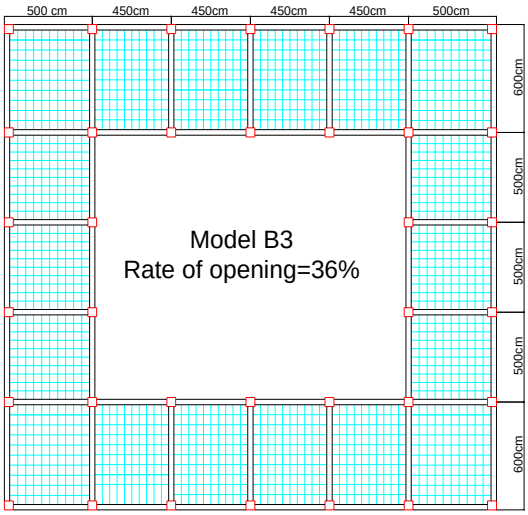

Figure 5. B 3 irregular model

B. Earthquake Parameters and Local Site Conditions

Table 1 shows selected earthquake accelerations properties used in dynamic analysis. The seismic records have been selected from the PEER Strong Motion Database [7] and scaled in order to be compatible with the design spectrum according to seismic zones and local site conditions in TSC. Soil classes (from Z1 to Z4) are characterized in term of periods T_A and T_B. The design spectrums are given according to local site classes in *Fig.* 6.

Table 1. Selected earthquake acceleration records for dynamic analysis

Eartquakes	Kocaeli	Loma Prieta	İmperial Valley
Station	Sakarya	Corralitos	El Centro Array
Direction	North-South	East-West	East-West
Date	August 17, 1999	October 18, 1989	May 19, 1940
Magnitude	7.4	6.9	7.0
PGA(g)	0.376	0.644	0.313

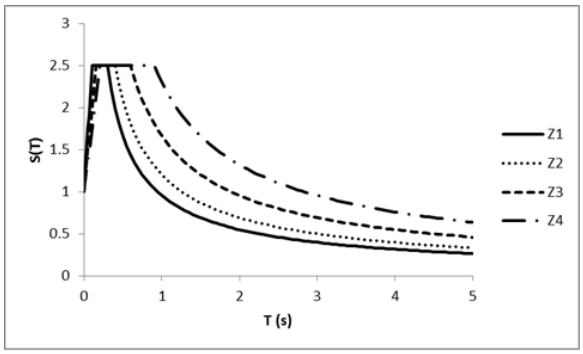

Figure 6. Recommended elastic response spectra for ground types Z1 to Z4 (for 5% damping)

Selected earthquake records were scaled in frequency content in order to be compatible with the target design spectrum of four effective ground accelerations and different soil classes (Fig. 7a-d). The records were scaled using SeismoArtif and SeismoSignal programs.

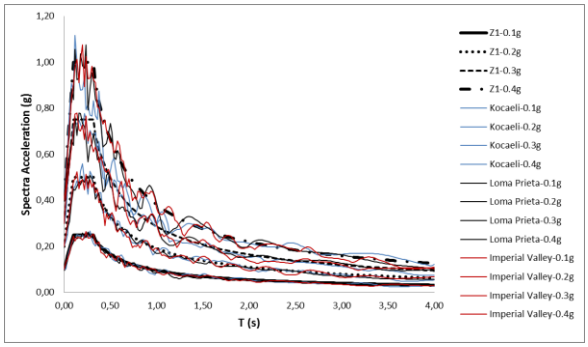

a) Response spectra of the earthquake acceleration records scaled according to the elastic design spectrum for Z1 soil class and effective ground accelerations

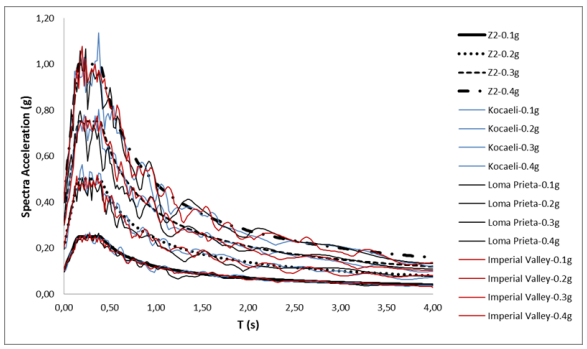

b) Response spectra of the earthquake acceleration records scaled according to the elastic design spectrum for Z2 soil class and effective ground accelerations

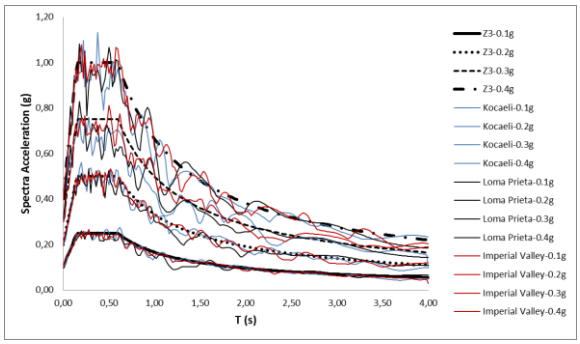

c) Response spectra of the earthquake acceleration records scaled according to the elastic design spectrum for Z3 soil class and effective ground accelerations

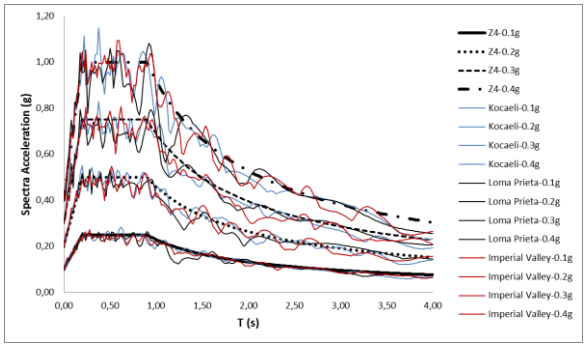

d) Response spectra of the earthquake acceleration records scaled according to the elastic design spectrum for Z4 soil class and effective ground accelerations

Figure 7. Response spectra of the earthquake acceleration records scaled according to the elastic design spectrum for four soil classes and effective ground accelerations defined in TSC

3. Results

Maximum responses of the incremental dynamic time history analyses are given in Figs. 8-10 for the x direction and Figs. 11-13 for the y direction. Dynamic envelopes are obtained according to these responses. Each irregular models are compared with regular building. According to these figures, the correlation coefficient values, are exceed 0.90 for x direction. Also, it is seen that dynamic envelopes of each irregular building models exceed the dynamic envelope of regular building. This situation is a evidence of the irregularity causes more shear forces.

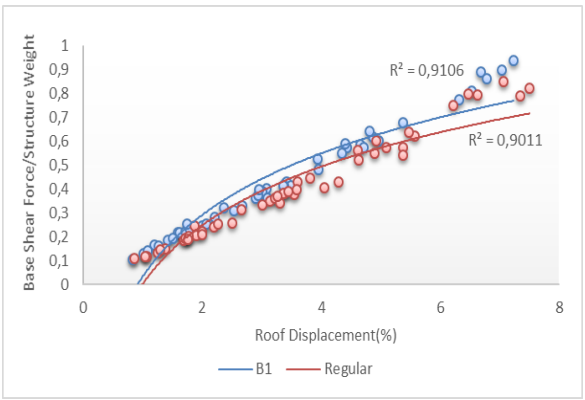

Figure 8. Comparision of dynamic envelopes of B1 irregular model and Regular model for x direction

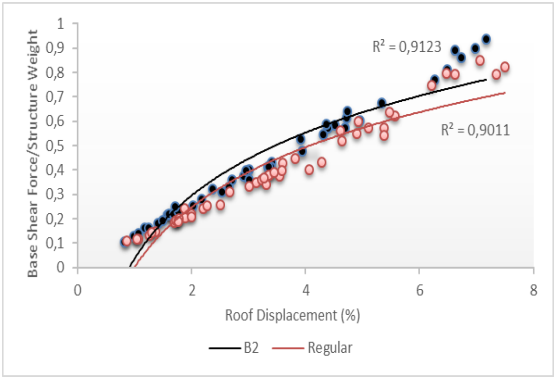

Figure 9. Comparision of dynamic envelopes of B2 irregular model and Regular model for x direction

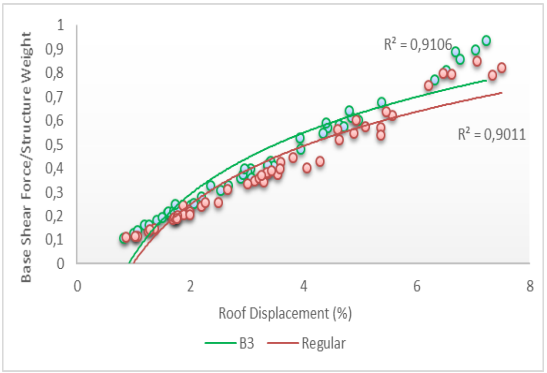

Figure 10. Comparision of dynamic envelopes of B3 irregular model and Regular model for x direction

According to Figs.11-13, the correlation coefficient values are approximately 0.90 for regular building and for the other coefficient exceed the 0.90 for y direction. Seismic actions obtained from the scaled earthquakes follow the same trend and shape to that of the dynamic envelopes, similar to that in the x direction.

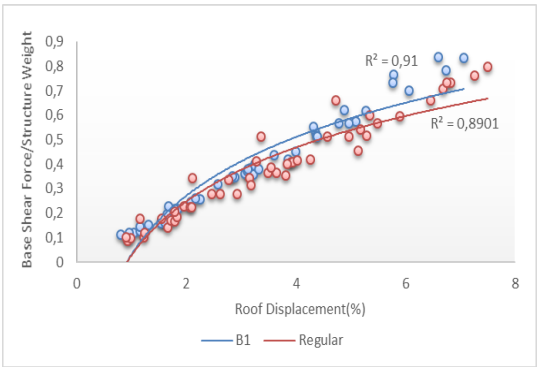

Figure 11. Comparision of dynamic envelopes of B1 irregular model and Regular model for y direction

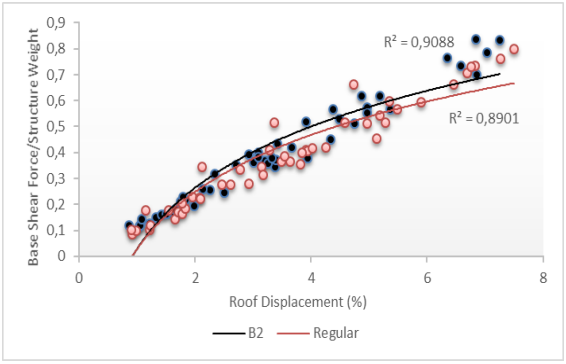

Figure 12. Comparision of dynamic envelopes of B2 irregular model and Regular model for y direction

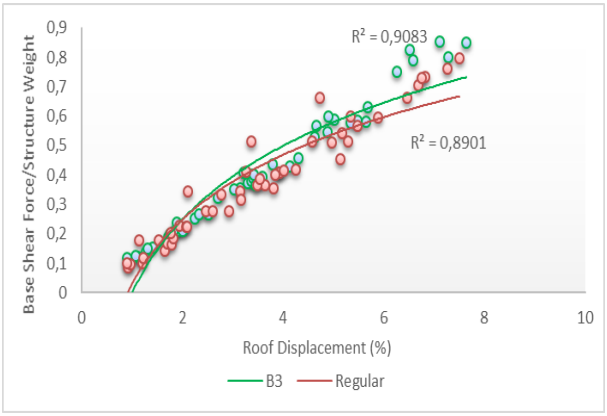

Figure 13. Comparision of dynamic envelopes of B3 irregular model and Regular model for y direction

4. Discussion

In this paper, the effect of slab discontinuity in plan on seismic behaviors of multi-storey reinforced concrete structures was investigated by using incremental dynamic analysis method. To investigate this irregularity situation, one regular and three irregular multi-storey reinforced concrete building models were selected. Dynamic envelopes of the structures were obtained from the analysis results.

According to analysis results, dynamic envelopes obtained from each irregular building models exceed the dynamic envelope of regular building for x and y directions This situation shows that this type of irregularity causes more shear forces. So, it is should be abstain from the application of this irregularity.

5. References

1.Özmen, C. and Ünay, A.İ. (2007). Commonly Encountered Seismic Design Faults due to the

Architectural Design of Residential Buildings in Turkey. *Building and Environment,* **42,** 1406–1416.

2.Ulucan Z.Ç. and Yön B. (2008). Nonlinear Earthquake Response of A2 Slab Discontinuity Irregularity Structures Using Rigid and Elastic Diaphragm Assumptions. *Science and Engineering Journal of Fırat University,* **20,** 315–323.

3.Yön B., Öncü M.E, and Ulucan ZÇ. (2010). Investigation of Effect of Slab Opening Location to the Shear Stress. *Journal of Pamukkale University Engineering Science,* **16,** 45-51.

4.Celep Z. and Kumbasar, N. (2004). Introduction to Earthquake Engineering and earthquake resistant structural design. pp. 700. Beta Distribution, İstanbul.

5.Turkish Sesimic Code, (2007). Anakara-Turkey.

6.SAP 2000 V9.0.1. (2004). Integrated Finite Element Analysis and Design of Structures, Computer and Structures Inc. Berkeley, California.

7.Pacific Earthquake Engineering Research Center Strong Motion Database

8.SeismoArtif v2.1: A computer program for generating artificial earthquake accelerograms matched to a specific target response spectrum. Available at: www.seismosoft.com [July 19, 2013]

9.SeismoSignal v5.1 - A computer program for the processing of strong-motion data. Available at: www.seismosoft.com [July 19, 2013]

Turkish Journal of Science & Technology
Volume 13(1), 93-98, 2018

Determining Dynamic Characteristics Of Reinforced Concrete Minarets And Updating Of Their Finite Element Models Using Environmental Vibration Data

Musa Yetkin[1*], Yusuf Calayır[1], Hakan Erkek[2]
[1]Firat University Engineering Faculty Civil Engineering Department Elazığ
[2]Osmaniye Korkut Ata University Engineering Faculty Civil Engineering Department Osmaniye
[*]musayetkin@firat.edu.tr

(Received: 05.02.2017; Accepted: 01.04.2017)

Abstract

Structures are exposed to various dynamic effects such as earthquake, wind and traffic load. It need to be taken various measures for surviving the structures under dynamic loads. Taking the appropriate measures depends on the well-known of dynamic behavior of existing structures. This behavior of the structure can be known through analytical or experimental methods. In the analytical methods, many acceptance is made in finite element modeling of the structure and it is considered that the created model represents its existing case. However, it is rather difficult to fully represent of the existing structure with the accepted assumptions. In experimental methods, the dynamic characteristics of the structure (natural frequencies, mode shapes and damping ratios) are determined for the present case. Using these dynamic characteristics, the existing analytical model of the structure can be updated and the evaluation of the structure according to this new model can be made more realistic. In this study, analytical and experimental analyses of the minaret of Firat University Engineering Campus Mosque were carried out. The finite element model has been updated depending on the dynamic characteristics obtained from the experimental analysis.

Keywords: Dynamic characteristics; Reinforced concrete minaret; Analytical model; Environmental vibration data; updating of finite element model.

Betonarme Minarelerin Dinamik Karakteristiklerinin Çevresel Titreşimler Kullanılarak Belirlenmesi Ve Sonlu Eleman Modellerinin Güncelleştirilmesi

Özet

Yapılar deprem, rüzgâr, trafik yükü gibi çeşitli dinamik etkilere maruz kalmaktadır. Yapıların dinamik yükler altında ayakta kalabilmeleri için çeşitli tedbirlerin alınması gerekmektedir. Uygun tedbirlerin alınması mevcut yapıların dinamik davranışlarının iyi bilinmesine bağlıdır. Yapının bu davranışının bilinmesi, analitik ya da deneysel yöntemler yardımıyla mümkün olabilmektedir. Analitik yöntemlerde, sonlu elemanlar modeli oluşturulurken birçok kabul yapılmakta ve oluşturulan modelin mevcut yapıyı temsil ettiği düşünülmektedir. Oysaki yapılan kabullerle mevcut yapının tam olarak temsil edilmesi oldukça zordur. Deneysel yöntemlerde ise, yapının dinamik karakteristikleri (doğal frekansları, mod şekilleri ve sönüm oranları) mevcut durum için belirlenmektedir. Bu dinamik karakteristikler yardımıyla yapının mevcut analitik modeli güncelleştirilebilir ve bu yeni modele göre yapının değerlendirilmesi daha gerçekçi olarak yapılabilir. Bu çalışmada, Elazığ ili Fırat Üniversitesi Mühendislik Kampüsü Camisinin minaresinin analitik ve deneysel analizleri gerçekleştirilmiştir. Deneysel analizden elde edilen dinamik karakteristiklere bağlı olarak yapının sonlu elemanlar modeli güncelleştirilmiştir.

Anahtar Kelimeler: Dinamik karakteristikler; Betonarme minare; Analitik model; Çevresel titreşim verileri; Sonlu elamanlar modelinin güncelleştirilmesi.

1. Introduction

As depending on the fast progress of the technology, the produced electronic devices enable easy observation of the behaviors of living things and also enable observation of the behaviors of the structures [1]. The analysis of the acceleration signals obtained with the help of accelerometers gives some information about the

structure. By comparing the results obtained for different situations, it can be determined whether there is any change in the behavior of the structure. Experimental Modal Analysis method is widely used for this purpose [2]. The basis of experimental modal analysis studies, which have application scope in many engineering disciplines, is based on the 1940s. At early times, non-practical approaches was mostly used since transformers measuring dynamic forces were simple. In the 1960s, the modern era of experimental modal analysis began as depending on the development of digital computers and Fast Fourier Transforms [3].

Structures are exposed to various dynamic effects such as earthquake, wind and traffic load. It need to be taken various measures for surviving the structures under dynamic loads. Taking the appropriate measures depends on the well-known of dynamic behavior of existing structures. While the dynamic characteristics of the structures (natural frequencies, mode shapes and damping ratios) are used to determine its dynamic behavior with using the mode superposition method, it also helps to control the accuracy of the analytical model. These characteristics cannot be at the expected values due to cracking, fatigue, collapse of support in the structures and/or workmanship faults during construction [4]. Therefore, it is considered that using of the dynamic characteristics obtained from analytical methods in determining dynamic response of the structures can be given incorrect results. Since experimental methods are applied on the current state of the structures, dynamic characteristics obtained by these methods reflect the current situation. Updating of analytical models of structures with respect to results of experimental methods will lead to more realistic results [5-7].

There are many studies on determining the dynamic characteristics of structures based on experimental measurements [8-14]. In these studies, the dynamic characteristics of many structures such as minaret, tower, mosque, church, etc., which are constructed as reinforced concrete/masonry, are determined.

2. Experimantal Method

Vibration is the behavior of structures under initial conditions or under applied external loads. Basically, there are two types of vibration, free and forced vibration [7,15]. Free vibration occurs under the initial conditions of the structure and ends with the effect of damping after a while. In this type of vibration, the fundamental frequency is the smallest frequency and usually the most effective frequency of the structure. If an external load is applied to the structure, the name of this vibration is the forced vibration. As long as the structure is exposed to external load, vibration of the structure continues [16]. The experimental method to be used varies depending on whether vibration is known or not. If the numerical values of vibration applied to the structure are known, Conventional Modal Analysis method, if the numerical values of the vibration are unknown and the structure vibrates under of environmental effects, Operational Modal Analysis (OMA) method is used. OMA method are not needed expensive devices when compared to the conventional modal analysis method at large volume structures for artificial excitation [5,17].

OROS-OR36 Multichannel Noise and Vibration Analyzer is used in experimental measurements based on the OMA method (Figure 1).

Figure 1. OROS-OR36 Multichannel Noise and Vibration Analyzer.

3. Numerical Application

In this study, theoretical and experimental analyses of the minaret of Firat University Engineering Campus Mosque (Figure 2) were carried out. This minaret had built as reinforced concrete.

3.1. Theoretical analysis

The analytical model of the selected reinforced concrete minaret was created with shell elements by using SAP2000 finite element package program. In the initial analytical model, the modulus of elasticity of the concrete was taken as $11*10^3$ MPa (Figure 3). The values of first three frequencies obtained from the modal analysis using the initial analytical model are 2.30, 2.45 and 8.77, respectively.

Figure 2. Minaret of Firat University Engineering Campus Mosque.

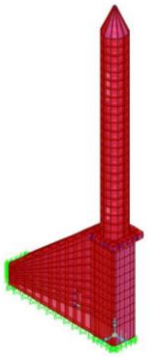

Figure 3. Finite element model of Minaret.

3.2. Experimental analysis

Creating Experimental Model: OMA method were used in the experimental measurements of the structure. Measurements were taken with the accelerometers attached to 4 different points of the structure. The measurement points on each floor are selected as points having the same coordinates in the "x" and "y" directions. 8 accelerometers were totally used for the measurement without reference as two accelerometers each of which are placed in x and y directions for each point (Figure 4).

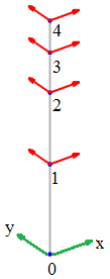

Figure 4. The accelerometer system for without reference measurement.

Experimental Measurement and Updating Analytical Model: After the preliminary tests of structure carried out, (finite element model solutions and in-situ wide frequency range measurements), the measurement frequency range, time and other parameters were determined. The Modal Indication Function was created by processing raw signals obtained from measurements. With the help of this function, first three frequencies were selected and values of that are 2.15, 2.32 and 9.56 Hz, respectively. Mode shapes with related these frequencies were given in Figure 5-6.

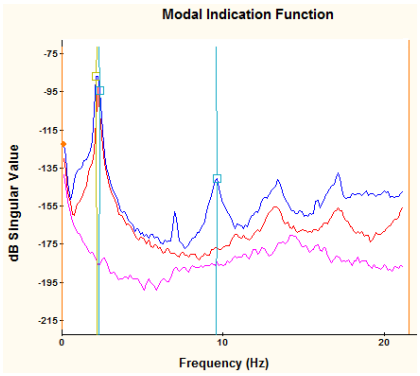

Figure 5. Selected frequencies from modal indication function.

The compatibility of analytical and experimental modes was controlled by a criterion called Modal Assurance Criteria (MAC). This criterion [16] is defined by the (1) equation.

$$MAC\ (\psi_a, \psi_d)=\frac{|\psi_a{}^T\psi_d|^2}{(\psi_a{}^T\psi_a)(\psi_d{}^T\psi_d)} \quad (1)$$

where ψ_a and ψ_d refer to analytical and experimental mode shape, respectively. If the analytical and experimental mode shapes are

entirely the same, the MAC value must be 1, otherwise this value must be less than 1.

In comparison of the initial analytical model solutions and experimental results (Table I), the frequency and MAC values were seen to be compatible for both method. It was also given experimental damping ratios in Table I. It is thought that differences between analytical and experimental frequencies can be minimized if the initial model of the structure is updated. The minaret mass is considerably known. There is more uncertainty in stiffness. Factors affecting the stiffness can be expressed as concrete elasticity and boundary conditions. Here, elasticity module of concrete was updated as $10*10^3$ MPa.

Table 1. Comparison of Initial Analytical Model Solutions and Experimental Results.

Mode Number	Analytical Frequencies (Hz)	Experimental Frequencies (Hz)	Experimental Damping Ratios (%)	MAC (%)
1	2.30	2.15	4.09	96.281
2	2.45	2.32	3.29	91.841
3	8.77	9.56	2.89	90.419

Modal analysis of the updated analytical model was performed and, the first three frequencies and mode shapes were presented in Table II and Figure 7, respectively. Now, the frequency and MAC values of first two modes for the updated analytical model are closer to the results of the experimental method.

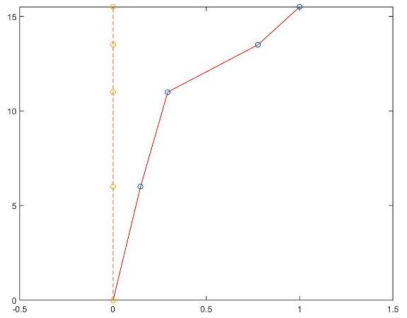

1. Mode

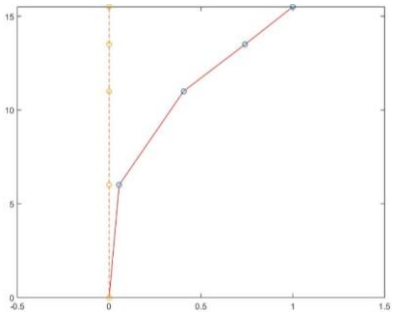

2. Mode

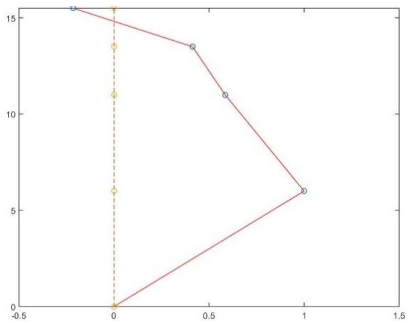

3. Mode

Figure 6. Mode shapes for selected frequencies.

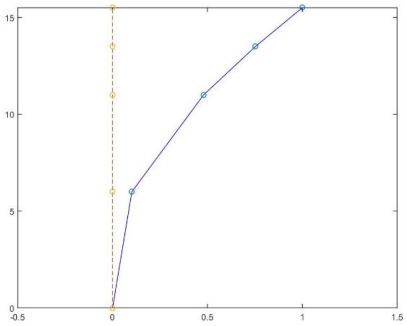

1. Mode

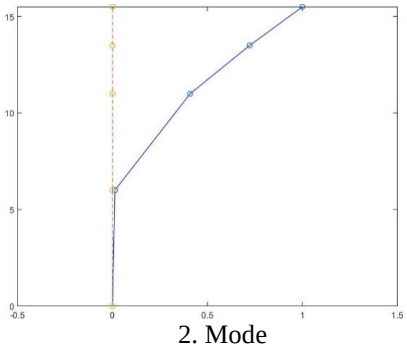

2. Mode

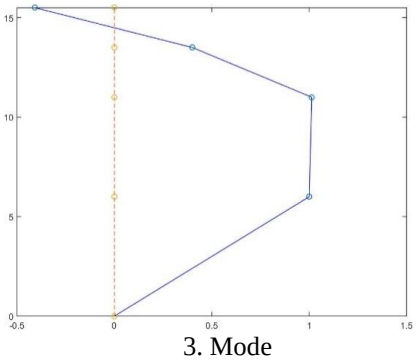

3. Mode

Figure 7. The first three modes obtained using updated analytical model

Table 2. Comparison of Updated Analytical Model Solutions and Experimental Results.

Mode Number	Updated Analytical Frequencies (Hz)	Experimental Frequencies (Hz)	MAC (%)
1	2.24	2.15	96.366
2	2.34	2.32	95.898
3	8.58	9.56	90.397

4. Conclusions

In this study, dynamic characteristics of a reinforced concrete minaret were determined by using Operational Modal Analysis (OMA) method and the analytical model of this minaret was updated. The analytical model solution was obtained by using SAP2000 finite element package program. Modal analysis of the analytical model was performed to find the dynamic characteristics and the first three frequencies were obtained at the range of 2.30-8.77 Hz.

The OROS-OR36 Multichannel Noise and Vibration Analyzer was used for experimental measurements. In these measurements, the first three frequencies are in the range of 2.15-9.56 Hz and the damping ratios related to these frequencies are in the range of 2.89-4.09%.

In comparison of the initial analytical model solutions and experimental results, the frequency and MAC values were seen to be compatible for both method. Differences between analytical and experimental frequencies can be minimized if the initial model of the structure is updated. The minaret mass is considerably known. There is more uncertainty in stiffness. Factors affecting the stiffness can be expressed as concrete elasticity and boundary conditions. Here, elasticity module of concrete was updated. The first three frequencies of the modal solutions of the updated model were obtained in the range of 2.24-8.58Hz. For the frequency and MAC values of first two modes, modal solution of the updated analytical model are closer to the results of the experimental method.

It has also been shown in this study that the dynamic characteristics of structures can be obtained using experimental methods and the analytical models can be updated according to the results of the experimental methods.

5. References

1.Rainieri, C., and Fabbrocino, G., (2011). Operational modal analysis for the characterization of heritage structures. *Geofizika*, **28.1**: 109-126.

2.Türker, T. (2011). Çevresel Titreşim Verileri Kullanılarak Yapıların Hasar Durumlarının Tespiti Ve Değerlendirilmesi, Doctoral Thesis, Karadeniz Technical University, Institute of Science and Technology, 247s.

3.Şahin, A. (2009). Yapıların Deneysel ve Operasyonel Modal Analizleri İçin Sayısal Sinyal İşleme, Dinamik Karakteristik Belirleme ve Sonlu Eleman Model İyileştirme Yazılımları: SignalCAD - ModalCAD – FemUP, Doctoral Thesis, Karadeniz Technical University, Institute of Science and Technology, Trabzon, 361s.

4.Turan, F.N. (2012). Dengeli Konsol Betonarme Köprülerin Dinamik Karakteristiklerinin Çevresel Titreşim Verileri Kullanılarak Belirlenmesi, Master's Thesis, Karadeniz Technical University, Institute of Science and Technology, Trabzon, 84s.

5.Yetkin, M. (2016). Betonarme Yapıların Çevresel Titreşim Verileri Kullanılarak Dinamik Davranışının İncelenmesi, Master's Thesis, Firat University, Institute of Science and Technology, Elazig, 68s.

6.Bayraktar, A., Altunışık, A.C., Sevim, B., Türker, T., and Birinci, F., (2010). Tarihi Yapıların Deprem Güvenliklerinin Tahribatsız Deneysel Yöntemlerle Belirlenmesi. *İMO İstanbul*, **98**: 10-20..

7.Yetkin, M., Calayır, Y., and Erkek, H., (2016). Çevresel Titreşim Verileri Kullanılarak Yapıların Dinamik Karakteristiklerinin Belirlenmesi Ve Sonlu Eleman Modellerinin Güncelleştirilmesi. *International Symposium on Natural Hazards and Hazard Management (Uluslararası Doğal Afetler ve Afet Yönetimi Sempozyumu - DAAYS'16)*, Karabük Üniversitesi, Karabük, 2-4 Mart, 2016, 133-138.

8.Bayraktar, A., Sevim, B., Altunişik, A.C., and Türker, T., (2007). Tarihi Yığma Minarelerin Deprem Güvenliklerinin Operasyonal Modal Analiz Yöntemiyle Belirlenmesi. *Tarihi Eserlerin Güçlendirilmesi ve Geleceğe Güvenle Devredilmesi Sempozyumu 1*, Ankara, Türkiye, 415-428.

9.D'Ambrisi, A., Mariani, V., and Mezzi, M., (2012). Seismic assessment of a historical masonry tower with nonlinear static and dynamic analyses tuned on ambient vibration tests. *Engineering Structures*, **36**: 210-219.

10. Bartoli, G., Betti, M., and Giordano, S., (2013). In Situ Static and Dynamic Investigations on the Torre Grossa Masonry Tower. *Engineering Structures*, **52**: 718-733.

11.Çalık, İ., Demirtaş, B., Bayraktar, A., and Türker, T., (2012). Yığma Taş Minarelerin Analitik Ve Deneysel Yöntemlerle Güvenliğinin Belirlenmesi:

Trabzon Muhittin Camii Minaresi Örneği. *Vakıflar Dergisi*, **38**: 121-139.

12. Choi, Park, S., Hyun, C.H., Kim, M.S., and Choi, K.R., (2010). Modal Parameter Identification Of A Containment Using Ambient Vibration Measurements. *Nuclear Engineering and Design*, **240**: 453-460.

13. Ventura, C., Laverick, B., Brincker, R., and Andersen, P., (2003). Comparison of Dynamic Characteristics of Two Instrumented Tall Buildings. *In Proceedings of IMAC-21: A Conference on Structural Dynamics*, February 3-6, The Hyatt Orlando, Kissimmee, Florida, 236-242.

14. Vivo, A.D., Brutti, C., and Leofanti, J.L., (2013). Modal shape identification of large structure exposed to wind excitation by operational modal analysis technique. *Mechanical Systems and Signal Processing*, **39**: 195–206.

15. Heerah, A.R.P. (2009). Field Investigatıon of Fundamental Frequency of Bridges Using Ambient Vibration Measurements. Master of Engineering, McGill University Montreal, Canada, 148s.

16. Ewins, D.J., (2000). Modal Testing: Theory Practice and Application, Research Studies Press, Baldock, Hertfordshire, UK, 576s.

17. Mendes, P., Baptista, M.A., Agostinho, L., Lagomarsino, S., and Costav, J.P., (2005). Structural and dynamic analysis of N. Sra. do Carmo churchs. *Proceedings EURODYN2005, Structural Dynamics*, Lagos Portugal, 311-318.

Turkish Journal of Science & Technology
Volume 13(1), 99-103, 2018

Deformation Measurements and Analysis with Robust Methods: A Case Study, Deriner Dam

Berkant Konakoğlu*, Ertan Gökalp
Karadeniz Technical University, Department of Geomatics, Trabzon, TURKEY
*bkonakoglu@ktu.edu.tr

(Received: 15.02.2017;Accepted: 22.04.2017)

Abstract

Dams, one of the country's most natural and cheapest way to product energy, are built for energy production, agricultural activities and flood protection. Dams with high construction costs are subject to deformation due to some physical factors. Therefore, dams should be kept safe to prevent possible dam accidents, loss of life and property. Engineering structures (such as dams) should be monitored periodically by geodetic and non-geodetic techniques. Deriner dam is Turkey's highest double-curved concrete arch dam. In this study, we monitored deformation with GPS measurements. For this purpose, two period static GPS measurements were performed on the reference and object points in the study. Afterwards, GPS measurements were adjusted separately with respect to free adjustment method and then deformation analysis were carried out by using the adjusted coordinates and their cofactor vectors. Iterative Weighted Similarity Transformation (IWST) and Least Absolute Sum (LAS) methods were used as deformation methods to detect the displacement of the reference and object points.

Keywords: Concrete arc dam, Deformation, Analysis, IWST, LAS, GPS.

Deformasyon Ölçmeleri ve Robust Yöntemler ile Analizi: Deriner Barajı Örneği

Özet

Bir ülkenin enerji üretiminin en doğal ve en ucuz yolu olan barajlar enerji üretimi, tarımsal faaliyetler ve taşkın koruma amacıyla inşa edilmektedir. Yapım maliyeti oldukça yüksek olan barajlar çeşitli fiziksel faktörlerinden dolayı deformasyona maruz kalırlar. Olası baraj kazalarını önleyebilmek, can ve mal kaybını önlemek için barajlar güvenlik altında tutulmalıdır. Baraj gibi büyük mühendislik yapıları jeodezik ve jeodezik olmayan yöntemlerle periyodik olarak izlenmelidir. Deriner barajı sahip olduğu gövde yüksekliği ile Türkiye'nin en yüksek çift eğrilikli beton kemer barajıdır. Bu çalışmada deformasyonlar GPS ölçüleri ile belirlenmiştir. Bu amaçla referans ve obje noktalarında iki periyot statik GPS ölçüleri gerçekleştirilmiştir. GPS ölçüleri serbest dengelenerek, dengelenmiş koordinatlar ve kofaktör matrisler kullanılarak deformasyon analizi yapılmıştır. Referans ve obje noktalarındaki hareketleri belirlemek için deformasyon analiz yöntemi olarak İteratif Ağırlıklı Benzerlik Dönüşüm ve En Küçük Mutlak Toplam yöntemleri kullanılmıştır.

Anahtar Kelimeler: Beton Kemer Baraj, Deformasyon, Analiz, IWST, LAS, GPS.

1. Introduction

The dams are one of the most important engineering structures used for water supply, flood protection and agricultural activities. Besides, it is the most natural and cheapest way of energy production for a country. Dams constructed with high cost expenditures are subjected to deformation due to various loading factors such as water level, air, water temperature and rock deformability. Controlling these dams has become compulsory in order to prevent disasters. In the literature, many deformation monitoring based studies have been reported [1]-[8]. Reference [1] investigated the surface movements of Alibey dam by means of geodetic and geotechnical methods. Geodetic displacement measurements were analysed using the Karlsruhe method. Also, Finite Element Method (FEM) was used to determine the behaviour of the dam. The results of geodetic measurements were compared with those of the FEM analyses. Reference [2] examined the long-term settlement behaviour of the Mornos dam in Greece. The result of geodetic monitoring analysis

and that of the finite element back analysis were compared. The findings showed a very good agreement between the measured and computed displacements. Reference [3] utilized the Global Positioning System (GPS) technique for monitoring horizontal movements in the Altınkaya dam. A deformation network consisting of 6 reference points and 11 object points along the dam crest were observed for 4 periods. Geodetic displacement measurements were analysed using the IWST and LAS methods to determine the points stability. Reference [4] investigated the magnitude and the direction of radial deformations of the Atatürk dam by means of conventional and GPS techniques. No significant correlation was detected between the radial movements on embankment and reservoir water level. Reference [5] investigated the relationship between displacement and reservoir water levels of the Koyna dam in India by means of GPS technique. The results indicated that a significant correlation between the movements and reservoir water level was detected. Reference [6] evaluated the horizontal movements of the Ermenek dam based on periodic conventional geodetic measurement campaigns during the first filling of the reservoir. Geodetic measurements were compared with those of the FEM. The aim of this work is to investigate the horizontal movements at the Deriner dam with GPS measurements. The coordinates of the GPS measurements are in WGS-84 coordinate system. The coordinates of the points were converted from Cartesian to the local topocentric coordinate system in order to examine the real directions of the displacements. Deformation analysis was performed with the Iterative Weighted Similarity Transformation (IWST) and the Least Absolute Sum (LAS) methods. Finally, the results of these two methods have been compared.

2. Materials and Methods

2.1. Robust Methods

Robust methods are used when there is no previous information about the movement of the points within the network [9]. In this study, the IWST and LAS methods are used to estimate the movements of a monitoring network. The IWST, proposed by [10], is a robust method. According to [11], the Danish, LAS and Huber methods are some of the frequently used robust methods. The IWST and LAS methods are based on S-transformation [10]-[12]. Both methods are applied as follows;

Adjusted coordinates of the points x_1, x_2 and their cofactor matrix Q_{x1}, Q_{x2} are calculated with two separate free adjustments. The displacement values (d) and cofactor matrix of d Q_d are calculated as;

$$d = x_2 - x_1 \tag{1}$$

$$Q_d = Q_{x1} + Q_{x2} \tag{2}$$

Then displacement values (d) are calculated as (3);

$$\begin{aligned} & d^{(k+1)} \\ & = \left[I - H\left(H^T W^{(k)} H\right)^{-1} H^T W^{(k)}\right] d^{(k)} \\ & = S^{(k)} d^{(k)} \end{aligned} \tag{3}$$

$\boldsymbol{d}$ = displacement vector

$\boldsymbol{k}$ = number of iterations

$\boldsymbol{I}$ = identity matrix

$\boldsymbol{W}$ = weight matrix

$\boldsymbol{S}$ = S-transformations matrix

H matrix for the 3D networks is written as;

$$H = \begin{bmatrix} e & 0 & 0 & 0 & -z_0 & -y_0 & x_0 \\ 0 & e & 0 & -z_0 & 0 & x_0 & y_0 \\ 0 & 0 & e & y_0 & -x_0 & 0 & z_0 \end{bmatrix}_{3m*7} \tag{4}$$

where, $e^T = (1, \dots\dots\dots, 1)$ x_0, y_0 and z_0 are the coordinates of points P_i, which are reduced to the centre of the network (5).

$$X_0^i = X_i - \frac{1}{m}\sum_{i=1}^{m} x_{i0},$$

$$Y_0^i = Y_i - \frac{1}{m}\sum_{i=1}^{m} y_{i0}, \quad (5)$$

$$Z_0^i = Z - \frac{1}{m}\sum_{i=1}^{m} z_{i0}$$

Above, z_0^i, y_0^i and x_0^i the i^{th} elements of z^0, y^0 and x^0 respectively, and z_i, y_i and x_i are approximate coordinates of point P_i and m is the number of the points in the network [13]-[15]. The main difference between the IWST and LAS method is in forming the weight matrix. In the first transformation $(k = 1)$ the weight matrix is taken as identity $\left(W^{(k)} = I\right)$ for all common points, then in the (k+1) transformation the weight matrix is defined as;

For the IWST method,

$$W^{(k)} = diag\{1/|d^{(k)}|\} \quad (6)$$

For the LAS method,

$$W^{(k)} = diag\left\{\frac{1}{\sqrt{(dx_i^{(k)})^2 + (dy_i^{(k)})^2}}\right\} \quad (7)$$

In equation (6), d is the displacement vector. However, in equation (7), dx_i and dy_i refer to the displacement components in x and y axis respectively. The iterative procedure continues until the differences between displacements of all common points $\left(d^{(k+1)} - d^{(k)}\right)$ are smaller than a tolarence value Ɛ (i.e. 0.0001 m.). In the final iteration cofactor matrix is calculated as;

$$Q_d^{(k+1)} = S^{(k)} Q_d \left(S^{(k)}\right)^T \quad (8)$$

The IWST method minimizes the total sum of absolute values of the displacement components,

$$\left(\sum |d_i| \Rightarrow min\right) \quad (9)$$

while the LAS method minimizes the sum of the lengths of the displacement,

$$\left(\sum \sqrt{(dx_i^{(k)})^2 + (dy_i^{(k)})^2} \Rightarrow min\right) \quad (10)$$

Equation (11) can be used in order to determine unstable reference and object points in the deformation network with a single point test as shown below [14];

$$T_i = \frac{\left(d_i^{(k+1)}\right)^T \left(Q_{di}^{(k+1)}\right)^{-1} d_i^{(k+1)}}{u_d \hat{\sigma}_0^2} \sim F(\alpha, u_d, df) \quad (11)$$

d_i = displacement vector of point i

Q_{di} = cofactor matrix of point i

u_d = dimension of the confidence region (1, 2 or 3)

$\hat{\sigma}_0^2 = \frac{df_i \hat{\sigma}_i^2 + df_j \hat{\sigma}_j^2}{df_i + df_j}$ = pooled variance factor

$\hat{\sigma}_i^2, \hat{\sigma}_j^2$ = a posteriori variance factors of epoch i and j

df_i, df_j = degrees of freedom of epoch i and j

α = significance level

If the test is passed, the point is assumed to be stable, otherwise, it is considered unstable.

3. Application

The Deriner dam, a double-curvature concrete arch dam, is located on the Coruh River at Artvin province in the north-eastern part of Turkey. It is the highest dam with a body height of 249 meters in Turkey. The underground powerhouse near the dam includes four units, with an overall capacity of 670 MW. Also, the powerhouse annually generates 2.118 GWh of electricity. The picture of

the dam and technical specifications are given in Figure 1 and in Table 1, respectively.

Figure 1. Deriner dam

Table 1. Technical characteristics of the Deriner dam

Type	Double-curvature concrete arch
Dam crest elevation	397.00 m
Length of dam crest	720.00 m
Height of crest	249.00 m
Total reservoir area	26.40 km^2
Total reservoir volume	1969 hm^3
Electric production capacity	2.117,75 GWh per year

In order to determine the possible horizontal movements on the dam crest, 14 reference and 7 objects points were used (Figure 2).

Figure 2. Distribution of reference and object points in Deriner dam

The deformation measurements of Deriner dam involved two measurement campaigns. The first campaign was carried out in May 2016 and the second one in September 2016. During the GPS measurements, Topcon Hiper Pro and Topcon GR-5 dual-frequencies receivers were used. The observation period was selected as 2 hours and 1.5 hours for reference and object points, respectively. The sampling rate was chosen as 10 seconds and the satellite elevation mask was selected at 15°. The baselines were processed with the Topcon Tools v.8.2.3 software. MATLAB script was used for network adjustment and deformation analysis. The significance level for deformation detection was specified as 0.05. The adjusted coordinates (WGS-84) and cofactor matrix were obtained from a free network adjustment. Deformation analysis was made with respect to the first period measurement. The two dimensional deformation analysis was made. All WGS-84 coordinates (X, Y, Z) and cofactor matrices were transformed to the local coordinate system (E, N, U). The displacement values (d) were computed by the IWST and LAS methods are shown in Tables 2 and 3. These tables also depicts whether or not the points are stable. Water levels were 389.33 m in the first period and 377.22 m in the second period. The reduction of water level in between the two periods is 12.11 m.

Table 2. Stable and unstable points determined by IWST

		Between 1-2 periods		
		IWST		
		dN	***dE***	
		cm	***cm***	
Object Points	1139	-0.19	0.18	stable
	1133	0.91	-0.59	unstable
	1127	1.17	-1.15	unstable
	1121	1.09	-1.93	unstable
	1115	0.52	-2.01	unstable
	1109	-0.45	-0.82	unstable
	1103	-0.25	-0.16	stable
Reference Points	105	-0.37	0.53	unstable
	108	0.02	0.24	unstable
	109	-0.09	0.32	unstable
	112	-0.01	-0.12	stable
	118	0.00	0.14	unstable
	101	0.00	-0.03	stable
	102	0.56	0.16	unstable
	104	-0.16	0.47	unstable
	107	-0.13	0	stable
	111	-0.14	0.06	stable
	113	0.01	0.23	stable
	114	0.08	-0.27	stable
	116	0.02	-0.13	stable
	117	-0.14	0.24	unstable

Table 3. Stable and unstable points determined by LAS

Between 1-2 periods				
LAS				
		dN	***dE***	
		cm	***cm***	
Object Points	1139	-0.17	0.17	stable
	1133	0.93	-0.61	unstable
	1127	1.19	-1.16	unstable
	1121	1.11	-1.93	unstable
	1115	0.53	-2.00	unstable
	1109	-0.43	-0.82	unstable
	1103	-0.24	-0.17	stable
Reference Points	105	-0.35	0.52	unstable
	108	0.04	0.23	unstable
	109	-0.07	0.31	unstable
	112	0.00	-0.13	stable
	118	0.02	0.14	stable
	101	0.03	-0.02	stable
	102	0.59	0.17	unstable
	104	-0.13	0.47	unstable
	107	-0.11	0.00	stable
	111	-0.13	0.06	stable
	113	0.04	0.23	stable
	114	0.12	-0.26	stable
	116	0.05	-0.13	unstable
	117	-0.12	0.24	unstable

4. Conclusion

Since we have no prior information about the movement of the points within the network, the IWST and LAS methods were used in this study. The IWST and LAS were used to perform 2D deformation analysis. It can be concluded from the results of the analysis that the displacements are dependent on the water level on the reservoir. The maximum horizontal displacement was experienced in the middle of the dam crest. These results will also be examined with new measurements to be conducted in further periods. Also, precise differential levelling of levelling line along the dam crest will be performed.

5. Acknowledgment

The authors would like to thank the Turkish General Directorate of State Hydrologic Works (DSI), the 26th Regional Directorate Artvin. This research was supported by the Scientific Research and Projects Unit (5482, 5252) of Karadeniz Technical University.

6. References

1. Guler G., Kilic H., Hosbas G. and Ozaydın K. (2006). Evaluation of the movements of the dam embankments by means of geodetic and geotechnical methods. Journal of surveying engineering, **132**(1): 31-39.

2.Gikas V. and Sakellariou M. (2008). Settlement analysis of the Mornos earth dam (Greece): Evidence from numerical modeling and geodetic monitoring. Engineering Structures, **30**(11): 3074-3081.

3. Taşçi L. (2008). Dam deformation measurements with GPS. Geodezijair kartografija, **34**(4): 116-121.

4.Kalkan Y. (2014). Geodetic deformation monitoring of Ataturk Dam in Turkey. Arabian Journal of Geosciences, **7**(1): 397-405.

5.Radhakrishnan N. (2014). Application of GPS in structural deformation monitoring A case on Koyna dam. Journal of Geomatics, **8**(1): 48-54.

6. Yigit C. O., Alcay S., and Ceylan A. (2016). Displacement response of a concrete arch dam to seasonal temperature fluctuations and reservoir level rise during the first filling period: evidence from geodetic data. Geomatics, Natural Hazards and Risk, **7**(4): 1489-1505.

7. Ehiorobo J. O. and Irughe-Ehigiator R. (2011). Monitoring for horizontal movement in an earth dam using differential GPS, Journal of Emerging Trends in Engineering and Applied Sciences, **2**(6): 908-913.

8. Pytharouli S. I. and Stiros S. C. (2005). Ladon dam (Greece) deformation and reservoir level fluctuations: evidence for a causative relationship from the spectral analysis of a geodetic monitoring record, Engineering Structures, **27**(3): 361-370.

9. Singh R. and Setan H. (1999). Comparison of different datum definitions in detection of deformation of a geodetic monitoring networks, in Presented at Research Seminar on Construction, Materials and Environmental Technology, Universiti Teknologi Malaysia, Johor, Bahru.

10. Chen Y. Q. (1983). Analysis of Deformation Surveys - A Generalized Method," Technical Report No. 94, Department of Surveying Engineering, University of New Brunswick, Fredericton, N.B.

11. Caspary W. F. and Borutta H. (1987). Robust estimation in deformation models. Survey Review, **29**(223): 29-45.

12. Chen Y. Q., Chrzanowski A. and Secord J. M., (1990). A strategy for the analysis of the stability of reference points in deformation surveys, CISM JOURNAL ACSGC, **44**(2): 141-149.

13. Kuang S. (1996). Geodetic network analysis and optimal design: concepts and applications, Ann Arbor Press Inc.

14. Setan H. and Singh R., (2001). Deformation analysis of a geodetic monitoring network. GEOMATICA-OTTAWA, **55**(3): 333-346.

15. Taşçi L. (2010). Analysis of dam deformation measurements with the robust and non-robust methods, Scientific Research and Essays, **5**(14): 1770-177

Turkish Journal of Science & Technology
Volume 13(1), 105-111, 2018

Determination of the Resistance of Hot Mix Asphalt Samples Prepared Under Different Conditions Against Wheel Tracking

Taner Alataş[1,*], Mehmet Yilmaz[1], Baha Vural Kök[1]
[1]Fırat University, Engineering Faculty, Civil Engineering Department, Elazığ.
[*] talatas@firat.edu.tr
(Received: 12.02.2017; Accepted: 24.02.2017)

Abstract

The present study aimed to examine the resistance of pure hot mixes and those prepared with 4% of three different polymers two types of SBS (styrene-butadiene-styrene) and one type of EVA (ethylene-vinyl-acetate) against permanent deformation. Samples were prepared with application of vibration so that they would have 4% void ratio using a roller compactor and without this application. The effect of vibration application during sample preparation on the wheel track formation was also assessed in the current study. Wheel track tests demonstrated that use of additives increased the resistance of hot mixes against wheel track formation. It was also determined that the most effective additive was EVA. Furthermore, it was determined that application of vibration during sample preparation increased the resistance of specimens against permanent deformation.

Keywords: Wheel tracking, Hot mix asphalt, Styrene-butadiene-styrene, Ethylene-vinyl-acetate.

Farklı Koşullarda Hazırlanan Bitümlü Sıcak Karışım Numunelerinin Tekerlek İzi Oluşumuna Karşı Dayanımlarının Belirlenmesi

Özet

Bu çalışmada, saf ve %4 oranında üç farklı polimer (iki tür stiren-butadien-stiren ve bir tür etilen-vinil-asetat) içeren bağlayıcılarla hazırlanan karışımların kalıcı deformasyona karşı dayanımları incelenmiştir. Numuneler merdaneli sıkıştırıcı kullanılarak %4 boşluk oranına sahip olacak şekilde vibrasyon uygulanarak ve vibrasyon uygulanmadan hazırlanmıştır. Böylece numune hazırlama esnasında vibrasyon uygulamasının tekerlek izi oluşumu üzerindeki etkisi de mevcut araştırmada değerlendirilmiştir. Tekerlek izi oluşumu deneyleri, katkı maddelerinin, bitümlü sıcak karışımların tekerlek izi oluşumuna karşı direncini arttırdığını göstermiştir. Tekerlek izi oluşumuna karşı en etkin katkı maddesinin EVA olduğu tespit edilmiştir. Ayrıca numune hazırlama esnasında vibrasyon uygulanmasının numunelerin kalıcı deformasyona karşı direncini arttırdığı tespit edilmiştir.

Anahtar Kelimeler: Tekerlek izi, Bitümlü sıcak karışım, Stiren-butadien-stiren, Etilen-vinil-asetat.

1. Introduction

Two basic components of bituminous hot mixes (BHM) are aggregate and bitumen and aggregates used in BHMs consist 90-95% of the total BHM weight. 1.6 billion tons of bituminous hot mix is produced every year worldwide. For this purpose, approximately 1.5 billion tons of aggregate is used. Environmental damages caused by highway construction are those resulting from construction activities (CO_2 emissions, use of nature lands, change in current conditions and ecological balance, change in natural structure) and the damages caused by the material utilized for construction (destruction of natural lands, technological equipment causing chemical pollution, noise and vibration) [1].

One of the most encountered deformations observed with bituminous hot mixes, permanent deformations occur as a result of two basic conditions. The first occurs due to the inappropriate construction of the base course or the asphalt base course. In the second condition, while there is no deformation in lower layers, the permanent deformation (wheel tracks) form on the wearing course [2].

Wheel track formation is frequently observed on pavement courses in hot temperatures and on roads where heavy vehicle traffic is present. Deformations cause expensive rehabilitations or reconstruction, as well as new

material needs, resulting in harming the environment again.

To improve the features of BHMs, postponing expensive rehabilitation and reconstructions, additive substances are utilized. Polymers used as the most common additive substances used in modification of bituminous binders are grouped in four categories of plastomers, elastomers, fibers and pavements. To improve the features of bitumen, selected polymer should form a new bond in bitumen, chemically reacting with bitumen. Obtaining a high performance polymer modified bitumen is dependent on the better distribution of the polymer in bitumen and the chemical structure of the bitumen [3]. Most frequently used bitumen additives are styrene-butadiene-styrene (SBS) from the elastomer group and ethylene-vinyl-acetate (EVA) from the plastomer group [4]. Several studies demonstrated that resistance against ageing [5], permanent deformation [6], low temperature fractures [7], and moisture damage [8] increased by the use of SBS modified bitumen. EVA especially increases resistance against permanent deformation [9] , [10].

It is possible to adjust the polybutadiene structure of SBS block copolymers using a special catalyzer. Thus, it is possible to obtain an SBS with the same molecular weight, but with a shorter polymer chain. This means low viscosity, and a better and more homogenous mixture with bitumen [11], [12].

It is of utmost significance to prepare bituminous hot mixes in laboratory environment reflecting the field conditions, for the accuracy of the design and accurate determination of the material that would be applied in the field. In the present study, bituminous hot mix samples containing pure bitumen and bitumen modified by three different additives (two types of SBS and one type of EVA) were prepared using roller compactor. The mixes were compacted with and without vibration to create the same void ratio. Afterwards, wheel track tests were conducted on these mixes. Thus, the effect of mix preparation method on permanent deformation performance of the mixes was assessed.

2. Materials and Methods

Limestone type aggregate procured from Karayazı region in Elazığ province in Turkey was used in the study. Properties of the aggregate is presented in Table 1 and the gradation selected according to Superpave method is given in Figure 1. Triangular signs depict control points, closed field shows forbidden zone, and square signs show utilized gradation points in Figure 1.

PG 58-35 bitumen procured from TÜPRAŞ refinery was used as the main binder in the present study. Two different types of SBS produced by Shell Corporation (Kraton D 1101 and Kraton MD 243) and EVA produced by Arkema Corporation (Evatane® 2805) were used as additives. A four-bladed mixing head was used in preparing modified bitumen. Pure bitumen and additives were mixed in a special mixer for 60 minutes at 180°C temperature and 1000 rpm.

To evaluate the effect of these additives on the performance of bituminous hot mixes, all additives were used at a rate of 4% (Table 2). Dynamic shear rheometer (DSR) and beam bending rheometer (BBD) test results for pure and with 4% SBS D1101 (MB_{SBS-D}), SBS MD243 (MB_{SBS-M}), and Evatane® 2805 (MB_{EVA}) bitumen are presented in Table 3. It was determined that the performance levels for MB_{SBS-D} and MB_{SBS-M} modified bitumen were similar (PG 70-34), and the low temperature value for MB_{EVA} modified bitumen was one level higher (PG70-28).

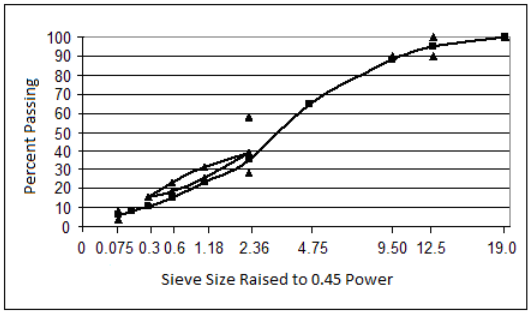

Figure 1. Used aggregate gradation.

Table 1. Physical properties of aggregate.

Properties	Standard	Limit	Coarse	Fine	Filler
Abrasion loss (%) (Los Angeles)	ASTM D 131	Max 30	27.8	-	-
Abrasion loss (%) (Micro Deval)	ASTM D 6928	Max 15	13.6	-	-
Frost action (%) (with Na_2SO_4)	ASTM C 88	Max 10	5.8	-	-
Specific gravity (g/cm^3)	ASTM C127		2.544	2.571	2.675

Table 2. Abbreviations used for modified bitumen.

Additive type and ratio	%4 SBS-D1101	%4 SBS-MD243	%4 EVA
Denomination	MB_{SBS-D}	MB_{SBS-M}	MB_{EVA}

Table 3. DSR and BBR test results of binders.

DSR test results				
Temperature	G*/sinδ (Pa) (Specification limit min. 1000 Pa)			
(°C)	PG 58-34	MB_{SBS-D}	MB_{SBS-M}	MB_{EVA}
58	1258	4890	4204	4534
70	-	1326	1183	1512
	G*/sin δ (Pa) RTFOT residue (Specification limit min. 2200 Pa)			
58	7862	-	-	-
70	-	5599	5171	6862
	G*.sin δ ($Pa*10^6$) PAV residue (Specification limit max. $5*10^6$ Pa)			
16	1.83	-	-	-
22	-	1.69	1.52	-
25	-	-	-	1.34
BBR test results				
Temperature	m-value (Specification limit min. 0.300)			
(°C)	PG 58-34	MB_{SBS-D}	MB_{SBS-M}	MB_{EVA}
-18	-	-	-	0.306
-24	0.309	0.314	0.325	0.277
-30	0.266	0.221	0.291	-
	Creep stiffness (Mpa) (Specification limit max. 300 MPa)			
-18	-	-	-	131.3
-24	108.3	144.7	98.5	160.6
-30	140.9	242.6	121.9	-
	Performance Grade (PG)			
	58-34	70-34	70-34	70-28

Rotational viscometer tests were conducted on unaged pure and modified bitumen under 135°C and 185°C temperatures to determine the workability of the binders and aggregate mixing and compacting temperatures. For workability, the viscosity values for the binders should be below 3 Pa.s (3000 cP) at 135°C [13]. Furthermore, it is required that the viscosity value of bituminous binders during mixing with aggregate should be 170 ± 20 cP, and during compacting it should be 280 ± 30 cP [14]. Utilizing the viscosity-temperature graphs plotted in the study, aggregate mixing and compacting temperature for each binder was identified. Results of viscosity tests are displayed in Table 4.

Data presented in Table 4 shows that all binders met the workability criterion. Furthermore, using additives increased viscosity values and mixing and compacting temperatures rose as a result. Modification indices were obtained by division of viscosity values of

modified bitumen by viscosity value of pure binder. As could be seen in Table 4, the highest modification index value was obtained with MB_{EVA} modified bitumen at both 135ºC and 165ºC temperatures. This situation indicates that more energy would be required in the plant during mixing with aggregate with EVA use.

During preparation of bituminous hot mixes, aggregate and bitumen were heated to mixing temperature and mixed using a special mixer. Non-compacted samples were placed in trays 21-22 kg per square meter and aged for a short period of time for 4 hours in an incubator at 135ºC. Then, the mixtures were heated to mixing temperatures and compacted using a 1.25º angle gyratory compactor for 100 revolutions. The design was determined based on the volumetric properties of bitumen content mixtures. It was determined that design bitumen content increased with modified bitumen use. Volumetric properties of mixtures in design bitumen content and Superpave specification criteria are presented in Table 5. It was confirmed that all mixtures met Superpave specification criteria.

Table 4. Rotational viscosity test results.

Properties	Standard	PG 58-34	MB_{SBS-D}	MB_{SBS-M}	MB_{EVA}
Viscosity (cP, 135°C)	ASTM D4402	275.0	1125.0	825.0	1250.0
Viscosity (cP, 165°C)	ASTM D4402	112.5	350.0	262.5	375.0
Mixing temperature range (°C)	-	151-158	171-173	169–171	171-173
Compaction temperature range (°C)	-	129-140	167-169	163–166	167-169
Modification index (135°C)		-	4.09	3.00	4.54
Modification index (165°C)		-	3.11	2.33	3.33

Table 5. Volumetric properties of mixtures.

Mixture properties	Specification limits	Binder type			
		PG 58-34	MB_{SBS-D}	MB_{SBS-M}	MB_{EVA}
Design binder content (%)	–	4.88	5.27	5.35	5.07
Air Voids (Va, %)	4.0	4.04	4.09	4.09	3.99
Voids in mineral aggregate (VMA, %)	min. 14.0	14.61	15.39	15.50	14.86
Voids filled with bitumen (VFA, %)	65–75	72.37	73.42	73.63	73.13
Dust ratio (DP)	0.8–1.6	1.07	0.98	0.97	1.02

3. Wheel Track Tests

Wheel track formation on pavement layer was examined in the study. The tests were conducted based on EN 12697-22 standard B procedure to examine the wheel track resistance of samples that contained pure PG 58-34, 4% SBS-D, SBS-M and EVA modified binders. Since maximum aggregate grain diameter was 19 mm according to the standard, sample height was selected as 6.0 cm. Initially 30.5 * 30.5 * 6 cm plate samples were compacted using rolling compactor so that they would have 4% air void ratio. Some samples were compacted with application of vibration, and the others were compacted without. Required BHM amount for plate samples was determined using the following equation:

$$M = 10^{-6} * L * l * e * \rho_m * ((100 - v)/100) \quad (1)$$

where M is sample weight (kg), L is inner length of the mold (mm), l is the inner width of the mold (mm), e is the final height of the sample (mm), ρ_m is the maximum density of the bituminous mixture (kg/m^3), and v is the void ratio of the sample (%).

In wheel track experiment the samples were tested at 60°C temperature. The device took 27 deformation measurements, out of which one was taken from the center of the sample, and 13were taken from the left of the center and right of the center. At the end of 10,000 wheel revolutions, wheel track depths were determined using the average of these 27 values. For each mixture sample, two samples were tested and

average of the values were taken. According to EN 12697-22 standard, the test is terminated either after 10,000 load repetitions or when 20 mm wheel track depth is formed. In mixtures containing pure binder, 20 mm wheel track depth was obtained after 2,940 load repetitions and the test was ended. The tests conducted with modified bitumen were terminated after 10,000 load repetitions. The relationship between wheel track depth and number of load repetitions in mixtures prepared with vibration is presented in Figure 2, while relationship between wheel track depth and number of load repetitions in mixtures prepared without vibration is displayed in Figure 3. The load that caused 20 mm deformation in mixtures prepared with pure binder is displayed with a dashed line.

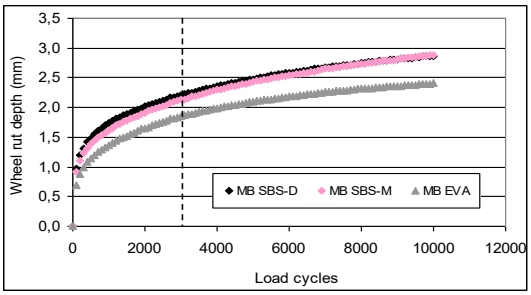

Figure 2. The wheel track depth-number of load repetition relationship in mixtures prepared with vibration.

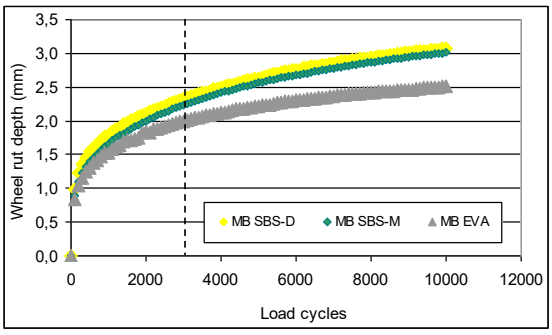

Figure 3. The wheel track depth-number of load repetition relationship in mixtures prepared without vibration

It was determined that wheel track values for mixtures prepared with MB_{SBS-D} and MB_{SBS-M} were close to each other as displayed in Figures 2 and 3. Comparison of mixtures prepared with modified bitumen showed that the lowest wheel track value was obtained with the mixture prepared with MB_{EVA}, and the highest wheel track value was obtained with the mixture prepared with MB_{SBS-D}. Deformation values for 5,000 and 10,000 load repetitions are presented in Table 6.

As could be observed in Table 6, wheel track depths for 5,000 and 10,000 load repetitions in mixtures prepared without vibration and using EVA modified bitumen were 18.5% and 22.7% lower than the mixture prepared using SBS-D modified bitumen, respectively. Furthermore, wheel track depths for 5,000 and 10,000 load repetitions in mixtures prepared using EVA modified bitumen were 15.3% and 20.3% lower than the mixture prepared without vibration using SBS-D modified bitumen, respectively.

As could be observed in Table 6, wheel track depths for 5,000 and 10,000 load repetitions in mixtures prepared with vibration and using EVA modified bitumen were 18.1% and 19.1% lower than the mixture prepared using SBS-D modified bitumen, respectively. Furthermore, wheel track depths for 5,000 and 10,000 load repetitions in mixtures prepared with vibration and using EVA modified bitumen were 15.7% and 19.9% lower than the mixture prepared using SBS-M modified bitumen, respectively.

As a result of vibration application, wheel track formation in mixes prepared using SBS-D modified bitumen decreased 5.7% after 5,000 load repetitions and 6.8% after 10,000 load repetitions. As a result of vibration application, wheel track formation in mixes prepared with SBS-M modified bitumen decreased 5.1% after 5,000 load repetitions and 4.3% after 10,000 load repetitions.

Table 6. Wheel track values for mixtures under different load repetitions.

Mixtures prepared without vibration				
Deformation (mm)	Mixture type (according to used binder)			
	PG 58-34	MB_{SBS-D}	MB_{SBS-M}	MB_{EVA}
@5000 load cycles	-	2.63	2.56	2.22
@10000 load cycles	-	3.08	3.02	2.51
Mixtures prepared with vibration				
Deformation (mm)	Mixture type (according to used binder)			
	PG 58-34	MB_{SBS-D}	MB_{SBS-M}	MB_{EVA}
@5000 load cycles	-	2.48	2.43	2.10
@10000 load cycles	-	2.87	2.89	2.41

As a result of vibration application, wheel track formation in mixes prepared using EVA modified bitumen decreased 5.4% after 5,000 load repetitions and 4.0% after 10,000 load repetitions.

Overall consideration of mixes showed that vibration application decreased wheel track formation. This finding demonstrated that, although the mixes had the same volume, the mix compacted better as a result of implementation of vibration. As a result of comparison of additive types, values obtained after 10,000 load repetitions showed that the mix affected by vibration the most was the one prepared with SBS-D and the mix affected by vibration the least was the one prepared with EVA based on permanent deformation. It was observed that compacting especially the SBS-D modified bitumen using vibration was more significant for wheel track formation.

4. Results

In the present study, initially the effect of three different bitumen additives (SBS-D, SBS-M and EVA) on the resistance of bituminous hot mixes against wheel track formation was examined. Later on, the effect of vibration application on the preparation of wheel track samples was attempted to be identified. Additive ratio was kept constant at 4% for all additives. Thus, the convenient comparison of all additive types was aimed. In the field, vibrating rollers are used to compact bituminous hot mixes. A roller compactor with vibration capabilities was used to obtain compatible samples with the field conditions. Samples were prepared using modified bitumen both by using and not using vibration. Wheel track tests were conducted on these samples to assess the effects of vibration.

It was determined that performance levels for modified bitumen that contained SBS-D and SBS-M equal to 4% of bitumen weight were PG 70-34, and the performance level of those that contained EVA were PG 70-28. It was identified that design bitumen content of the mixes prepared with SBS-D, SBS-M and EVA modified bitumen were 5.27%, 5.35%, and 5.07%, respectively.

Wheel track samples that contained pure and modified bitumen with 4% void ratio consistent with the field applications were prepared with roller press. Samples were prepared both using vibration and without using vibration. It was determined that mixes prepared with EVA modified bitumen had the lowest wheel track depth for both vibration applied and not vibration applied mixes. Furthermore, it was identified that wheel track values for mixes prepared with SBS-D and SBS-M modified bitumen were similar. It was also determined that vibration applied mixes displayed lower wheel track formation when compared to mixes that were not applied vibration.

It was determined that vibration was more effective especially in mixes prepared with SBS-D modified bitumen. It was considered that this condition was due to better compacting of the mixes as a result of vibration. To determine the compatibility of vibrated and non-vibrated samples with the field conditions, it would be beneficial to compare the test results for samples

obtained from the field with the test results for the samples prepared at the laboratory in the future.

5. Acknowledgements

The support for this work was provided by FUBAP (Fırat University Scientific Research Projects Unit) with project number MF.11.30, which we gratefully acknowledge.

6. References

1. Nicuta, A. M., (2011). Life Cycle Assesment Study for New and Recycled Asphalt Pavements, *Bulletin of the Polytechnic Institute of Iasi*, Vol. 61, Issue 2, pp. 81-91.

2. Said, S. F., Hakim, H., Oscarsson, E. and Hjort, M., (2011). Prediction of Flow Rutting in Asphalt Concrete Layers, *International Journal of Pavement Engineering*, Vol. 12, Issue 6, pp. 519-532.

3. Isacsson, U. and Lu, X., (1995). Testing and Appraisal of Polymer Modified Road Bitumens, State of the Art, *Materials and Structures*, Vol.28, pp. 139-159.

4. Sengoz, B. and Isıkyakar, G., (2008). Evaluation of the Properties and Microstructure of SBS and EVA Polymer Modified Bitumen, *Construction and Building Materials*, Vol. 22, Issue 9, pp. 1897-1905.

5. Cortizo, M. S., Larsen, D. O., Bianchetto, H. and Alessandrini, J. L., (2004). Effect of the Thermal Degradation of SBS Copolymers During the Ageing of Modified Asphalts, *Polymer Degradation Stability*, Vol. 86, Issue 2, pp. 275-282.

6. Tayfur, S., Ozen, H. and Aksoy, A. (2007). Investigation of Rutting Performance of Asphalt Mixtures Containing Polymer Modifiers, *Construction and Building Materials*, Vol. 21, pp. 328-337.

7. Isacsson, U. and Zeng, H.Y., (1997). Relationships Between Bitumen Chemistry and Low Temperature Behavior of Asphalt, *Construction and Building Materials*, Vol. 11, Issue 2, pp. 83–91.

8. Shuler, S. and Douglas, I., (1990). Improving Durability of Open-Graded Friction Courses, *Transportation Research Record*, Vol. 1259, pp. 35–41.

9. Airey, G., (2002). Rheological Evaluation of Ethylene Vinyl Acetate Polymer Modified Bitumens, *Construction and Building Materials*, Vol. 16, pp. 473-487.

10. Topal, A., (2010). Evaluation of the Properties and Microstructure of Plastomeric Polymer Modified Bitumens, *Fuel Processing Technology*, Vol. 91, pp. 45-51.

11. Vonk, W., Scholten, E., Korenstra, J. and Novel, J. (2010). Class of SBS Polymers for Enhanced Effectiveness in Bitumen Modification, Australian Asphalt Paving Association, *Thirteenth International Flexible Pavements Conference*, Queensland, Australia.

12. Scholten, E. J., Vonk, W. and Korenstra, J., (2010). Towards Green Pavements with Novel Class of SBS Polymers for Enhanced Effectiveness in Bitumen and Pavement Performance, *International Journal of Pavement Research Technology*, Vol. 3, Issue 4, pp. 216-222.

13. McGennis, R. B., Shuler, S. and Bahai, H. U., (1994). Background of Superpave Asphalt Binder Test Methods, *Report* No. FHWA-SA-94-069.

14. Zaniewski, J. P. and Pumphrey, M.E., (2004). Evaluation of Performance Graded Asphalt Binder Equipment and Testing Protocol, *Asphalt Technology Program.*

Turkish Journal of Science & Technology
Volume 13(1), 113-117, 2018

Finite Element Solution of the Contact Problem

Pembe Merve Karabulut[1*], Murat Yaylacı[2], Ahmet Birinci[3]

[1]Karadeniz Teknik Üniversitesi Of Teknoloji Fakültesi İnşaat Mühendisliği Bölümü Trabzon

[2]Recep Tayyip Erdoğan Üniversitesi Mühendislik Fakültesi İnşaat Mühendisliği Bölümü Rize

[3]Karadeniz Teknik Üniversitesi Mühendislik Fakültesi İnşaat Mühendisliği Bölümü Trabzon

[*]pembemerve.karabulut@ktu.edu.tr

(Received: 02.02.2017; Accepted: 03.04.2017)

Abstract

In this paper, continuous and discontinuous contact problems for an elastic layer loaded by symmetrical distributed loads whose lengths are 2a on an elastic semi-infinite plane is solved using finite element method. The elastic layer also subjected to uniform vertical body force because of effect of the gravity. Thickness in z direction is taken to be unit. It is assumed that the contact surfaces are frictionless, only normal tractions can be transmitted through the contact areas. The contact along the interface between elastic layer and half plane is continuous if the value of load factor is less than a critical value. In continuous and discontinuous contact cases, the stress distribution on the contact interface are plotted for different dimensionless quantities. The finite element model of the problem is constituted using ANSYS software and analysis of the problem is carried out. Finally, the results obtained from the finite element solution are verified by comprasion with the analytical results.

Keywords: Mechanic, Continuous contact, Discontinuous contact, Elasticity, Half plane, Finite element analysis.

Temas Probleminin Sonlu Elemanlar Çözümü

Özet

Bu çalışmada, simetrik 2a genişliğindeki yayılı yük ile yüklenmiş elastik tabakanın sürekli ve süreksiz temas problem sonlu elemanlar yöntemi kullanılarak çözülmüştür. Elastik tabakaya ayrıca yer çekimi etkisinden doğan kütle kuvvetleri etkimektedir. z yönündeki kalınlık birim olarak alınmıştır ve temas yüzeylerinde sürtünmenin etkisi dikkate alınmamıştır. Yük faktörünün kritik değerden küçük olması durumunda tabaka ve yarım düzlem arasında sürekli temas durumu oluşmaktadır. Sürekli ve süreksiz temas durumları için temas yüzeylerindeki gerilme dağılımları çeşitli boyutsuz büyüklükler için elde edilmiştir. Problemin sonlu eleman modeli ANSYS yazılımı kullanarak oluşturulmuş ve problemin analizi gerçekleştirilmiştir. Son olarak sonlu elemanlar yönteminden elde edilen sonuçlar analitik sonuçlarla karşılaştırılarak doğrulanmıştır.

Anahtar Kelimeler: Mekanik, Sürekli temas, Süreksiz temas, Elastisite, Yarım düzlem, Sonlu elemanlar metodu.

1. Introduction

Since contact problems have possible application to a variety of structures of practical interest such as foundation grillages, pavements in roads and runways, railway ballats and other structures consisting of layered media, there has been an increasing attention on the contact problems. There is large body of literature concerned with contact problems both analytically [1-9] and numerically [10-15].

Except for these papers, El-Borgi et al. investigated a receding contact problem between a functionally graded layer and a homogeneous substrate and they studied the effect of the material nonhomogeneity parameter and the thickness of the graded layer on the contact pressure and on the contact lengths. Kahya et al. studied a receding contact problem for an anisotropic elastic medium consisting of a layer and a half plane and they obtained contact stresses and contact lengths for different fibre orientations. A axisymmetric double receding contact problem between a functionally graded layer and a homogeneous half plane is solved Rhimi et al.. Effects of surface tension on axisymmetric Hertzian contact problem and they obtained helpful results to characterize and

measure the mechanical features of soft materials or biomaterials through micro-indentation. El-Borgi et al. considered a frictional receding contact problem between a functionally graded layer and a homogeneous semi-infinite plane and they analyzed the effect of friction coefficient and nonhomogeniety factor on the contact pressure distribution and contact lengths. Gun and Gao presented a quadratic boundary element formulation for continuously nonhomogeneous, isotropic and linear elastic functionally graded material contact problems with friction. Yan and Li analyzed double receding contact problem between functionally graded layer and elastic layer. Li et al. are presented fundamental contact solutions of a magneto-electro-elastic half space indented by a smooth and rigid half infinite punch. Comez studied moving contact problem for a rigid cylindrical punch and a functionally graded layer and he obtained an effect of relative moving velocity for contact problem of functionally graded layer.

In this paper, continuous and discontinuous contact problem for infinite layer on an elastic semi-infinite plane is solved using FEM. The load which will occur by initial separation and the bigger values than this load, the stress distribution on the contact surfaces are plotted for different dimensionless quantaties. Finally, the results obtained from FEM are verified by comprasion the analytical results.

2. Definition of the Problem

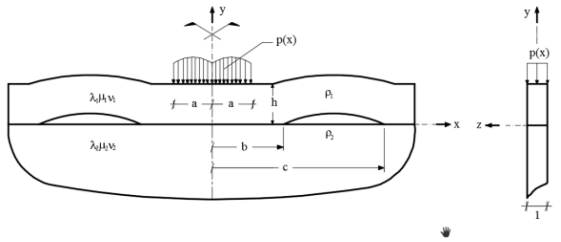

Figure 1. Geometry and the loading of the contact problem

In this paper continuous and discontinuous contact problems for an elastic layer on an elastic semi-infinite plane is solved using finite element method. The layer are loaded by symmetrical distributed loads whose lengths are 2a and thickness in z direction is taken to be unit. It is assumed that the contact surfaces along the interfaces is frictionless, only normal tractions can be transmitted through the contact surfaces, body forces of elastic layer is taken into account and body force of semi-infinite plane is neglected.

As shown in Fig. 1, consider the symmetric plane strain problem consist of an infinitely long homogeneous layer of thickness h in smooth contact with semi-infinite plane. μ_1, ν_1 and ρ_1 are the shear modulus, poisson ratios and density of a layer respectively. Similarly μ_2, ν_2 and ρ_2 are the shear modulus, poisson ratios and density of a half space respectively.

3. The Finite Element Solution

The finite element method is a numerical method for solving problems of engineering and mathematical physics. In this method, problem divides into simpler parts that are called finite elements and the model transform into large system of equations. With recent developments in computer technology and package programs for FEM solution of large system of equations is fulfilled.

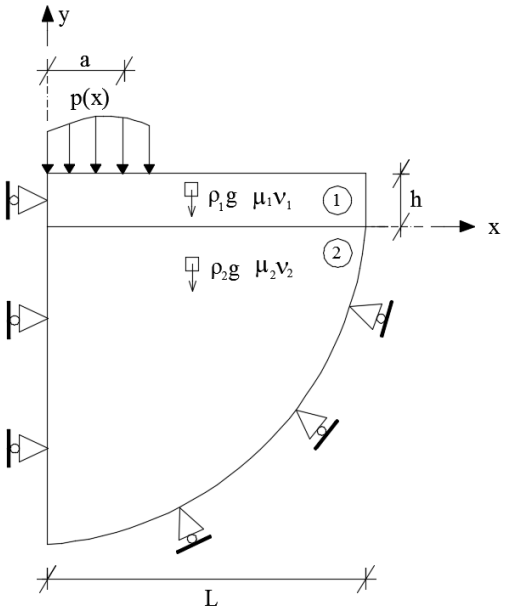

Figure 2. Schematic model of the contact problem (symmetric finite element model)

In this study, the finite element analysis is performed by ANSYS software program. The

geometrical model is created with the standart tools in ANSYS software. Because of the problem exhibits symmetry in geometry, material proportions and loading, only half of the problem is modeled. The geometry and the applied load are shown symmetrically in Fig. 2. The layer and semi-infinite plane are considered as lineer elastic and isotropic. In the analysis, geometric properties are taken as L=12 m (length of the layer in x direction), h_1=1m (thickness of the layer in y direction). Other parameters are choosen such that $p_0/(\rho gh)$, μ_1/μ_2, κ_1/κ_2. Are compatible with analytical values.

PLANE183 element is used for the modeling elastic layer and semi-infinite plane. PLANE183 element consist of eigth nodes having two degrees of freedom: translations in the nodal x and y directions. Frictionless surface-to-surface 2D contact elements are used to model the interaction between the contact surfaces: CONTA172 and TARGE169. CONTA172 is used to represent contact. Target surfaces is defined by TARGE169 for the associated contact elements CONTA172. Several numerical solution methods have been proposed to solve the variational equation of elastic contact problem, including penalty method, augmented Lagrangian method, Lagrange multiplier method method and augmented Lagrangian multiplier method. These methods incorporated to general finite element analysis (FEA) technology, are applied to solve the contact problem that involves complex geometry shapes. In the penalty method, the accuracy of the solution depends on the choice the penalty parameter. Too small a penalty parameter may cause unacceptable error in the solution. Also the penalty method suffers from ill-conditioning as the penalty parameter becomes large. The augmented Lagrangian method is an iterative series of penalty methods. The contact tractions (pressure and frictional stresses) are augmented during equilibrium iterations so that the final penetration is smaller than the allowable tolerance. Compared to penalty method, the augmented Lagrangian method usually leads to better conditioning and is less sensitive to the magnitude to contact stiffness.The Langrange multiplier method introduces new unknowns for each constraint. Therefore, it always increases the dimension of the system equations to be solved. For large scale problems where the contact surface consist of a large number of nodes, the number of unknowns introduced by the Lagrange multiplier method is also large. This increases the CPU time to solve the problem. For the augmented Lagrangian multiplier method, both penalty parameters and Lagrangian multipliers are applied, and penetration is admissible but controlled by allowable tolerance [28]. In this study, Augmented Lagrangian method is used as the contact algorithm. And the deformed shape after analysis is shown in Fig. 3.

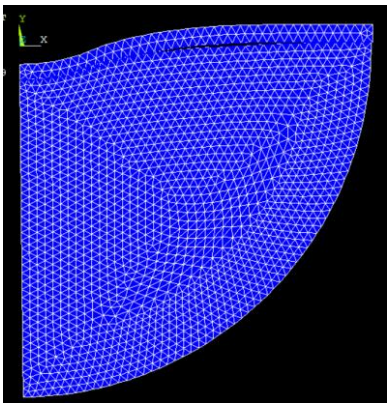

Figure 3. Deformed shape after finite element analysis.

4. Conclusions

In this paper, continuous and discontinuous contact problem for an infinite layer and a semi-infinite plane is solved by using finite element method and results obtained from finite element method are verified by comparing with analytical results in literature. Note that all quantaties are dimentionless.

Fig. 4-5 shows contact stress distributions for the continuous contact cases. It can be seen that the initial separation point x_{cr} seems to increase as a/h increases.

The variation of the normalized contact stress $\sigma_y(x,0)/(\rho_1 gh)$ between the infinite layer and semi-infinite plane for the discontinuous contact case is shown Fig. 6-7. As it can be seen in graphics, there are three regions in the discontinuous contact between the layer and semi-infinite plane. These are the continuous contact region, separation zone, and the discontinuous contact region where the effect of the external load (P) decreases and disappears infinitely. If the a/h increases, initial separation point occurs a

longer distance from the origin and separation zone decreases for similar material proportions.

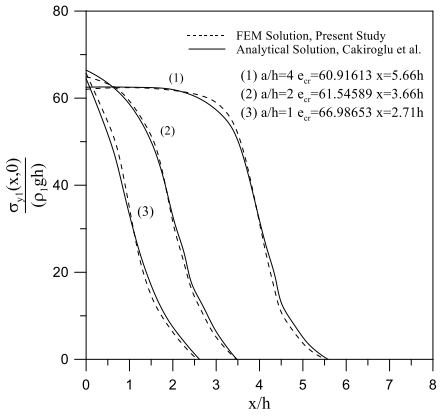

Figure 4. Contact stress distrubutions for the cases of continuous ($e=e_{cr}$) for the first loading condition.

$$(\mu_1/\mu_2 = 1/3,\ e_{cr} = p_0/(\rho g h))$$

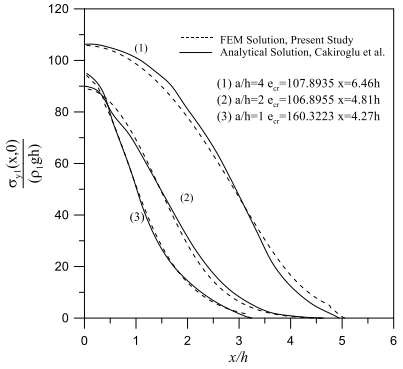

Figure 5. Contact stress distrubutions for the cases of continuous ($e=e_{cr}$) for the second loading condition.

$$(\mu_1/\mu_2 = 3,\ e_{cr} = p_0/(\rho g h))$$

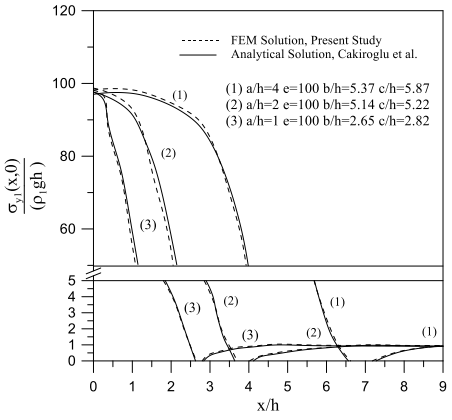

Figure 6. Contact stress distrubutions for the cases of discontinuous ($e>e_{cr}$) for the first loading condition.

$$(\mu_1/\mu_2 = 1/3,\ e_{cr} = p_0/(\rho g h))$$

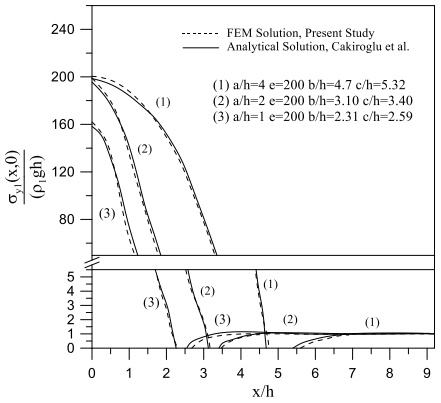

Figure 7. Contact stress distrubutions for the cases of discontinuous ($e>e_{cr}$) for the second loading condition.

$$(\mu_1/\mu_2 = 1/3,\ e_{cr} = p_0/(\rho g h))$$

Finally, based of the comprasion of numerical values obtained from finite element solution and analytical solution in literature [11], difference between finite element solution and analytical solution in literature is in a acceptable range.

5. References

1. Chan, S. K. and Tuba, I. S. (1971). A finite element method for contact problems of solid bodies - part I: theory and validation. *International Journal of Mechanica Sciences*, **13**(7): 615-625.

2. Keer, L. M., Dundurs, J. and Tsai, K. C. (1972). Problems involving a receding contact between a layer and a half space. *Journal of Applied Mechanics*, **39**(4): 1115-1120.

3. Erdogan, F. and Gupta, G. D. (1972). Numerical solution of singular integral equations. *Quarterly of Applied Mathematics*, **29**(4): 525-&.

4. Ratwani, M. and Erdogan, F. (1973). On the plane contact problem for a frictionless elastic layer. *International Journal of Solids and Structures*, **9**(8): 921-936.

5. Francavilla, A. and Zienkiewicz, O. C. (1975), A note on numerical of elastic contact problems. *International Journal for Numerical Methods in Engineering*, **9**(4): 913-924.

6. Adams, G. G., Bogy, D. B. (1977), The plane symmetric contact problem for dissimilar elastic semi-infinite strips of different widths. *Journal of Applied Mechanics-ASME*, **44**(4): 604-610.

7. Civelek, M. B., Erdogan, F. and Cakiroglu, A.O. (1978). Interface seperation for an elastic layer loaded by a rigid stamp. *International Journal of Engineering Science*, **16**(9): 669-679.

8. Gecit, M. R. (1986). Axisymmetric contact

problem for a semi-infinite cylinder and a half space. *International Journal of Engineering Science*, **24**(8): 1245-1256.

9. Abdou, M. A. (1999). Integral equation and contact problem for a system of impressing stamps. *Applied Mathematics and Computation*, **106**(2-3): 141-148.

10. Francavilla, A. and Zienkiewicz, O. C. (1975). A note on numerical computation of elastic contact problems. *International Journal for Numerical Methods in Engineering*, **9**(4): 913-924.

11. Cakiroglu, A. O. and Cakiroglu, F.L. (1991). Continuous and discontinuous contact problems for strips on an elastic semi-infinite plane. *International Journal of Engineering Science*, **29**: 93-111.

12. Jing, H. -S. and Liao, M. -L. (1990). An improved finite element scheme for elastic contact problems with friction. *Mathematical and Computer Modeling*, **15**: 143-154.

13. Gorrido, J. A., Foces, A. and Paris, F. (1991). BEM applied to receding contact problems with friction. *Mathematical and Computer Modeling*, **15**, 143-154.

14. Gorrido, J. A., Foces, A. and Paris, F. (1991). BEM applied to receding contact problems with frictions. *Mathematical and Computer Modeling*, **15**(3-5), 143-153.

15. Gorrido, J. A. and Lorenzana, A. (1998). Receding contact problem involving large displacements using the BEM. *Engineering Analysis with Boundary Elements*, **21**(4), 295-303.

16. El-Borgi, S., Abdelmaula, R. and Keer, L. (2006). A receding contact plane problem between a functionally graded layer and a homogeneous substrate. *International Journal of Solids and Structures*, **43**(3-4): 658-674.

17. Kahya, V., Ozsahin, T. S., Birinci, A. and Erdol, R. (2007). A receding contact problem for an anisotropic elastic medium consisting of a layer and a half plane. *International Journal of Solids and Structures*, **44**(17): 5695-5710.

18. Rhimi, M., El-Borgi, S. and Lajnef, N. (2011). A double receding contact axisymmetric problem between a functionally graded layer and a homogeneous substrate. *Mechanics of Materials*, **43**(12), 787-798.

19. Long, J. M. and Wang, G. F. (2013). Effects of surface tensionon axisymmetric Hertzian contact problem. *Mechanics of Materials*, **56**: 65-70.

20. Gun, H. and Gao, X. W. (2014). Analysis of frictional contact problems for functionally graded materials using BEM. *Engineering Analysis with Boundary Elements*, **38**: 1-7.

21. Li, X. -Y., Zheng, R. -F. and Chen, W. -Q. (2014). Fundemental solutions to contact problems of a magneto-electro-elastic half space intended by a semi-infinite punch. *International Journal of Solids and Structures*, **51**(1): 164-178.

22. El-Borgi, S., Usman, S. and Guler, M. A. (2014). A frictional receding contact plane problem between a functionally graded layer and a homogeneous substrate. *International Journal of Solids and Structures*, **51**(25-26): 4462-4476.

23. Adiyaman, G., Yaylaci, M. and Birinci, A. (2015). Analytical and finite element solution of a receding contact problem. *Structural Engineering and Mechanics*, **54**: 69-85.

24. Oner, E., Yaylaci, M. and Birinci, A. (2015). Analytical solution of a contact problem and comprasion with the results from FEM. *Structural Engineering and Mechanics*, **54**: 607-622.

25. Birinci, A., Adiyaman, G., Yaylaci, M. and Oner, E. (2015). Analysis of continuous and discontinuous cases of a contact problem using analytical method and FEM. *Latin American Journal of Engineering Science*, **12**: 1771-1789.

26. Yan, J. and Li, X. (2015). Double receding contact plane problem between a functionally graded layer and an elastic layer. *European Journal of Mechanics A-Solids*, **53**: 143-150.

27. Comez, I. (2015). Contact problem for a functionally graded layer intended by a moving punch. *International Journal of Mechanical Sciences*, **100**: 339-344.

28. Liao, X. and Wang, G. G. (2015). Non-lineer dimentional variation analysis for sheet metal assemblies by contact modeling. *Finite Elements in Analysis and Design*, **44**: 34-44.

Turkish Journal of Science & Technology
Volume 13(1), 119-124, 2018

CFD Analysis of Ilısu Dam Sluice Outlet

M. Cihan Aydin[1*], Ali Emre Ulu[1], Çimen Karaduman[1]
[1]Department of Civil Engineering, Bitlis Eren University, Bitlis, TURKEY
[*]mcaydin@gmail.com

(Received: 18.02.2017; Accepted: 04.03.2017)

Abstract

Ilisu Dam is one important energy projects in Turkey. After it is completed, it is expected that it will contribute to the country economy approximately $300 million annually. One of the most remarkable engineering designs of the dam is the conversion of diversion tunnels of 12 m in diameter and about 1 km in length into sluice outlet structure. In this study, the CFD simulation of Ilısu Dam sluice outlet were performed with 1/40 scale. The obtained CFD results were compared with physical model observations conducted by the State Water Works (SWW). A good agreement was achieved between both results, and some useful results of CFD were presented for design of the outlet.

Keywords: Ilisu Dam; Sluice Outlet; CFD.

Ilısu Barajı Dipsavağının HAD Analizi

Özet

Ilısu Barajı Türkiye'deki en önemli enerji projelerinden biridir. Tamamlandığında ülke ekonomisine yaklaşık olarak yıllık 300 milyon dolar katkı sağlaması beklenmektedir. Barajın en dikkat çekici mühendislik tasarımlarından biri, 12 m çapında ve yaklaşık 1 km uzunluğundaki derivasyon tünellerinin dipsavağa dönüştürülmesidir. Bu çalışmada, Ilısu Baraj dipsavağının CFD simülasyonu 1/40 ölçek ile gerçekleştirilmiştir. Elde edilen CFD sonuçları Devlet Su İşleri (DSİ) tarafından yapılan fiziksel model gözlemleri ile karşılaştırılmıştır. Her iki sonuç arasında iyi bir mutabakat sağlanmış ve CFD'nin bazı kullanışlı sonuçları dipsavak tasarımında sunulmuştur.

Anahtar Kelimeler: Ilısu Barajı; Dipsavak; HAD.

1. Introduction

Sluice outlet is a hydraulic structure which is designed to completely discharge the dam when necessary, to reduce the spillway capacity and to release the water to be left to the downstream of the river. The sluice outlet can be of different shapes and lengths depending on the needs or shapes of the dams. An important consideration when designing the sluice way is to prevent cavitation damage. In order to avoid this problem engineers may choose different solutions in the sluice outlet design. Experimental studies are conducted to observe how the cavitation phenomenon will actually have an effect. However, these experiments may be time consuming, costly and require a lot of attention. Instead, using the developed computational fluid dynamics (CFD) is now a more functional and reliable method that has been tested many times. There are many studies exist in the literature that was performed using the CFD. Some of those studies can be seen as follows:

Khan et al. [1] establishes a 3D CFD model of The Dalles Dam forebay. The aim of the model is to investigate the effects of clogging resulting from the accumulation of debris in the 12.3 m section above the turbine intake. The model includes approximately 0.80 million cells consisted from 22 power plant units, two fish turbine units, station services unit and a forebay bathymetry. The CFD model has quite well simulated the velocity distributions observed in a physical model. Numerical simulations indicated that blocked garbage pits would change velocity distributions around the powerhouse to a significant extent [1]. Cassan and Belaud [2] defines the flow properties at a large opening to improve the discharge calculation for submerged channel gates. To do so, the technical note

investigated the upstream and downstream flow characteristics of the channel inlet gates experimentally and numerically by means of a fluid method using average Navier-Stokes two-dimensional simulations by Reynolds [2]. Zhang et al. [3] develops a dynamic numerical model to investigate a laboratory experiment. Through analysis and modeling of the observed data, the river water quality and quantity (WQQ) operations under the water channel regulation were examined and the interaction between the WQQ and the regulatory capacity downstream of a water channel was investigated [3]. Li et al. [4] developed a numerical model to simulate the flow of probable maximum flow (PMF) on a system consisting of an existing service spillway and a new auxiliary spillway. In the study, approach channel geometries consisted from different combinations were simulated. The article demonstrates the successful implementation of a CFD model in the design process of an auxiliary spillway and encourages the hydraulic engineers and CFD modelers for designing the hydraulic structures [4]. Ebner [5] investigated CFD model used applications to reveal its limitations and to make some assumptions. At the end, article noted that CFD numerical models are a good way to recognize the hydraulic conditions [5].

A technical report modified a previously computed fluid dynamics model, and it was used to characterize tailrace hydraulic and sluice outlet exit conditions for low total river and low level spillway flows [6]. Kökpınar and Çelik [7] investigated the preliminary test results obtained from a large scale Deriner Dam of tunnel spillway model are presented. A number of test models have also been carried out for the original and final project cases. In the article it was seen that the original designed ventilator did not work effectively from the values obtained according to the original project status. For this reason, it became necessary to change the original progeny in terms of location and geometry of the aerator [7].

From the current literature, it can be said that CFD models are valuable, useful and reliable tools for the hydraulic structures. As one can understand that there is limited study about the CFD models of the sluice outlet. This study investigates the working principle of sluice outlet of Ilısu Dam by using CFD model.

2. Ilisu Dam and HPP

Ilısu Dam and Hydroelectric Power Plant (HPP) is one of most important energy project with 1200 MW installed capacity in Turkey. After completed, the total produced energy will be 3833 GWh/year, and it is expected to bring about $300 million incomes to the economy annually. This energy corresponds to 10% of the hydroelectric energy to be produced in Turkey. The general project characteristics of Ilısu Dam and its sluice outlet structures were given in Table 1 [8], [9].

DT2 derivation tunnel of Ilısu Dam was converted to the outlet structure. DT1 derivation tunnel parallel to DT2 tunnel also were designed as an aeration tunnel for air supply purpose. Two tunnels were connected by a horseshoe cross-section air gallery. The detail of outlet structures converted from DT2 derivation tunnel were showed in the Fig. 2.

Table 1. Ilisu Dam and HPP Project Characteristics

Type of Dam	Embankment, concrete-face rock-fill
Purpose	HP, flood control and irrigation
Status	Under construction
Location	Dargeçit County, between Mardin and Şırnak
River	Dicle River
Construction cost	1.7 billion $
Height from thalweg	135 m
Length	1.820 m
Dam volume	43,800,000 m^3
Installed capacity	1,200 MW
Average annual energy production	6 x 200 MW Francis-type
Hydraulic head	122.6 m
Annual generation	3,833 GWh
Derivation slope	0.1%

Derivation structures	DT1+DT2+DT3 derivation tunnels
Sluice outlet	DT2 derivation tunnel
Diameter of sluice outlet	12 m
Length of the outlet	1016.1 m
Type of control valve	Sluice valve
Number of control valve	2
Dimensions of control valve	2.65x4.00 m
Spillway type	Service overflow, controlled-chute
Spillway capacity	18,000 m^3/s

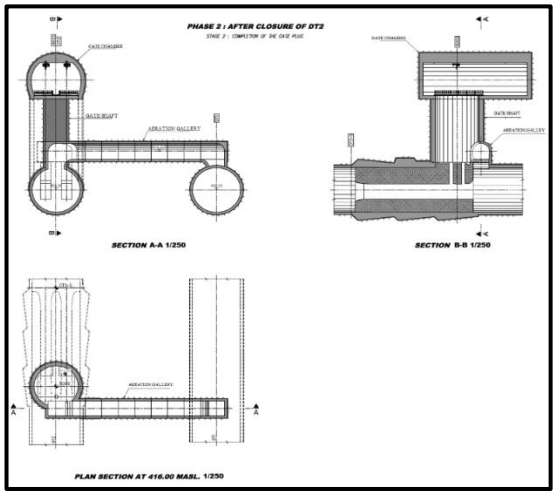

Fig. 1. Details of the sluice outlet converted from DT2 derivation tunnel of Ilısu Dam [8].

3. Method

In this study, a three-dimensional (3D) numerical simulation using FLOW-3D software was applied to Ilısu Dam sluice outlet to determine the two-phase (air-water) flow properties. FLOW-3D is a general purpose CFD program which is especially effective free surface flows for one and two phase flows. The program solves the mass continuity and the Navier-Stokes equations as the momentum equation for each element to estimate properties of fluid motions. These equations can be given as follows respectively for Cartesian coordinate system [10].

$$V_F \frac{\partial p}{\partial x} + \frac{\partial}{\partial x}(\rho u A_x) + \frac{\partial}{\partial y}\left(\rho v A_y\right) + \frac{\partial}{\partial x}(\rho w A_z) = R_D + R_S \quad (1)$$

where, V_F is volume fraction, ρ is the density of fluid; R_D is a turbulent diffusion term; R_S is a mass source; A_x, A_y, and A_z are the fractional areas in the x, y and z; u, v and w are velocity components. The Navier-Stokes are used to describe three-dimensional fluid dynamics.

$$\begin{aligned}
\frac{\partial u}{\partial t} + \frac{1}{V_F}\left[uA_x\frac{\partial u}{\partial x} + vA_y\frac{\partial u}{\partial y} + wA_z\frac{\partial u}{\partial z}\right] &= -\frac{1}{\rho}\frac{\partial p}{\partial x} + G_x + f_x - \frac{R_S}{\rho V_F}(u - u_w - \delta u_s)\\
\frac{\partial v}{\partial t} + \frac{1}{V_F}\left[uA_x\frac{\partial v}{\partial x} + vA_y\frac{\partial v}{\partial y} + wA_z\frac{\partial v}{\partial z}\right] &= -\frac{1}{\rho}\frac{\partial p}{\partial y} + G_y + f_y - \frac{R_S}{\rho V_F}(v - v_w - \delta v_s)\\
\frac{\partial w}{\partial t} + \frac{1}{V_F}\left[uA_x\frac{\partial w}{\partial x} + vA_y\frac{\partial w}{\partial y} + wA_z\frac{\partial w}{\partial z}\right] &= -\frac{1}{\rho}\frac{\partial p}{\partial z} + G_z + f_z - \frac{R_S}{\rho V_F}(w - w_w - \delta w_s)
\end{aligned} \quad (2)$$

where; G_x, G_y, G_z are body acceleration components, f_x, f_y, f_z are viscous accelerations components, u_w,v_w,w_w are the components of velocity source; u_s, v_s, w_s are the velocity components at the surface.

Physical Model

The experimental studies on the revised design of the sluice outlet structure and aeration tunnel were conducted by State Hydraulic Works in Turkey. In the first design of the Ilısu Dam sluice outlet, the transport tunnels to the sluice outlet vane chamber were planned as ventilation galley providing air flow. However, in the tests and analyzes conducted, it was understood that the air in the narrowing sections would reach a speed as high as 100 m/s and eventually air explosions and operational problems would occur. For this reason, one of the two sluice outlet (DT1) was planned as an air gallery with a diameter of 12 m and a length of about 1000 m, and the air for the DT2 sluice outlet was provided by an air gallery with a horseshoe section here. Different alternatives of this system have been experimentally investigated by DSI with 1/40 model and solution proposal has been introduced. The experimental setup of the outlet

and aeration tunnels performed by DSI was showed in Fig. 2.

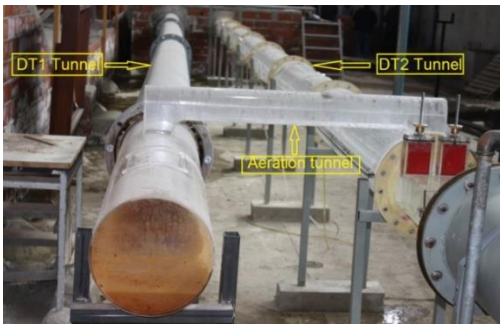

Fig. 2. Experimental setup of the outlet and aerations tunnels [8]

Numerical Model

The 3D numerical model was given in the Fig. 3. Numerical model was divided into 3,900,000 structured 3D hexahedral elements. The simulation duration is approximately 7 hours with two real core xenon processor and 8 GB ram. Two phases model with *renormalized group (RNG)* turbulence model were used in the numerical solution. Numerical model with 12 m diameter of DT1 and DT2 tunnels were scaled by 1/40 scale similar to the experimental model. The dimension of the rectangular sluice section is 2.65x4.00m. The height and width of the horseshoe air tunnel are 4.5 m and 4.20 m respectively.

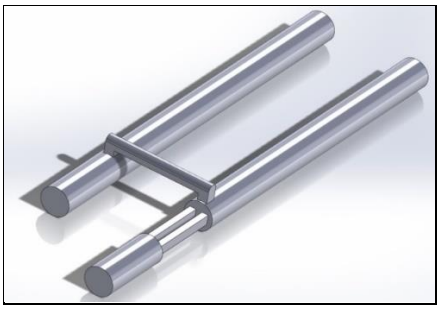

Fig. 3. Geometry of 3D numerical model

The CFD analysis were performed for 24.75 m of the hydraulic head and 430 m^3/s of water outlet discharge with laboratory model dimensions (1/40 scale). The solution convergence was achieved in 5.0 second. The solution convergence curves and water velocity of the sluice flow were illustrated in Fig. 4. As seen at the convergence curves in Fig. 5, the air flow rate in the aeration tunnel is almost steady while approaching to 0.012 m^3/s and velocity of 1.2 m/s. This corresponds 121.43 m^3/s and 7.58 m/s of prototype values. The air entrainment discharges and average air velocity were observed by DSI as 118.76 m3/s and 7.35 m/s experimentally [8]. The air entrainment rates ($\beta=Q_a/Q_w$) are calculated as 0.303 of experiment, and 0.309 of CFD. The relative percent error between experimental and numerical (CFD) results is approximately 2%. These comparisons were given in Table 2.

Table 2. Comparison of experimental and CFD results

	Hydraulic Head, H_t (m)	Water discharge, Q_w (m^3/s)	Air entrainment discharge, Q_a (m^3/s)	Average Air Velocity, V_a	Air entrainment coefficient ($\beta=Q_a/Q_w$)
Experiments	24.75	392	118.76	7.35	0.303
CFD	24.75	392	121.43	7.58	0.309
Error (%)			2.2	3.0	2.0

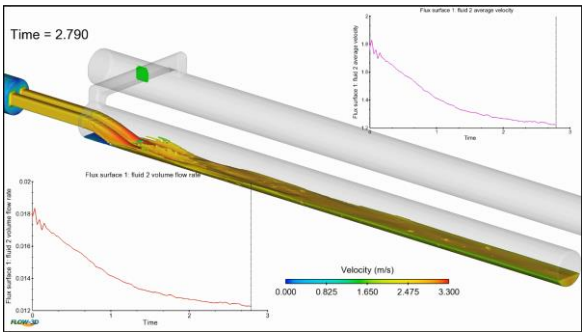

Fig. 4. Solution of the numerical model with convergence curves.

The maximum velocity of water flow was observed in jet near to impact region at the downstream of sluice gate. The streamlines of the water flow are shown in the Fig. 5. This figure also indicates same the maximum water velocity position.

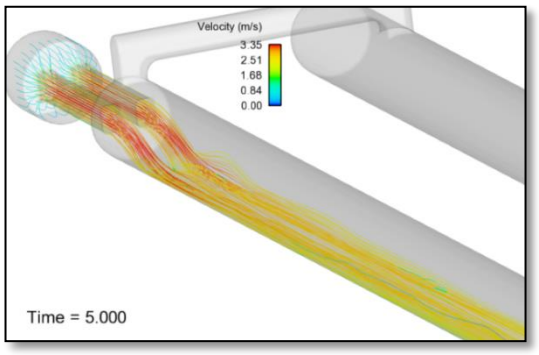

Fig. 5. Streamlines of the water flow in the sluice outlet

Fig. 6 shows the streamlines of air flow (on the left) and velocity contours at the middle section of aeration tunnel (on the right). It is observed in these figures that the air velocity on the section is irregular and the maximum velocity occurs at the top of the section while the velocity at a lower part of the section was almost zero. The maximum air velocities in the DT2 tunnel were observed near to water surface probably owing to slip velocities between air and water flow.

In Fig. 7, the pressure and velocity contours on the water flow profiles are given with colored scales. In the upper figure, the maximum pressure occurs at the impact point of the water jet while the minimum pressure is formed at the upper of the sluice. The velocities inside (in the lower figure) the sluice is higher than that of the edges of the sluice due to the wall effects.

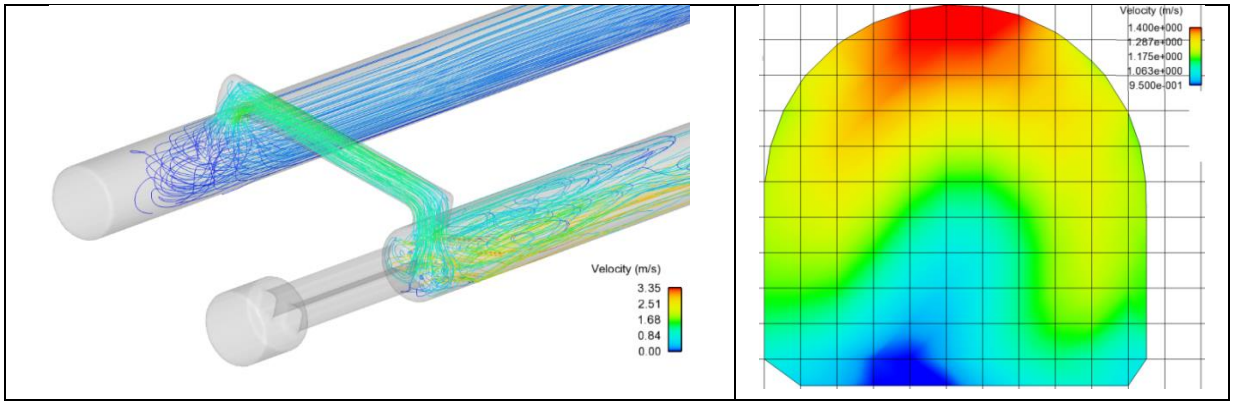

Fig. 6. Streamlines of air flow (on the left), and the velocity distribution at the cross-section of the aeration tunnel (on the right).

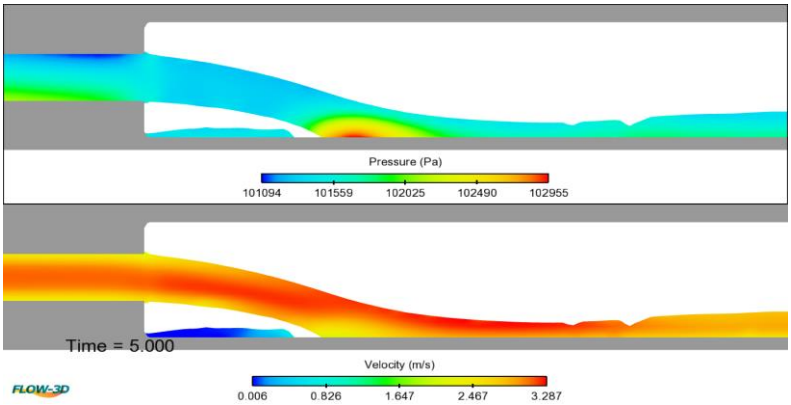

Fig. 7. Pressure and velocity contours of water flow jet downstream of sluice gate.

4. Conclusions

In this study, Ilısu Dam's sluice outlet, which have 12 m diameter, was analyzed by using CFD simulation technic, and was discussed. The results of CFD analysis were compared to the experimental tests with 1/40 scale performed by DSI, and a good agreement was achieved in

terms of air entrainment by air supply tunnel. The CFD results are reasonably compatible with the experimental observations with the percent errors from 2.00 to 3.00%. The experimental study is more expensive and required more effort than CFD analyses. Bu still, the CFD models need to be calibrated with some experimental data. The calibrated numerical models may be more useful and easier to determine hydraulic characteristics than experimental studies. The results encouraged the further researches for detailing the design of the Ilısu Dam outlet and the other similar projects.

5. Acknowledgement

- This study has been supported by Scientific Research Project Department of Bitlis Eren University in Turkey with Project No: BEBAP 2017.04.
- We thanks to Fırat University Department of Civil Engineering, the State Water Works (SWW) and IOG Engineering for their valuable contribution.
- This paper is also available in Oral Submision Book of International Conference on Advances and Innovations in Engineering (ICAIE) May 10-12 2017, Elazığ.

6. References

1.Khan, L.A., Wicklein, E.A., Rashid, M., Ebner, L.L. and Richards, N.A. (2008). Case study of an application of a computational fluid dynamics model to the forebay of the Dalles Dam, Oregon, *Journal of Hydraulic Engineering*, **134(5):** 509-519.

2.Cassan, L. and Belaud, G. (2011). Experimental and numerical investigation of flow under sluice gates. *Journal of Hydraulic Engineering*, **138(4)**, 367-373.

3.Zhang, Y., Xia, J, Shao, Q and Zhang, X. (2011). Experimental and simulation studies on the impact of sluice regulation on water quantity and quality processes. *Journal of Hydrologic Engineering*, **17(4):** 467-477.

4.Li, S., Cain, S. Wosnik, M., Miller, C., Kocahan, H and Wyckoff, R. (2010). Numerical modeling of probable maximum flood flowing through a system of spillways, *Journal of Hydraulic Engineering*, **137(1)**: 66-74.

5.Ebner, L.L: (2014). Practical Use of Computational Fluid Dynamic Models as a Design Tool-Limitations and Assumptions. *Critical Transitions in Water and Environmental Resources Management*, 2004, pp. 1-10.

6.Rakowski, C.L, Richmond, M.C. Serkowski, J.A. and Perkins, W.A. (2010). Computational Fluid Dynamics Modeling of the Bonneville Project: Tailrace Spill Patterns for Low Flows and Corner Collector Smolt Egress (No. PNNL-20056), Pacific Northwest National Laboratory, (PNNL), Richland, WA (US).

7.Kökpinar, M.A. and Çelik, H.Ç. (2002). Deriner Baraji Tünelli Dolusavak Havalandiricilari Büyük Ölçekli Hidrolik Model Çalişmalari.

8.DSİ, (2013). Ilısu Barajı ve HES Projesi Dipsavak Tüneli Ek Hidrolik Çalışmaları (M-398), Fiziksel Model Deney Raporu, DSİ TAKK Dairesi Başkanlığı Hidrolik Model Laboratuvarı Şube Müdürlüğü. Ankara. Rapor No: Hİ-1022, 119 s.

9.Wikipedia, (2017), Ilısu Dam. https://en.wikipedia.org/wiki/Il%C4%B1su_Dam, Accessed date: 26 Feb. 2017.

10.FLOW-3D (2016). User Manual, Theory Guide

.

Turkish Journal of Science & Technology
Volume 13(1), 125-128, 2018

Ms Excel Macro Aplications of Finite Differece and Integration Method for Simply Supported Rectangular Plates Under Sinusoidal Load

Sedat Savaş
Firat Univ. Eng. Faculty Civil Eng. Dept. Elazig/Turkey
ssavas@firat.edu.tr

(Received: 19.01.2017; Accepted: 20.03.2017)

Abstract
In this study, the finite differences and the method of integration were compared to find displacements in an elastic plate under sinusoidal loading. This question type, which is one of the common examples in the literature, is available with various methods. Application engineers mostly use Microsoft Excel excel macro program, VBA, has written program codes for both finite element method and integration method. The difference between the results of these programs and the CPU time is calculated.

Keywords: Finite Difference Method, Integration Method, Elastic Plate, Microsoft Excel Macro

Sinüzoidal Yükleme Altında Basit Mesnetlenmiş Dikdörtgen Plaklarda Sonlu Farklar ve İntegrasyon Metodunun Ms Excel Makro Uygulaması

Özet

Bu çalışmada sinüzoidal yükleme altındaki bir elastik plaktaki deplasmanları bulmak için sonlu farklar ve integrasyon yöntemi karşılaştırılmıştır. Bu soru tipi literatürde yaygın olup, çeşitli metotlarla çözüzümü yapılmıştır. Bu soru tipinin uygulama mühendislerinin çoğunlukla kullandığı Microsoft Excel' in makro programında her iki metod için çözümü sunulmuştur. Yapılan çözüm sonuçları ve çözüm zamanı arasındaki farklar elde edilmiştir.

Anahtar Kelimeler: Sonlu farklar metodu, integrasyon metodu, elastik plak, Microsaft Excel Makro

1. Introduction

Numerous calculations have been made up to now on the solution of elastic plates. These studies were carried out by varying the dimensions of the elastic plaques from time to time and changing the loading conditions applied on the bases, changing the boundary conditions at the bases. In this study, four edges under sinusoidal loading resolve a simple supported elastic plate problem [1]. These solutions were compared with manual solutions and also within themselves.

In this analysis, VBA programming language in Microsoft Excel is used. The reason for choosing this applet is that it is easy to access and is easy to implement by every engineer. In addition, the ability to read data from the file and write data to the file is easier, as well as the wide selection of graphics. However, the CPU time is not the performance seen in other programming languages .

2. Sinusoidal Load Under Elastic Plate

2.a. System geometry and loading condition

In the coordinate system given 2.1, the rectangular plate with long side a, short side b is simply supported. We assumed that the sinusoidal load distributed over surface of rectangular plate is given by the expression

$$q = q_0 \sin\left(\frac{\pi x}{a}\right)\cos\left(\frac{\pi y}{a}\right) \tag{1}$$

in which q_0 represents the intensity of th"e load at the center of the plate.

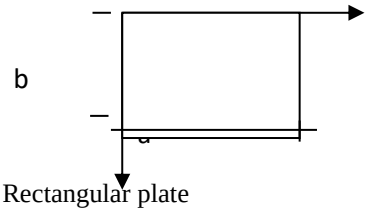

Figure 1. Rectangular plate

3. Integration Method

Generally, numerical approximation methods require reaching in several steps of solving by dividing time or space region into specific intervals, or in most cases require successive iteration solutions [2,3,4]. Numerical methods developed for this reason. They have various advantages or disadvantages in terms of the computational needs they require, the time spent on the solution or the CPU (Central Processing Unit) time, the stability of the equations, the number of node points used, the preprocessing for problem solving, and most importantly the time spent on this solution.
In this method, Elastic curve equation for (1) equation loading condition ;

$$\frac{\partial^4 w}{\partial x^4} + 2\frac{\partial^4 w}{\partial x^2 \partial x^2} + \frac{\partial^4 w}{\partial y^4} = \frac{q}{D} \qquad (2)$$

The differential equation (2) for the deflection surface in this case becomes;

$$\frac{\partial^4 w}{\partial x^4} + 2\frac{\partial^4 w}{\partial x^2 \partial x^2} + \frac{\partial^4 w}{\partial y^4} = \frac{q_0}{D}\sin\left(\frac{\pi x}{a}\right)\cos\left(\frac{\pi y}{a}\right) \qquad (3)$$

in which the quantity D, taking the place of the quantity EI in the case of beams, is called the flexural rigidity of the plate. The boundary conditions for simply supported edges are

$w=0$ $M_x=0$ for $x=0$ and $x=a$
$w=0$ $M_y=0$ for $y=0$ and $y=b$

we can represent the boundary conditions in the following form:

$$w=0 \quad \frac{\partial^2 w}{\partial x^2} = 0 \qquad \text{for } x=0 \text{ and } x=a$$

$$w=0 \quad \frac{\partial^2 w}{\partial y^2} = 0 \qquad \text{for } y=0 \text{ and } y=b$$

All boundary conditions are satisfied if we take for deflections the expression;

$$w = C\sin\left(\frac{\pi x}{a}\right)\cos\left(\frac{\pi y}{a}\right) \qquad (4)$$

in which the constant C must be chosen so as to satisfy Eq. (3). Substituting expression (4) into Eq. (3), we find

$$\pi^4\left[\frac{1}{a^2}+\frac{1}{b^2}\right]^2 C = \frac{q_0}{D} \qquad (5)$$

and we conclude that the deflection surface satisfying Eq. (3) and boundary conditions is

$$w = \frac{q_0}{\pi^4\left[\frac{1}{a^2}+\frac{1}{b^2}\right]^2 D}\sin\left(\frac{\pi x}{a}\right)\cos\left(\frac{\pi y}{a}\right) \qquad (6)$$

In the light of these equations, we have applied this equation to find the displacements along the entire plate surface with the aid of the program we have done in excel macro.

Step of program:
1- Once plates surface is defined.
2- The plate lengths are divided into equal parts
3- Cyclic increments are made in the x and y directions
4- These values are placed in the equation
5- Program is stopped

1. Finite Difference Method

Boundary value problems do not have many definite and closed solutions. Approximate solutions are available for this. Approximate methods are divided into characters. Some agrees with the provision of boundary conditions, but requires that the differential equation be precisely met. In the second group of methods, there is approximation in the presence of the differential equation, even if the boundary conditions are precise. The finite difference method is a method

that can be applied to almost every other form entering this second group[].
It is possible to approximate the derivative of a function $y = f(x)$ at a certain set of discrete points, using known values. Similarly, approximate partial derivative formulas can be given for multivariable functions of type $z = f(x, y)$. Considering the definition of derivative, advanced difference approach, backward difference approach and central difference approach are emphasized.

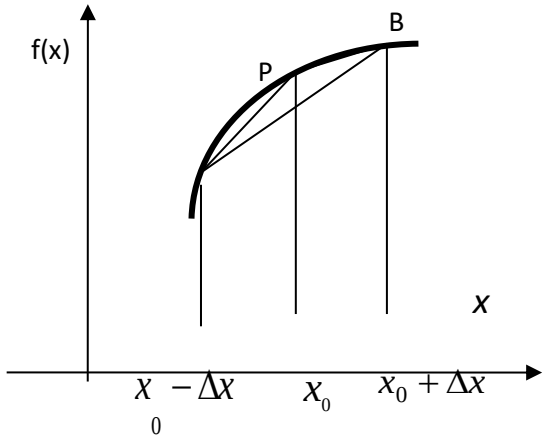

Figure 2. The derivation of f (x) at point P using forward and backward and central differences

Advanced difference formula:

$$f'(x_0) = \frac{f(x_0 + \Delta x) - f(x_0)}{\Delta x} \quad (7)$$

Back difference formula:

$$f'(x_0) = \frac{f(x_0) - f(x_0 - \Delta x)}{\Delta x} \quad (8)$$

Central difference formula:

$$f'(x_0) = \frac{f(x_0 + \Delta x) - f(x_0 - \Delta x)}{2\Delta x} \quad (9)$$

The theory of elasticity is a branch of the theoretical physics, and the strain and shape changes that occur in elastic bodies under the influence of the objective external loads are calculated precisely by moving from a certain set of differential equations. In this case, the vehicle used for the solution is the differential equation theory[3].

The principal equation of plane elasticity theory;

$$\Delta(\sigma_x + \sigma_y) = \Delta\Delta F = \frac{\partial^4 F}{\partial x^4} + 2\frac{\partial^4 F}{\partial y^2 \partial x^2} + \frac{\partial^4 F}{\partial y^4} = 0 \quad (10)$$

From the boundary conditions:

$$F_s = M(s)_{\text{and}} \left(\frac{dF}{dn}\right) = -Q_t(s) \quad (11)$$

Here;
Fs : Stress function,
M(s) : Static moment,
Qt : It is the trace of the boundary value forces on the tangent.
The way to solve the problem of boundary value:
- Equation (11) calculates the values of the den function at the boundary precisely,
- The coefficients of the finite difference are calculated
- We extend the function to the outside of the region to be calculated,
- Divide the calculated shape into the desired number of node points to form the finite difference equations,
- Since the gauss-elimination method is used, conversion of the results to square matrix
- By solving these results into a matrix format.

5. Summary and Conclussion

In this study, an elastic plate finite difference method and a generalized computer program were used to obtain the elastic plate deflection graph for a complex loading situation of the geometry. The results were compared and the solutions were made. In the comparison made, 0.01 percent error was observed between the integration method and the final difference method. Displacement graphics have topped. The reason is that the number of segment is excessive. But the solution time is ten times more in the finite difference method.

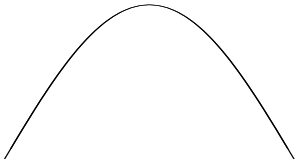

Figure 3. Exaggerated displacement curve in the long side

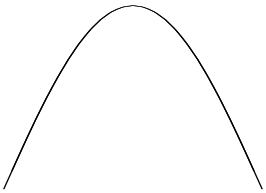

Figure 4. Exaggerated displacement curve in the short side

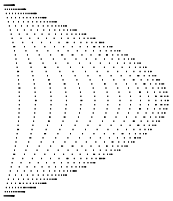

Figure 5. Plate displacement view

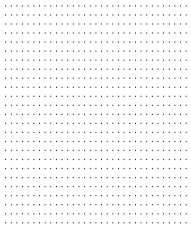

Figure 6. Plate top view

6. References

1. M. İnan, (1976). Düzlemde Elastisite Teorisi. Matbaa Teknisyenleri Basımevi,bölüm 4.

2. C. F. Gerald and P. O. Wheatley, (1997) "Applied Numerical Analysis," by Addision Wesley Longman, Inc.

3. S. Tameroğlu, (1991). "Elastisite Teorisi" İTÜ Matbaası.

4. Ö. Civalek, M. Ülker, (2006). "Polinomal Diferansiyel Quadrature(PDQ) ve Sonlu Farklar (SF) Metod Çifti ile Elastik Zemine Oturan Dikdörtgen Plakların Geometrik Bakımdan Lineer Olmayan Analizi"*İMO Teknik Dergi, (2006) 3739 -3760, Yazı 246

Turkish Journal of Science & Technology
Volume 13(1), 129-136, 2018

Investigation of Live-Bed Scour at Labyrinth Side Weirs

Mustafa Tunç[1*], M. Emin Emiroğlu[1]
[1]Fırat Üniversitesi, Mühendislik Fakültesi, İnşaat Mühendisliği Bölümü, Elazığ.
*mtunc@firat.edu.tr

(Geliş/Received: 27.01.2017; Kabul/Accepted: 12.04.2017)

Abstract

Side weirs, also known as lateral weirs, and overflow dams are free overflow regulation and diversion devices commonly encountered in hydraulic engineering. The lateral loss of water is reducing the sediment transport capacity in the main-channel and the formation of a local sediment deposit in the downstream of weir. The head over the side weir rises and the side overflow discharge as well. The design discharge to be diverted over the weir is increased by this flow-sediment transport interaction. Although there were no studies that scrutinized the scouring depth and geometry that occurs around the labyrinth side weirs in channels with movable bed, there are limited number of studies that examined the scouring geometry around the classical side weir. In the present study, local scour depths formed in the periphery of triangular labyrinth side weir mounted in a live-bed rectangular cross-section straight channel were experimentally investigated under steady state flow and free overflow from the side weir conditions. To provide for live-bed conditions, the sediment was added to bed material in the experiments. A series of experiments were conducted for live-bed scouring conditions (for flow intensity greater than one) to determine the maximum scour depths that occur around the triangular labyrinth side weir with different flow depths, different main channel discharges, different volumetric amounts of sediment feed, different crest heights, different Froude numbers, different flow intensities and using uniform bed material. In the experiments, the dimensions of the scours and sediment deposits that occur upstream and downstream of the weir exhibited a periodic change (increase and decrease). The maximum depth of scour occurred at the downstream end of the triangular labyrinth side weir frequently.

Keywords: Triangular labyrinth side weir, Flow intensity, Local scour, Live-bed scour, Sediment transport.

Labirent Yan Savaklarda Hareketli Taban Oyulmasının İncelenmesi

Özet

Yan savaklar; baraj, bağlama ve tersip benti gibi su yapılarında serbest savaklama akım yönünü değiştirme gibi amaçlarla hidrolik mühendisliğinde yaygın olarak kullanılmaktadırlar. Yanal savklanmadan dolayı, ana kanaldaki sediment taşınım kapasitesi azalmakta ve savağın mansap bölgesinde sediment birikimi gözlenmektedir. Yan savak yüksekliğine bağlı olarak savaklanma debisi de artmaktadır. Literatürde klasik yan savaklardaki oyulmayı inceleyen sınırlı sayıda çalışma bulunurken, labirent yan savaklarda oluşan oyulma derinliğini ve geometrisini inceleyen hiç bir çalışmaya rastlanmamıştır. Mevcut çalışmada dikdörtgen enkesitli alüvyal tabanlı bir kanalda kararlı akım şartları ve serbest savaklanma durumu için üçgen labirent yan savak civarındaki yerel oyulma derinlikleri deneysel olarak araştırılmıştır. Deneylerde hareketli taban koşullarını sağlamak için, kanala belirli miktarlarda taban malzemesi ilavesi yapılmıştır. Üçgen labirent yan savak etrafında oluşan maksimum oyulma derinliklerini belirlemek için; farklı akım derinlikleri, farklı ana kanal debileri, farklı hacimlerde beslenen sediment miktarları, farklı kret yükseklikleri, fraklı Froude sayıları, farklı akım şiddetleri ve nüiform taban malzemesi dikkate alınarak hareketli taban oyulması koşulları altında (akım şiddetinin birden küçük olduğu durum) bir dizi deney gerçekleştirilmiştir. Deneylerde savağın membasında ve mansabında farklı boyutlarda oyulma ve kum birikintileri oluştuğu gözlemlenmiştir. Maksimum oyulma derinliğinin, çoğunlukla üçgen labirent yan savağın mansap ucunda oluştuğu gözlenmiştir.

Anahtar Kelimeler:

1. Introduction

A structure, located in a stream bed or built later, could change certain properties of the flow. If these changes in flow could be predicted beforehand, the structure would be designed in a sounder manner, or necessary precautions against the problems that are caused by these changes

would be taken. Otherwise, this case leads to damages in the structure or to the failure in fulfilling its function. The scouring observed in the intake structure, scouring formed in the downstream of the spillway, and the scouring occurring in the abutment wall and midfoot of the bridges and the scouring observed in the downstream of the baffle structures are of major problems encountered in hydraulic engineering.

The decrease in velocity and shear stress due to the lateral over flow causes the realization of a reverse current via creating a stagnation region in the downstream of the side weir. Scouring is formed between the main channel axis in the downstream region of the side weir and the outer bank, as a result of the changes in the shear stress.

Although there were no studies that scrutinized the scouring depth and geometry that occurs around the labyrinth side weirs in live-bed channels, there are limited number of studies that examined the scouring geometry around the classical side weir. Rosier et al. (2011) conducted an experimental research on the geometrical behavior of bed forms in a classical side weir region placed in a rectangular channel [1]. Paris et al. (2012) researched the applicability of De Marchi hypothesis on the determination of discharge capacity of side weirs under subcritical flow regime and live-bed conditions. This study presents experiments demonstrating the relationship between bed morphology and overflow discharge. The experiments were conducted in a main channel with small dimensions (0.30 m x 5 m x 0.30 m) and within a small discharge range (2-12 L/s). Studies reported that De-Marchi approach could be used in live-bed channels [2]. Onen and Agaccioglu (2013) conducted an experimental research examining clear-water scouring and live-bed scouring conditions in rectangular cross-section side weirs with L = 0.25, 0.40 and 0.50 m weir opening and p = 0.07, 0.12 and 0.17 m crest height from the sand bed in a live-bed 180o curved channel, considering subcritical flow regime and overfall conditions [3].

Since there are limited number of studies in the literature on the change in bottom topography and the scouring problem, which both occur around the labyrinth side weir that are placed in the streams, a complete theoretical basis on this subject was not constituted. Therefore, it is considered that it would be useful to examine the scouring problem, especially in our country that is rich in rivers. The aim of the present study is; to investigate the maximum scouring depth and the bottom geometry in the labyrinth side weirs, under the live-bed scouring conditions.

2. Hydraulics of Side Weir Flow

The most important function of the side weir is to discharge the excessive water, when the optimum capacity, determined by taking into account the requirement and economy, is exceeded. Side weirs are used in numerous engineering applications. As the water level in the reservoir reaches a level that could damage the dam, side weirs are used to discharge the water (Fig. 1). Although they are built next to the reservoir due to the flow conditions in the reservoir, these weirs act as normal weirs. This condition should be taken into consideration while conducting the hydraulic design.

Figure 1. Walshaw Dean Reservoir [4]

Figure 2 presents the side weir plan and section. It is stated that; y_1 = flow depth at the upstream end of the side weir at the centerline of the main channel (m), y_2 = flow depth at the downstream end of the side weir at the centerline of the main channel (m), y = flow depth at any point in the main channel (m), Q_1 = main channel discharge (m^3/s), Q_2 = main channel discharge after the side weir (m^3/s), Q_w = total flow over side weir (m^3/s), V_1 = mean approach flow velocity at the upstream of the side weir in thw main channel (m/s), V_2 = mean approach flow velocity at the downstream of the side weir in the main channel (m/s), V_s = mean approach flow

velocity of the side weir in the collection channel (m/s), B = main cahnnel width (m), L = around a triangular labyrinth side weir of width (m), Ψ = angle of deflection (°), p = weir crest height (m), x = longitudinal coordinate (m).

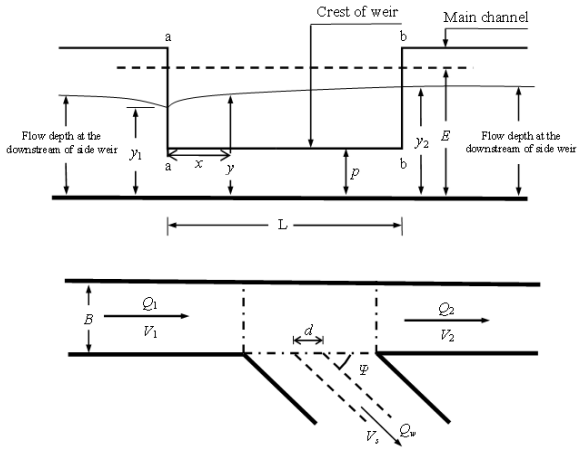

Figure 2. Plan and section of the side weir flow [5].

3. Labyrinth Weirs

Increasing the flow rate that could overflow in a particular lake level or transmitting a constant flow rate by a smaller crest water load is aimed via the labyrinth spillways, through increasing the effective length of the spillway crest. These weirs could be considered as an alternative, which are advantageous in conditions where the space in the upstream is restricted for the reservoir water level that would especially be created by the flood discharge or in conditions where the spillway width is limited due to topography. Labyrinth weirs could be constructed in trapezoidal, triangular, and circular-shaped (Fig. 3). Most preferred type is the trapezoidal-shaped type. Equation (1) is used to find the rate of flow, that pass over the labyrinth weir. Total crest length should be considered instead of the distance "L" in Eq. (1) [6].

$$Q = 1.83.(L\text{-}0.2h).h^{3/2} \quad (1)$$

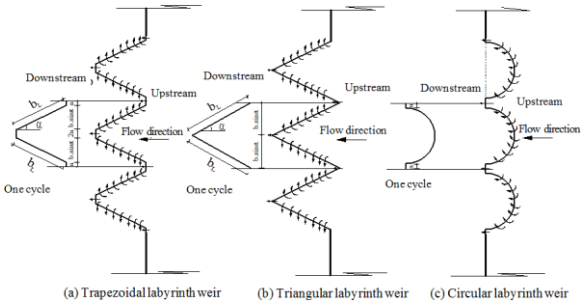

Figure 3. Labyrintyh weirs [7].

4. The Deterioration of Equilibrium in Sediment Transportation

In the case that the amount of solid material transported in an alluvial stream changes locally, changes such as sediment deposit in the bed and scouring could occur. As the amount transported increases scouring is observed, and when decreases, sediment deposit is observed.

The construction of a hydraulic structure such as a weir might cause changes in the stream bed. Such changes in the bed of the stream are observed either as sediment deposit in some parts or as scouring in others, depending on the amount of material that comes from the upstream, on the amount of material that is transported and on the amount of material that is over flown (Fig. 4). Both the sediment deposit and the scouring phenomena continue until they obtain a stable cross-sectional shape. Sediment deposit starts primarily with the sediment deposit of coarse particles, with their departure from the bed the velocity increases and the suspension discharge increases due to the decrease of the mean diameter of the material transported in suspension. Thus, due to the increase in the transported material, equilibrium condition is approximated. On the other hand, as the material coming from the upstream is smaller than the discharge transport capacity, the coarse particles remain in the bed since initially the fine particles in the bed would be scoured. In addition, occurrence of ripples in the bed would as well cause the decrease of the discharge transport capacity. Thereby, either in case of scouring or in sediment deposit, several secondary degree factors accelerate the achievement of the equilibrium condition [8].

Figure 4. Sediment deposit and scouring observed in the present study.

In a bed with cohesionless loose-material, the movement starts when the bed conditions reach a critical value required for movement. The particles that depart the bed due to the bed movement are washed away along the bed by depositing.

Bed shapes encountered in the rivers are as follows:

a. Ripples
b. Dunes
c. Plane bed
d. Antidunes

The order of the bed shapes provided above is made according to the change depending on the velocity of the flow. In other words, sand ripples occur with lower velocity flows, and as the velocity increases the bed has the shapes of ripple, dune, plane bed and antidune, respectively. Various shapes that the bed could take are given in Fig. 5 [9].

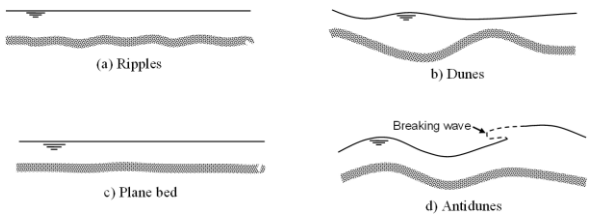

Figure 5. Bed forms developed in alluvial channels [9].

Ripple and dune formations observed in this study are presented in Fig. 6.

Figure 6. Ripple and dune formations observed in this study.

5. Experimental Study

This study was conducted at the Firat University Hydraulics Laboratory using the experimental setup depicted in Figure 7. The experimental setup was 18.20 × 0.50 m and the side wall of the main channel was made of glass. The slope of the main channel bottom was approximately 0.1%. The collection channel was 0.50 m wide and 0.70 m high. The main channel and collection channel were separated by a steel wall. The section of the collection channel where the side weirs would be *installed* was built in a circular form with a diameter of 1.30 m to provide free nape overflow from the labyrinth side weir (Fig. 7).

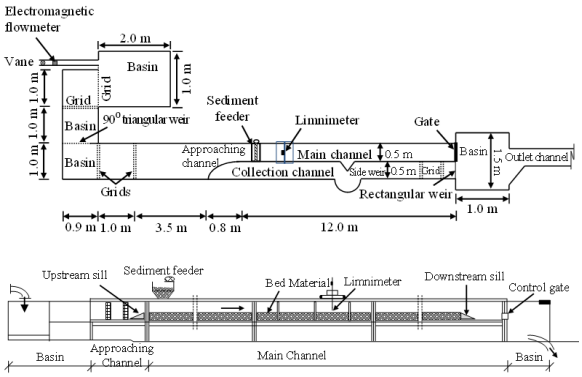

Figure 7. Experimental setup plan and longitudinal cross-section: Plan view (a), Longitudinal section (b).

The experiments are conducted in a linear channel with a rectangular cross-section; for a side weir opening of L = 0.25 meters, and for triangular labyrinth side weirs, with crest height of p = 0.07, 0.12 and 0.16 meters from the sand bed and with an apex angle of $\theta = 90^0$. The experiments were carried out under steady flow conditions, and in the case of bed scouring (V_1/V_c>1) for free over flowing condition. The experiments were conducted at a discharge of 50

- 90 L/s. The flow depth (y_1) was measured at the channel axis at the upstream end of the side weir. The water depth at the main channel axis upstream of the side weir was used as the side weir upstream water depth. Novak and Cabelka (1981) suggested a minimum upstream water depth of 30 mm [10]. Thus, in this study a minimum upstream water depth of 30 mm was used to prevent surface tension affects.

Two sills of 20 centimeters height are placed at the upstream and downstream ends of the main channel, as seen in Figure 8. Quartz sand was placed between the upstream and downstream sills on the main channel. For this sand laid on the channel bed, following values are determined, d_{50} = 1.16 millimeters and γ_s = 26 kN/m^3. The parts before the upstream sill and after the downstream sill are made up of sheet metal with an approximate slope angle of 15^0, reaching the channel bed. Thus, the provided sand base was protected against deterioration. In order to ensure stable flow conditions (i.e. to provide time-invariant flow conditions), hollow bricks are placed at the upstream part of the channel and in front of the specific points at the end of the collecting channel. The aim is to ensure taking accurate measurements over the weir.

This experimental study was carried out for the labyrinth side weirs placed in the middle part of a linear channel. The bed material was laid 4 meters forth and 4 meters backwards from the center of the side weir, covering 8 meters of the channel. Experiment system application assembly is shown in Fig. 8.

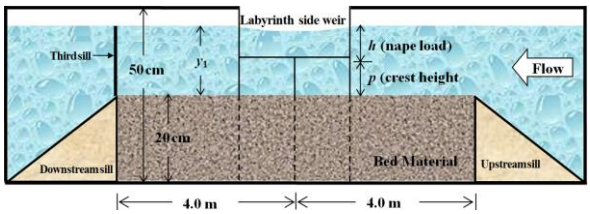

Figure 8. Experiment system application assembly.

Prior to each experiment, the sand was mixed and compacted and the bed was leveled. After the channel bed is compressed and flattened, water was supplied slowly to the channel by turning on the valve very little. As the water slowly flowed over the sand by rising slowly from the ramp in front of the sill of the upstream end of the channel, a third sill is placed 20 centimeters above the sill on side of the downstream (i.e., as it should be 40 centimeters high from the channel bed). In such way, deformation the flat shape of the sand in the bed is prevented. Then, it was waited until the depth of water in the next section of the downstream sill of the main channel reached the same water depth in the main channel. After all water level along the channel became even, the requirement flow was attained and the experiment was commenced by slowly removing the third sill that prevented the deformation of the shape of the sand in the bed, on the sill at the downstream part. By keeping the flow rate constant, flow height in the channel (y_1) was adjusted to the required level via the radial caps at the end of the channel.

Once the experiment is completed, the valve was slowly turned off, and the third sill was placed back on the downstream sill of the channel in order to preserve the topography that was formed on the bed, and thus the discharge of the water from the channel was provided. Consequent to all these processes, maximum scouring depth that occurred at the side weir area was measured via a digital limnimeter. In addition, for the bed topography, bed level measurements were taken at the side weir area at 268 points with particular intervals through the aid of the digital limnimeter. Figure 9 presents the points, at which the bed topography measurements were taken.

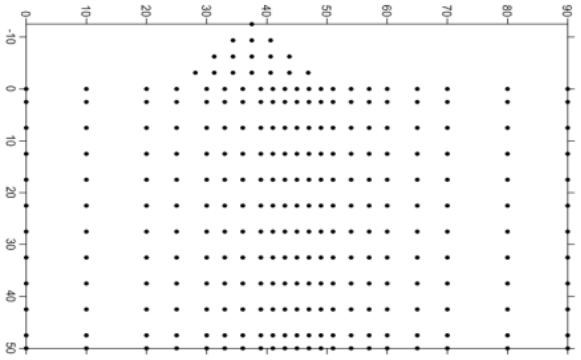

Figure 9. The demonstration of the points of topography measurements at the labyrinth side weirs that were tested: L = 0.25 m.

Initially pilot experiments were conducted in order to determine the bed load flow for various flow conditions. In case of a moving bed (V_1/V_c >

1), since bed ripples occur in a short time, and the bed is constantly in a movement, solid material transportation occurs at a high level, and the amount of the overflown material increases constantly due to the increase in the flow rate (V_1/V_c). Thus, in order to provide the moving bed condition, constant supply of solid material was provided in the channel via the portative machine, which is designed in the Hydraulics Laboratory of the Firat University's Civil Engineering Department, seen in Fig. 10. The velocity of the volumetric amount of sediment feed ($Q_{s,up}$) was adjusted by taking into consideration the "V_1/V_c" values through this machine.

Figure 10. Portative machine that provide solid material supply to the channel.

Side weir properties and flow conditions in this study are presented in Table 1.

Table 1. Side weirs and flow conditions tested in the experiments

Experiment No	p (m)	L (m)	Q_1 (L/s)	y_1 (m)	$Q_{s,up}$ (m^3/s)	V_1/V_c (-)	F_1 (-)
1	0.07	0.25	50	0.12	0.00075	1.94	0.77
2	0.12	0.25	55	0.16	0.00019	1.52	0.55
3	0.16	0.25	90	0.19	0.00020	2.06	0.69

6. Evaluation of the Experiment Results

In this section, non-dimensional maximum scouring depth's (d_{smax}/p) change in non-dimensional time (t/t_{max}) was investigated in case of moving bed scouring, for side weirs with L = 0.25 meters opening and p = 0.07, 0.12, 0.16 meters crest height, and is presented in Figure 11(a-c). For moving bed scouring, "V_1", which is the velocity value in the main channel, is selected greater than the "V_c" value, which is the initial velocity of the movement in the bed. The experiments were carried out in the range between V_1/V_c = 1.0-3.0 and each experiment were carefully elaborated to be sustained for 1080 minutes. Figure 4 presents the areas in which maximum scouring depths were observed. The experiments pointed out that the duration required to obtain the maximum scouring depth during equilibrium for moving bed scouring is approximately 480 minutes. For larger "V_1/V_c" values, this duration was around maximum 900 minutes. After this duration, maximum scouring depths were observed to exhibit amplitudes close to the equilibrium scouring depths (Fig. 11). On the other hand, for the same "V_1/V_c" values in side weirs with larger crest heights, scouring depth at the time of equilibrium was observed to be smaller, and the equilibrium time was attained in a shorter duration. Scouring depth-duration graphics for each experiment is presented in Figs. 11 (a-c) and the flow characteristics are presented in Table 1. The tendency of the experiment results is parallel to the change of scouring depth as a function of time graphics in the studies of Tsujimoto and Mızukami (1985) and Yanmaz and Altinbilek (1991) [11 and 12].

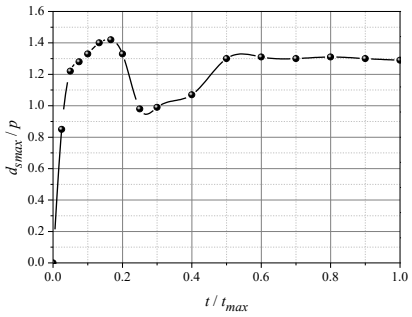

a) No.1 experiment

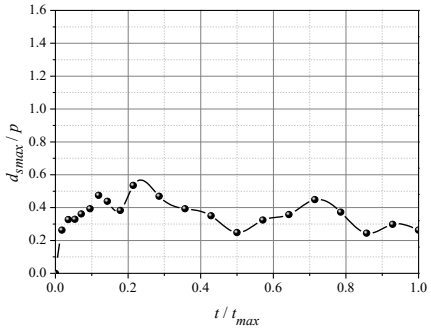

b) No.2 experiment

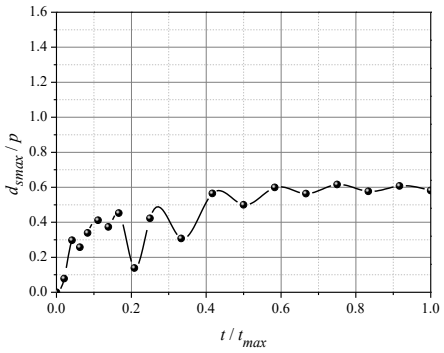

c) No.3 experiment

Figure 11. Time-dependent change of the scouring depth for L=0.25 m in the maximum scouring area: p=0.07 m (a), p=0.12 m (b), p=0.16 m (c).

Bathymetric contour lines of the bed occurrence as a result of the experiment for L = 0.25 m and p = 0.07, 0.12 and 0.16 m and the related images are presented in Figs. 12 (a-c).

In Figure 12 (a), it is possible to observe that the topography at the interior edge of the channel did not change significantly. Scours and peaks were observed in the labyrinth triangular side weir area placed at the exterior edge. Scouring depth at equilibrium time occurred at a certain distance from the weir area.

Scouring depth at equilibrium time in Figure 12(b) was formed in an elliptical shape from the center of the downstream of the weir to the downstream end. At the upstream overflow part, a small peak formation was observed. Due to the increasing crest height and decreasing flow rate (V_1/V_c), less material was transported to the collection channel.

In Figure 12(c), it was observed that the topography at the interior edge of the channel did not alter significantly and small-dimensioned sand ripples were formed. However, at the exterior edge of the channel, it was observed that scours and peaks were formed. Scouring depth was formed with an elliptical shape at the weir's downstream end. Bed ripple formation is observed. Maximum scouring formation is observed at the downstream overflowing part. Due to the large crest height and lower side weir length of the side weir used for this experiment, little amount of material was overflown.

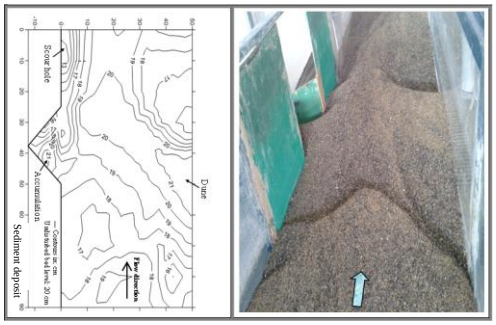

a) No.1 experiment

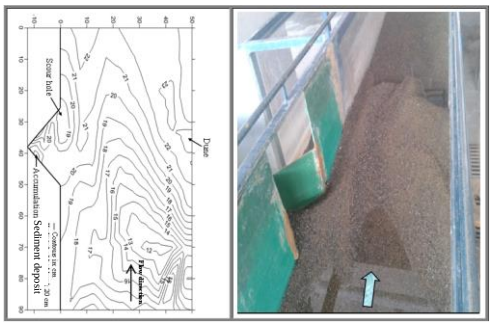

b) No.2 experiment

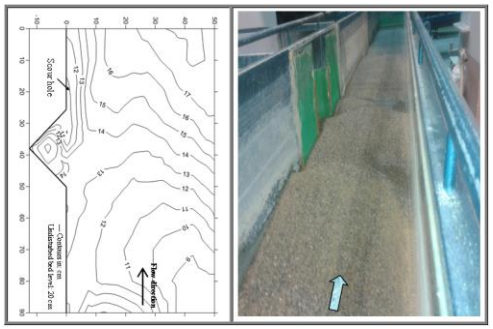

c) No.3 experiment

Figure 12. Bed bathymetry and related images for L=0.25 m: p=0.07 m (a), p=0.12 m (b), p=0.16 m (c).

7. Conclusions

Along a linear, rectangular cross-section channel with a moving bed, in constant flow and free overflowing conditions; following results are obtained from this study, which scrutinized the topographical changes that occur around the side weir and at the main channel bed and the scouring depths at the non-dimensional equilibrium time, in conditions of moving bed scouring in labyrinth side weirs with L = 0. 25 m length and p = 0.07, 0.12 and 0.16 m crest height from the sand bed.

- In this experimental study (V_1/V_c = 1.0 - 3.0), it was observed that scouring depth became

evident after a short duration from the initiation of the experiment and this duration shortened due to the increase of the flow rate.

- For the flow rate V_1/V_c = 1.52 value, while usually ripple formation was observed in the bed, mostly dune formations were observed at 1.94 and 2.06 values.
- The transformation of the channel bed from ripple form to dune form, scatterings were observed in the scouring depths due to the changing bed roughness.
- While the duration to reach the maximum value of the scouring pit decreased due to the increase of the side weir crest height, the duration for obtaining the maximum value in larger "V_1/V_c" values increased.
- The place of the scouring pit formation was determined as around the side weir and close to the downstream end. As the "V_1/V_c" value increased, it was observed that the place of the scouring pit was shifted from the downstream end of the side weir to the downstream.
- With the larger values of flow rate (V_1/V_c), scouring depth at the non-dimensional equilibrium time (d_{se}/p) also reached larger values.
- Larger scouring depths were obtained in side weirs with large crest heights.
- When the flow conditions were considerably same, bed scouring started earlier as the side weir crest height decreased, and bed scouring started later as the side weir crest height increased.
- It was determined that scouring shape that occurred in the bed was directly related to the flow rate (V_1/V_c) and non-dimensional side weir crest height (y_1/p) in the rectangular cross-section linear channel, under moving bed flow conditions.
- While the side weir height is 0.07 meters, the shape of the scouring in the bed is formed with circular cross-sections due to the vortex occurrence, and when the side weir crest height increases to 0.12 and 0.16 meters, the scouring was observed to have an elliptical shape.
- It was determined that the scouring depth at non-dimensional equilibrium time (d_{se}/p) changed directly with the increase in flow rate (V_1/V_c) and after a certain period it presented an amplitude around the peak values.

8. References

1. Rosier, B., Boillat, J. L., and Schleiss, A. J. (2011). "Influence of lateral water withdrawal on bed form geometry in a channel." *Journal of Hydraulic Engineering*, 10.1061/(ASCE)HY.1943-7900.0000472, 1668-1675.

2 . Paris, E., Solari, L., and Bechi, G. (2012). "Applicability of the De Marchi hypothesis for side weir flow in the case of movable beds." *Journal of Hydraulic Engineering*, 10.1061/(ASCE)HY.1943-7900.0000566, 653-656.

3. Onen, F., and Agaccioglu, H. (2013). "Live bed scour at a side-weir intersection located on an alluvial channel." *Irrigation and Drainage*, 62(4), 488-500.

4. Tunc, M., and Emiroglu, M. E. (2014). "Effect on bed topography of labyrinth side weirs located in movable bed rivers." *With International Participation 4th National Symposium and Exposition on Dam Safety*, 759-770 (in Turkish).

5. Emiroglu, M. E., Kaya, N., and Agaccioglu, H. (2010). "Discharge capacity of labyrinth side weir located on a straight channel." *J. Irrig. and Drain. Eng.*, 10.1061/(ASCE)IR.1943-4774.0000112, 37-46.

6. USBR., 2001. Water measurement manual, *3rd Edition*, Water Resources Research Laboratory, Bureau of Reclamation, U. S. Department of the Interior.

7. Emiroglu, M. E., Kaya, N. ve Dogan, Y. (2010). The effect of shape of crest on discharge coefficient in weirs, *DSI Technical Bulletin*, 108, 57-70 (in Turkish).

8. Tunc, M. (2014). An investigation of the hydrodynamics of flow at the labyrinth side weirs in the movable bed rivers, *Firat University, Graduate School of Science* (in Turkish).

9. Bayazit, M., and Avci I. (2010). Flow in streams and sediment transport, *Istanbul Technical University, Civil Engineering Faculty Press*, Istanbul (in Turkish).

10. Novak P. and Cabelka J. (1981). Models in Hydraulic Engineering, *Pitman Publishing Limited*, London.

11. Tsujimoto, T. and Mizukami T. (1985). Effect of migration to local scour around a bridge pier, *Memoirs, Faculty of Technology, Kazanawa University*, 19(1): 23-34.

12. Yanmaz, A. M., and Altınbilek, H. D. (1991). "Study of time –dependent local scour around bridge piers." *Journal of Hydraulic Engineering*, 10.1061/(ASCE)0733-9429(1991)117:10(1247) 1247-1267

TURKISH JOURNAL OF SCIENCE & TECHNOLOGY (TJST)

INSTRUCTIONS FOR AUTHORS

Turkish Journal of Science & Technology is an international journal covering all aspects relating to science, engineering and technology.
The following types of article will be considered:
1. Research Articles: Original research in various fields of science, engineering and technology will be evaluated as research articles. Papers must include an English abstract and if possible a Turkish abstract.
2. Research Notes: These include articles such as preliminary notes on a study, manuscripts.
3. **Reviews:** Reviews of recent developments, improvements, discoveries and ideas in various fields of selected subjects will be requested by the editor or advisory board.
4. Letters to the Editor: These include opinions, comments relating to the publishing policy of Turkish J. of Sci. & Tech., news and suggestions. Letters are not to exceed a single page.
All manuscripts will be subject to multiple **peer review** before publication. Submitted manuscripts must not be under consideration for publication elsewhere or have already been published. The editor reserves the right to decide that a paper may be treated as a Research Note.
Manuscripts should be sent to below address:
Fırat University, Fen Bilimleri Enstitüsü,
Turkish Journal of Sci. & Tech. Editörlüğü,
23119 Elazığ- TURKEY
There are **no page charges**.

SUBMISSION OF MANUSCRIPTS

1. Manuscripts must be submitted in typewritten on one side of the page in a legible font, double-spaced with ample margins. All manuscripts must be accompanied by the **Copyright Release Form**, which can be found following the Instructions. This form must be completed and signed by all the authors before processing of the manuscript can begin. If the manuscript is submitted by e-mail a high quality scan of the Copyright Release Form is acceptable.

Manuscripts must be written in **English**. Contributors who are not native English speakers are strongly advised to ensure that a colleague fluent in the English language, if none of the authors is so, has reviewed their manuscript. Concise English without jargon should be used. Repetitive use of long sentences and passive tense should be avoided. All abbreviations and acronyms should be defined at first mention. To facilitate reader comprehension, abbreviations should be used sparingly. After the manuscript has been accepted for publication, i.e. after referee-recommended revisions are complete, the authors will not be permitted to make any additions. Before publication, the **galley proof** is always sent to the authors for correction. Mistakes or omissions that occur due to some negligence on our part during the final printing will be rectified in an errata section of a later issue. However, this does not include those errors left uncorrected by the authors in the galley proofs.
All due care will be taken with material submitted, but the Advisory Board and the publisher cannot be held responsible for any loss or damage.

2. Manuscripts should have the following **format**: title, name(s) of author(s), key words (3-6), abstract, text, references.
3. The **abstract** must be brief and informative and must not exceed 200 words. It should include all new names, combinations and rank transfers.
4. The text may be divided into reasonable subdivisions by the authors with numbered (1, 2,..), but the aim of the article, results and discussion must be included. An Introduction and Materials and Methods section may also be included if appropriate.

Within the main text, **author citations** should follow:
Brummitt and Powell, [1] …….For three or more authors use 'et. al.' for example Özcan et. al. [1]

References in the text should be numbered in square brackets as [1]. Multiple references should be arranged chronologically.

5. In the **reference list**, references should be numbered in the order of appearance in the text and should appear in the following style:
Journal articles: (i) Surname(s) and initial(s) of author(s), (ii) Year of publication (in parentheses), (iii) Title of article (in lower case), (iv) Title of journal (in italics), (v) Volume number, (vi) Page numbers.

For example, Emiroglu, M. E., and Baylar, A. (2003). Study of the Influence of Air Holes along Length of Convergent-Divergent Passage of a Venturi Device on Aeration. *Journal of Hydraulic Research*, **41** (5), 513-520.

Chapters in books: (i) Surname(s) and initial(s) of author(s), (ii) Year of publication (in parentheses), (iii) Title of chapter (in lower case), (iv) Name of editor (if applicable), (v) Title of book (in upper case and italics), (vi) Page numbers,

(vii) Place of publication, (viii) Name of publisher.
For example, Endler JA (1982). Pleistocene forest refuges: Fact or fancy? In: Prance GT (ed.) Biological Diversification in the Tropics, pp. 641-657. New York: Plenum Press.
Books: (i) Surname(s) and initial(s) of author(s), (ii) Year of publication (in parentheses), (iii) Title of book (in upper case and italics), (iv) Place of publication, (v) Name of publisher.
For example, Mabberley DJ (1987). The Plant-Book. A Portable Dictionary of the Higher Plants. Cambridge: Cambridge University Press.

Ahmed, A. (1974). Aeration by Plunging Liquid Jet. Ph.D. thesis, Loughborough University of Technology, Leicestershire, UK.
References to web sites, computer programs, and unpublished theses or reports are unacceptable.

6. All scientific names cited in the running text, irrespective of rank, **must be italicised**. In headings, scientific names must be in bold and not italicised. **Authors of genera and lower taxa** must be cited at the first mention of the taxa in both the abstract and the text.

7. Figures and Tables
All illustrations (photographs, line drawings, graphs, maps, etc.), not including tables, must be labelled "Figure".
The **correct position** of each table and figure must be clearly **indicated** in the paper
All tables and figures must have a number (Table 1, Figure 1) and a caption or legend. All tables and figures must be numbered consecutively. All captions and legends must also appear on a separate sheet, double-spaced and labelled according to the relevant table or figure.
Tables and figures, including caption, title, and column heads, **must not exceed** 16 x 20 cm and should be no smaller than 8 cm in width. Tables must be clearly typed, each on a separate sheet, and double-spaced. Tables may be continued on another sheet if necessary, but the dimensions stated above still apply.
Figures must be the originals. Reduced photocopies are not acceptable. **Photographs** must be clear, black and white, and on glossy paper. **Three sets of photographs** must be submitted.
Before submitting your manuscript, ensure that all the following requirements have been met:
-- The **Copyright Release** Form, appearing on the following page, has been completed and **signed by all the authors**
-- Spell check and grammar check have been performed
-- **Paper** is submitted in **triplicate** (one original, two copies)
-- **Entire paper** is **double-spaced** including abstract, tables, captions/legends, and references (NOT 1.5)
-- Margins are c. 3 cm each side
-- Font size is 12 pt or 3 mm
-- There are **no word breaks** at the ends of lines
-- **Decimals** are shown by a **decimal point** (e.g., 10.24) and **not by a comma** (e.g., NOT 10,24)
-- The percent sign appears after the number (e.g., 53%) and not before (e.g., NOT %53)
-- **Names of authors** are written in full (not abbreviated)
-- English address is given
-- Turkish address (if applicable) is given
-- English title is given
-- Turkish title is given (if possible)
-- English abstract is given
-- Turkish abstract is given (if possible)
-- English key words are given
-- Turkish key words are given (if possible)
-- **Authors of genera and lower taxa** are cited at first appearance in both the abstract and the text
-- **Unpublished references** (theses, project reports, etc.) are not referred to or cited
-- Three sets of **photographs** are enclosed
-- **Original figures** are enclosed
-- **Figures** are prepared according to the instructions
-- Figures are max 16 x 20 cm; min 8 x 20 cm wide
-- Figures are referred to consecutively in the paper
-- **Tables** are max 16 x 20 cm; min 8 x 20 cm wide
-- Tables are referred to consecutively in the paper
-- Table and figure legends/captions are typed on a separate sheet
-- **References** are listed in alphabetical order in the style shown in the instructions
-- All pages are numbered

Further details can be found on our web site. **http:/www.firat.edu.tr**

C O P Y R I G H T R E L E A S E F O R M

TURKISH JOURNAL OF SCIENCE AND TECHNOLOGY (TJST)
Published by Firat University

Firat University, Fen Bilimleri Enstitüsü Müdürlüğü
Turkish Journal of Science & Technology Editörlüğü
Elazığ-TURKEY,
Manuscript title: .....
.....
.....
Full names of all authors (in order to appear on manuscript): .....
.....
Name, address etc. of corresponding author: .....
.....
.....
ID Number: ..... Telephone: .....
E-mail: ..... Mobile phone: .....

The author(s) warrant(s) that:
a) the manuscript submitted is his/her/their own original work;
b) all authors participated in the work in a substantive way and are prepared to take public responsibility for the work;
c) all authors have seen and approved the manuscript as submitted;
d) the manuscript has not been published and is not being submitted or considered for publication elsewhere;
e) the text, illustrations, and any other materials included in the manuscript do not infringe upon any existing copyright or other rights of anyone. Notwithstanding the above, the Contributor(s) or, if applicable the Contributor's Employer, retain(s) all proprietary rights other than copyright, such as
a) patent rights;
b) to use, free of charge, all parts of this article for the author's future works in books, lectures, classroom teaching or oral presentations;
c) the right to reproduce the article for their own purposes provided the copies are not offered for sale.
However, reproduction, posting, transmission or other distribution or use of the article or any material contained therein, in any medium as permitted hereunder, requires a citation to the Journal and appropriate credit to Firat University as publisher, suitable in form and content as follows:
Title of article, author(s), journal title and volume/issue, Copyright© year.
All materials related to manuscripts, accepted or rejected, including photographs, original figures etc., will be kept by Turkish Journal of Science and Technology editority for one year following the editor's decision. These materials will then be destroyed.
I/We indemnify Firat University and the Editors of the Journals, and hold them harmless from any loss, expense or damage occasioned by a claim or suit by a third party for copyright infringement, or any suit arising out of any breach of the foregoing warranties as a result of publication of my/our article. I/We also warrant that the article contains no libelous or unlawful statements and does not contain material or instructions that might cause harm or injury.
This copyright form must be signed by all authors. Separate copies of the form (completed in full) may be submitted by authors located at different institutions; however, all signatures must be original.

ID number: ..... ID number: .....
Full name (block letters) ..... Full name (block letters) .....
Signature ..... Date ..... Signature ..... Date .....
ID number: ..... ID number: .....
Full name (block letters) ..... Full name (block letters) .....
Signature ..... Date ..... Signature ..... Date .....
ID number: ..... ID number: .....

Turkish authors must supply their ID card number; foreign authors must supply their passport number (if possible)